SHELF-TO-CANYON SEDIMENTATION ON THE SOUTH WESTLAND CONTINENTAL MARGIN, WESTLAND, NEW ZEALAND

A thesis submitted in partial fulfilment

of the requirements for the degree

of

Master of Science in Geology

at the

University of Canterbury

by Josh Radford

2012

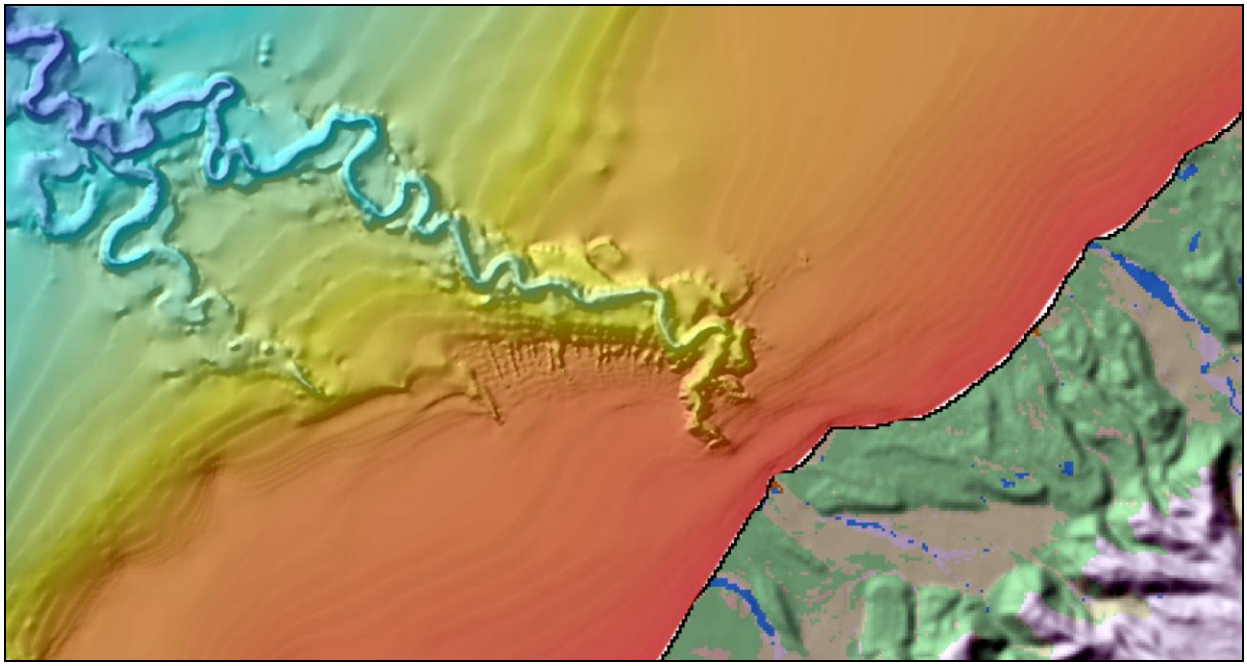

The Cook Canyon incising the South Westland shelf to within 4 km of the Cook River mouth. Image is based on digital elevation model data from NIWA.

ABSTRACT

The South Westland Continental Margin (SWCM) is incised by two major active canyon channels, the Hokitika and Cook Canyons, which export large volumes of terrigenous sediment from the active New Zealand landmass to the deep ocean basins. This thesis examines modern sediment textures and compositions of shelf and canyon heads, to interpret depositional and transport processes in shelf-canyon interactions and the dispersal and provenance of SWCM surface sediments. This is the first detailed study of modern sediments south of the Whataroa River which focuses on both shelf and canyon head sediments. Submarine canyons that incise active continental shelves are major conduits for sediment transfer. The frequency and magnitude of this transfer has important implications for ocean nutrient cycling (i.e. organic carbon), the stratigraphy and morphology of continental shelves, and the development of economic mineral deposits. Grain size analysis, petrology, geochemistry, detrital magnetite analysis (microprobe), swath bathymetry, and wave hindcast data are used to interpret the spatial distribution, dispersal, and provenance of surface grab samples, canyon cores, and beach and river samples on the SWCM.

Four main surficial facies are defined from textural and compositional results, primarily reflecting the supply and storm dominated nature of the SWCM. Facies 1 is comprised of inner shelf very fine to medium sand sized quartz, metamorphic lithics, and feldspar. This facies occurs above the mean H_{sig} wave base (48 m) where silts, clays, and sand sized micas are bypassed further offshore. Facies 2 is a transitional sand to mud facies between 40 -70 m depth where increasing clay, silt, and mica reflect a decrease in the frequency and magnitude of wave orbital remobilisation. Facies 3 is a mud dominated (80-90%), clay rich (7-9%) facies with the highest mica and Al_2O_3 content of all the SWCM facies. The shelves south of the Hokitika Canyon are blanketed beyond the inner shelf in facies 3 towards the shelf break. Facies 4 is restricted to the canyon head north rims and is characterised by mixed relict and modern terrigenous sediments and glaucony. Net transport on the SWCM shelf is to the north, particularly during south-westerly storms where wind drift and storm swells may stir and transport the deeper Facies 2 and 3 sediments. The SWCM has an energetic wave climate and numerous high yield mountainous rivers. As a result the shelf has an extensive coverage of silts and clays with sediment transport most likely dominated by nepheloid layers and fluid mud flows during wet storms. North of the Hokitika Canyon, shelf width increases as fluvial supply falls, resulting in a more storm dominated shelf as the prevailing hydraulic conditions prevent modern silts and clays from blanketing the outer shelf. Narrower shelf widths and higher fluvial supply between the Hokitika Canyon and the Haast region results in more fluvial dominated shelves.

Contrasting canyon rim textures and compositions reflect the major influence the Hokitika and Cook Canyon Heads impose on the SWCM by intercepting modern net northward shelf transport paths. This interception creates a leeward sediment deficit on the canyon north rims where low sedimentation rates prevail and relict sediments are partially exposed. The south and east rims of both canyons are characterised by modern fine grained terrigenous textures and compositions similar to the SWCM middle to outer shelf facies 3. The build-up and storage of these unconsolidated sediments at the south and east rims provides favourable environments for sediment gravity flows that feed into the canyon systems. Wave orbitals can resuspend fine sands up to 50 m below the canyon rims during large storms. This resuspension will be a main driver of canyon head sedimentation in the form of fluid mud flows. Gully networks along the south and east rims of the Hokitika and Cook Canyons indicate active submarine erosion, unconfined fluid flow, and sediment gravity flows operate here.

In contrast, the north canyon rims are characterised by gravels and coarse sands out of equilibrium with the prevailing modern hydraulic regime. Relict gravels are particularly prevalent on the Hokitika Canyon north rim between 90 – 150 m depth. A lack of active gully networks and the presence of relict terraces and cuspate channels provide further evidence for a relict origin of HCH north rim sediments and little influx of modern fine sediments. North rim sediments on the Hokitika Canyon between 90 – 125 m have features characteristic of relict beach and littoral environments. These features include pebble and coarse sand sized siliciclastics, high heavy mineral percentages (i.e. garnet), high Zr and Y levels, elevated SiO_2/Al_2O_3 ratios, and relict shell fragments. Mature glaucony is common on the north rims of both canyons, especially between 180 -200 m depth providing further evidence for extended periods of little to no modern sediment deposition in the canyon lee. Glaucony grains have experienced limited transport and are probably *parautochthonous.*

The bulk composition of SWCM shelf, canyon, river, and beach sediments is controlled mainly by the hydrodynamic sorting of Alpine Schist derived material. Regional changes in catchment geology are identified in modern SWCM shelf sediments. Ultramafic signals (i.e. enriched trace element patterns and Cr/V and Ni/Y ratios) from the Pounamu Ultramafics and Dun Mountain Ultramafics were identified on the North and Cascade shelves respectively. The contribution of other lithologies to the bulk composition of SWCM sediments is localised due to rapid dilution with Alpine Schist detritus. The low carbonate and skeletal content on the SWCM is due to the energetic wave climate and high fluvial supply on the shelves.

A variety of Cr-rich spinels and magnetites are supplied to the SWCM shelves and vary with regional changes in catchment geology. The Cascade Shelf is rich in chromites (containing up to 215,000 ppm Cr) and Cr – rich magnetites sourced from the Dun Mountain Ultramafics via the Cascade River. Shelf, beach, and river samples between the Haast River and Waitaha River are dominated by low-Cr magnetite grains which represent the 'background' magnetite composition sourced from rivers draining the Alpine Schist dominated catchments. The dispersal of Cr-rich spinels is limited due to the dilution with low Cr-magnetites from rivers and littoral sediments.

Glacio-eustatic lowstands such as the Last Glacial Cold Period (LGCP), represented periods of robust connection of local rivers with the Hokitika and Cook Canyon Heads, increased interception of littoral transport paths, and compartmentalisation of inter-canyon shelves. Hokitika Canyon cores reflect these changes with textural and compositional 'spikes' indicating higher terrigenous input during the LGCP. The geochemistry of the terrigenous fraction in the Hokitika Canyon provides evidence for enrichment in ferromagnesian and Cr-rich minerals during the LGCP. This is due to the increased connectivity of the Cr-spinel bearing Hokitika River to the canyon head. The Cr/V ratio in particular demonstrates its effectiveness as a proxy for interglacial – glacial change in submarine canyon stratigraphy. Increases and decreases in the connectivity of Cr-bearing fluvial systems during lowstands and highstands respectively can be observed with this ratio.

Key words: *submarine canyon, Hokitika Canyon, sediment transport, geochemistry, relict, last glacial cold period*

Table of Contents

List of Figures

List of Tables

Acknowledgements

A huge thanks to my supervisors Dr Kari Bassett, Dr Helen Neil, Dr Deirdre hart, and Dr Kate Pedley for your comments, reviews, and support throughout my thesis. You each brought ideas and concepts from different perspectives which I am grateful for. Kari, cheers for keeping me on track and helping me through when things got a bit tough, Helen for all the incredible data and resources from NIWA, Deirdre for the coastal 'spin' on things and forcing me to consider the international context, and Kate for GIS help and your enthusiasm for submarine canyons!

A special thanks for all the support from Helen Neil and the staff at NIWA. Cheers for making the time for my visits, allowing me access to data and sediment archives, and granting additional funding. In particular the use of the laser sizer at short notice due to the CHCH quakes! Helen Bostock and Lisa Northcote for help with the carbonate analysis, how are the chooks doing Lisa?

A massive thanks to Richard Wysoczanski and Victoria University for use of the Microprobe. Thanks Richard for making the time to get me through all those magnetites and the advice on dealing with the data!

Thanks to the University of Canterbury Masters scholarship and the Mason trust from the Department of Geological Sciences for funding during this thesis.

Derek Todd for the discussions on West Coast stirring potentials and your absolute passion for coastal science.

Thanks to all the technical and academic staff in the UC Department of Geology who helped make this happen. Kerry Swanson for your help with the magnetites, photomicrographs, and the good yarns. Rob Spiers for making thin sections, helping me with the microprobe stubs, and showing me how to use the ring mill (sorry the sand was so fine). Chris Grimshaw for thin section staining, microscope access, use of the sed lab, and the beats you put on to sieve to. Huge thanks to Stephen Brown for all the bulk XRF and XRD analyses and making the time to explain how it all works. John Southward for my random IT questions. Thanks to Catherine Reid, Courtney and Janelle for enlightening me on fossils.

Lastly a special thanks the support of my family and friends. Mum and Dad especially for sparking my curiosity in the world around me. Matt Tapps and Chris Bohan for joining me on the West Coast missions to sample rivers and beaches, cheers Matt for pointing out the car had a 6^{th} gear after arriving at Hari Hari.

CHAPTER 1 : INTRODUCTION

1.1 INTRODUCTION

Tectonically active continental margins represent an important interface between terrestrial and marine environments where large volumes of terrigenous sediment is transferred to the deep ocean basins. Submarine canyons often incise active continental shelves close to the coast, becoming a major conduit for sediment transfer to offshore basins (Suter 2006; Puig et al. 2003). The frequency, magnitude, and nature of this transfer has important implications for ocean nutrient cycling (i.e. organic carbon) and the stratigraphy and morphology of continental shelves (Walsh & Nittrouer 2003; Hedges & Keil 1995). In addition, glacio-eustatic sea level fluctuations have major consequences for the flux of terrestrial sediments exported into these canyon systems (Walsh & Nittrouer 2003). The Westland shelf off New Zealand's South Island is a supply dominated active margin shelf characterised by high sedimentation from the rapid tectonic uplift of the Southern Alps and an extremely wet climate. The narrower southern half of this shelf is incised by the Hokitika - Cook Canyon system. This system has recently become the focus of a National Institute of Water and Atmosphere (NIWA) research program looking at the canyon system morphology and stratigraphy to better understand the Late Quaternary glacial history of New Zealand (NIWA Voyage Report 2005).

Previous work on the Westland shelf has focused mainly on the more northern shelf sediments (Probert & Swanson 1985; Stoffers, et al. 1984) north of the Whataroa River. Earlier research has also been traditionally conducted on shelf sediments, with little work on surface sediments within and surrounding the Hokitika and Cook Canyon Heads.

This thesis is focused on the modern distribution, texture, and composition of shelf and canyon head surface sediments on the South Westland shelf, and the implications for modern shelf sediment dispersal, transport mechanisms, and provenance. By investigating the relationships between shelf and canyon head sediments, a more detailed picture of the role and nature of shelf-canyon interactions on the Westland shelf will be achieved. A secondary focus is to examine the effects of sea level change on the texture and composition of canyon stratigraphy.

This chapter introduces the study region, referred to as the South Westland Continental Margin (SWCM) herein, and provides relevant background information on the region, and conveys the specific aims of this thesis.

1.2 STUDY AREA

The South Westland Continental Margin (SWCM) area is focused on a ~320km northeast trending portion of the Westland coastal margin. It includes elements from the continental shelf, the canyon heads,

beaches, and rivers between the Grey River mouth (-42.441˚, 171.94˚) in the north to the Cascade River mouth (-44.031 ˚, 168.362 ˚) in the south (Figure 1-1). Shelf width decreases southwards from 50 – 60 km on the North, to 20 – 30 km wide on the shelves near the Cook and Haast rivers. Most rivers included in this study are major South Westland Rivers that drain westwards from the main divide of the Southern Alps. The location of several cores further offshore in the Hokitika Canyon system are displayed and discussed in section 1.5.

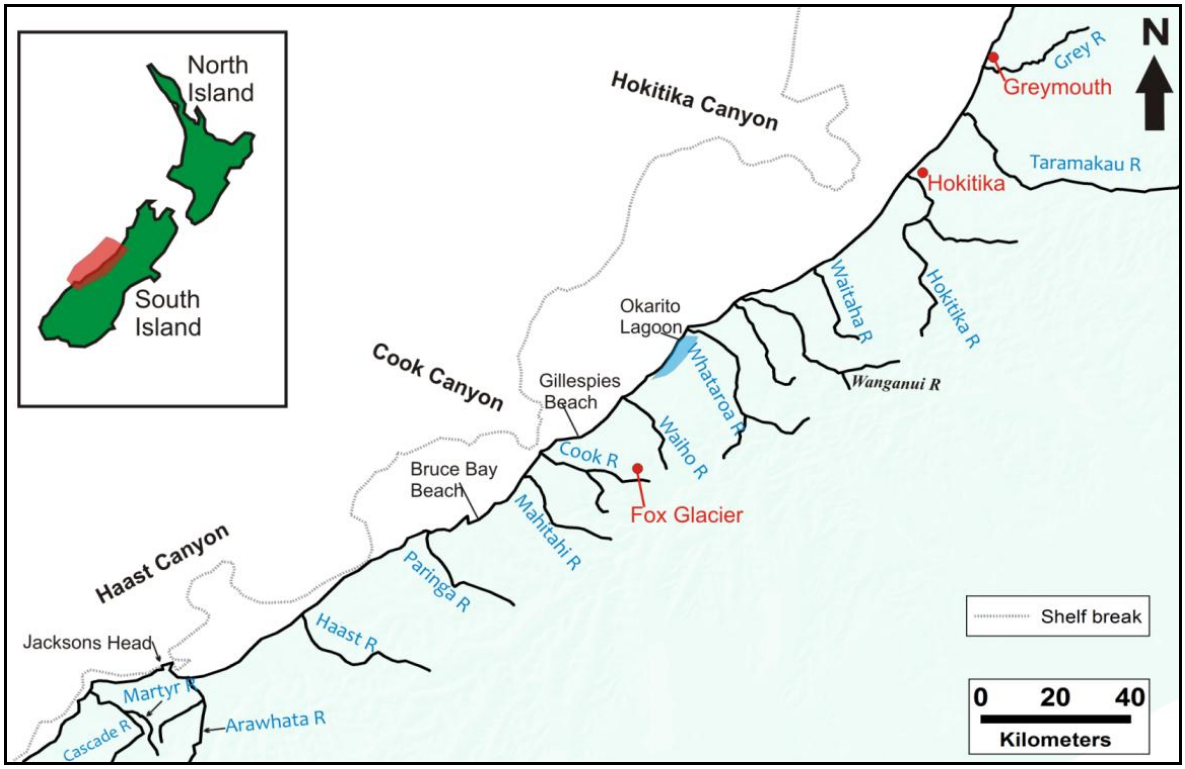

Figure 1-1 The South Westland shelf, canyon heads, and the main rivers considered in this thesis.

1.3 FINE GRAINED SEDIMENTATION ON ACTIVE CONTINENTAL MARGINS

Active continental margin shelves frequently receive large fluvial inputs from high sediment yield mountainous rivers. With ca. 90% of this sediment flux comprised of suspended terrigenous fine sand to clays (Walling & Fang 2003), most of the shelf becomes blanketed in fine sediments except for the energetic inner shelf. The net result is a supply dominated shelf, where terrigenous sedimentation exceeds the rate of accommodation space creation (Suter 2006). Fine grained shelf sediments are very sensitive to oceanic processes; hence their transport and deposition is a complex interplay between wave climate, tides, geostrophic and wind driven currents, and shelf morphology (Walsh & Nittrouer 2009).

1.3.1 Transport Mechanisms

International research into fine grained sediment transport and dispersal has identified three main transport mechanisms relevant for shelf to canyon sedimentation (Suter 2006; Walsh & Nittrouer 2009; Puig et al. 2003 and refernces therein) (Figure 1-2).

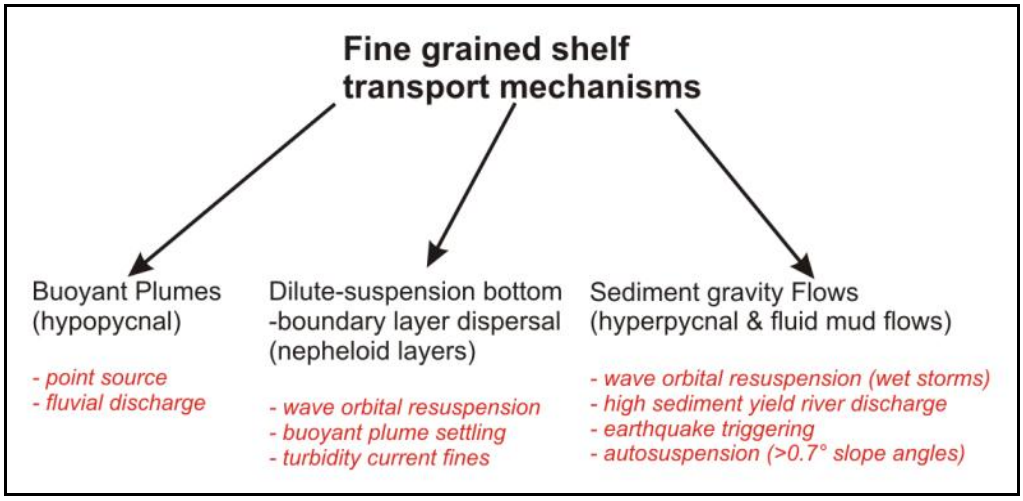

Figure 1-2 Key transport mechanisms on fine grained active continental margin shelves. Different ways each mechanism is generated is given in red text.

1.3.1.2 Wave Orbital Resuspension

Water particles in waves move in circular paths (orbitals) in the direction of wave travel. The diametre of the orbitals decreases with depth until there is no motion, typically at a depth equivalent to half the wavelength (Carter & Heath 1975; Griffin et al. 2008). The passage of shoaling waves on shallow shelves can generate near-bed orbital velocities that can accelerate back and forth at velocities much higher than unidirectional currents (i.e. tidal or wind driven currents) (Porter-smith et al. 2004). Consequently sands can be entrained off the shelf surface and then transported by unidirectional currents operating on the shelf.

1.3.1.3 Buoyant Plume (hypopycnal) Transport

Buoyant surface plumes develop where low salinity water discharges from a point source (river or estuary) on top of higher salinity seawater (Boggs 2001). Suspended sediments are deposited on the shelf as the plume loses momentum and as silt and clay particles flocculate, resulting in deposition mainly on the inner and middle shelves (Walsh & Nittrouer 2009; Boggs 2001). Buoyant plumes are not considered a major transport agent on continental shelves due to this flocculation of particles that restricts dispersal (Walsh & Nittrouer 2009). However, the deposition of buoyant plume fines on the shelf provide a ready source of silt and clay for more significant transport mechanisms.

1.3.1.4 Nepheloid Layers (dilute-suspension bottom-boundary layer dispersal)

This form of transport involves turbid bodies (several 10's of mg/l) of suspended sediment that can extend from the seafloor to several hundred metres above the seafloor (Boggs 2001; Sommerfield et al. 2007). They are generated mainly from the resuspension of fines via storm wave orbitals, but settling particles from buoyant plumes or injections of fines from turbidity currents may also create these dilute suspensions (Sommerfield et al. 2007). Nepheloid layers are denser than ambient seawater but do not sink rapidly. Transport is typically via slow advection offshore or in the direction of various currents operating on the shelf (i.e. tides, wind driven currents, or geostrophic currents) (Walsh & Nittrouer 2009). Nepheloid layers are a major mechanism for off-shelf transport of fine sediments beyond the shelf break, or into canyon heads that incise the shelf (Puig et al. 2003).

1.3.1.5 Sediment Gravity Flows (e.g. hyperpycnal plumes and fluid mud flows).

Sediment gravity flows are a key transport mechanism on many continental shelves and submarine canyon systems. These include hyperpycnal flows, fluid muds flows, and debris flows. Fluid mud flows are near bottom, gravity driven layers of dense sediment suspensions (>10 g/l) that are a major transport process on supply dominated shelves with high fluvial input like the SWCM (Sommerfield et al. 2007; Puig et al. 2004; Walsh & Nittrouer 2009). Fluid mud flows may be generated by the resuspension of fines from storm waves (Puig et al. 2003), or represent an extension of hyperpycnal flows from high yield mountainous river discharge at the coast (Addington et al. 2007). Earthquake triggering of sediment gravity flows (debris flows) are significant for canyon head processes, while autosuspending flows on slopes over 0.7˚ are important on both shelf and canyon heads (Puig et al. 2003). The various forms of sediment gravity flow are critical for the erosion and maintenance of canyon heads which would otherwise become draped in modern fine sediments like the shelves.

1.3.2 Continental Margin Sediment Types

a) ***Terrigenous*** sediment (allochthonous sediment) is land derived sediment supplied to the shelf by rivers, estuaries, and cliff erosion (Carter 1975; Suter 2006). Supply dominated active margin shelves (like the SWCM) are commonly draped in a blanket of modern fine grained terrigenous sediment, with terrigenous sands restricted to the energetic inner shelf (Boggs 2001; Suter 2006).

b) Biogenic sediments are the skeletal remains of benthic and pelagic organisms mainly of calcareous composition. The main skeletal components on the Westland shelf of the South Island are foraminifera tests, molluscs, gastropods, and byozoan fragments (Carter 1975).

c) ***Authigenic sediments*** are those formed in-situ on the sea floor (Carter 1975). Glaucony is a generic term for a mixed group of authigenic hydrated Fe and K-rich clays formed at over 60 m water depth on shelves (Odin & Fullagar 1988). The presence of glaucony is a strong indication of low terrigenous input, and can provide useful information on shelf sedimentation and dispersal patterns. Glaucony is the

predominant authigenic mineral found on the western shelves off New Zealand's South Island (typically < 5% of bulk sediment) (Stoffers, et al. 1984). The distribution and significance of glaucony on the SWCM is discussed in detail in Chapters 3 and 5.

d) ***Relict*** sediments are remnant shelf sediments of a different, earlier shelf environment (Carter 1975; Suter 2006). They may be terrigenous, biogenic or authigenic in origin. Relict terrigenous sediments are usually coarse sands and gravels out of equilibrium with the prevailing hydraulic regime, deposited on the shelf by glacial or fluvial systems during sea level lowstands (Boggs 2001). Exposures of relict sediments on active margin shelves are rare, but where found they can provide valuable information about past shelf history and modern sediment dispersal patterns. Common features of relict shelf sediments include: an unusually coarse grain size for a given location, an association with relict topography (i.e. old channels or gravel ridges), bored and iron stained shells, and rounded quartz pebbles with iron staining (Carter et al. 1985; Carter 1975; Suter 2006).

d) ***Palimpsest*** sediments represent relict sediments reworked by waves and currents and brought into partial or complete equilibrium with the modern hydraulic regime (Boggs 2001).

1.4 PHYSICAL SETTING

1.4.1 Tectonic Setting

The New Zealand landmass is the subaerial portion (~ 10%) of a vast area of submerged continental crust called Zealandia (Mortimer 2004). Until the Late Mesozoic, Zealandia was a small portion of the much larger Gondwana continental landmass. Separation of Zealandia from the Gondwana margin occurred in the Late Cretaceous, and has remained in isolation from other continental blocks ever since (Nathan et al. 1986). The SWCM lies on the Australian plate, close to the active plate boundary between the Australian and Pacific plates where convergence rates are ca. 37 mm/year (Figure 1-3) (Rattenbury et al. 2010). Most of this plate boundary motion is expressed as dextral-reverse slip along the southeast dipping, Alpine Fault (Vry et al. 2008; Rattenbury et al. 2010). This structure has a regional strike of ~055˚and extends for up to 480 km along the South Island (Vry et al. 2008).

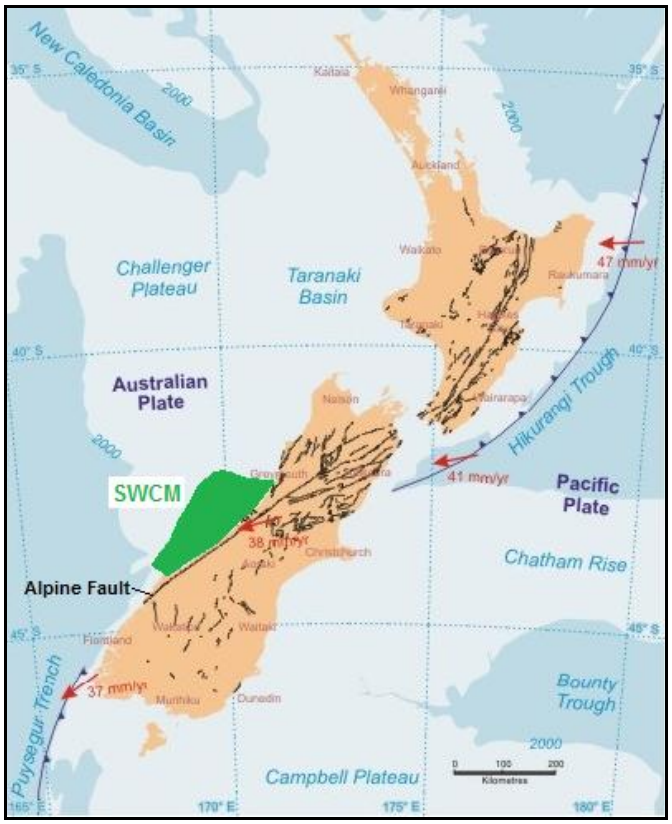

Figure 1-3 The modern plate boundary setting of New Zealand. Green area is approximate region of the South Westland Continental Margin (SWCM). Map modified from Rattenbury et al. (2010)**.**

The collision along this plate boundary is also characterised by the uplift of the Southern Alps, which rise to the southeast of the Alpine Fault and form the Main Divide drainage boundary between the western and eastern sides of the South Island (Rattenbury et al. 2010). Modern uplift rates are high (8 -12 mm/year) with the high elevation of these mountains intercepting moist Tasman sea air masses, resulting in very high precipitation (Vry et al. 2008). The Western Southern Alps between the Alpine Fault and the Main Divide are especially relevant to the SWCM. This is because all rivers discharging to the SWCM have their middle to upper catchments within the Western Southern Alps.

The Western Platform

The SWCM lies on the Western Platform to the west of the South Westland and Cape Foulwind fault zones (Figure 1-4). It is a mainly offshore province comprised of flat lying to gently dipping Cretaceous - Cenozoic strata (up to 4km thick) which thin to the west (Nathan et al. 1986).

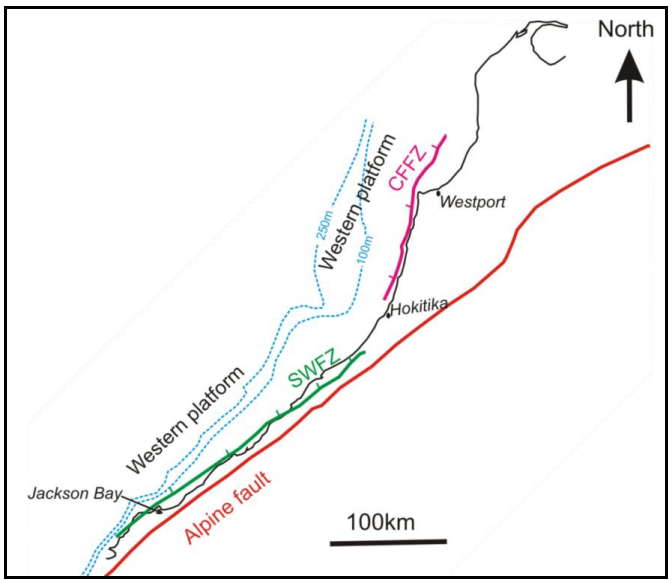

Figure 1-4 The Western Platform on the South Islands West Coast which lies on the downthrown, western side of the Cape Foulwind and South Westland fault zones (CFFZ and SWFZ respectively). Map based on Nathan (1986).

These faults are 'recent', reverse slip structures associated with the modern plate boundary. Both fault zones cut Late Tertiary and Early Quaternary strata, but it is unclear whether Late Quaternary strata have been offset (Norris 1978). These faults are particularly relevant to the SWCM as subsidence on the downthrown sides creates accommodation space for modern shelf sediment deposition.

1.4.2 Coastal Morphology

The coastal morphology of the SWCM is characterised by moraine ridges, fluvio-glacial outwash plains, and sand and gravel beaches. Major coastal embayments are rare, with only the Okarito and Saltwater lagoons found to the north and south of the Whataroa River respectively. These lagoons were originally bays which became enclosed by sand and gravel bars during post glacial sea level rise (Cox & Barrell 2007). Headlands are typically lateral moraine and outwash features often truncated by coastal cliff erosion. Between the Waitaha to Grey rivers, beaches are more common with limited active coastal cliff erosion. South of the Waitaha River towards Bruce Bay, moraines and outwash complexes are more pronounced, perturbing the coastline and forming numerous coastal cliffs (i.e. Cook, Waiho, Whataroa, and Wanganui lateral moraines). Further south more resistant headlands of Cretaceous – Pliocene rocks prevail at Tititira Head and the Jackson Bay area.

1.4.3 Postglacial Deposition on the SWCM

At the end of the Last Glacial Cold Period (LGCP) (ca. 18 ka), a rapid, episodic marine transgression ensued until 6.5 ka when sea levels became relatively stable at the present day level (Carter et al. 1986; Alloway et al. 2007). A modern wedge or prism of mainly fine grained sediment developed as the uppermost layer on the SWCM, termed the Hawea series (Norris 1978). The Hawea Series unconformably

overlies older Quaternary and Tertiary deposits and epitomises shelf sedimentation on the modern SWCM during the present hydraulic regime (Norris 1978). Sedimentation became more focused on the SWCM shelves during the present highstand, with a marked reduction in the export or bypassing of terrestrial sediments to the ocean basins.

Thicknesses of the Hawea prism range from 20 -30 m on the inner shelf to up to 70 m thick ~8km offshore in 50-60 m water depth (Figure 1-5). Beyond the middle shelf the formation thins again to 30-40 m (Norris 1978). Along the SWCM, the geometry of the Hawea prism is variable, but a lenticular profile is the most common (Figure 1-5 A) (Norris 1978).

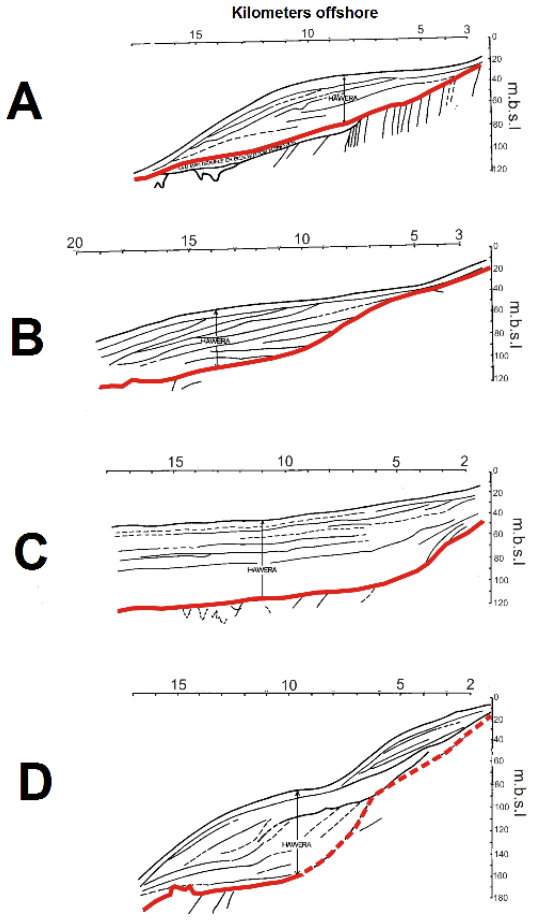

Figure 1-5 Cross sections showing the four types of geometry of the Late Quaternary to Holocene Hawea Series present on the SWCM. Red line represents the unconformity between the Hawea Series and underlying mid to late Quaternary and Tertiary deposits. Type A is the most common profile on the SWCM with a well developed lenticular form. Type C is from the shelf bulge just south of the HCH. Type D is a 'deltaic' complex of overlapping units common offshore from SWCM rivers. Modified from seismic interpretations by Norris (1978).

1.4.4 West Coast Canyon Systems

The Hokitika – Cook Canyon complex is a major feature comprised of four canyons incising the SWCM shelf and slope further offshore (Figure 1-6). The two main active canyons are the Hokitika and Cook Canyons which have been mapped by NIWA's *RV Tangaroa* for 700 km using multibeam swath bathymetry (NIWA Voyage Report 2005). The outer limits of the system have not been reached. The other two canyons terminate at the shelf edge of the Central Shelf and represent abandoned glacial lowstand structures (NIWA Voyage Report 2005). On the continental shelf and slope the canyons typically have a sinuous, ox bowed, and meandering form reflecting low slope gradients and frequent channel avulsion (Figure 1-6) (NIWA Voyage Report 2005). Further offshore beyond the continental slope they become deeply incised, erosive, and straight in form. At the confluence of the Hokitika and Cook Canyons, a waterfall indicates the Cook Canyon has had the most recent 'flow' or the largest recent 'flow'.

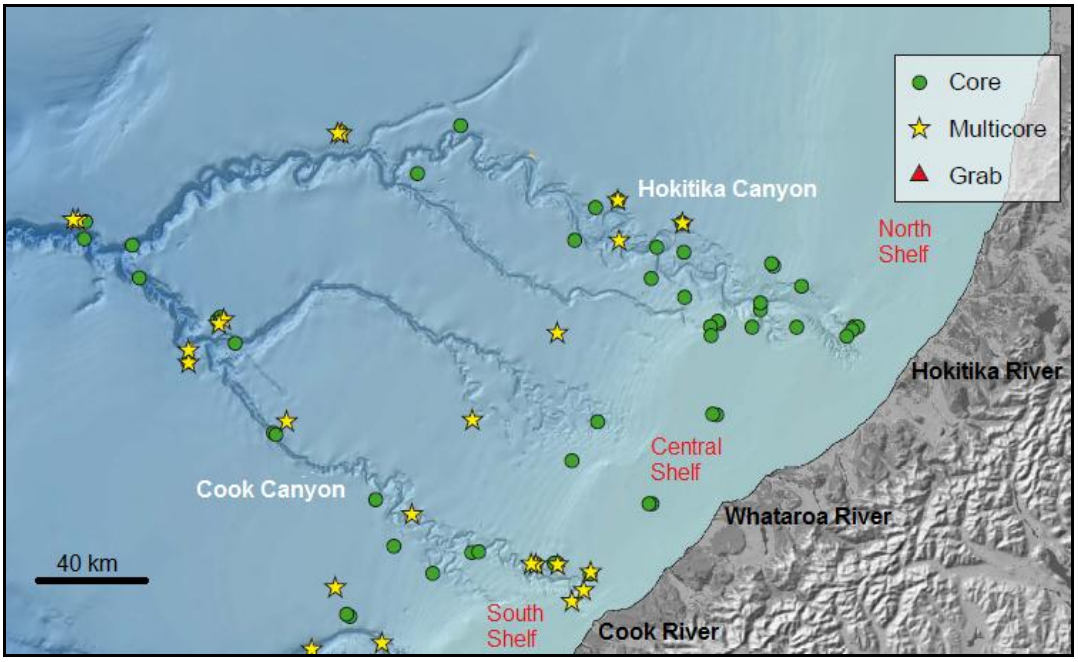

Figure 1-6 Bathymetry of the Hokitika – Cook Canyon complex and the SWCM shelves. Note the change from meandering, ox bowed forms in the upper reaches to deeply incised straight forms further down the system. Image provided by NIWA. Sample locations are from the 2005 *RV Tangaroa* voyage.

The Hokitika and Cook Canyons have actively prograded with post glacial sea level rise (NIWA Voyage Report 2005; Norris 1978). The canyons would have incised the shelf via erosive agents such as turbidity currents (Norris 1978), fed by high volumes of terrigenous material that otherwise blanketed the smooth and featureless SWCM shelves. Strong evidence for recent active incision is seen in the numerous channels which incise Tertiary, lower Quaternary, and Hawea series strata (Norris 1978).

1.5 OCEANOGRAPHY AND CLIMATE

1.5.1 Oceanographic Setting

New Zealand straddles the convergence zone between two major surface currents; the Trade Wind Drift (a sub-tropical southwestern pacific water mass flowing southwest) and the West Wind Drift (a cold sub-antarctic water mass flowing northeast) (Figure 1-7) (Carter 1975). The deflection of the warm Trade Wind Drift against the Eastern Australian coast sets up the southwards flowing East Australian current (Heath 1985). A series of eddies from the East Australian current generates the northeast flowing Tasman Current, a warm, slow moving water mass that approaches New Zealand's West Coast (Carter 1975). The Tasman Current is partially deflected towards the South Island's West coast by the southwest flank of the Challenger Plateau (Figure 1-7) (Heath 1985; Carter 1975; Stanton 1976). Near Jacksons Bay (~ 44˚ S) the Tasman Current bifurcates into the northeast flowing Westland Current and the south flowing Southland Current (Carter 1975; Stanton 1976).

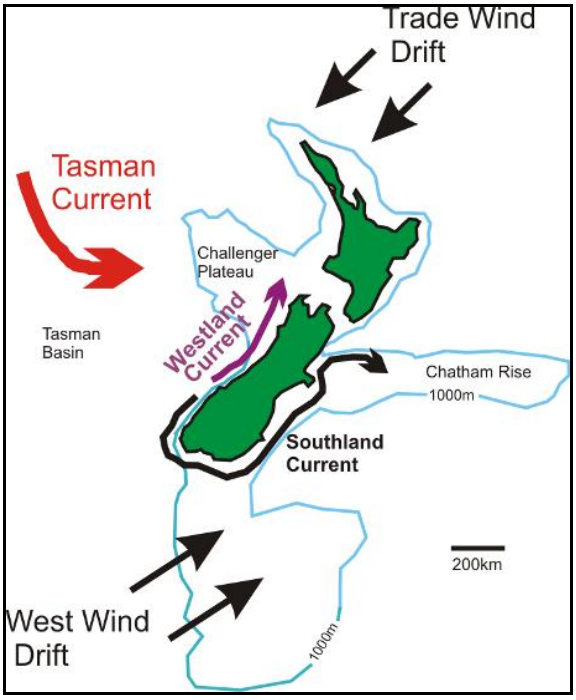

Figure 1-7 Surface circulation in the New Zealand region showing the position of the main regional currents (West Wind drift, Trade Wind drift, and the Tasman Current) and the local surface currents of the South Island. Based on work of Carter (1975) and Heath (1985).

The Westland Current is a variable, mainly northeastward flowing current partially driven by the prevailing southwesterly winds and differences in sea surface elevation (Heath 1985; Stanton 1976). The mean velocity of the Westland current ranges from 1.3 – 9.6 cm/s (Carter & Heath 1975), typically too low to entrain fine sands. During calm periods with little wind, the Westland current can reverse to a weak southwestward coastal flow (Stanton 1976). The Southland Current flows around the bottom of the South Island and up much of the South Island's east coast (Figure 1-7).

Inshore upwelling is well documented on the South Island's West Coast (Stanton 1971; Probert & Swanson 1985). These events are common due to the prevailing southwesterly winds, and can last from 2 – 12 days (Stanton 1971). Southwest of the Hokitika Canyon at Wanganui Bluff upwelling was observed by Bradford (1983). Jets or squirts of inshore SWCM water into the deeper ocean have been observed by (Moore & Murdoch 1993). These low salinity, coastal squirts are often directed by the bathymetry of the Hokitika Canyon well beyond the shelf break. These events were not seasonal or related to upwelling (Moore & Murdoch 1993).

1.5.2 Weather

New Zealand's weather is dominated by the weekly passage of eastward moving anticyclones in the north and low pressure troughs towards the south of the country (Stanton 1998). The West Coast of the South Island is dominated by a strong and persistent westerly circulation for much of the year (Alloway et al. 2007). High rainfall in the SWCM catchments reflects the barrier that the Southern Alps present to these moisture bearing westerly air masses. On South Westland lowlands annual rainfall ranges from 3 400 – 4 900 mm, and reaches up to 14 000 mm at the Main Divide (Henderson & Thompson 1999; Hessell 1982). The prevailing winds on the West Coast are from the southwest, with northwest winds also common. The orographic effect of the Southern Alps on winds can cause the northwesterly winds to deflect and flow north-eastwards down the coast (Stanton 1998). The wind stress from southwesterlies contribute to the mean northward flow of the Westland Current along the South Westland continental shelf (Heath 1982).

1.5.3 Wave Climate

Wind generated swells incident on the SWCM have significant implications for the physical and biological features in the region. New Zealand is exposed to ocean swells dominantly from the southwest and west, and to a lesser extent, storm waves generated north of New Zealand (Heath 1985; Carter 1980). The SWCM is directly exposed to these predominant west and south west swells, which typically range between 1-3 m in height with wave periods between 4 – 8 seconds (Figure 1-8) (Heath 1985; Carter 1980; Gorman et al. 2003). A short period cycle of wave height is common, lasting up to 5 days due to the quasi-rhythmic cycles of the weather (Heath 1985). Twenty year wave hind cast data from offshore of the Wanganui River are presented in Figure 1-8. This hind cast site is centrally located in the SWCM region, and shows a dominance of west-southwest swells ranging between 1 - 4 m in height with a mean monthly significant wave period of 7 - 9 seconds. Wave period and wave height increase slightly during winter months (Figure 1-8 B & Heath 1985).

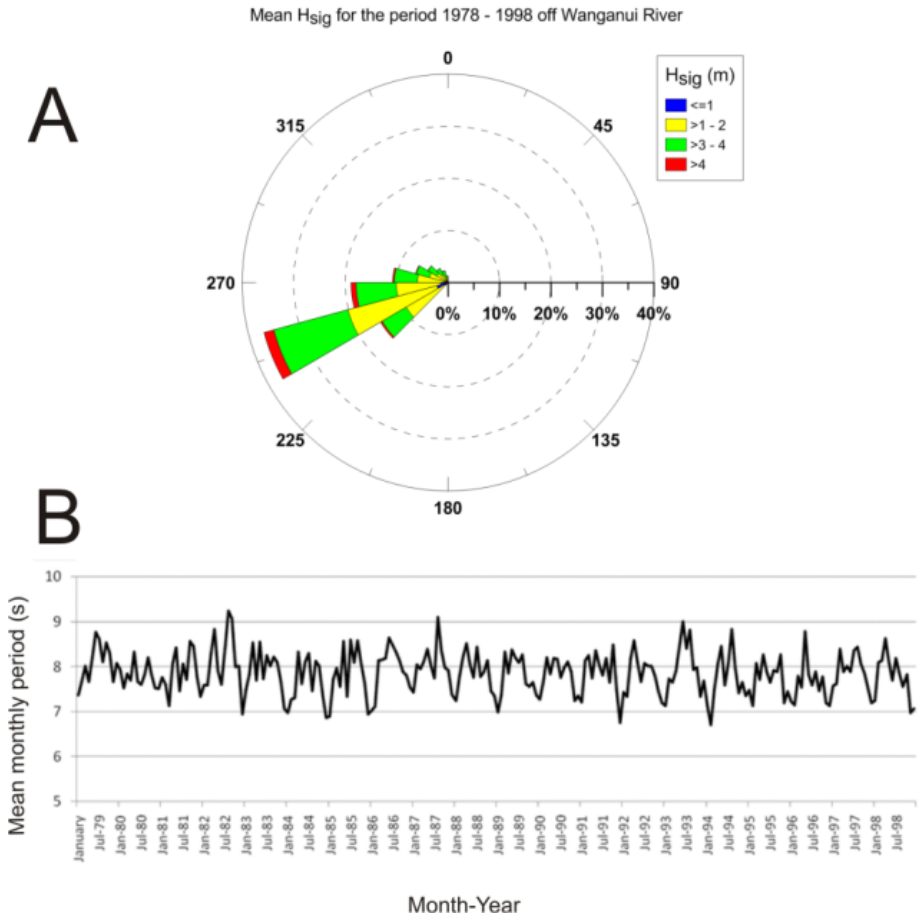

Figure 1-8 Plots of the typical SWCM wind wave climate. Plot A) Mean significant wave height (H_{sig}) and direction swells are from, and plot B) Mean monthly significant wave period (T_{sig}). Graphs are based on 20-year hindcast data from 1978 – 1998 for the Wanaguni River site ('Greens Beach') courtesy of NIWA.

1.5.4 Tides

Tidal currents generated by the gravitational attraction of the moon and sun are typically too weak to entrain sediments on the open West Coast shelves. This is in contrast to more constricted regions such as the Cook Straight between the North and South islands (Heath 1985; Carter 1980). On the SWCM, the M_2 tide has a period of 12.42 hours and is the dominant progressive wave component which is trapped along the Westland continental shelf (Heath 1985). The S2 tide operates mainly as a standing wave with a 12 hour period. Internal tides generated by the vertical movement of density surfaces (in contrast to the movement of the sea surface itself) are a significant feature on the SWCM (Heath 1985). Major variations in water flow and the depth of isopleths during tidal cycles are thought to create these strong internal tides which can influence sediment movement and nutrient mixing (Heath 1985). The Hokitika and Cook Canyons may exert some control on the pattern of tidal currents on the SWCM, but little research has been undertaken to date to investigate this. In other canyon systems internal tides can be an order of magnitude more energetic than on the surrounding shelves (i.e. Monterey Canyon in Kunze et al. 2002).

1.6 PREVIOUS WORK ON THE WESTLAND SHELF

The extent of previous studies on modern shelf sediments on the SWCM are displayed in Figure 1-9. An early study by Carter (1980) assessing the iron sand (ilmenite + magnetite) content of western North and South Island shelf sediments included a broad assessment of surface textures in the SWCM. Later studies by Stoffers et al. (1984) and Probert & Swanson (1985) provided more focus on the South Island's West Coast shelf, concentrating on modern sediment composition (geochemistry and mineralogy) and textures respectively between the Whataroa and Karamea Rivers (Figure 1-9). Apart from Carter (1980), the focus has been on the modern shelf and slope sediments north of the Whataroa River, encompassing the northern half of the Central Shelf, the Hokitika Canyon Head (HCH), and the North Shelf regions considered in this study.

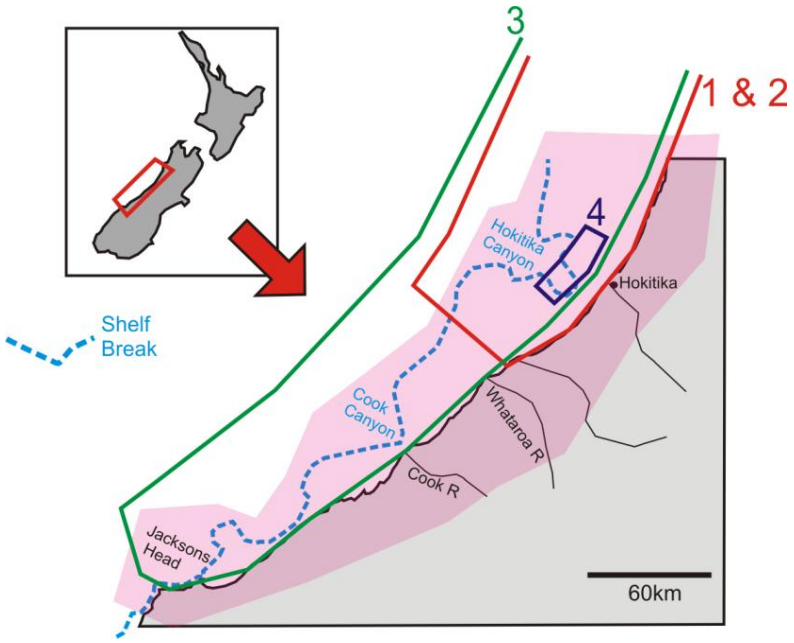

Figure 1-9 Locations of previous work in the SWCM region. Pink area is the continental shelf and catchments considered in this study. 1 & 2 = Stoffers et al. (1984) and Probert & Swanson (1985), 3 = Carter (1980), 4 = The 'Harvester Prospect' from Price (1983) and Youngson (2006).

1.6.1 Textures

All these previous studies were primarily focused on the modern fine grained shelf sediments. This highlighted a lack of work on the surface textures within and near the Hokitika Canyon Head (HCH) and their implications for shelf – canyon interactions. An exception to this is the 'Harvester Prospect', a small, several km^2 area in 70 -100 m water depth just north of the HCH where extensive exploration for placer gold was conducted in the 1980s by CRA Exploration Ltd (CRA) (Figure 1-9) (Price 1983; Youngson 2006). Here, coarser gravelly muds were encountered in dredging and vibrocoring programs, providing the first extensive documentation of coarse sediments on the otherwise fine grained SWCM shelves.

Perpendicular to shore and along shelf textural patterns are generally well defined, especially in the northern half of the SWCM (Figure 1-10) (Carter 1980; Probert & Swanson 1985; Stoffers et al. 1984). The typical perpendicular to shore trend includes an inner shelf (< c.50 m depth) of fine sand grading into muddy sand, sandy mud, and muds on the middle shelf (c.50 – c.150 m depth). An important difference in outer shelf textures north and south of the HCH was recognized by Probert & Swanson (1985) and Stoffers et al. (1984). Sediments were shown to coarsen to muddy sands Northwards from the HCH, but not to the south offshore from the Whataroa River. During the exploration for placer gold deposits by CRA, modern terrigenous fine grained sediments were encountered in most exploration licences except the Harvester Prospect (Price 1983), highlighting the pervasive blanket of modern sediment on the West Coast shelf.

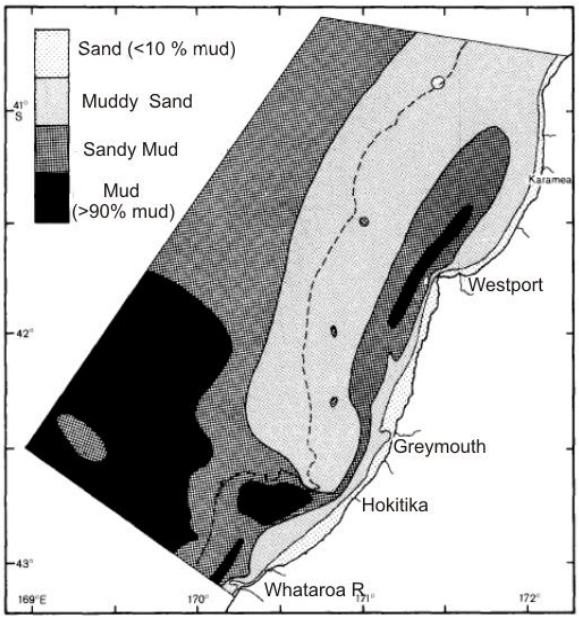

Figure 1-10 Surface sediment textures north of the Whataroa River from Probert & Swanson (1985). Muddy sands were found to dominate the outer shelf north of the HCH while sandy muds were more typical to the south.

The gravelly muds in the Harvester Prospect are interpreted as relict Pliestocene deposits, formed in a submarine fan environment rather than a beach environemnt given the chaotic, poorly sorted, muddy texture in the prospect (Youngson 2006).

1.6.2 Sediment Supply

In Probert & Swanson (1985) and Stoffers et al. (1984) the distribution of shelf textures were considered a function (in order of importance) shelf sediment supply, shelf width, and possibly upwelling. Fluvial supply to the shelf increases greatly south of Greymouth, resulting in larger volumes of fine suspended sediment delivered to the shelf. Probert & Swanson (1985) consider this increase in supsended load causes the lack of outer shelf coarsening south of the HCH and a general decrease in mean grain size.

Sedimentation rates between 1.1 – 2.3 mm/year on the Westland shelves were estimated by Probert & Swanson (1985) which the authors note will be significantly higher south of the Whataroa River.

The dominant shelf sediment transport direction on the Westland shelves is to the northeast (Carter & Heath 1975; Carter 1980). The ability of tides and the Westland Current to entrain and transport modern shelf material alone is widely considered insufficient (Carter & Heath 1975; Carter 1980; Probert & Swanson 1985). However, in combination with resuspension via storm waves and wind drift during southwesterly storms, transport of shelf surface sediments is far more efficient.

The absence of a modern sediment cover in the Harvester Prospect provides the first indication the Hokitika Canyons are influencing SWCM textures. A possible explanation from Price (1983) is that the export of northward propagating modern terrigenous sediments into the canyon creates an area of no deposition in the lee of the canyon head.

The supply of fluvial sediment to the West Coast shelves is notably high by global standards. South Westland catchments are characterised by steep, densely spaced, high energy mixed bedrock and gravel rivers flowing to the SWCM due to maximum uplift rates (up to12mm/year), high erosion rates, and high precipitation (up to 15 m/year) in the Western Southern Alps (Korup et al. 2005).

In addition, the short length of SWCM rivers and the lack of coastal embayments to trap fluvial sediments contributes to the large terrigenous input to the shelves (Carter 1975). A strong north to south increase in sediment load is evident on the South Islands West Coast. The suspended sediment yield (Mt/year) between the Taramakau and Arawhata rivers (i.e. the SWCM) is an order of magnitude higher than all catchments combined further north (i.e. Grey to Karamea Rivers) (Table 1-1).

Table 1-1 Catchment area and suspended sediment yields for selected Westland rivers. Note the general increase in yields towards the south within the South Westland rivers.

River	Catchment Area (km^2) [a]	Suspended Sediment Yield (Mt/year) [b]
Aorere	709	0.11
Karamea	1242	0.15
Mokihinui	752	0.29
Buller	6484	2.7
North Westland Total	**-**	**6.5**
Grey	3948	2.1
Taramakau	1005	2.2
Hokitika	1069	6.2
Waitaha	-	2.8
Whataroa	-	4.8
Waiho	-	3.4
Haast	1349	5.9
Arawhata	-	7.2
South Westland Total	**-**	**62**

[a]Catchment area from (Griffiths & Glasby 1985)
[b]Suspended sediment yield from (Hicks & Shankar 2003)

Within the SWCM catchments, southern rivers such as the Haast and Arawhata rivers supply 2-3 Mt/year more suspended sediment than river further north such as the Waitaha, Whataroa, and Taramakau rivers. An exception is the Hokitika River which is the second largest supplier of suspended sediments after the Arawhata River in the SWCM catchments.

1.6.3 Mineralogy

Studies of shelf sediment mineralogy on the South Islands West Coast are limited but generally reflect the primary control of metamorphic followed by plutonic outcrops in West Coast catchments (Carter 1975; Stoffers et al. 1984). North of the Whataroa River, quartz, feldspar, and rock fragments dominate the inner shelf, while mica-chlorite silts and illite-chlorite clays dominate the middle shelves (Stoffers et al. 1984). The presence of authigenic minerals (especially glaucony) 30 km north of the HCH were highlighted by Stoffers et al. (1984) with up to three varieties present. Heavy minerals in Westland beach and river sediments have received considerable attention, primarily due to the potential economic resource they may present. Diverse heavy mineral suites occur in SWCM beaches and rivers, with broad regional trends in mineral species and chemistry evident (Bradley et al. 2002; Bradley 1977; Chew 1981; Ooi 1982). For example, Bradley et al. (2002) and Chew (1981) identified spikes in the Cr content of detrital magnetites in beaches linked to catchments with ultramafic outcrops. The Cr content of magnetites is applied in this study to investigate dispersal and provenance of shelf sediments on the SWCM (Chapter 4).

1.6.4 Geochemistry

Stoffers et al. (1984) provide the only study of shelf sediment geochemistry of Westland sediments. Bulk composition is governed by Ca and Si, depending on the levels of biological productivity and terrigenous supply to the shelf. North of the Whataroa River, the inner shelf is high in silica, with a high SiO_2/Al_2O_3 ratio and low Ca (Stoffers,et al. 1984). Higher Fe, Al, K, and Mg on the middle shelf is common due to the mica and chlorite rich muds and sandy muds.

1.7 SUMMARY OF THE SWCM SETTING AND PREVIOUS WORK

The SWCM environment is the product of a complex and dynamic interplay between geological, geomorphic, climatic and oceanographic factors. The Westland current is the major surface current influencing SWCM sedimentation. The low velocity of the Westland Current (and tidal currents) is insufficient to entrain shelf sediments on the SWCM alone. However, in combination with predominantly southwesterly storm waves and winds, maximum transport rates of SWCM shelf sediments to the northeast can occur.

The SWCM shelves are characterised by a smooth, featureless bathymetry and a decrease in shelf width towards the south. The Hokitika-Cook Canyon complex is a major feature in the region comprised of two

active channels that incise the SWCM shelves (HCH and CCH) and extend offshore, meandering across the continental slope, and eventually becoming deeply incised and less sinuous further offshore.

Previous work on the Westland shelves has included the northern half of the SWCM, identifying well developed across and along shelf textural patterns. Fines sands to muds dominate the modern SWCM sediments, with coarse terrigenous material only found in a small area just north of the HCH. Fluvial supply to the SWCM is very high due to high rates of erosion, uplift, and precipitation, and numerous, steep, short, rivers which rarely encounter coastal embayments. The net result is a supply dominated shelf where fine sediments (fine sand to mud) blanket the shelf with relict sediments rare except in association with the HCH.

1.8 METHODS

1.8.1 Surface Samples

Surface samples from the SWCM shelf and canyon heads are the main sample type used in this thesis. Access was kindly granted to the NIWA sediment archives, from which a total of 46 surface samples were selected. These surface sediments were originally collected on a series of NIWA (formerly known as the New Zealand Oceanographic Institute) voyages off the South Islands West Coast between the 1960s and 1980s. Over half the samples used in this thesis were collected on the June 1975 voyage.

The selected surface samples range from 14m to 454m water depth from both the shelf and canyon heads (Figure 1-11). Details of the location and depth of these surface samples is provided in Appendix A2. The samples mostly lie on a series of transects perpendicular to the shelf (Figure 1-11). These transects are referred to throughout this study and provide a useful means to assess shelf sediment trends and make regional comparisons. The sample locations cover the inner shelf (0-50 m), middle shelf (50 -150 m) outer shelf (150 – 220m) and the upper slope (>220 m depth) of the SWCM. Canyon head samples were more abundant in the Hokitika Canyon Head (HCH), with few samples collected from the Cook Canyon Head (CCH) during NIWA voyages.

1.8.2 Canyon Cores

Several kasten cores from the Hokitika – Cook Canyon complex were available for use from NIWA to investigate glacial – interglacial fluctuations in sediment texture and composition. These cores were collected by NIWA's research vessel the *RV Tangaroa* during the 'West coast canyons 1' 2005 voyage (NIWA Voyage Report 2005). Three cores from the Hokitika Canyon north levee (TAN 0513-15, 19, and 21) were the main cores used in this thesis (Figure 1-11). Five samples from each of the 2-3 metre long cores were obtained. The depth intervals of these samples and other core details are provided in Appendix A4.

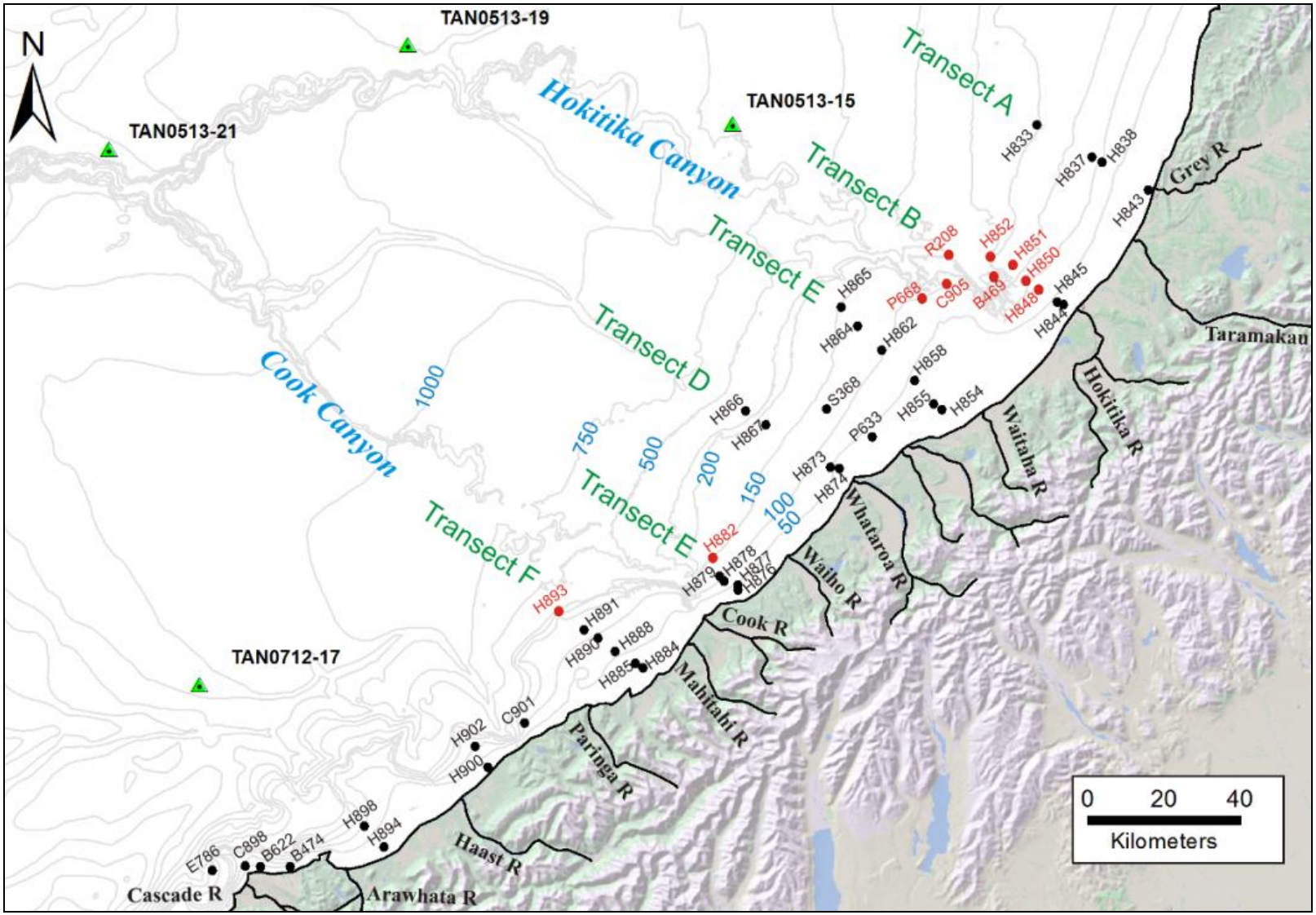

Figure 1-11 The location of surface grab samples (dots) and kasten cores (triangles) on the South Westland Continental Margin and Hokitika – Cook Canyon system. Black dots are shelf surface samples, red dots are surface samples from canyon heads.

1.8.3 Beach & River Sampling

To investigate the dispersal and provenance of SWCM shelf sediments, a selection of beach and river samples were collected over 2 field trips (October 2010 and February 2011). The locations of these samples are displayed in (Figure 1-12), with detailed descriptions of sampling localities provided in Appendix A3.

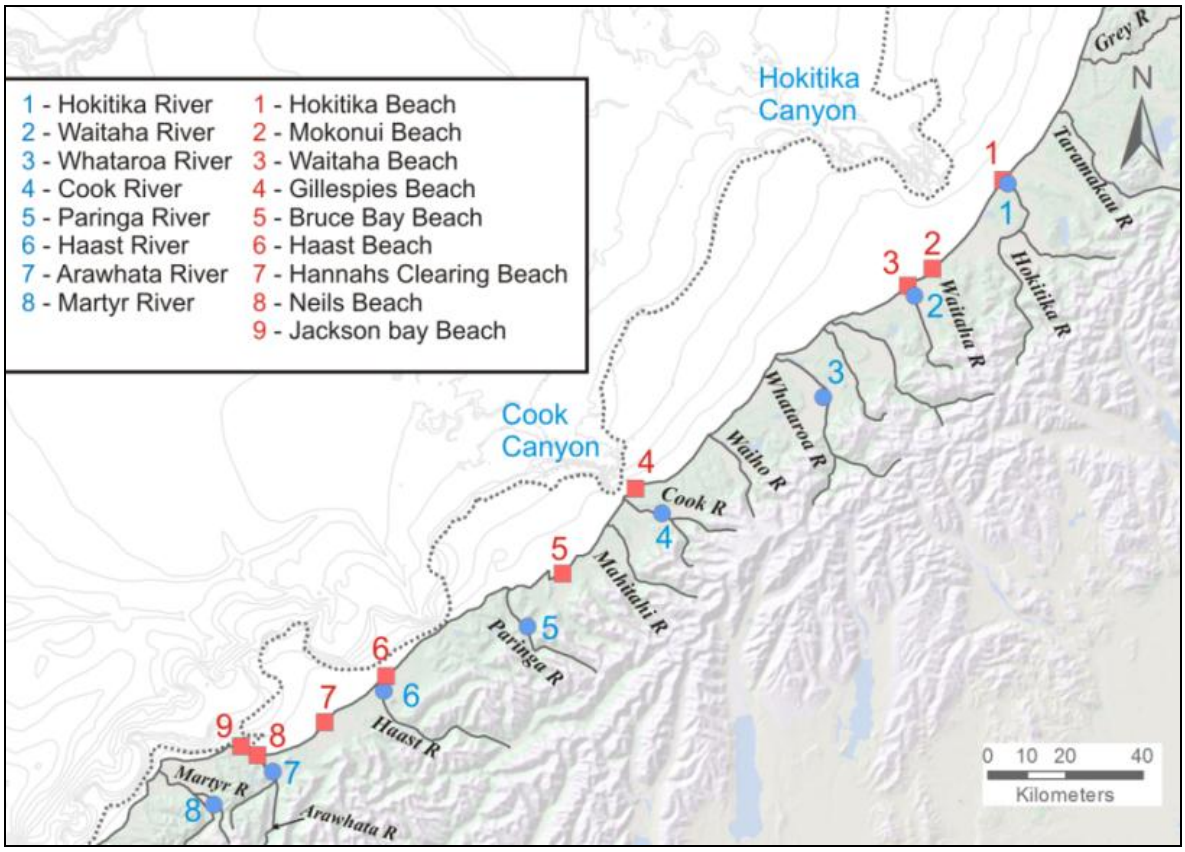

Figure 1-12 Beach and river sample locations from the SWCM region used in this study. Red squares are beach samples, blue circle are river sample sites.

Two to three samples were obtained at each locality with an emphasis during sample collection to obtain enough from the sand to clay fractions to be comparable to the SWCM shelf samples. River samples were taken from the active river channel (mainly longitudinal bars) and beach samples from the active swash zone (Figure 1-13). One of the samples collected from each location was selected at random (out of 2-3 samples) and used for all subsequent laboratory techniques.

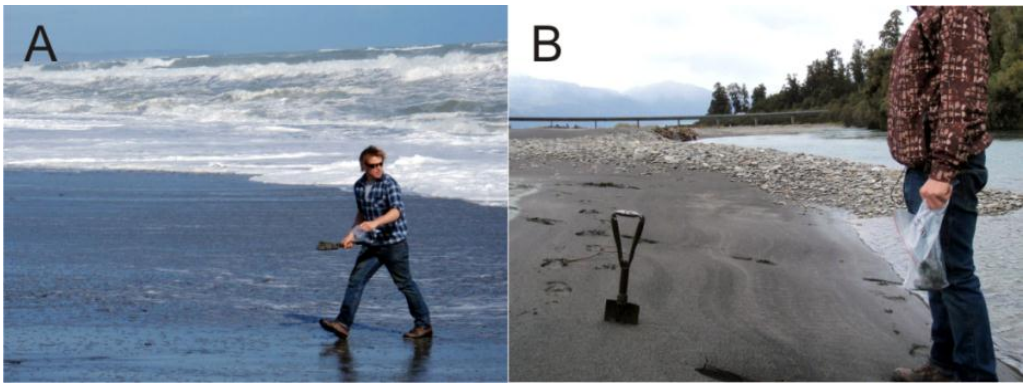

Figure 1-13 A) Beach sampling at Ross Beach. B) Sampling of an active bar on the Waitaha River

1.8.4 Wave Hind Casts and Wave Orbitals

To study the effects of wave orbitals on SWCM surface sediments, a 20-year wave hind cast was obtained from NIWA (Richard Gorman). The wave generation model WAM (WAve Model) provides data on the generation and propagation of deep water waves incident on the New Zealand coastline. Treatment of this data is discussed in more detail in Chapter 2 and Appendix G.

1.8.5 GIS DATA

All GIS work was conducted using ESRI's ArcGIS® suite of software. A 75 by 75 cell Digital Elevation Model (DEM) provided by NIWA is employed throughout this thesis in maps to depict bathymetry and hillshade imagery of the SWCM. In hillshades, a Z – factor of 5 was used to highlight particular features.

1.8.6 Analytical Techniques

A variety of laboratory techniques were used to analyse the texture and composition of shelf, canyon, river and beach samples from the SWCM. These techniques are summarised below but are discussed in more detail in the relevant chapters and appendices. An inventory of sample treatments is provided in Appendix A5.

Grain size analysis: Grain size analysis was conducted on all shelf and canyon head surface samples, as well as the canyon core samples. A combination of laser sizing (NIWA, Wellington) and sieving (University of Canterbury) allowed all grain size fractions to be assessed. Detailed methods are provided in Chapter 2 with results provided in Appendix B.

Mineralogy: All samples except those from the canyon kasten cores were examined for siliciclastic, skeletal and authigenic components by a combination of thin section petrography and inspection of the loose sand samples under a binocular microscope. Mineralogical results are provided in Appendix C. Heavy mineral separation was via the heavy liquid separation technique (LST), results and methods for this are provided in Appendix C10 and C11. The bulk mineralogy of selected samples was analysed by the XRD method (Appendix C7 to C9).

Bulk geochemistry: A selection of samples from each SWCM environment was analysed for bulk geochemistry via the XRF method at the University of Canterbury (Appendix E). Carbonate content was determined at NIWA (Wellington) via the gasometric quantitative analysis after acidification method (Appendix D).

Microprobe analysis of detrital magnetite composition: Detrital magnetites were used in provenance and shelf dispersal analysis. Grains were separated by a magnet from the separated heavy mineral fraction and mounted on epoxy stubs for microprobe analysis conducted at Victoria University, Wellington. Details on these methods and results are provided in Chapter 4 and Appendix F.

1.9 AIMS OF THIS WORK

The aims of this thesis include:

- To investigate the texture and composition of modern shelf and canyon surface sediments on the SWCM to permit interpretations of depositional and transport mechanisms.
- Develop an understanding of the extent and nature of modern day shelf to canyon head interactions on the SWCM.
- Employ the use of wave hind cast data and bathymetry to predict the frequency of wave orbital stirring of SWCM surface sediments.
- Create an overall picture of modern sedimentation on the SWCM from textural, compositional, geomorphic, and wave hind cast data.
- Investigate the dispersal and provenance of modern SWCM surface sediments from bulk sediment geochemistry and microprobe data on detrital magnetites. Are there regional trends in catchment geology which can be traced on the SWCM shelf?
- Study the texture and composition of Hokitika Canyon core stratigraphy to detect glacial-interglacial cycling effects on the flux and composition of terrigeous sediments. To accompany this, the effects of sea level change on the SWCM shelves and the connectivity between fluvial and canyon systems are assessed.

1.10 THESIS STRUCTURE

This thesis is organised into 7 chapters. These include: 1) Introduction; 2) Sediment textures and Geomorphology of the SWCM; 3) Dispersal and Provenance of SWCM Detrital sediments; 4) Provenance of Detrital Magnetites; 5) Geochemistry, Provenance, and Relict Sediments; 6) Late Quaternary History and Core Stratigraphy; 7) Sedimentary facies, Interpretations, and Conclusions.

Chapter 1 introduces the region and the focus of this thesis. Chapter 2 examines the surfaces textures and geomorphology of SWCM shelves and canyon heads as well as the frequency of sediment stirring from

wave orbitals. Chapters 3 to 6 are focused on the composition of SWCM surface sediments and the implications for dispersal and provenance. Most chapters contain a discussion and interpretation section specific to the results presented in that chapter. Chapter 7 is the final chapter which draws all the interpretations and conclusions together to provide a picture of modern and Late Quaternary sedimentation on the SWCM and the role of submarine canyons in the region.

CHAPTER 2 : SEDIMENT TEXTURES AND GEOMORPHOLOGY OF THE SWCM

Shelf sediment textures are commonly used to interpret shelf processes and provide a means to compare different shelf types (Boggs 2001). Surface sediments on the SWCM vary perpendicular to and along shore due to the dynamic interactions between oceanography, shelf and canyon morphology, and sediment supply (Carter 1975; Probert & Swanson 1985; Stoffers et al. 1984). In this thesis, textural analyses of surface sediments are dominantly from depths above the shelf break. The shelf break is approximately defined using bathymetric contours and slope angle analysis of digital elevation data (Section 2.2). Surface sediment textures are characterised for each of the SWCM shelves, and the intervening Hokitika and Cook Canyon Heads. The geomorphology of the SWCM shelves and canyon heads are examined using a digital elevation model (DEM) provided by NIWA. In addition, a 20 year wave hindcast is used to approximate the frequency of sediment stirring by ocean swells on the SWCM. The use of this DEM and wave hindcast data will assist with interpretations of possible transport mechanisms and pathways on the SWCM.

Transects E, F and the Haast to Cascade Shelf samples provide the opportunity to characterize shelf textures south of the Whataroa River, beyond the southern limits of previous work on the SWCM (Probert & Swanson 1985; Stoffers et al. 1984). In addition, transect B and to lesser extent, transect E will provide insight into surface textures near and within the Hokitika and Cook Canyon Heads (HCH and CHC respectively).

2.1 METHODS

2.1.1 Laser Sizing

All marine samples finer than 1600 µm were analyzed using a Beckman Coulter LS13 320 Laser Diffraction Particle Analyzer located at NIWA (Wellington). A 3-5 g split from each bulk sample was taken using a riffle splitter. Each sample was dry sieved first using a 1600 µm mesh to separate any coarser sediments that could potentially jam in the sample chamber. This coarser fraction was analysed in a separate analysis (Section 2.1.1.2). Each split was soaked in calgon for at least 12 hours and subjected to 10 seconds in a sonic bath to disaggregate any clumped silts and clays before adding to the laser sizer. The machine settings included a pump speed of 1275 rpm and a 90 second run length. Grain size results were processed using GRADISTAT Version 4.0 (Blott & Pye 2001) with the silt - clay boundary at 4µm. Calculated mean grain size, sorting, and skew were derived from GRADISTAT using geometric graphical calculations detailed in Blott & Pye (2001). All grainsize analyses are provided in Appendix B. Grain size

classes used are displayed in Figure 2-1 and sorting values (in µm) and corresponding classifications are provided in Table 2-1.

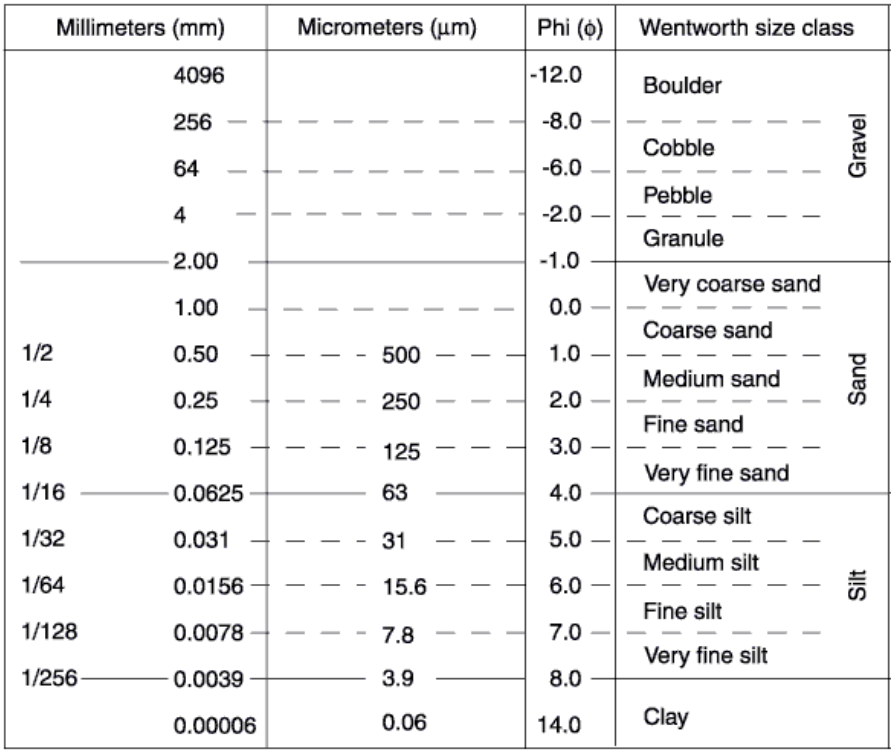

Figure 2-1 The Wentworth grain size classes and corresponding phi and mm boundaries for these classes. Figure modified from Boggs(2001).

Table 2-1 Sorting values in microns (µm) and corresponding sorting classifications.

SORTING	STANDARD DEVIATION (µm)
Very well sorted	< 1.2
Well sorted	1.27 – 1.41
Moderately well sorted	1.41 – 1.62
Moderately sorted	1.62 – 2.00
Poorly sorted	2.00 – 4.00
Very poorly sorted	4.00 – 16.00
Extremely poorly sorted	> 16.00

2.1.2 Coarse Fraction Analysis by Sieving (> 1600 µm)

The aim of sieving was to determine the proportion of sediment above the upper limit of the laser sizer used (1600 µm) for all marine samples. Depending on the amount of bulk sample available, a split ranging from 10 – 25 g was weighed (dry weight) prior to wet sieving using 1600 µm and 2000 µm sieves. The retained fractions were then dried at 60°C for at least 12 hours and reweighed. The percentages of material between 1600 - 2000 µm and above 2000 µm (gravel) were then recorded as a weight percentage (Appendix B3).

Laser sizer data (<1600 µm) and sieving data (>1600 µm) were combined to calculate the gravel, sand, and mud percentages. The gravel percentage from sieving was normalized with the sand and mud

percentages from laser sizing to achieve this. Mean grain size, sorting, and skew are based solely on laser sizing data. The mean grain size and sorting will be undervalued for the 9 samples (of 46) containing gravel sized clasts because of this. However, most of these 9 samples contain less than 3 % gravel, and the omission of the gravel fraction for mean grain size and sorting calculations will not be dramatic.

2.2 SWCM GEOMORPHOLOGY & BATHYMETRY

Shelf geometry is an important factor contributing to the nature of sediment transport and dispersal (Walsh & Nittrouer 2003). The general bathymetry of the SWCM is displayed in Figures 2-2 and 2-3. A slope analysis using ArcGIS helped to define the approximate position of the shelf break for the SWCM region (Figure 2-3 B). The shelf break was traced where the slope angle became consistently greater than 1 degree. Bathymetric profiles of the shelf transects are provided in Figure 2-4. The geomorphology of the Hokitika and Cook Canyon Heads and their relationship with the surrounding shelves are examined in this section also in Figure 2-6 & Figure 2-7. To improve clarity in the canyon heads, bathymetric contours are reduced to just the 100 m isobaths.

2.2.1 General Bathymetry

The shelves of the SWCM are dominantly shallow, seaward dipping shelves trending northeast to southwest along the Westland coast (Figure 2-2 and Figure 2-3). They are generally smooth and featureless due to an extensive blanket of Late Quaternary sediments (Norris 1978). The only major interruptions are the Hokitika and Cook Canyons which incise the shelf to within ~ 10 and ~2-3 km of the Westland coastline respectively. A more detailed discussion of the bathymetry and geomorphology of the canyon heads is found in section 2.2.2.

To characterise regional changes in surface sediment texture and composition in the SWCM, the canyon heads and intercanyon shelves are divided into the sub-regions displayed in Figure 2-2. The North Shelf extends northeast for 80 km from the HCH to an arbitrary northern limit just north of the Grey River. It includes transect A and the inner shelf of transect B, covering an area of ca. 3 820 km^2. This region has the widest shelf width of the SWCM shelves (~60 km in the north) with the shelf break near the 250 m isobath (Figure 2-2). The Westland shelf continues to broaden north of the SWCM towards the Karamea Bight. Just north of the HCH, a more irregular shelf surface occurs is present in Figure 2-3 A & B.

The Central Shelf is a large intercanyon shelf (ca. 3835 km^2) between the HCH and CCH with a shelf break typically at 200 m depth (Figure 2-2). In the north, a prominent seaward bulge, first noted by Norris (1978), is clearly defined by the 50 m isobath just south of the HCH (Figure 2-2).The western tip of this bulge lies ~26km offshore, while to either side the 50 m isobath is 10-12 km from the coast. This bulge was probably a low lying, blunt headland during sea level low stands Norris (1978). To the south the Central Shelf continues to narrow towards the CCH. A tributary canyon causes a landward inflection of

the shelf break in the middle of the Central Shelf (Figure 2-3 A). This tributary does not incise the Central Shelf, and eventually feeds into the Cook Canyon system to the south.

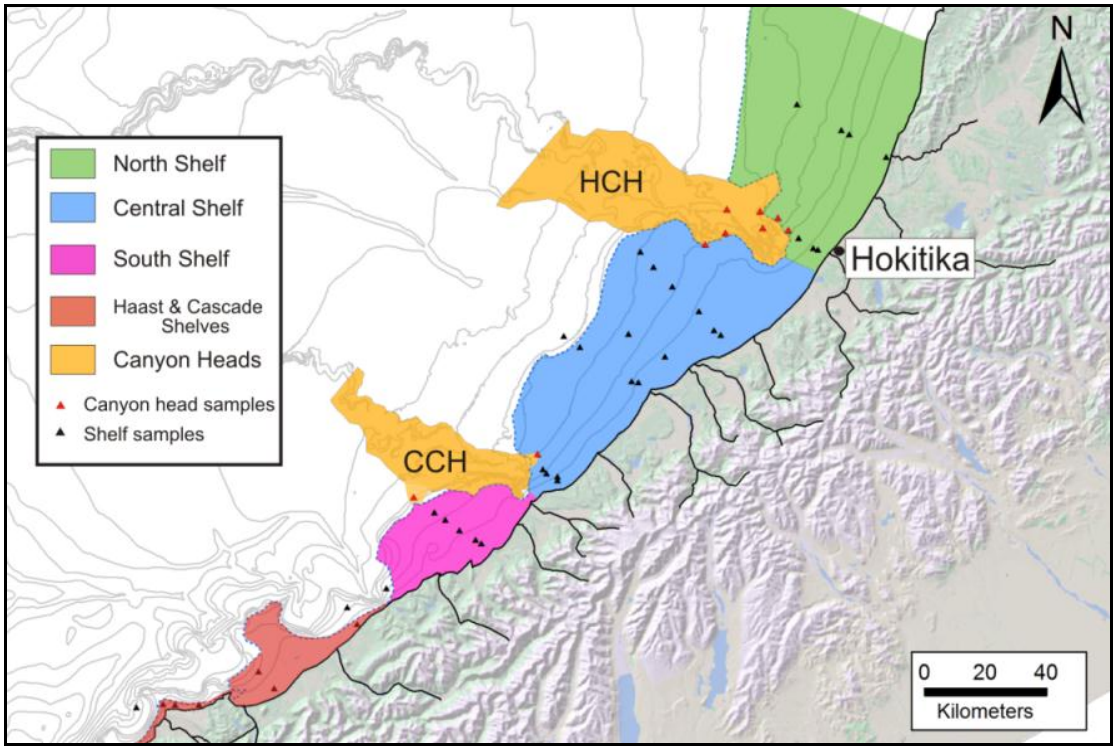

Figure 2-2 Shelf and canyon sub-regions of the SWCM discussed in this study. The seaward limit of each region if defined by the shelf break. HCH = Hokitika Canyon Head, CCH= Cook Canyon Head.

The South Shelf forms an intercanyon shelf between the CCH and the Haast canyon complex (Figure 2-3). The shelf break varies from 15 – 25 km offshore and lies near the 150 m isobath. The South Shelf is smaller than the Central Shelf with an area of ca. 1040 km^2. A tributary canyon of the CCH incises the upper slope near the outer most sample on transect F (H893).

A narrower, more irregular shelf characterizes the Haast and Cascade shelves. The Haast Shelf is bounded by the deeply incised Haast canyon head to the north and west, and by Jacksons Head to the south. The shelf break ranges from ~ 2 to 25 km offshore. Between the Haast and Arawhata rivers this shelf is widest. Shelf slopes are steep, ranging from 0.5 – 4 degrees (Figure 2-3 B). South of Jacksons Head a very narrow and steep shelf comprises the Cascade Shelf. The southern limit of the Cascade Shelf is an arbitrary boundary 30 km south of the Cascade River mouth.

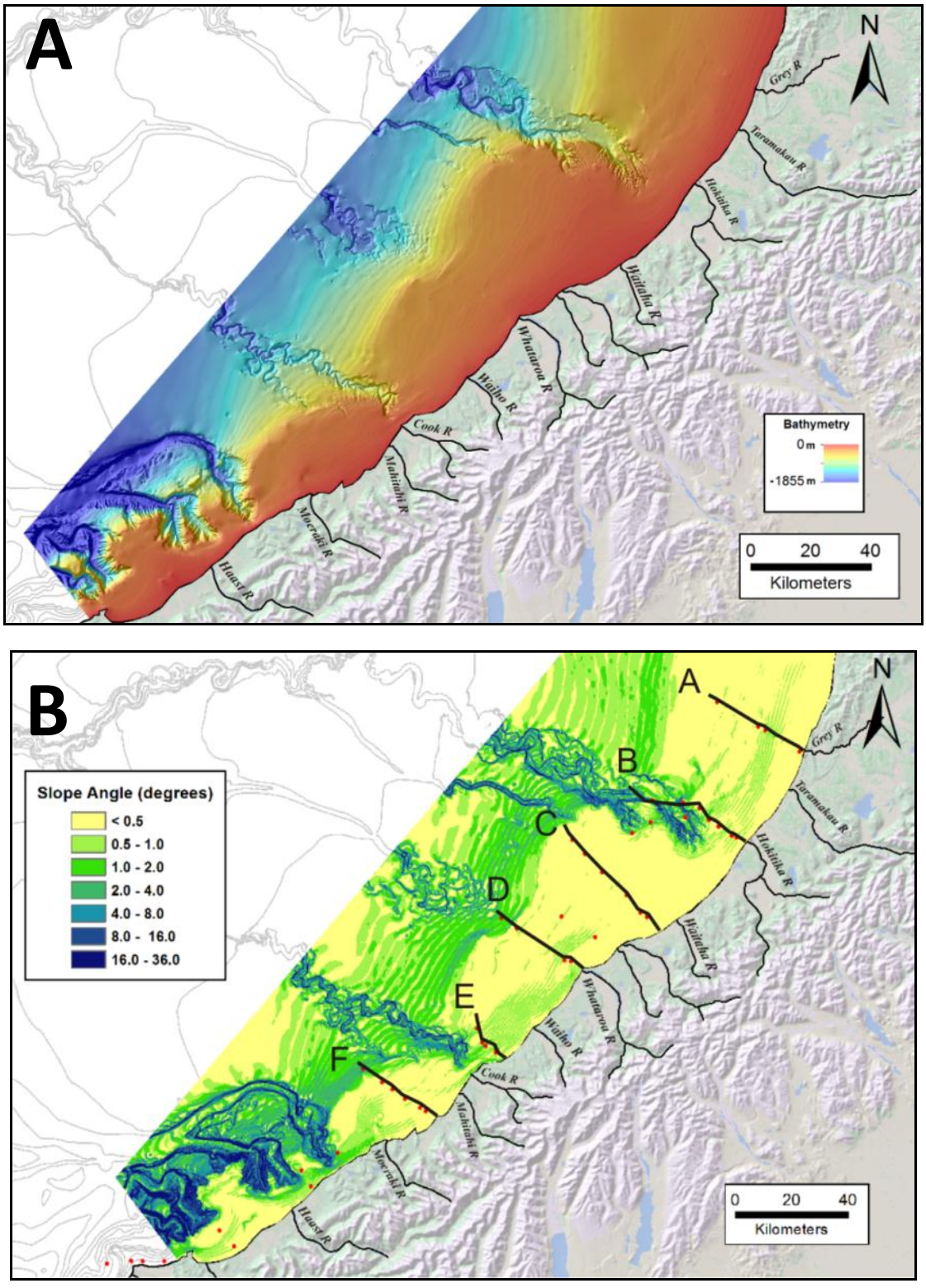

Figure 2-3 Bathymetric maps of the SWCM. A) Combined hillshade and DEM of the SWCM and B) Slope analysis of the SWCM and the location of transect section lines displayed in Figure 2-4.

2.2.2 Shelf Transect Profiles

The depth and distance offshore the shelf break is traversed by the the transects is summarised in table 2-2. Surface profiles of the transects are depicted in Figure 2-4. Transect A occurs on a relatively wide section of shelf offshore from Greymouth (North Shelf). The shelf slope is largely gentle with the shelf break occurring ca. 54 km offshore in ~255m water depth (Figure 2-4 A). This is the widest shelf transect included in this study. All samples occur on the shelf portion of this transect.

Table 2-2 Summary of the depth and distance offshore the shelf break occurs in the sub-regions of the SWCM. The position of the shelf break was picked where the slope angle was consistently greater than 1˚ in the slope analysis displayed in Figure 2-3 B.

Transect - Shelf	Approximate depth of shelf-slope break (m)	Distance offshore of shelf-slope break (km)
A - North Shelf	255	54
B - North Shelf/HCH	180	25
C - Central Shelf	164	52
D - Central Shelf	180	29
E - Central Shelf/CCH	230	25
F - South Shelf	150	27

Transect B is located offshore from Hokitika and includes a section of the inner North Shelf and the HCH. The shelf slope is gentle for the inner 10 - 15 km but becomes increasingly variable beyond 15 km offshore due to the influence of the HCH. Due to this influence, the shelf break occurs close to shore (~25 km). A dog leg in transect B was required to include a canyon floor sample (R208) that lies at the base of the south rim (Figure 2-4 B). Beyond the shelf break bathymetry drops steeply by >100 m into the upper reaches of the HCH. The outer most sample on the canyon floor occurs at 450 m depth (R208).

In transect C on the Central Shelf (Figure 2-4 C), shelf slopes are very gentle until the shelf break 52 km offshore. This transect lies on the shelf 'bulge' just south of the HCH. Beyond the shelf break the bathymetry drops away steeply. All samples are located on the shelf portion in transect C.

Further south on the Central Shelf, transect D slopes are slightly steeper than in transect C (Figure 2-4 D). The shelf break is ~ 29 km offshore in 180 m water depth with a relatively steep upper slope beyond this. Three samples occur on the shelf while one sample, H866, is located on the upper slope.

Transect E occurs in the narrower south end of the Central Shelf, just north of where the CCH incises the shelf (Figure 2-4 E). Shelf slopes are relatively steep, with the shelf break ca. 25 km offshore at 230 m depth. An abrupt break in slope occurs ~ 8 km offshore between H878 and H879. The outer most sample (H882) occurs close to the northeastern most reaches of the CCH where irregular bathymetry is present.

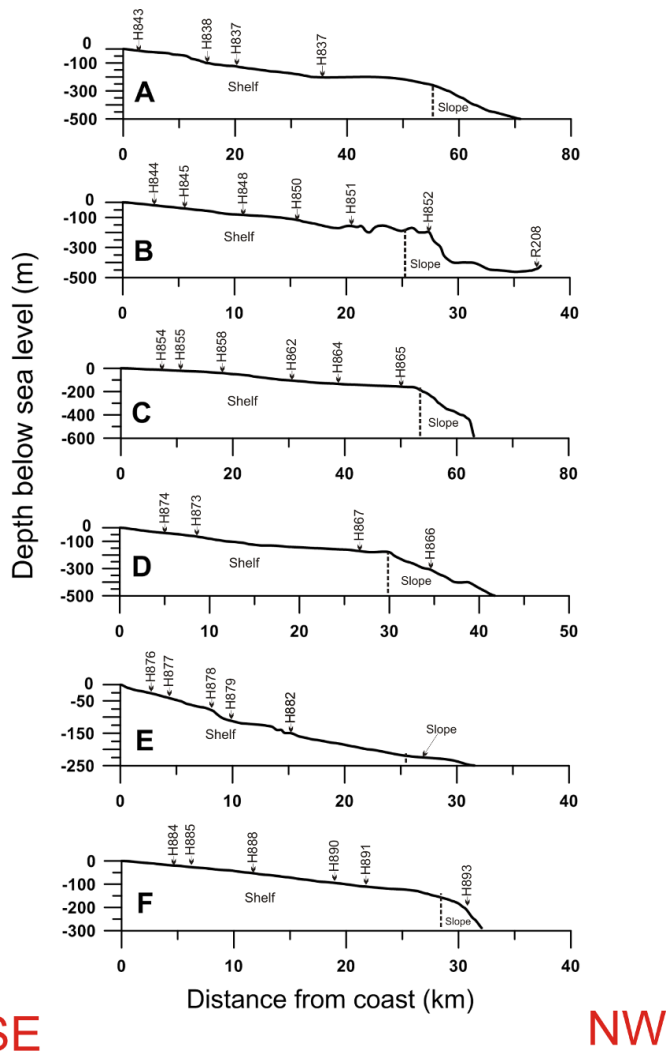

Figure 2-4 Surface profiles for transects A to F in the SWCM. Location of transect lines are displayed in Figure 2-3 B.

Transect F is the only transect on the South Shelf (Figure 2-4 F). A gentle shelf slope dips offshore until a shelf break ~ 27 km offshore in 150 m of water. The slope drops away steeply into what appears to be a tributary branch of the main CCH to the north.

2.2.3 Canyon Head Geomorphology

Hokitika Canyon Head (HCH)

The Hokitika Canyon is a major feature incising the SWCM and separating the North and Central Shelf regions. In cross section the HCH is characterised by an elevated south rim (100-200 m higher than the north rim) and an abrupt, steep decent to the canyon floor (Figure 2-5). Down canyon, increasing levels of incision and the very steep southwest canyon wall becomes more pronounced (Figure 2-5). The maximum landward extent of incision is ca. 10km offshore from the Hokitika coastline. The width of the main

canyon is ca. 13 km near the 50 m isobath, widening to ca. 20 km at 150-200 m depth. The general trend of the HCH is northwest – southeast, perpendicular to the trend of the SWCM.

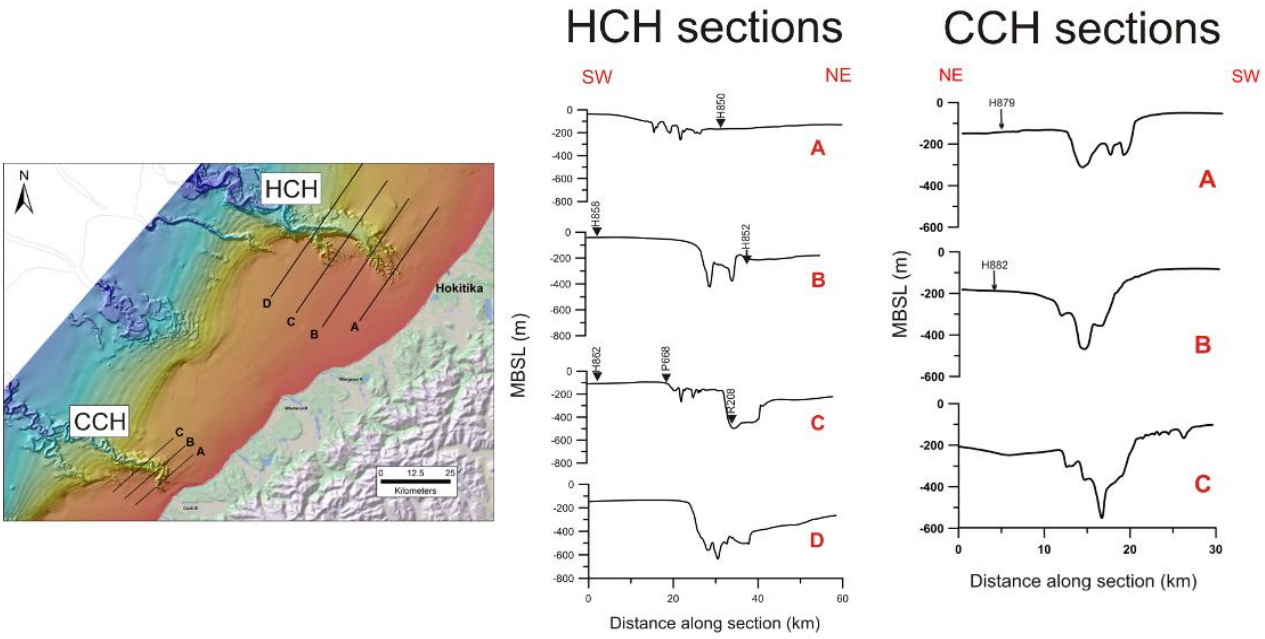

Figure 2-5 Cross sections of the Hokitika (HCH) and Cook (CCH) canyons and the approximate location of sediment sample sites. Note the different spacing of sections. MBSL = metres below sea level.

An eastern canyon system incises to within 2-3km of the 50m isobath and contains 3-4 main channels with both sinuous and straight forms (Figure 2-6). A smaller lobe ~12 km west-southwest of the larger eastern system incises the shelf to the 100 m isobath (sample site P668).

Along the south and east rims of the HCH, extensive gully systems are developed (Figure 2-6). These range from 1-4 km long, are spaced 0.3 – 1 km apart, and incise into the smooth Central Shelf. An abrupt escarpment trending west-southwest for 13 km runs along the south HCH rim between the two lobes (Figure 2-5 and Figure 2-6). A broad, smooth area occurs between the two lobes and terminates sharply at the south rim escarpment above sample site R208 (Figure 2-6).

On the north HCH rim, the geomorphology differs considerably from the south and eastern HCH rims. Most notably, the north HCH lacks any major gully networks (Figure 2-6). About 5-6 km north of sample site R208, a major cuspate escarpment may be an abandoned canyon channel. To the west of this, irregular features may also be relict in origin. The Central Shelf to the south of the HCH is smooth and featureless compared to the North Shelf adjacent to the HCH rim.

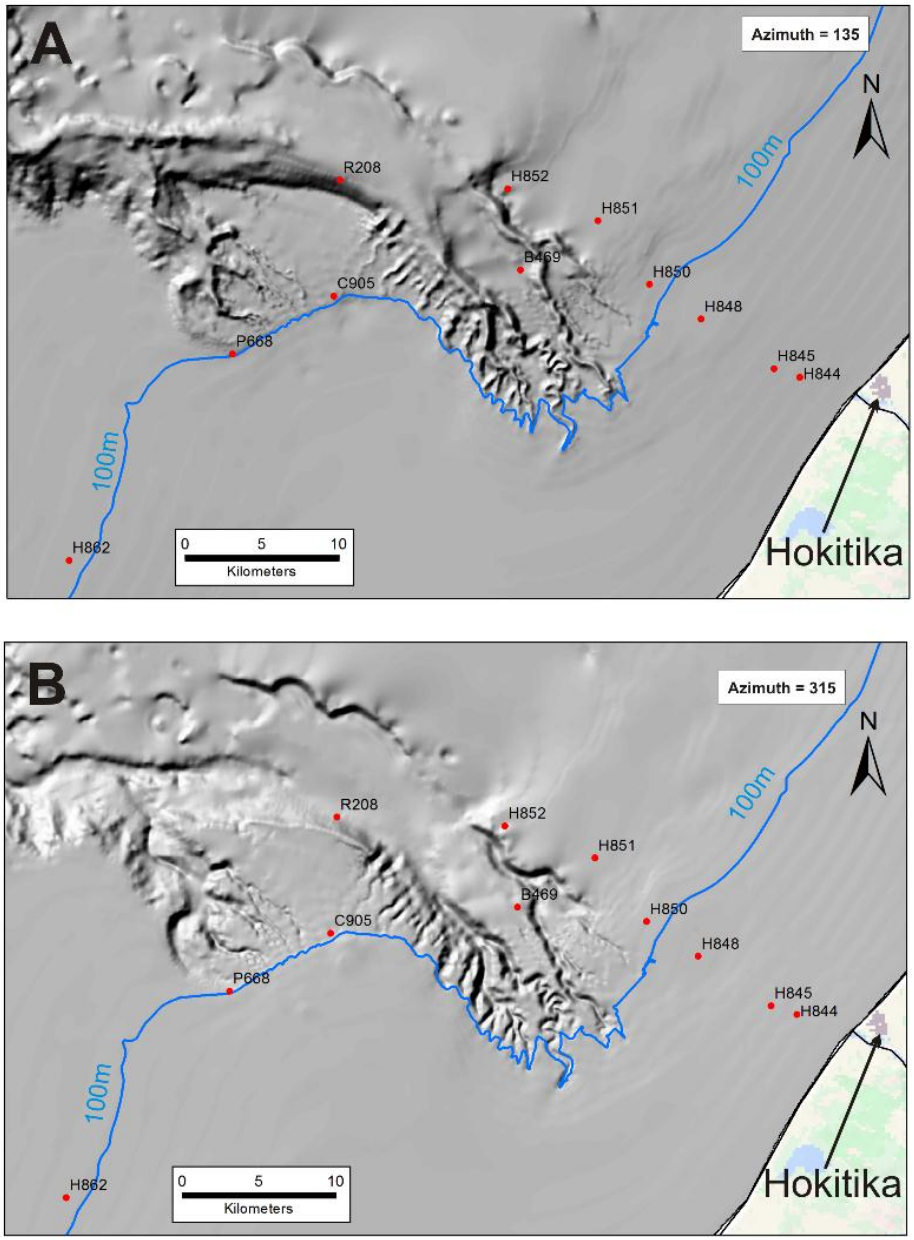

Figure 2-6 Hill shade images of the Hokitika Canyon Head with hill shade illumination from A) the Southeast and B) the Northwest. Note: a Z-factor of 5 was used in these images.

Cook Canyon Head (CCH)

The CCH is dominated by a deeply incised, sinuous channel which intersects the 50 m isobath. The eastern most incision of the CCH terminates ~3km offshore from the Cook River mouth (Figure 2-7). Cross sections show the very incised nature of the CCH (Figure 2-5). At the eastern most incision of the CCH, the shelf drops abruptly to the canyon floor by over 100 m. Along the south flank of the CCH a major escarpment runs for 12-13 km west of the main canyon channel.

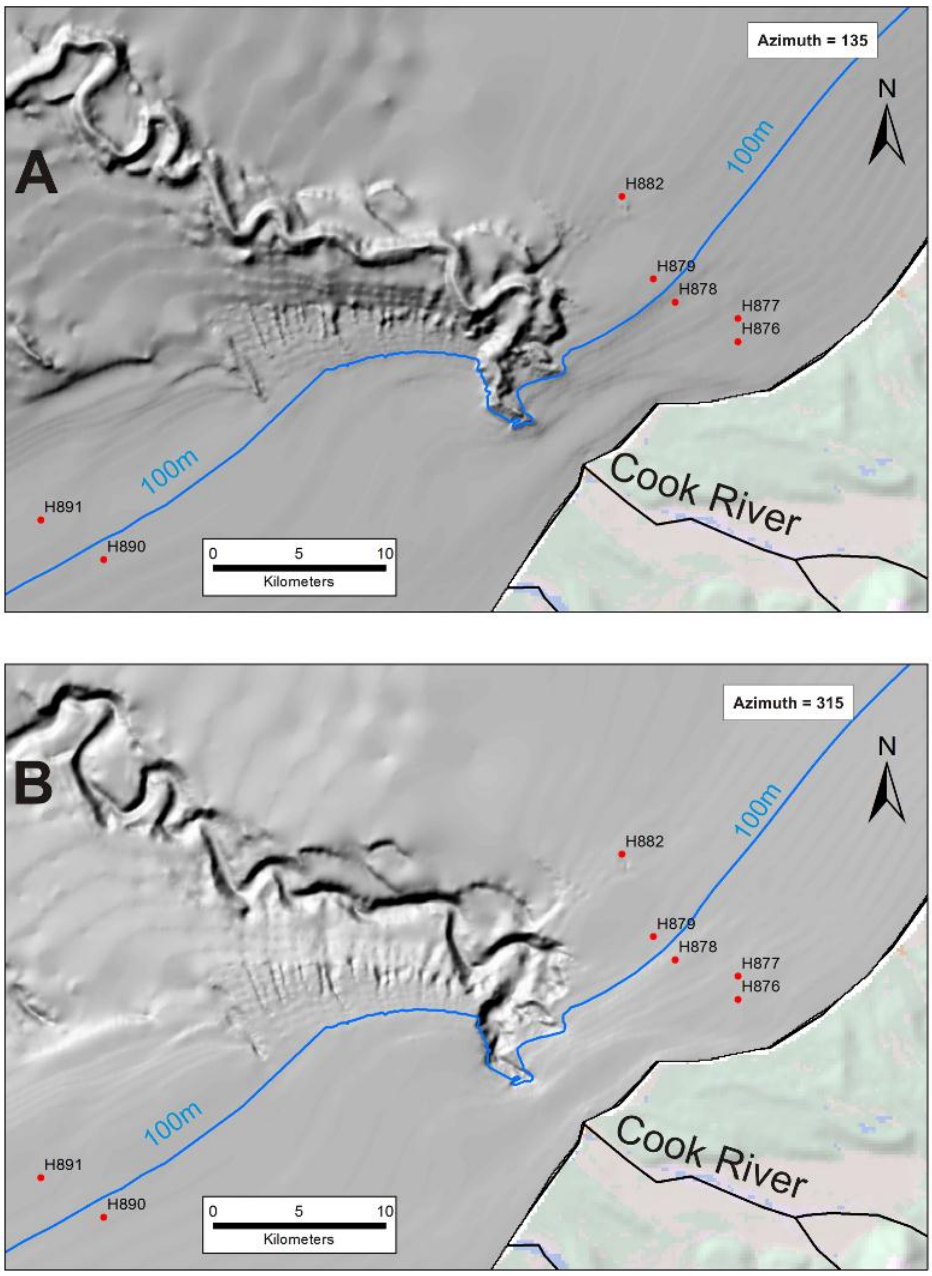

Figure 2-7 Hill shade images of the Cook Canyon Head with hill shade illumination from A) the south east and B) the north west. Note: a Z-factor of 5 was used in these images.

The slope leading towards this escarpment is incised by numerous northwest to southeast trending gullies up to 6 km long with an average spacing of 1km (Figure 2-7). The north rim shows no evidence for these gully systems. Unique to the north CCH rim is a series of curved, stepped escarpments up to 5km long and up to 5km north of the Cook Canyon rim. This contrasts with the smooth bathymetry of the South Shelf leading towards the CCH south rim. An irregular, possibly relict feature occurs in the vicinity of sample H882, 8km from the active CCH channel.

Canyon head surface sediments included in this study occur in both north and south rim environments. This provides the opportunity to investigate the relationships between these contrasting environments and the implications for shelf – canyon interactions on the SWCM. This includes five sample sites on the north rim and 3 on the south rim of the HCH (Figure 1-11). Only H882 occurs on the north rim of the CCH.

2.3 SHELF GRAIN SIZE ANALYSIS

2.3.1 Mean Grain Size of SWCM Sediments

Over the shelf and canyon head regions the mean grain size of bottom sediments range from 16.0 μm (medium silt) to 170.0 μm (fine sand). The most common mean grain size is medium silt (36%) followed closely by very fine sand (34 %), coarse silt (19%), and fine sand (11%).

Shelves

Across each shelf region a typical mean grain size pattern occurs. Inshore regions (< 50 m depth) are very fine sand to fine sand, the middle shelf (50 – 150 m) is medium silt, and medium to coarse silt is typical on the outer shelf (150 – 220 m) (Figure 2-8 & Figure 2-9). The distance between these grain size boundaries are broad on the North and Central shelves compared to the South Shelf, where a more condensed width of mean grain size contours exists.

Generally, inner shelf sediments range between 59 and 148 μm, with an average of 102 μm (very fine sand) (Appendix B1). An along shore trend from North to South is evident, with inner shelf mean grain size coarsening south of the CCH (Figure 2-9). Here, sediment over 125 μm becomes common, especially shallower than 30 m depth. At middle shelf depths (50-150 m), the mean grain size is generally medium silt, ranging from 16 – 62μm and averaging 27 μm. Middle shelf sediments have the least variation between samples, plotting as a tight group in Figure 2-8 and suggests a relatively uniform mud belt at these depths.

At outer shelf to upper slope depths (> 150 m) mean grain size ranges between 24 – 43 μm with an average of 29 μm, slightly higher than the middle shelf samples. At outer shelf depths coarse silts occur on the shelf transects (Transect A, C, D and E) while coarser sediments (very fine – fine sands) are found in the canyon heads (Transects B and E).

The sand – silt boundary (63 μm) generally follows the 50 m isobath on the SWCM (Figure 2-9). On the North, Central and South shelves, the 63 μm contour lies 5 – 15 km offshore. At the CCH, this contour follows closest to the coast than anywhere in the SWCM (3-4 km offshore). Progressing from the inner shelf, the coarse silt – medium silt boundary (32 μm) often coincides with the 100 m isobath. Beyond this boundary on the North and South shelves, medium silts continue offshore until a reversal to coarse silt occurs between 150 – 160 metres and 125 metres depth respectively. This outer shelf coarsening defines a

rough < 32 µm belt ranging from 20 km width on the North Shelf, to 10 km width on the South Shelf (Figure 2-9). On the Central Shelf this reversal to coarse silts was not observed.

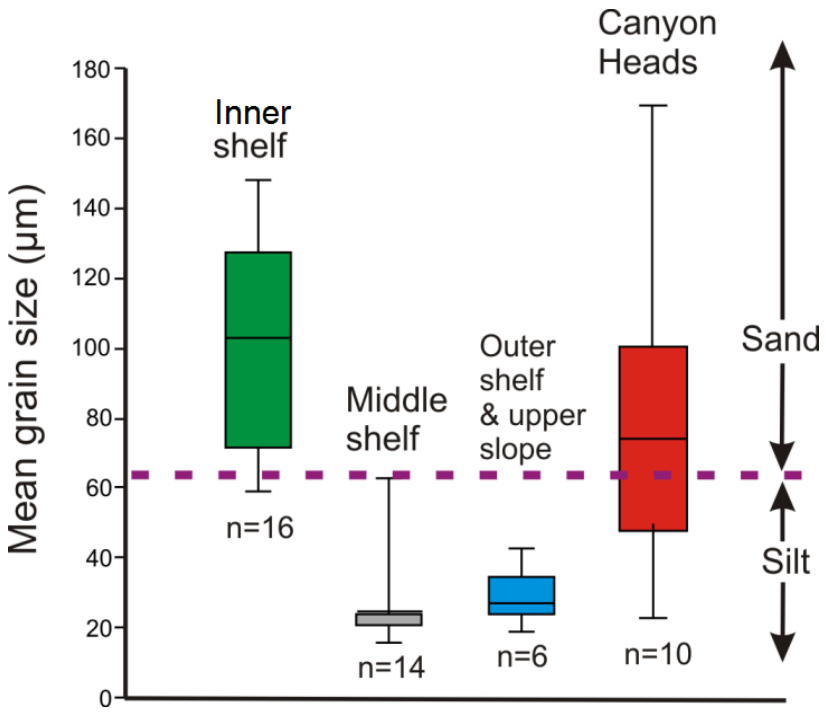

Figure 2-8 Box plot of mean grain size for all SWCM surface sediments. Values are for all sediments < 1600 µm analysed by laser sizing.

Canyon heads

The coarsest mean grain size occurs in the canyon heads with an average of 75 µm (Figure 2-8 & Figure 2-9). In the HCH, surface sediments are very fine sand at middle shelf depths (48 -110 µm),coarsening to fine sand (170 µm) at 200 m water depth. The coarsest mean grain size (170 µm) occurs at 198 m depth, 26 km offshore on the north rim of the HCH. North rim sediments are far coarser than the south rim sediments (averages of 94 µm and 31 µm respectively). Several kilometres north of the CCH (Transect E), the outer shelf mean grain size is coarser (very fine sand) than the surrounding shelves. The HCH and CCH perturb the typical SWCM mean grain size patterns with unusually coarse sediments (>63 µm and >125 µm) well into middle shelf depths (Figure 2-9).

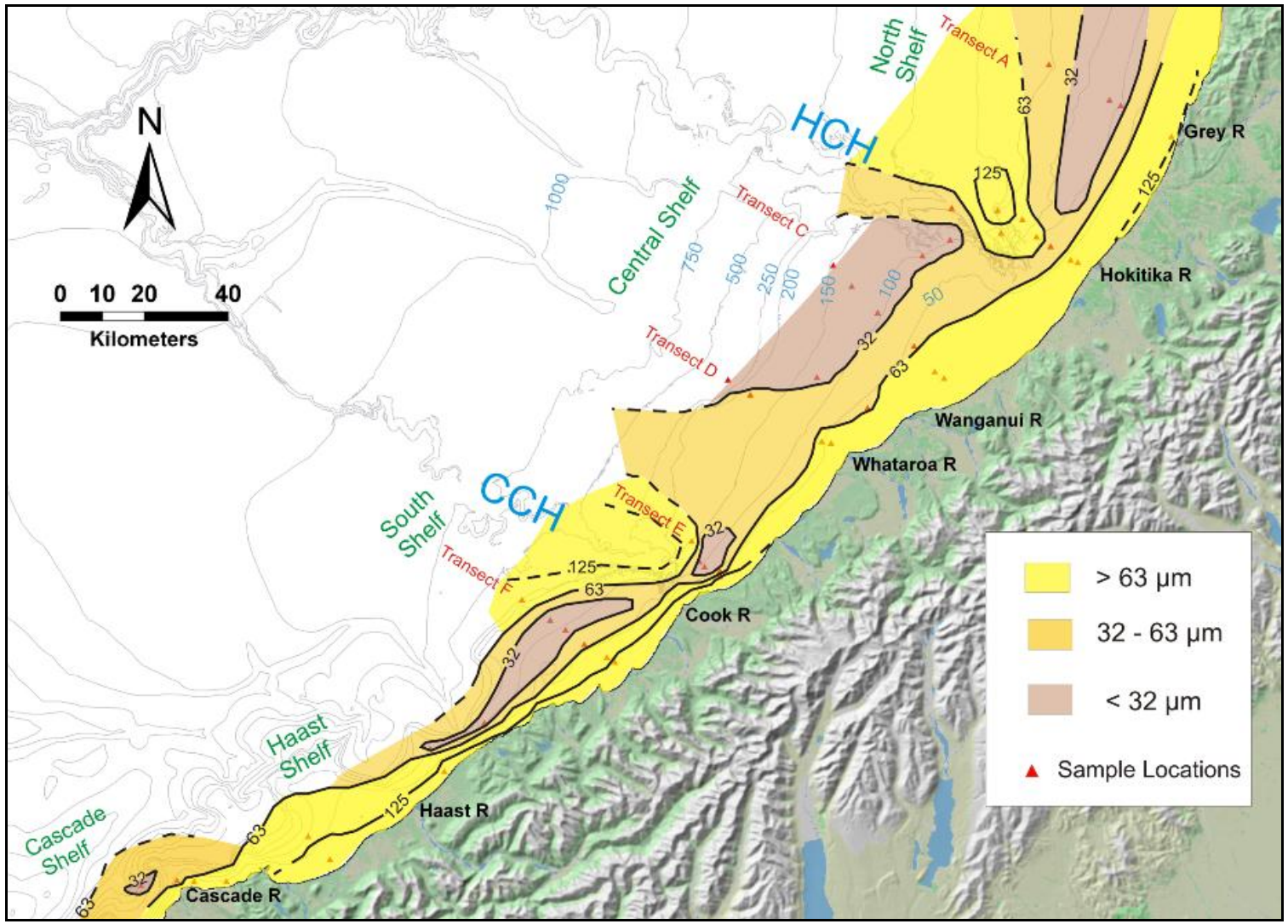

Figure 2-9 Graphic mean grain size distributions for continental shelf and canyon head surface sediments in the SWCM region.

2.3.2 Sorting of SWCM Sediments

The sorting of shelf and canyon sediments is displayed for the SWCM in Figure 2-10. Overall the region is dominated by poorly sorted sediments (66%).The average sorting for shelf sediments is 2.43 μm (poorly sorted), while canyon heads are less sorted with an average of 3.6 μm (Appendix B1)

Shelf

A general across shelf trend exists with moderate to well sorted sediment common on the inner shelf (< 50 m depth), and poorly sorted sediments on the middle to outer shelves (Figure 2-10). Shelf sediment sorting beyond the inner shelf ranges between 2.5 – 3.8 μm. For most of the SWCM, moderate to well sorted sediments cover the shelf within 5 -10 km of the coastline. This widens to up to 15 km of the shelf on the Haast Shelf (Figure 2-10). A general along-shelf trend occurs in the inner shelf sands (especially <30 m depth). Here, sands north of the CCH are mainly moderately sorted, while on the South Shelf, well sorted sands become common.

Canyon heads

Most canyon sediments are poorly sorted. On the HCH north rim, very poorly sorted sediments (> 4 μm) occur at 94 and 182 metres depth. Both samples from the CCH are very poorly sorted, with the least sorted sediments in the entire SWCM located in the upper reaches of the CCH tributary canyon (H893, Transect F, Figure 2-10).

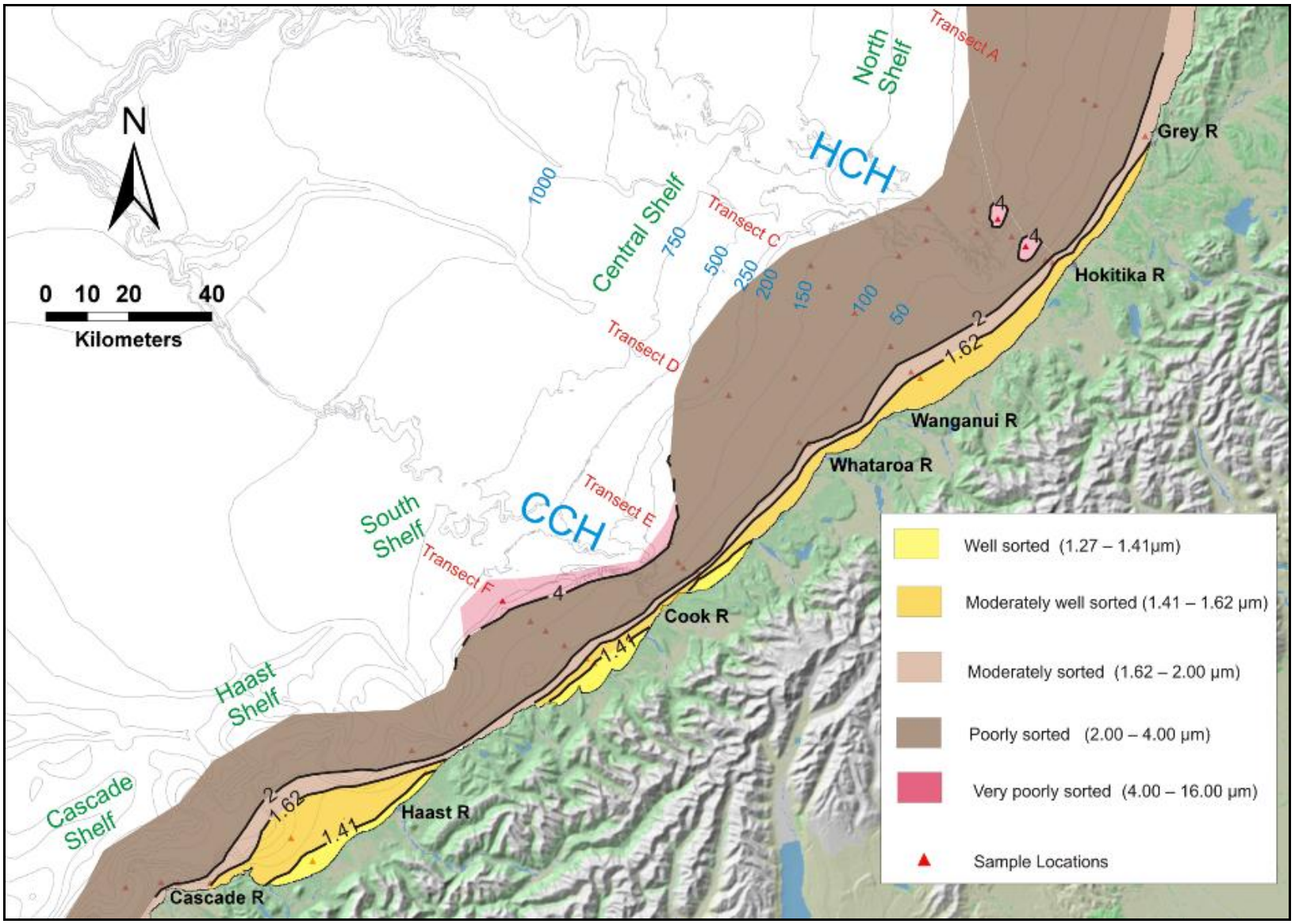

Figure 2-10 Map of sorting distributions for shelf and canyon head surface sediments in the SWCM region

2.3.3 Grain Size Distributions

Grain size distributions for each transect are plotted as normal and cumulative curves from laser sizing data in Figure 2-11. These help to characterise variations perpendicular to and along the North to Cascade Shelf regions.

The most common distribution in the region is unimodal. Bimodal distributions also feature in each transect but to less of an extent. Most samples are finely skewed (i.e. have a tail of excess fines) with only a few samples classed as symmetrical. Inner shelf sands (< 50 m depth) are strongly unimodal with steep cumulative curves reflecting the high degree of sorting in this zone (Figure 2-11). The inner shelf mode is generally very fine to fine sand. The middle shelf (50-150m depth) sediments are unimodal or bimodal with a dominant mode occurring between medium to coarse silt. Cumulative curves from depths beyond the inner shelf are less steep, reflecting poorly sorted sediments at these depths. The distinction between middle and outer shelf sample distributions is difficult.

The HCH (Transect B) has the most variable range of distributions, with both unimodal and polymodal surface sediments present. Inner shelf sediments to the east of the HCH (H845 & H844) are strongly unimodal, similar to the other SWCM shelves to the north and south. At middle to outer shelf depths HCH distributions become more variable than the shelves. Here, polymodal distributions contain modes commonly at 8-10 μm, 70-200μm, and >500 μm (i.e. H848 & H850, Figure 2-11). Near the HCH south rim (C905, P668), sediments have medium silt unimodal distributions similar to other shelf regions at comparable depths.

Sediments from transect E have typical shelf distributions similar to the central and northern shelves, except at 186 m depth north of the CCH. Polymodal (modes at 350 μm, 115 μm and 15 μm), very poorly sorted (shallow cumulative curve), sediments are located north of the CCH. In the tributary canyon south of the CCH (transect F, H893), polymodal (modes at 15 μm, 120 μm, 650 μm respectively), very poorly sorted sediment occur also.

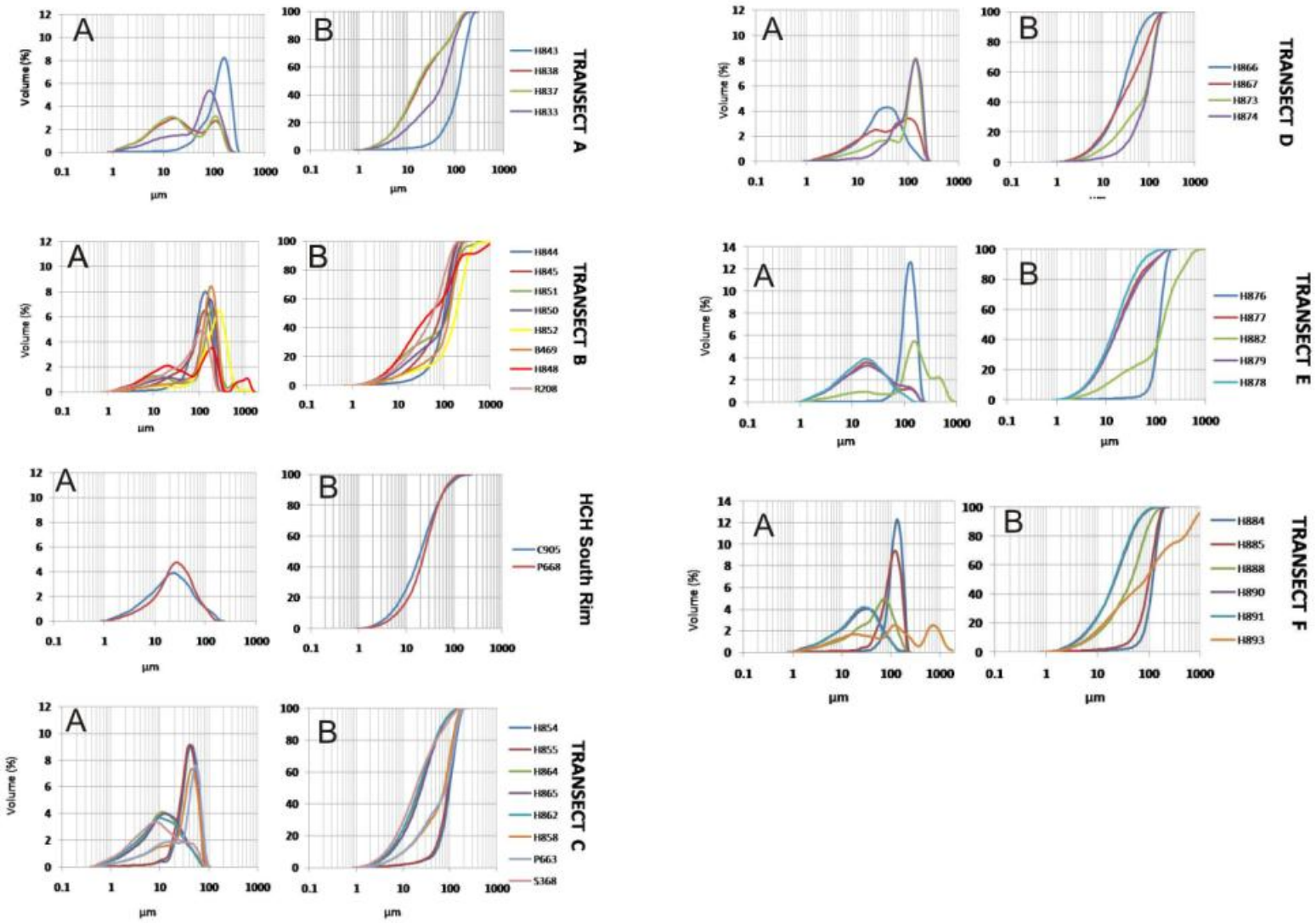

Figure 2-11 Grain size distributions for all SWCM transects (does not include Haast and Cascade Shelf sediments). Graph A = grain size distribution and Graph B = cumulative distributions. The y-axis is in percent volume, as determined by laser sizing.

2.3.4 Gravel, Sand, Mud, and Clay Fractions

This section describes the percentage of gravel to clay sized fractions present in SWCM sediments. The percentages are displayed as separate contour maps for each size fraction as well as transect graphs perpendicular to the coast (Figure 2-12 to 2-16).

Gravel (>2000 µm) and 1600 - 2000 µm fractions

Coarse sediments (i.e. medium sand to gravel) are generally rare on the SWCM. Of the 46 samples analysed, only 11contained any material greater than the upper limit of the laser sizer (1600 µm). Nine samples contained material in the 1600 - 2000 µm fraction, but this was typically < 0.5 % of the sample weight (Appendix B3).Only H848 from the HCH north rim contained an appreciable amount in this fraction (1.8% wt).

Gravel sized clasts were found in 9 samples from both the canyon heads and shelves (Figure 2-12). Only six of these samples contained over 1 % gravel by weight. The largest clast size was a 20mm worm tube on the Cascade Shelf, but gravel clasts usually range between 3 – 10 mm in diametre. The most gravel rich area is the HCH where 9.9 % (H848) and 2.8 % (H852) gravel occurs in sediments at 94 and 198 metres depth respectively (Figure 2-12). In the canyon heads, gravels are dominated by terrigenous clasts while on the shelves biogenic clasts are more common (Figure 2-12). No gravels were found on the North Shelf (transect A). On the Central Shelf, gravels are very rare, with only 3% found at 137 metres depth (transect C) and 0.5 % on the inner shelf of transect D. On the Haast to Cascade shelves, variable amounts of gravel sized clasts occur (up to 3 % wt.).

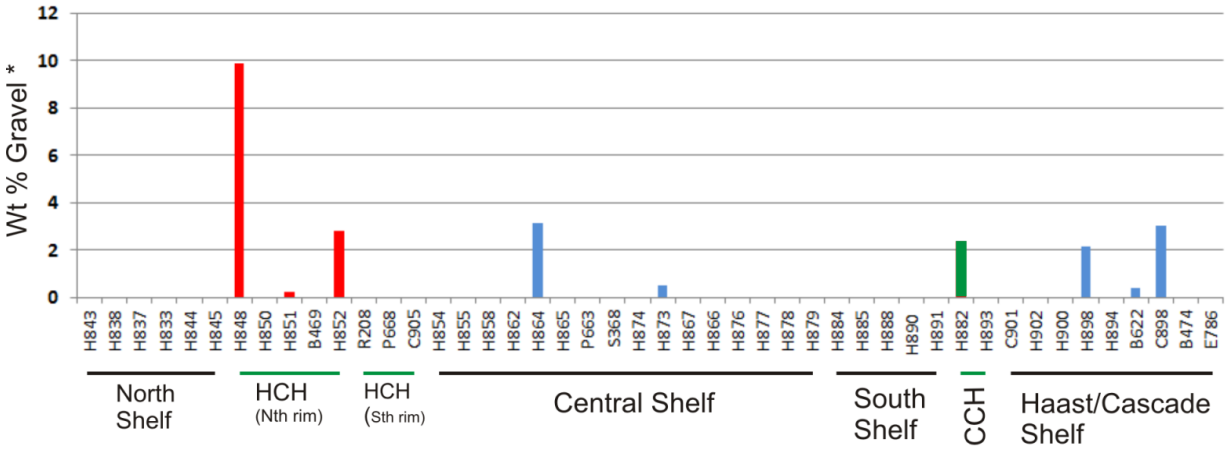

Figure 2-12 Bar chart showing the weight percentage of gravel sized clasts in SWCM sediments. *The gravel percentage has been normalised with the sand and mud fractions from laser sizing. Red bars are dominantly terrigenous gravel clasts, blue bars are dominantly biogenic clasts, and green bars are authigentic clasts.

Sands (63 – 2000 µm)

Sand sized sediment is a major component on the SWCM. The average sand percentage is 50 % for all samples (n= 46) and ranges widely perpendicular to and along the shelf regions (7 to 96 %). A general across shelf trend exists with high sand content on the inner shelf, low sand content at middle shelf depths, followed by an increase at outer shelf depths (Figure 2-13 & Figure 2-16).

The inner shelf (< 50 m) usually ranges between 60 – 96 % (average 81%) for all shelf regions. North of the CCH (transects A – E), inner shelf sand content is lower, averaging 75% (n=6), while on the South and Haast shelves, values are higher, averaging 90% (n=6).

At middle shelf depths (50-150 m), sand content falls dramatically in each shelf region (Figure 2-13). Here, shelf sand content ranges from 7 – 60% and averages 22 % (n=14). On the North Shelf (transect A), middle shelf sand content does not fall below 20 % like the central and South Shelf regions do (Figure 2-13). On the outer shelf, sand content usually increases to over 50% except on the Central Shelf transects.

In the canyon heads, sand distribution is more complicated than on the shelves. On the HCH north rim, sediments contain an average sand content of 68%, over twice the south rim content (25 %) (Appendix B1). Very high sand content (over 80 %) occurs in sediments at 200 metres depth on the north rim (Figure 2-13 & Figure 2-16). Similarly, several kilometres north of the CCH (transect E), 75% sand occurs at 186 m depth.

Muds (silts + clays)

The proportion of mud-sized grains (silts and clays) on the SWCM varies significantly (4 - 93 %) (Figure 2-14). On the inner shelf, mud content is low, averaging 19 % (n=16) for all inner shelf sediments. On the South and Haast shelves, inner shelf sediments are most depleted in mud-sized grains (< 10 %). At middle shelf depths (50-150 m) mud percentages increase to 73 - 93 % in most regions (Figure 2-14). Beyond the middle shelf, mud content falls below 50 % again; thus defining a broad middle-shelf ‘mud-belt’ most clearly developed on the North and South shelves. On the Central Shelf, the seaward boundary of this mud belt is not seen. Towards the outer shelf and upper slope, mud percentages decrease and become more variable (25 – 83%).

In the canyon heads, mud percentage is notably lower than at similar depths on the surrounding shelves(Figure 2-14). On the HCH north rim between 90 to 200 metres depth, mud content is less than 50 %, reaching below 20 % at 200 m depth. On the south rim mud content is much higher (averaging 74%).

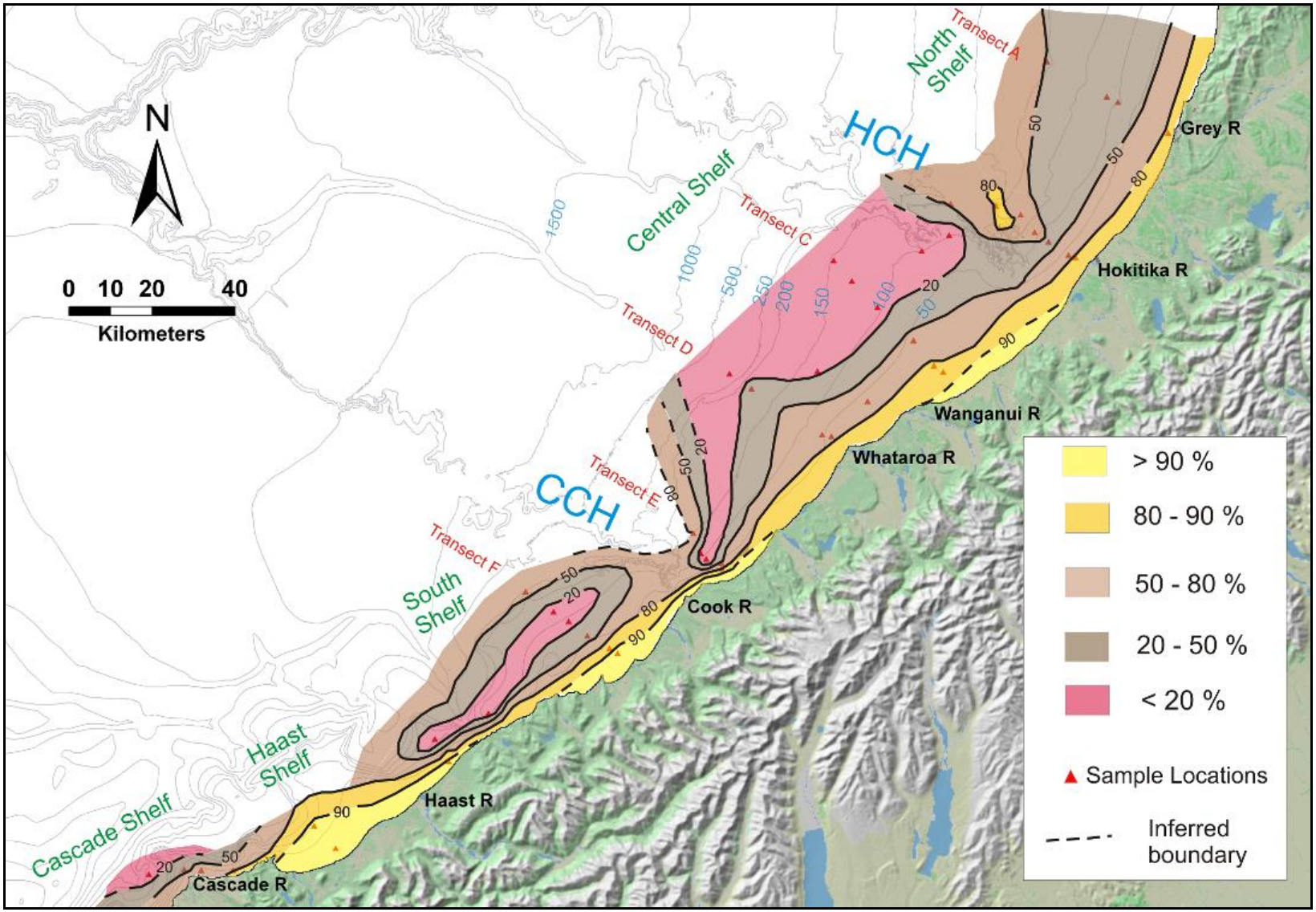

Figure 2-13 Sand percentage in surface sediments on the SWCM.

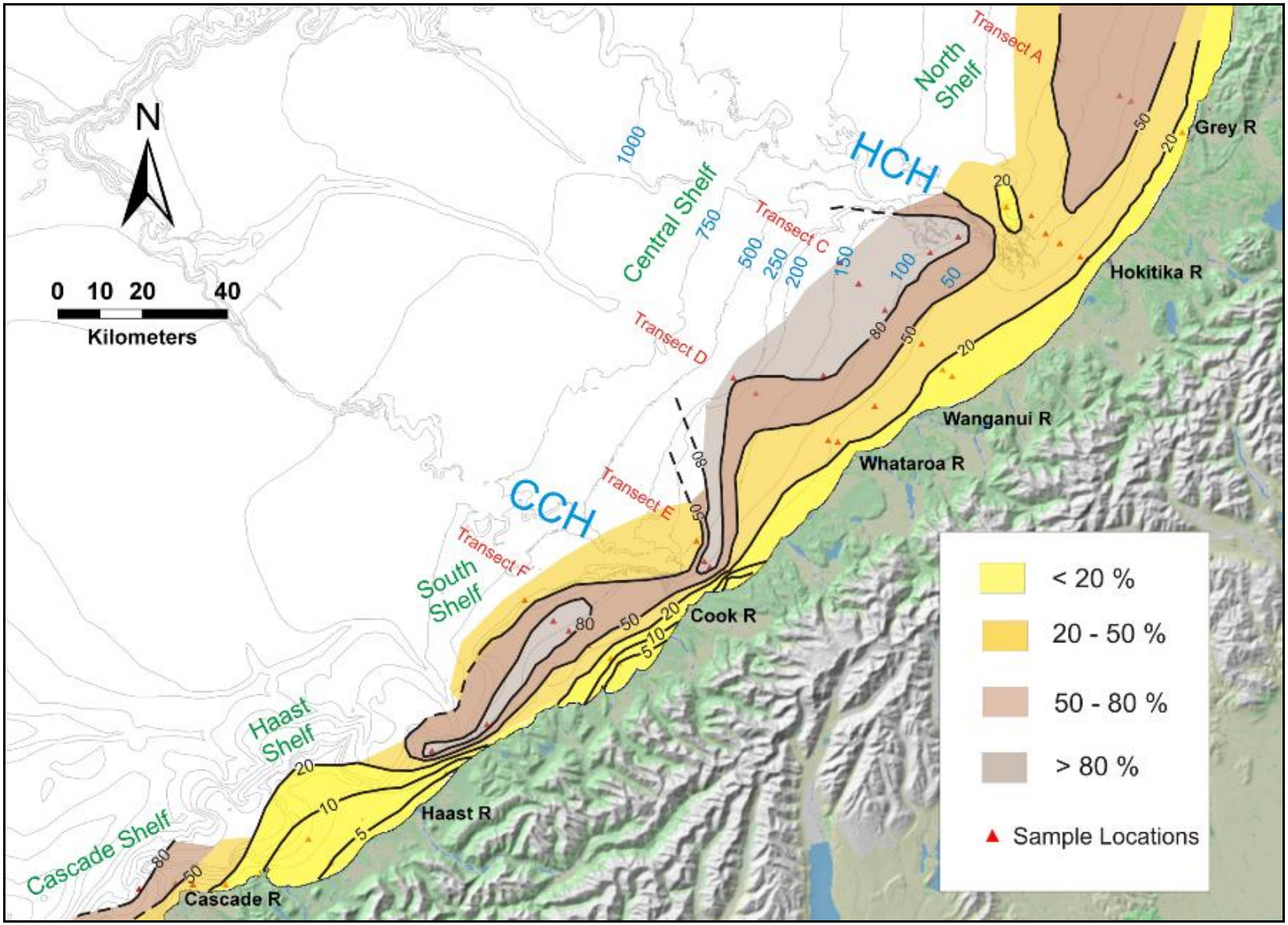

Figure 2-14 Mud (silts + clays) percentage in surface sediments on the SWCM.

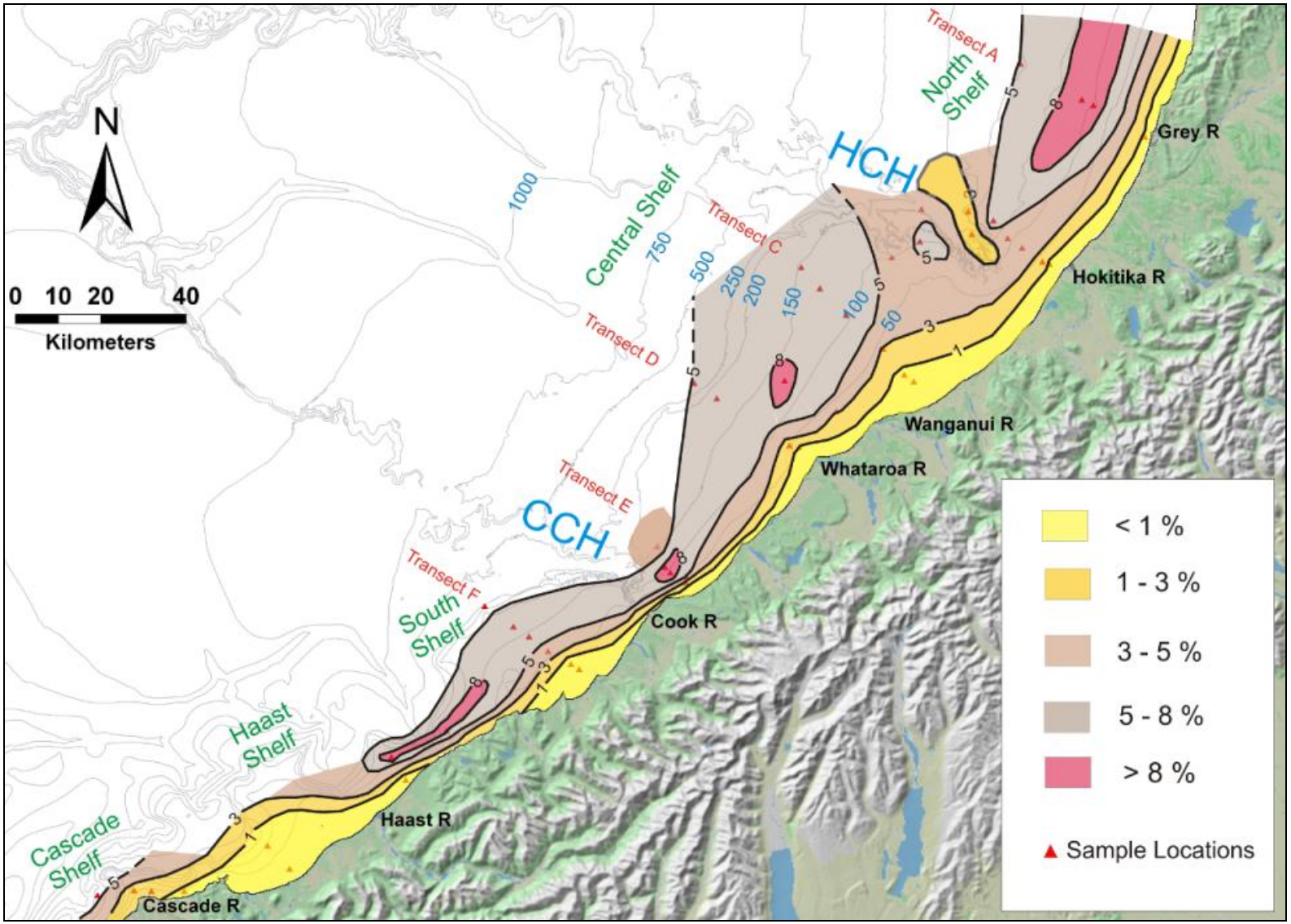

Figure 2-15 Clay (< 4 μm) percentage in surface sediments on the SWCM.

Clay (< 4 µm)

Clay-sized particles on the SWCM are a relatively minor component, with an average of 4.2% (n=46). The SWCM clay distribution is also variable, ranging from 0.3 % to 9.2. A low clay content (< 3 %) characterises the inner shelf, in contrast to the middle shelves which contain up to three times more clay (5 – 9 %) (Figure 2-15). Beyond the middle shelf, clay content decreases slightly. Hence, a clay-enriched belt bound to the east and west by more clay depleted sediments lies on the middle shelf. The narrow Haast and Cascade shelves are covered completely in clay poor (<3%) surface sediments.

In the HCH, low clay percentages (< 3%) on the north rim contrast with the more enriched south rim sediments (>5%).

Across shelf trends in sediment fractions

The percentage of each grain size fraction present in the transects A - F have been plotted against water depth to emphasize the across shelf trends on the SWCM (Figure 2-16).

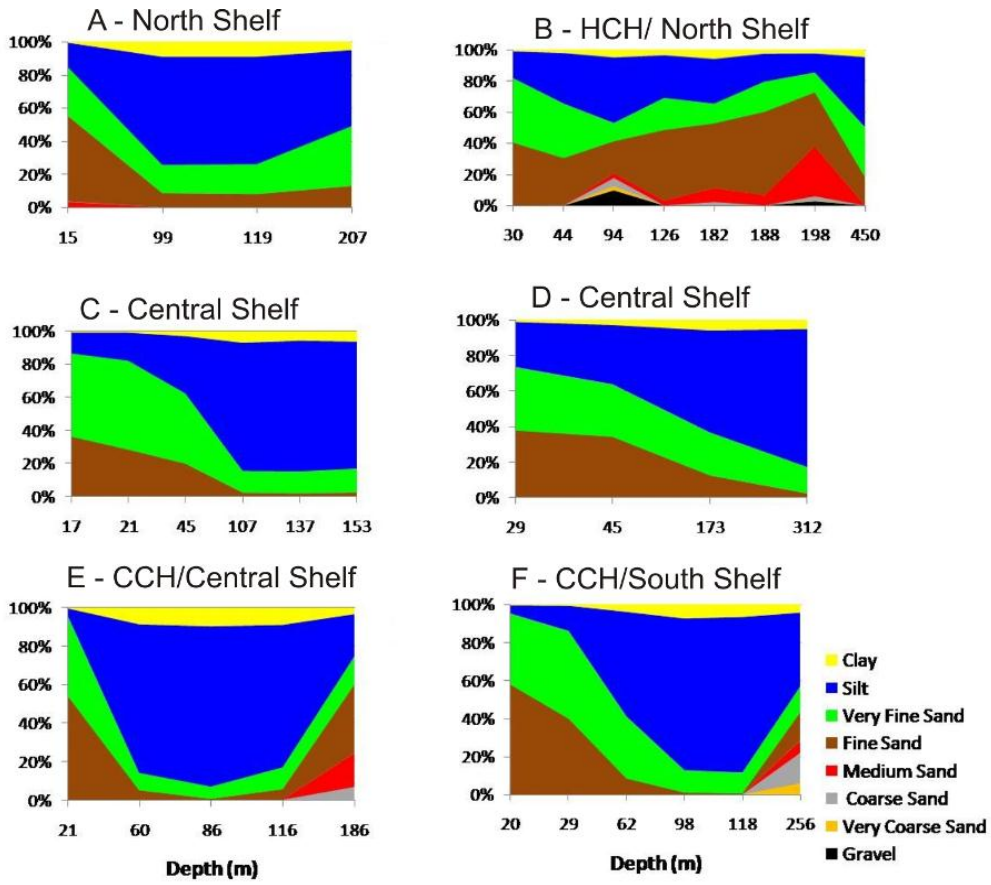

Figure 2-16 Percentage of clay to gravel fractions in transects A to F on the SWCM.

Silts to fine sands are clearly the most dominant fractions on the SWCM. Inshore areas (< 50 m) are dominated by the fine to very fine sands on all transects. Towards middle shelf depths (50 -150 m), silts and clays dominate the surface sediments on transects A, C, D, E and F. Silts and clays are more pronounced in the southern transects (E and F) than the Central and North Shelf transects. Except for the Central Shelf (transects C & D), sands become increasingly common towards outer shelf depths.

The influence of the HCH is demonstrated in transect B where medium sands to gravels become more common. No middle shelf increase in silts and clays occur at middle shelf depths on transect B like the other transects. The outer shelf samples for transects E and F contain notable amounts of coarse sand and gravels. This is probably due to the influence of the CCH and a Cook Canyon tributary respectively.

2.3.5 Textural Classifications

Results from the coarse fraction analysis (>1600 μm) and laser sizing (< 1600 μm) were used to classify the textural distribution of SWCM sediments after Folk (1968) and Lewis & McConchie (1994) (Figure 2-17 A & B, Appendix B). Most obvious in Figure 2-17 (A) is the distinct lack of gravels, with the majority of SWCM sediment plotting as sandy muds or muddy sands. One sample plots as mud (transect E) and several in the sand field (Haast – Cascade shelves). The finer, gravel free plot (Figure 2-17 B) shows that the mud sized fraction is dominated by silt-sized grains.

The textural classifications from Figure 2-17 (A) are mapped for the SWCM regions in (Figure 2-18). The inner shelf is dominated by muddy sands north of the CCH, while sands are more common in the south. A transition from muddy sand to sandy mud occurs on the Central and South shelves near the 50 m isobath. Sandy muds dominate the surface sediments beyond the inner shelf on the North to South shelves. Pure muds (> 90 % mud) occur in a small zone on the middle shelf, several kilometres north of the CCH (Transect E). Slightly gravelly muddy sands are found near the 50 m isobath offshore from the Whataroa River and further south near the Cascade River. The HCH (Transect B) is dominantly muddy sand out to 450 m depth, with slightly gravelly muddy sand and gravelly mud present at outer and middle shelf depths respectively.

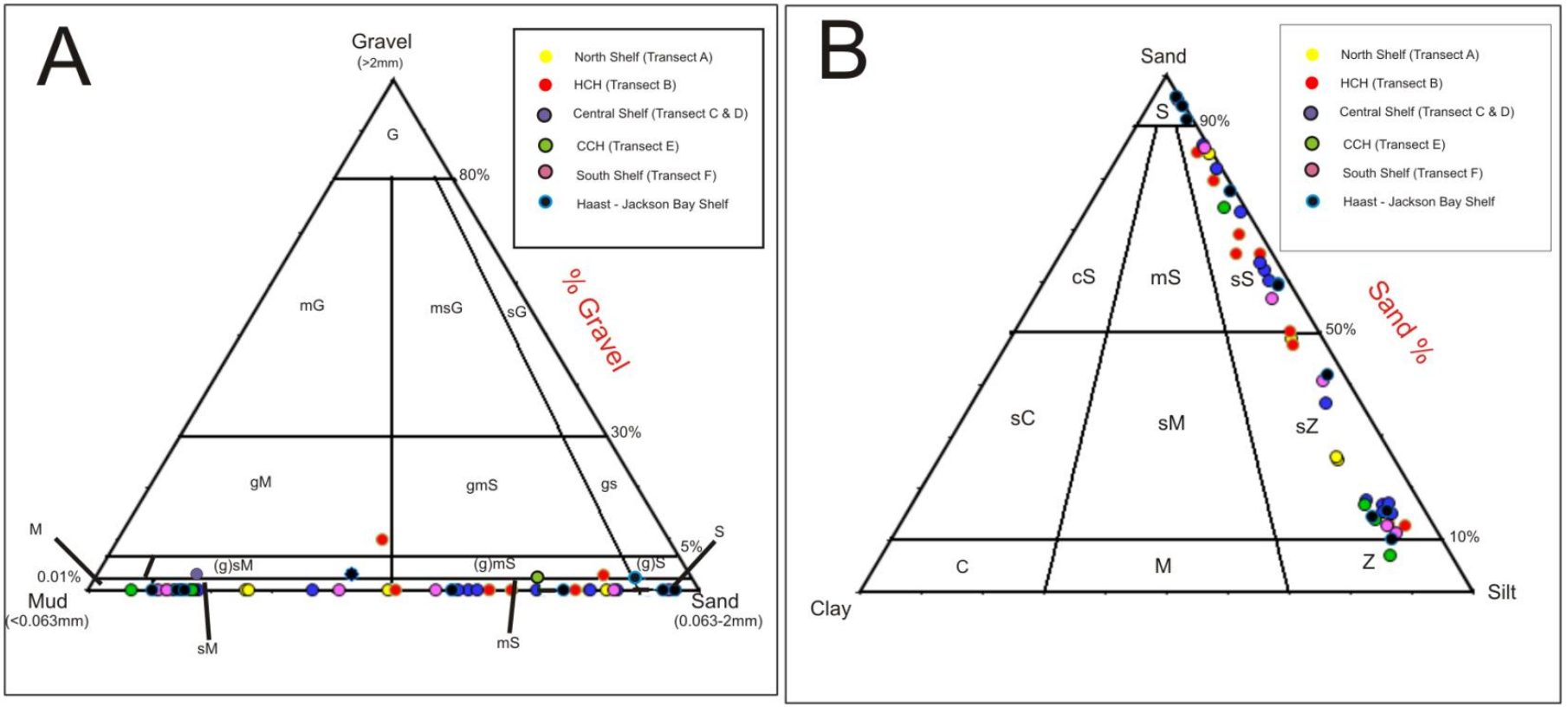

Figure 2-17 Textural classification of the SWCM surface sediments. Graph A: Gravel, sand, and mud fractions after Folk (1968). Graph B) Textural classification for gravel free sediments after Lewis & McConchie (1994). For graph A: G=gravel, S=sand, M=mud, g=gravelly, s=sandy, m=muddy, (g)=slightly gravelly. For graph B: S=sand, s=sandy, Z=silt, z=silty, M=mud, m=muddy, C=clay, c=clayey.

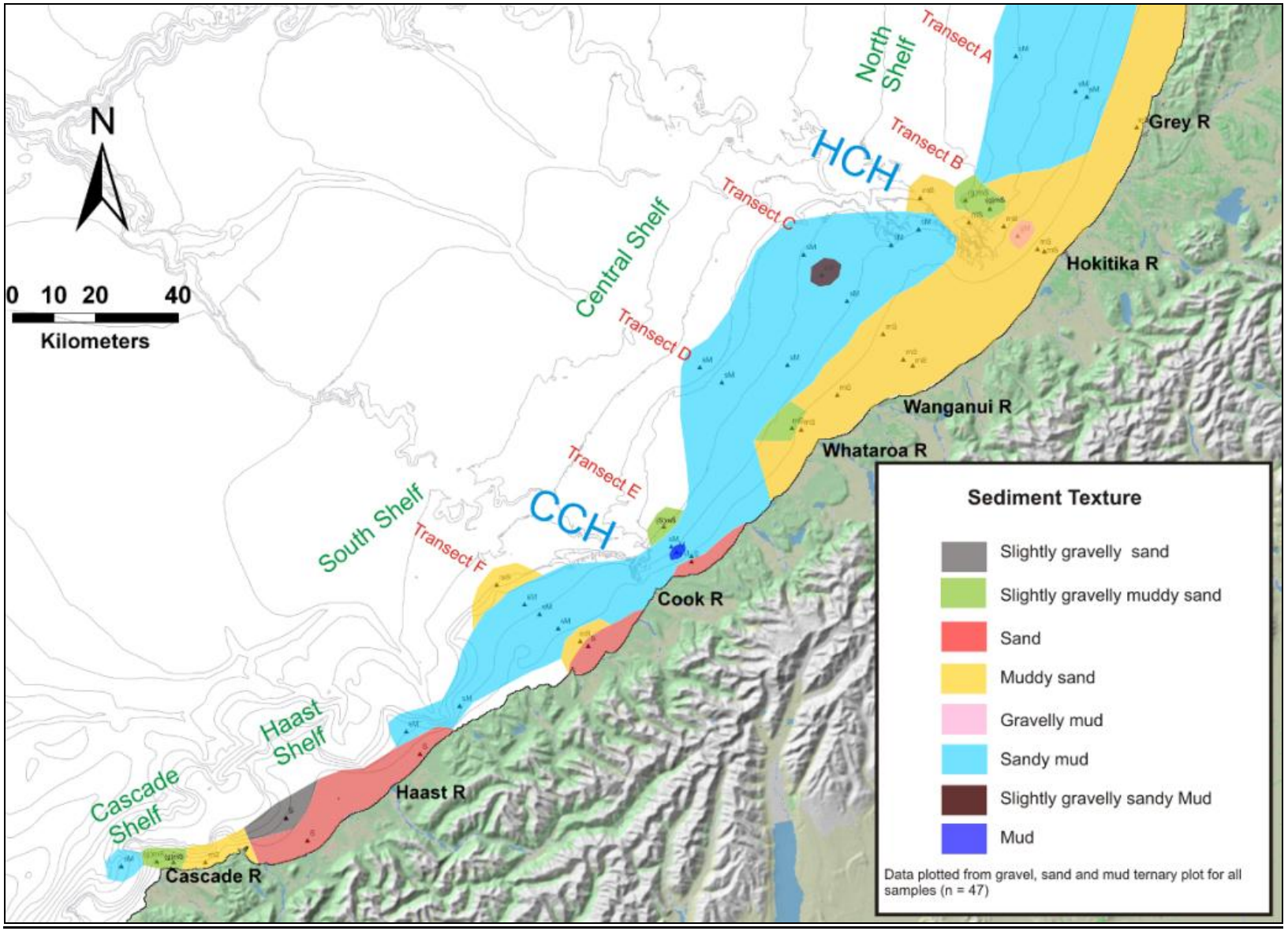

Figure 2-18 Map showing the textural classifications of SWCM surface sediments after Folk (1968).

2.4 SWCM SEDIMENT MOBILITY DUE TO WAVE ACTION

The frequency and magnitude of shoaling waves on the continental shelf have important implications for sediment transport (Le Roux 2010; Campos & Dominguez 2010; Porter-smith et al. 2004) and marine benthic habitats (Griffin et al. 2008). Passing shoaling waves can generate near bed orbital velocities which oscillate back and forth in water depths shallower than the wave base, i.e. half the wave length (L). These orbital velocities are often greater than unidirectional currents operating on the shelf, and can exceed the entrainment velocity (U_{cr}) for surface sediments of a given density and diametre (Porter-smith et al. 2004). This can result in the resuspension of shelf sediments which may then become transported by unidirectional currents such as wind drift, tides, or upwelling. New Zealand West Coast swells, predominantly from the west-southwest and southwest have long been recognized to influence Westland shelf sediment textures to at least 94 m depth under large storm waves (Carter 1980; Probert & Swanson 1985). On New Zealand's Canterbury shelf, Carter & Herzer (1979) have shown that threshold velocities for the entrainment of fine sands (125 -250 µm) under shoaling waves can be as little as 10 cm/s. Using 20 year wave hind cast data (WAM modeling) obtained from NIWA, this section aims to approximate the proportion of time when swells are strong enough to mobilise SWCM surface sediments. An understanding of the frequency of surface sediment resuspension on the SWCM will help put shelf and canyon head sediment textures into context with other dispersal mechanisms.

2.4.1 Methods and Data

The wave generation model WAM (WAve Model) allows the creation of a hindcast for the generation and propagation of deep water waves incident on the New Zealand coastline (Gorman et al. 2003). Details of the WAM data obtained from NIWA can be found in Appendix G1. Comparisons between the West Coast WAM sites revealed only small variations in wave direction, significant wave height (H_{sig}), and significant wave period (T_{sig}). Consequently, a single WAM hindcast site off the Wanganui River (lat -43.0 long 170.44) was chosen given its central location within the SWCM. Significant wave height is equivalent to the average height of the highest 1/3 of the waves, while significant wave period is the average period for the highest 1/3 of the waves. The hind cast period is between 01/01/79 and 31/12/98, with predictions of H_{sig}, T_{sig}, and mean wave direction every 3 hours. A total of 58,440 recordings of wave statistics are present in the data set. Calculations of the maximum orbital velocity (U_{max}) for a given water depth are based on Airy first order wave theory after Porter-smith et al. (2004), Dunbar & Barrett (2005), and Campos & Dominguez (2010) (Appendix G2, Eq. (1)). Values for the entrainment threshold velocity (U_{cr}) are determined from T_{sig} and grain diametre, D, using the empirical formulae of Clifton & Dingler (1984) for unconsolidated quartz grains (Appendix G2 Eq. (3)). Calculated values are approximations only due to several assumptions, including: a) the WAM

model assumes bathymetric contours are approximately parallel and b) sediment entrainment thresholds are based on flat-bed, spherical, unconsolidated, quartz silts and sands.

2.4.2 Near Bed Orbital Velocities on the SWCM

The maximum near bed orbital velocity (U_{max}) for ocean swells incident on the SWCM during the 20 year hind cast period are presented in Figure 2-19 A-C for 25, 50 and 100m depth. This gives an indication of the velocities sediment grains experience on different parts of the shelf during Westland swell conditions.

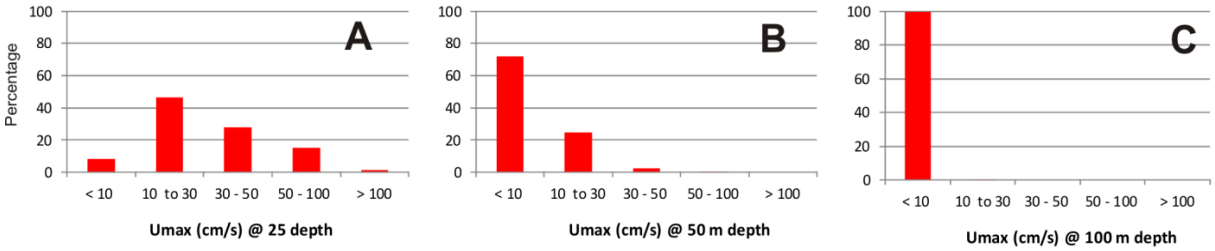

Figure 2-19 Calculated wave orbital velocities of swells during the 01/01/79 to 31/12/98 hindcast period at 25, 50, and 100 m depth offshore from the Wanganui River. Y-axis is the percentage of the entire hindcast period at the specified range of U_{max}.

Obviously the shallow inner shelf experiences high U_{max} values under most Westland swell conditions. At 25 m depth, maximum velocities commonly range between 10 – 50 cm/s (Figure 2-19 A), often above transport thresholds for fine sands. Near 50 m depth, orbital velocities fall dramatically with ca. 72 % of waves less than 10 cm/s and only 3% of waves exceeding 30cm/s. Orbital velocities rarely exceeded 10cm/s at 100 m depth (only 0.23 %) during the hindcast period. The highest U_{max} at 100 m depth of 21.5cm/s suggests on occasion shelf sediments are influenced at this depth.

Wave base (the depth that swells first 'feel' the shelf) for maximum H_{sig} and mean H_{sig} waves over the 20 year hind cast period are displayed in Figure 2-20 for the SWCM. The maximum H_{sig} depth, 144.5m, represents the general limit of storm swell influence on the SWCM. Since the maximum H_{sig} is based on significant wave height, rarer, very large swells may influence the SWCM beyond this depth. The mean H_{sig} roughly defines where typical fairweather swells begin to shoal and influence SWCM sediments. On the SWCM shelves, mud percentage is clearly affected by shoaling waves (Figure 2-20). Mud percentage is typically < 25 % below the mean H_{sig} wave base, reflecting the frequent stirring and resuspension of silts and clays on the inner shelf.

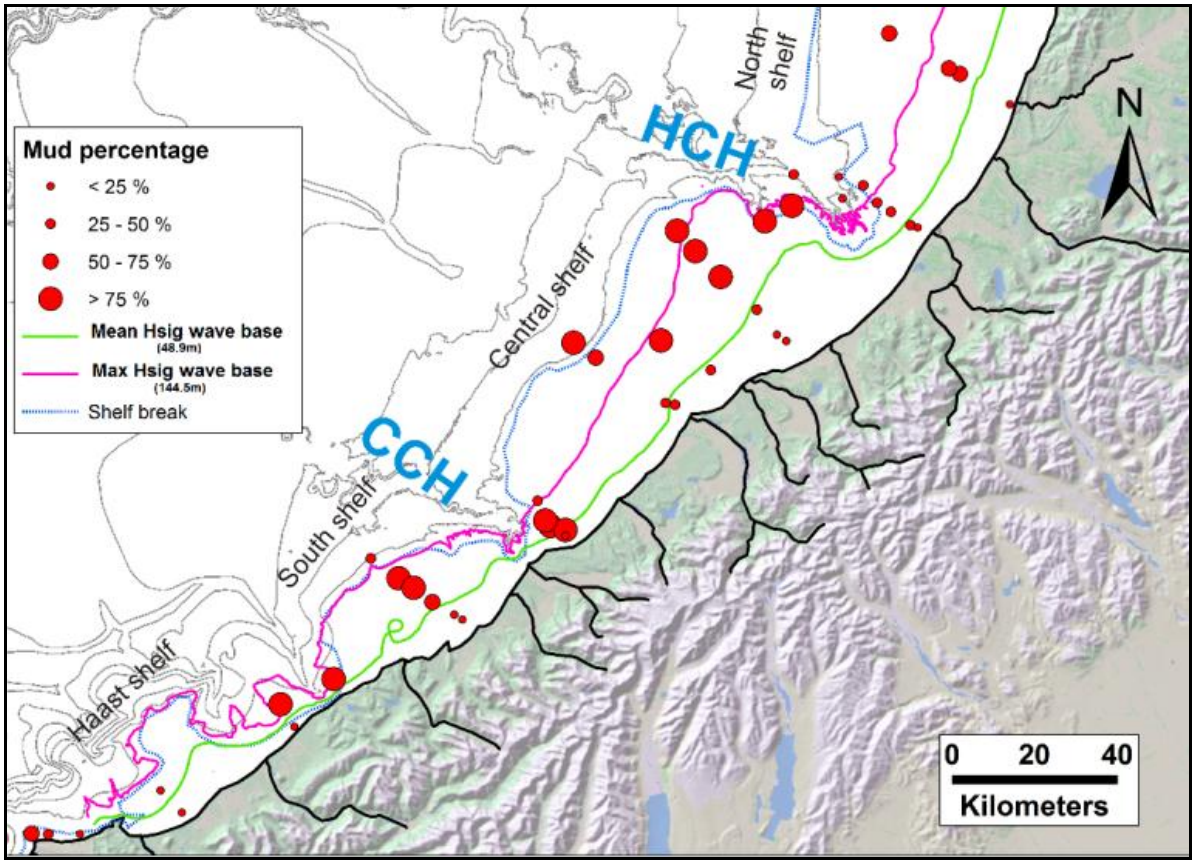

Figure 2-20 Map showing mud percentage and the depths of mean and maximum H_{sig} on the SWCM. Based on 20 year hind cast data offshore from the Wanganui River provided by NIWA.

The shelf break lies at progressively shallower depths south of the HCH. This results in a southward increase in the surface area of the shelf influenced by large storm swells. On the North Shelf, large storm swells begin to influence the shelf half way across the shelf (Figure 2-20). Beyond this depth, sediment entrainment by waves would be rare. Almost all of the northern Central Shelf experiences wave stirring to some degree due to the shelf bulge south of the HCH. Almost the entire South and Haast shelves are influenced by large storm swells, with the shelf break lying near the 150m isobath.

Different parts of the canyon heads experience different levels of sediment stirring. In the HCH, the shallower south rim and eastern lobe are more exposed to storm swells (Figure 2-20). Here, the maximum H_{sig} wave base lies up to 50 m below the HCH rim, especially in the eastern lobe. The gully networks highlighted in Section 2.2.3 are all well exposed to large storm swells. In contrast, the deeper north HCH rim is mostly beyond the influence of large storm swells. This north versus south rim contrast in wave orbital exposure exists in the CCH also. Storm waves commonly shoal below the CCH canyon rims including the heavily gullied rim areas (Figure 2-20).

2.4.3 Wave Threshold Exceedence Values

The entrainment threshold velocity (U_{cr}) has been calculated for common grain sizes found on the SWCM (Table 2-3). Details and assumptions for determination of U_{cr} are provided in Appendix G2.

Table 2-3 Calculated entrainment threshold values (U_{cr}) for different grain sizes using minimum, maximum, and mean significant wave periods (T_{sig}) from the Wanganui River hindcast.

Grain size description	Grain size (µm)	U_{cr} @ T_{sig}=4.305 [a] (cm/s)	U_{cr} @ T_{sig}=13.428 [b] (cm/s)	U_{cr} @ Mean T_{sig}
Coarse silt	31	8.0	11.7	9.8
Very fine sand	63	10.1	14.7	12.3
Fine sand	125	12.7	18.5	**15.5**[c]
Medium sand	250	16.0	23.2	19.5

[a] = minimum T_{sig} for 20 year hindcast,
[b] = maximum T_{sig} for 20 year hindcast.
[c] = U_{cr} value used to produce Figure 2-21

Where the maximum wave orbital velocity (U_{max}) is greater than the U_{cr} for a given grain size and water depth, the grains may become suspended. Grain sizes finer than this threshold will likely remain in suspension. This is an assumption since factors such as bed roughness, grain density, and grain shape can influence the U_{cr} values (Porter-smith et al. 2004). Using calculated values for U_{max}, U_{cr}, and the 20 year hind cast dataset, a map was produced to display the percentage of time U_{max} exceeds U_{cr} for 125µm sediments (fine sand) at 25, 50, and 100 m water depth on the SWCM (Figure 2-21). Since U_{cr} varies with T_{sig}, the mean T_{sig} for the entire hind cast was used to calculate the most *common* U_{cr} for 125µm sediment, i.e. 15.5 cm/sec.

The entrainment of sediment finer than 125 µm is strongly controlled by shelf morphology. The broad bulge of the Central Shelf demonstrates this with the widest zones of moderate – high entrainment of 125µm sediments on the SWCM (Figure 2-21). Below 25 m depth on the shelves, <125µm sediment is in suspension for at least 79% of the time (i.e. ~288 days of the year). Consequently, muds are rare and the coarser sand fractions dominate at these depths. Between 25 – 50 metres depth, 14 - 79 % of the time < 125 µm sediment is in suspension, with muds percentages remaining low.

The south and eastern rims of the HCH and CCH experience more frequent entrainment of <125µm sediments than their northern rims. Shelf sediments <125µm bordering the south and eastern rims may become entrained up to several percent of the time (well within the 'Low' entrainment zone). Gullies in the eastern HCH lobe experience entrainment of 125µm sediment with the low entrainment zone. The deeply incised main channel of the CCH almost enters the 'Moderate' entrainment zone, suggesting a more frequently 'stirred' canyon head than the HCH.

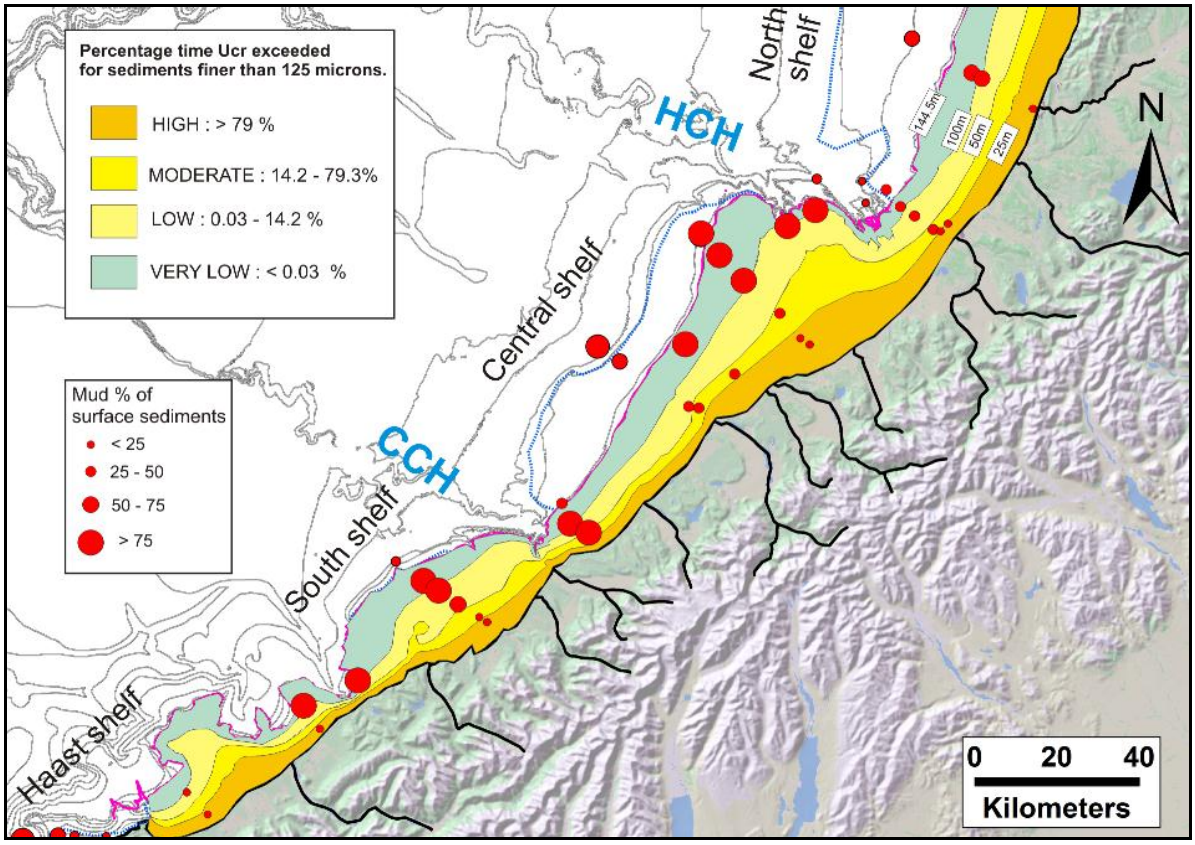

Figure 2-21 Proportion of time ≤ 125 µm sediments may experience resuspension due to wave orbitals. Based on the 20 year hindcast from 01/01/79 to 31/12/98 offshore from the Wanganui River, provided by NIWA. Assumes sediment resuspension when $U_{max} > U_{cr}$. Purple line is maximum Hsig from Figure 2-20. HCH = Hokitika Canyon Head, CCH = Cook Canyon Head. For details on calculations and data refer to appendix G.

2.5 DISCUSSION AND INTERPRETATIONS

2.5.1 Shelf Textural Interpretations

Surface sediments on the SWCM shelves are dominated by fine grained allochthonous sediments (fine sands to muds). This is typical of storm dominated active margin shelves where modern terrigenous sediment input is high (Boggs 2001; Walsh & Nittrouer 2009; Suter 2006). The active margin setting of the SWCM supplies large volumes of terrestrial sediments which overwhelm most of the shelves. Coarser material (i.e. coarse sands and gravels) on the SWCM shelves are uncommon and dominantly biogenic in origin where present. Terrigenous coarse material is restricted to canyon heads or isolated patches on the upper slope.

Generally the results of this textural analysis compare to previous studies focused on Westland shelves north of the Whataroa River (Probert & Swanson 1985; Stoffers et al. 1984). The pattern observed generally conforms to a 'wave graded shelf' pattern where sediments fine in an offshore direction as the influence of wave and current energy decreases (Boggs 2001; Dunbar & Barrett 2005; Nittrouer et al. 1984; Suter 2006). The inner shelf (< 50 m depth) is dominated by the coarsest (fine – very fine sand) and well sorted sediments, reflecting an environment where constant agitation and resuspension

via waves and currents occurs. The wave base for the mean H_{sig} from the hindcast data demonstrates this. South of the CCH inner shelf sediments appear better sorted and have a higher sand percentage and mean grain size than the Central and North shelves. It is possible that these higher sand percentages may be the result of more effective winnowing of fines. The narrower South and Haast shelves could allow deep water currents to impinge further onto the shelf, in contrast to the wider Central and North shelves.

Mud dominated sediments at middle shelf depths have long been recognized on the Westland shelves (Carter 1980; Probert & Swanson 1985). At middle shelf depths, sandy mud and muds dominate surface sediments in each shelf region. The transition to muddier sediments takes place near the 50 m isobath. This is shallower than portrayed in previous studies where the sand to mud transition is defined closer to the 100 m isobath (Probert & Swanson 1985). On the North and South shelves, these muddier sediments define a 'mud belt' which eventually grades seaward into coarser muddy sands again on the outer shelf. Sediments of the middle shelf are poorly sorted, reflecting the varying degrees of flocculation of the finer particles and an increasing abundance of biological organisms in the lower energy environment here.

Within the mud belt, medium silt to clay occurs in its highest concentration. Several factors may be contributing to the development of these muddy sediments. In recent decades, studies of modern shelf sediment accumulation using radionuclides (e.g. ^{210}Pb, ^{234}Th) have commonly found accumulation maximums coincident with mud dominated zones on the middle shelf (Carpenter et al. 1982; Nittrouer et al. 1979; Walsh & Nittrouer 2009). This accumulation maximum is largely due to a decrease in sediment resuspension relative to the more energetic inner shelf (Nittrouer et al. 1984). Fairweather swells on the SWCM shelves agitate bottom sediments at up to 50 metres depth (Figure 2-20), which correlates roughly with the transitional boundary from inner shelf sands to the silt and clay dominated mud belt.

Another contributor to the middle shelf muds may be from buoyant hypopycnal plumes. These plumes typically don't propagate beyond inner and middle shelf depths since they eventually become carried parallel to the coast via the coriolis effect (Nittrouer and Wright 1994; Boggs 2001). Hence, suspended sediment plumes from high sediment yield West Coast rivers may flocculate and settle through the water column, contributing to the mud belt. Suter (2006) notes that the alongshore projection of river plumes can lead to muddy deposits forming sub-parallel to shelf contours. The shelf transects in this study do show a general tendency of the mud belt to follow shelf contours and may be evidence that hypopycnal plumes are contributing to this depositional facies. However, their contribution to the total volume of sediment accumulated on shelf is generally small in comparison to other depositional processes (i.e. *hyperpycnal* deposition) (Nittrouer & Wright 1994, pg. 35). The contour following boundary between inner shelf sand and middle shelf muds is probably therefore more a function of decreasing wave orbital remobilization with increasing water depth.

Beyond the middle shelf, mean grain size generally coarsens from medium silt to coarse silt. Coarser muddy sands have been observed north of the HCH by Carter (1980); Probert & Swanson (1985). This coarsening beyond the middle shelf is not observed on the Central Shelf, where mean grain size and sand content increase only slightly on the outer shelf. The muds here appear to continue offshore beyond the study area. This coarsening may be the due to several factors, including: increases in the proportion of carbonate secreting organisms; mixing of modern sediments with relict or palimpsest material; or hydraulic energy (i.e. internal waves or ocean currents) that is remobilising or winnowing the fines on the outer shelf. Increased biological productivity due to a reduction in wave orbital disturbance will be contributing to the increase in sand sized grains on the outer shelves on the SWCM.

Shelf width is a key factor affecting shelf textures, where narrower widths become more easily inundated by modern fine grained terrigenous sediment (Walsh & Nittrouer 2003). This factor has been highlighted by previous work on shelf sediments north of the Whataroa River (Carter 1975,1980; Probert & Swanson 1985; Stoffers et al. 1984). Shelf width decreases southwards from 50 – 60 km on the North Shelf, to 35 – 50 km on the Central Shelf, and 25 – 30 km on the South Shelf. On the wider Central and North shelves, textural zones (i.e. sandy inner shelf, mid- shelf mud belt, to coarser outer shelf sediments again) are broader than on the South Shelf. The South Shelf represents a condensed pattern of textural zones. The narrower shelf widths of the Central and South shelves are more easily inundated by modern, fine grained terrigenous sediments. On the narrow South Shelf (Transect F), fine muds occur at middle shelf depths, but appear to coarsen towards the upper slope (Transect F). This pattern is contrary to the notion that narrower shelf are more easily blanketed in modern sediments, particularly with high fluvial input in this southern region. This may be due to currents sweeping farther across narrow shelves.

A north to south decrease in grain size is acknowledged from the North Shelf down to the Whataroa River on the Central Shelf (Probert & Swanson 1985; Stoffers et al. 1984). This has been attributed to an increase in suspended load towards the south (Probert & Swanson 1985). South of the Whataroa River, the middle shelf muds become more mud rich and the mud belt more clearly defined than to the north (Transect E & F). This suggests a continuation of the trend identified by Probert & Swanson (1985), where shelf sediments fine as fluvial suspended loads increase to the south. Estimates of sediment accumulation rates south of the Whataroa River support this ‘fining to the south’ trend where fluvial input between Jackson Bay and the Whataroa River is notably higher than West Coast rivers to the north (Table 1-1 and Hicks et al. (2003)). Sedimentation rates are especially high between the Whataroa and Arawhata Rivers due to very high precipitation and uplift rates, and steeper, more glaciated catchments than to the catchments further north (Korup et al. 2005).

2.5.2 Canyon Head Textural Interpretations

Generally, the canyon heads are defined by coarser landward projections of sands and occasional pebbles relative to shelf sediments from similar depths. Sand percentages are relatively high (45-85%), grain size distributions are often polymodal, sorting is poor to very poor, and coarse grains (medium sand to gravel) become common, especially on the north rim areas. Spatial variation in sediment textures is high compared to the shelves, with gravelly sands, muddy sands and sandy muds within a few kilometres of each other.

Modern canyon head textures and features

Modern fine grained textures dominate the south and eastern rims of the HCH and CCH. Here, poor sorting, fine unimodal grain size distributions, and high mud percentages all suggest a strong association with the modern middle to outer shelf SWCM sediments. The smooth, featureless shelves leading towards the south and east rims of the HCH and CCH indicate modern sediments are rapidly blanketing these areas (Figure 2-22). In addition, gully networks along the south and east rims of both canyon heads suggest submarine erosion and downslope sediment transfer is common here. Similar gully networks on other submarine canyons have been associated with active unconfined fluid or sediment gravity flows that propagate downslope (Micallef & Mountjoy 2011).

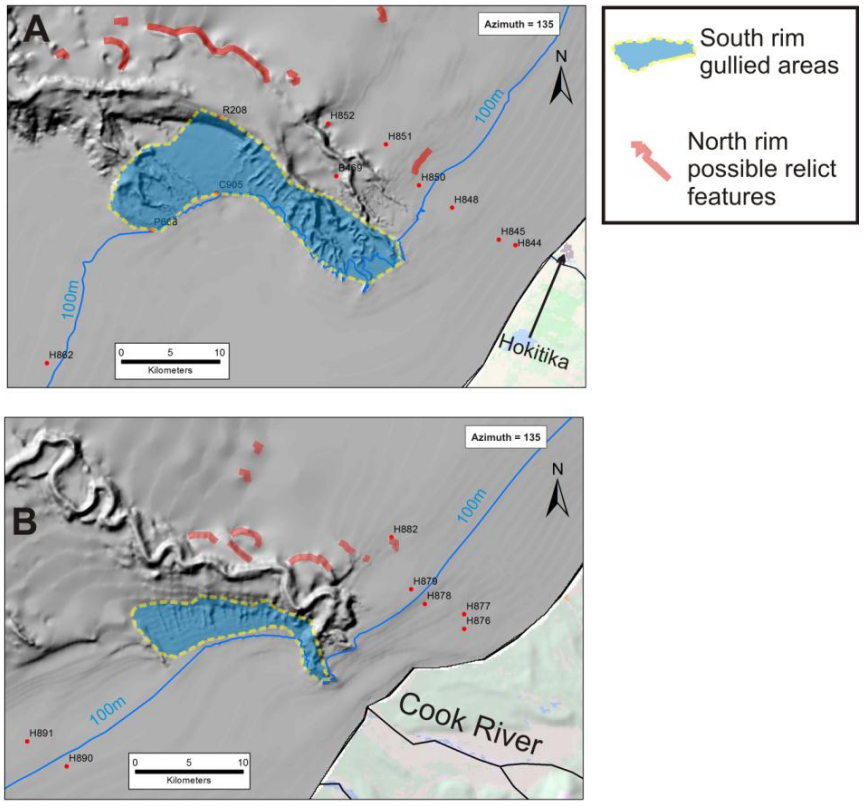

Figure 2-22 Hill shade maps showing contrasting geomorphologies on the north and south rims of A) the Hokitika Canyon Head and B) the Cook Canyon Head.

Relict textures and features

On the north canyon rim areas, coarser sediments contrast with the south and eastern rims, suggesting a significant relict component in surface sediments. Pebbles and coarse sands in the HCH are clearly out of equilibrium with the prevailing modern hydraulic regime. The polymodal grain size distributions on the north rims indicate reworking and mixing of coarser relict grains or clasts with finer modern sediments (Swift et al. 1971). The shallower HCH north rim sample locations (H848 and H850) are near the 'Harvester Prospect', where gravelly sand and muds were encountered during placer gold exploration in the 1980s (Price 1983). The shallower HCH samples in this thesis are most likely related to the Harvester relict sediments which Price (1983) interpret as Pleistocene gravels deposited during lowstands.

As highlighted in the hillshade images of the HCH (Figure 2-6 and Figure 2-7), the presence of 'relict topography' such as terraces and cuspate channels provides further evidence for a relict origin of HCH north rim gravelly sands (Figure 2-22). While samples from the CCH north rim are rare (only H882), given the relict topography it is probable that relict Pleistocene gravelly sediments are exposed in places here too. The lack of gully networks on the north canyon rims suggests active transport and sedimentation rates are low. This would allow for the preservation of relict terraces and channels (Figure 2-22).

Wave orbitals on the canyon heads

The effects of storm wave resuspension of modern fines on the south and east canyon rims is probably significant. The wave base for maximum H_{sig} waves is up to 50 m below the canyon rims in many places. Large storm waves could create high suspended sediment concentrations on the south and east rims (Puig et al. 2003). This may generate fluid mud flows that feed into the gully networks highlighted in Section 2.2.3. The higher elevation of the south rims in both the HCH and CCH would result in a higher frequency of resuspension events compared the deeper north rims.

Interception of shelf transport paths

The contrasting texture and morphology of SWCM canyon north and south rims provides an insight into shelf – canyon interactions. Canyon heads which incise the shelf to within several kilometres of the coast are widely documented to intercept shelf sediment transport pathways (Walsh & Nittrouer 2009; Puig et al. 2003). The interception of the net northward transport path of suspended sediments on the SWCM would help explain the lack of modern fine sediments on the north rims. Price (1983) first postulated this interception as the reason for exposure of the 'Harvester Prospect' between 70 – 100 m depth on the HCH north rim. More extensive sampling of the HCH and CCH indicates the effect of this interception is extensive on the northern rims, with textures and topography suggesting little deposition of modern fines to at least 200 m depth.

Canyon head bypassing

Results from this study are consistent with comments by Carter (1980) in terms modern littoral sediment by-passing of the canyon heads. The inner shelf landward of the HCH has typical near shore characteristics (moderate to well sorted, unimodal fine sands) suggesting constant agitation and reworking by waves, and littoral transport to the north under southwesterly swells. The lack of bathymetric features between the HCH and the shoreline suggest modern sediments thickly blanket the shelf here. Much of these modern sediments will be part of the North-east trending transport pathway that is well developed at inner shelf depths and ultimately bypassing the HCH northwards up the Westland shelf.

2.6 SUMMARY

- Surface sediments on the SWCM shelves are dominantly fine grained modern terrigenous sediments (fine sand to muds). This is typical of storm dominated shelves adjacent to active margins with high modern terrigenous input. Across shelf textures are well developed and are mainly a function of decreasing hydraulic energy with increasing water depth.
- The inner shelf is dominantly well sorted, fine to very fine sand, reflecting the constant resuspension and transport from waves and currents. Mud rich surface sediments (> 50 % mud) occur at middle shelf depths for all shelf regions. The transition from inner shelf sands to mud rich sediments occurs near the 50 metre isobath, consistent with the mean H_{sig} from the 20-year hindcast. The mud rich middle shelf textures represent areas of maximum sediment accumulation.
- On the North and South shelves sediments coarsen on the outer shelf but this is not observed on the Central Shelf, probably due to the high fluvial sediment supply to the Central Shelf.
- Storm wave orbitals are capable of stirring fine sediments on most of the SWCM shelves; this influence increases towards the south as shelves progressively narrow. Storm wave orbitals can may stir fine sediments up to 50 m below the South and east canyon rims.
- The canyon heads of the SWCM have strongly contrasting textures and morphologies on their north and south rims respectively. South and eastern rims are dominated by modern fine sediment blankets with gully networks suggesting active transport. North rims are characterised by relict sediment textures and irregular topography indicating little active transport or modern sedimentation.
- The canyon heads probably intercept the net northward transport of suspended sediments on the SWCM, creating a leeward deficit on the north rims.

CHAPTER 3 : DISPERSAL AND PROVENANCE OF SWCM DETRITAL SEDIMENTS

3.1 INTRODUCTION

The mineralogy of terrigenous sediments are considered in this chapter to provide insight into the dispersal and provenance of South Westland Continental Margin (SWCM) surface sediments. A selection of shelf, canyon head and terrestrial sediment samples were examined in thin section and as loose sediment samples (Figure 3-1). The inclusion of beach and river sediments in this analysis was purely for assessing any trends in provenance on the SWCM.

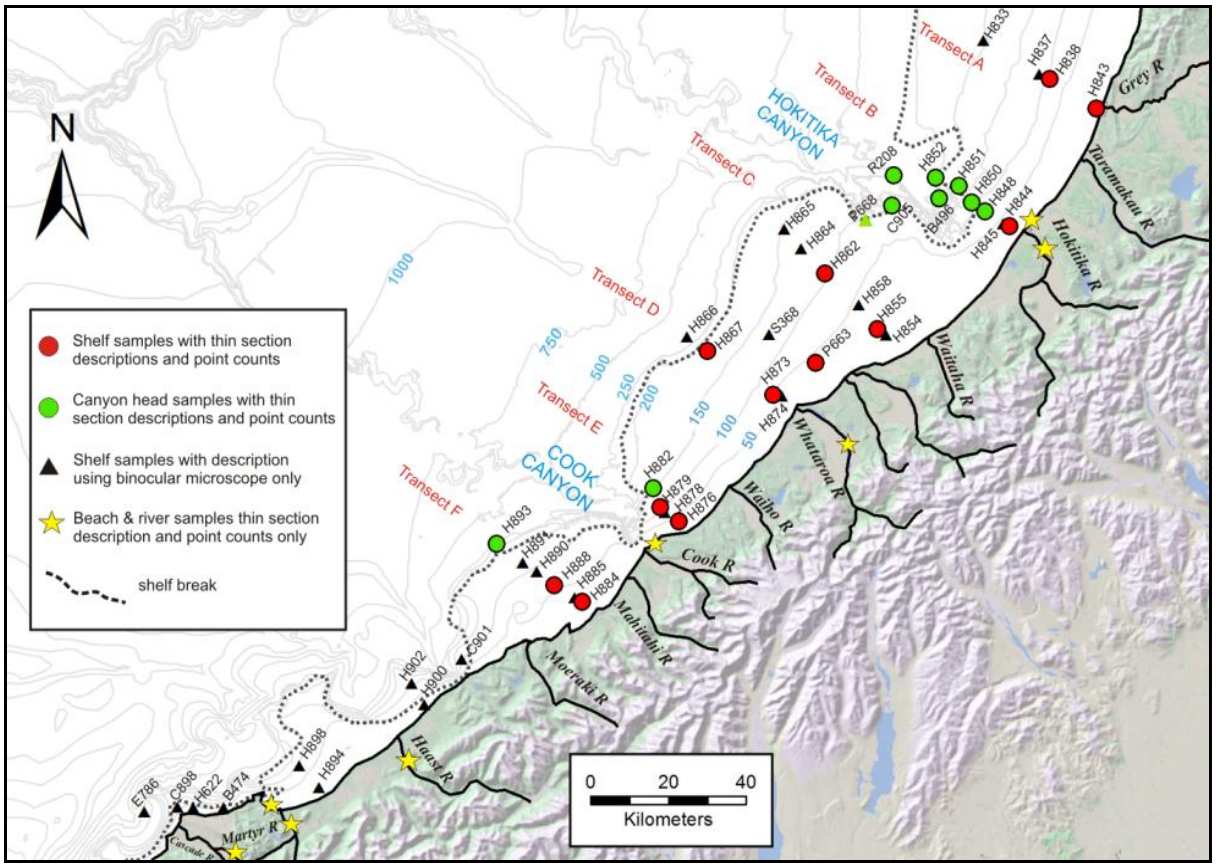

Figure 3-1 Map showing location of SWCM shelf, canyon head, beach, and river samples and the methods used to investigate sediment composition.

3.2 GEOLOGY OF THE SWCM CATCHMENTS

The basement geology of SWCM catchments is summarised here to aid discussion of the provenance of detrital shelf and canyon sediments. This summary is also applicable to subsequent chapters on detrital magnetites (Chapter 4) and the geochemistry of SWCM sediments (Chapter 5).

The geology of the catchments supplying the SWCM shelves span much of the geological history of New Zealand, with pre-Cretaceous basement units very widespread. For simplicity, these units are

discussed as three separate groups: Firstly, the Late Cambrian to Early Cretaceous basement terranes related to the convergent Gondwana margin. Secondly, the Cretaceous to Pliocene units related to 'rifting' and 'drifting' of the New Zealand continental block from Gondwana, and lastly, the Quaternary to recent lithologies related mostly to glacial-interglacial cycles and the modern plate boundary. The generalised regional stratigraphy is displayed in Figure 3-2. In Figure 3-3 the regional outcrop patterns of these three main rock groups are portrayed.

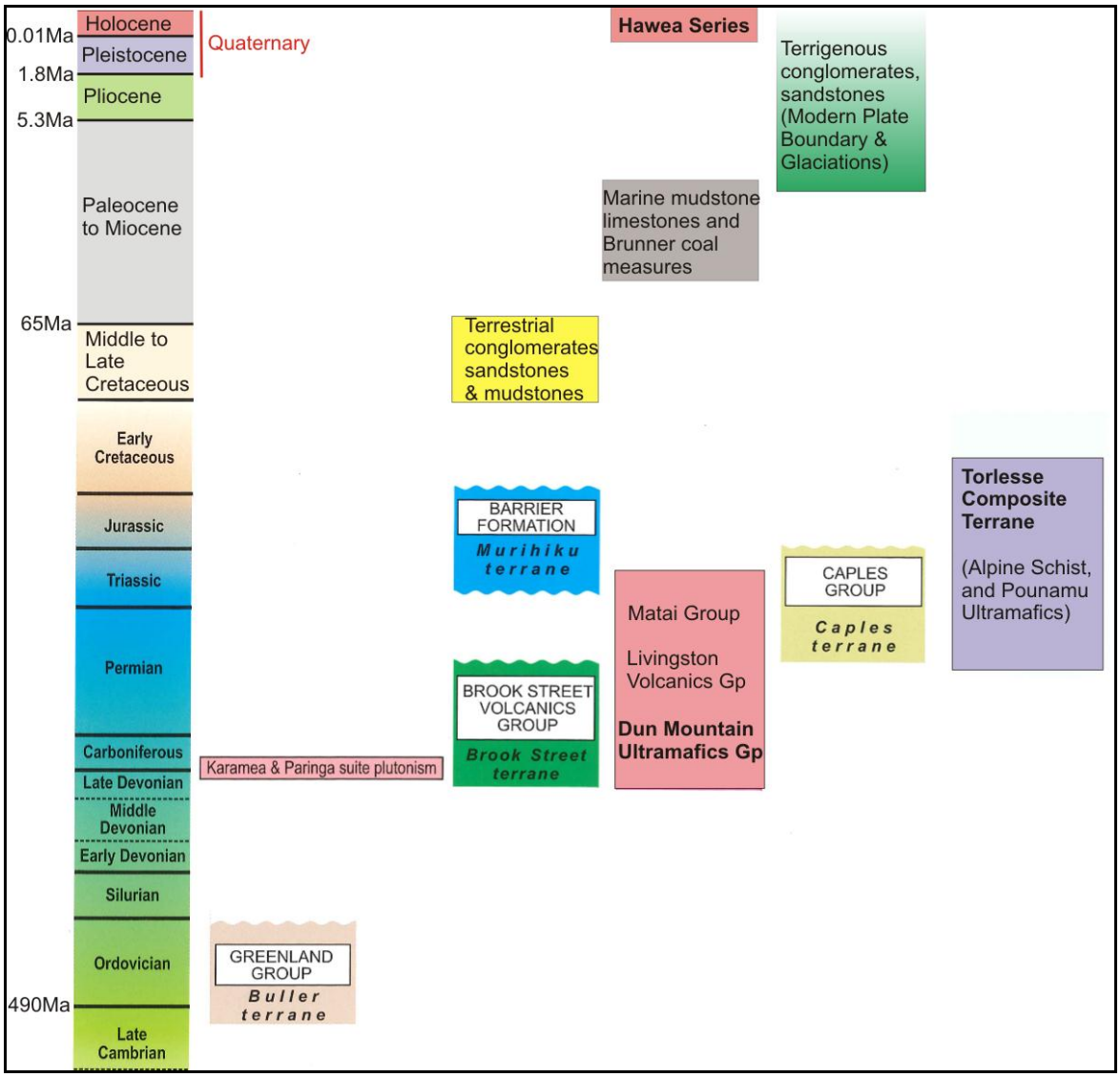

Figure 3-2 Simplified stratigraphic relationships of geological terranes and units relevant to the South Westland Continental Margin. Modified from Rattenbury et al. (2010)

3.2.1 Late Cambrian to Early Cretaceous (Basement Rocks)

Basement units in South Westland catchments are divided into the Western and Eastern provinces by the Alpine Fault. The Western Province is a mainly Early Paleozoic province (Rattenbury et al. 2010) of which the Greenland group is the only major outcrop in the region. The Eastern Province is represented in the region by up to five Late Paleozoic to Early Cretaceous terranes related to convergent tectonics and volcano-sedimentary processes at the Gondwana margin (Mortimer 2004;

Rattenbury et al. 2010; Coombs et al. 1976). The most extensive Eastern Province terranes outcropping in the region are the Dun Mountain Ultramafics and the Torlesse Composite terrane.

Greenland group

The Greenland Group was deposited at the paleo-pacific Gondwana margin in the Early Ordovician as a widespread turbidite succession (Laird 1972). It is comprised of quartz rich, greenish-grey sandstones and mudstones with modal quartz of 30 – 35 %, < 6 % plagioclase, and varying amounts of sedimentary and volcanic lithics (Roser & Nathan 1997; Laird 1972). During the Late Ordovician to Silurian the Greenland group was deformed and metamorphosed to lower green schist facies (Laird 1972; Rattenbury et al. 2010). Greenland Group outcrops occur to the west of the Alpine Fault in the middle to lower reaches of several South Westland catchments (Figure 3-3). Notable outcrops occur in the Cascade River and Jackson Bay, and the Paringa, Waiho, Waitaha, and Hokitika river catchments.

Brook Street and Murihiku Terranes

These terranes form minor outcrops in the study area, with elongate, northeast trending slices up to 2 km wide found only in the upper Cascade catchment. The Brook Street terrane is dominantly Early Permian mafic to felsic volcanics and related sedimentary rocks (Rattenbury et al. 2010). The Murihiku terrane is mainly volcaniclastic sedimentary rocks (Mortimer 2004).

Dun Mountain Ultramafics Group

The Dun Mountain Ultramafic Group (DMG) outcrops as a major lens up to 30 km long and 4.5 km wide in the study region between the Cascade and Arawhata rivers (Figure 3-3) (Rattenbury et al. 2010). The DMG is essentially a ‘slab’ of Permian oceanic crust tectonically emplaced against the Brook Street terrane (Coombs et al. 1976; Mortimer 2004). A diverse range of ultramafic to mafic lithologies are present, including: olivine pyroxenite, wherlite, lherzlite, harzbergite, and gabbro (Coombs et al. 1976; Rattenbury et al. 2010). Zones of serpentinite occur throughout and the group has endured two phases of metamorphism (Rattenbury et al. 2010). The DMG supplies the Cascade, Martyr, and Jackson rivers with unstable ultramafic to mafic minerals such as olivine, orthopyroxene, clinopyroxene and chromium spinels (Bradley et al. 2002; Morton & Smale 1990).

Livingston Volcanics Group, Maitai Group, and Caples Terrane

These Middle Permian to Triassic age units (Rattenbury et al. 2010) outcrop as minor elongate slices or wedges in the Cascade River upper catchment (Figure 3-3). The Livingstone Volcanics Group is comprised of gabbro and basalt outcrops, while the Maitai Group is dominated by volcanogenic sediments (Rattenbury et al. 2010; Mortimer 2004). The Caples terrane is composed of weakly metamorphosed volcaniclastic greywacke and argillite units which outcrop on the eastern side of the Dun Mountain Ultramafics (Figure 3-3) (Mortimer 2004).

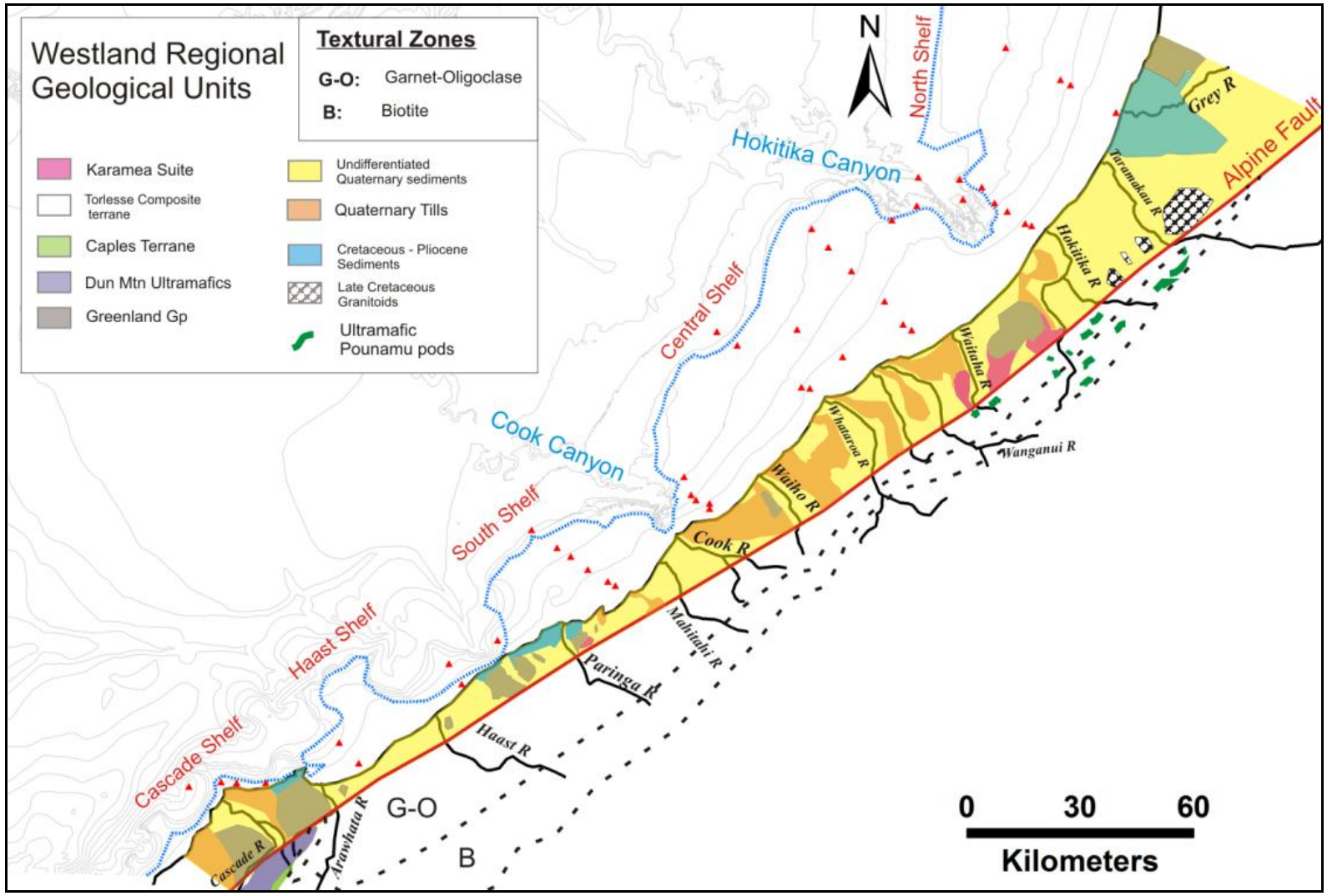

Figure 3-3 Regional geology of the SWCM catchments. Based on the work of Rattenbury et al. (2010), Cox & Barrell (2007) and Nathan et al. (2002).

Torlesse Composite terrane and the Alpine Schist

This is the most important lithology for the SWCM since the middle to upper catchments of most rivers discharging to the SWCM are dominated by this composition. The Torlesse Composite terrane is mainly composed of quartzofeldspathic, indurated sandstones and argillites (commonly termed greywackes) found east of the Alpine Fault (Rattenbury et al. 2010; Mortimer 2004). The terrane accumulated at the Gondwana margin between the Late Permian to Early Cretaceous as deep-water submarine fans sourced from a continental volcanoplutonic arc (Roser & Korsch 1986; Mortimer 2004). Within the Torlesse Composite terrane, an older Rakaia and a younger Pahau Terrane are distinguished (Bradshaw 1989), but only the Rakaia Terrane is present in the SWCM catchments.

Alpine Schists: Large parts of the Rakaia terrane were subjected to regional low grade metamorphism that peaked during the Jurassic to Cretaceous. This produced the semi-schists and schists of the Haast schist group common in the South Island (Vry et al. 2008). The Alpine Schist is part of this Haast schist group and runs east of and sub parallel to the Alpine Fault as a 12 - 25km wide belt (Figure 3-4) (Vry et al. 2008; Mortimer 2000).

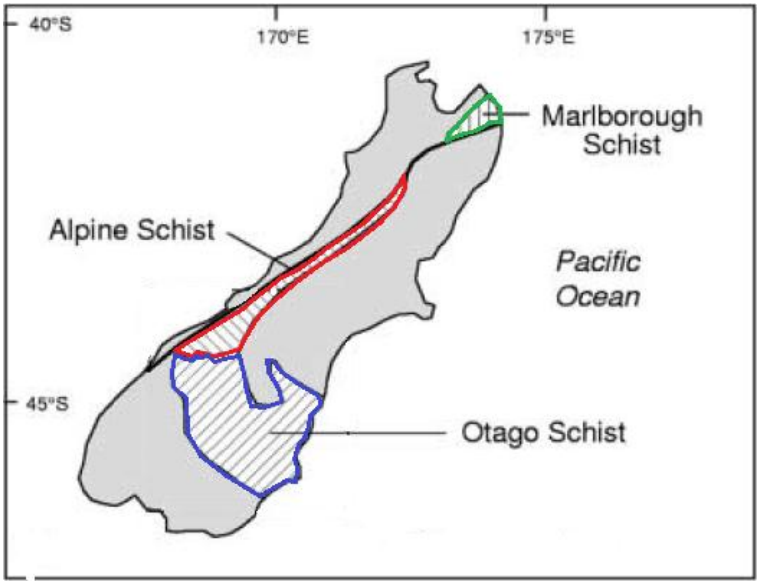

Figure 3-4 Subdivisions of the Haast Schist Group showing the Alpine Schist (red area), the main lithology of the middle to upper catchments of rivers discharging to the SWCM After Mortimer (2000).

Rapid uplift and denudation as the Southern Alps formed exposed the Alpine Schists, which essentially represent the 'upturned and obducted' edge of the Pacific plate along the Alpine Fault (R. H. Grapes 1995). Metamorphic grade in the Alpine Schists increases from east to west, from chlorite, biotite, garnet, and finally to an oligoclase zone at the Alpine Fault (Figure 3-3) (R. H. Grapes 1995; Vry et al. 2008).

The Alpine Schists generally consist of a fine grained, foliated matrix of quartz and muscovite with porphyroblasts ranging from ilmenite, titanite, chlorite, biotite, epidote, plagioclase (albite), garnet, and amphiboles (Vry et al. 2008). Regional variations of the above mineralogy is common, for example, in the Haast River region green schists and amphibolites become common due to a basaltic volcanogenic protolith (Cooper & Lovering 1970). Minor bodies incorporated into the Rakaia Terrane during accretion include metamorphosed limestone, chert, mudstone and ultramafic remnants of oceanic crust (Nathan et al. 2002).

Pounamu Ultramafics: In the Hokitika and Waitaha catchments Pounamu Ultramafics represent metamorphosed remnants of oceanic crust (including serpentinite, gabbro, and metabasite) hosted in the Rakaia terrane (Figure 3-3) (Nathan et al. 2002). These outcrop as northeast trending, elongate lenses up to several kilometres long and several hundred metres wide, and contain the rare, highly prized Pounamu (greenstone or nephrite). The Pounamu Ultramafics have been associated with chromium rich spinels found in the Hokitika and Waitaha River sediments, and local beaches (Bradley et al. 2002; Ooi 1982).

Granitoids

All Granitoids are restricted to the western side of the Alpine Fault. Late Devonian to Early Carboniferous granitoids from the Karamea suite outcrop mainly in the Waitaha River area in the study region (Figure 3-3). They are dominantly muscovite - biotite granites, tonalites, and orthogniesses which intrude the Greenland Group (Nathan et al. 2002; Cox & Barrell 2007). South of the Wanganui River, granitic outcrops are rare. An exception is the Paringa Suite in the Paringa River, a relatively large outcrop of Devonian age biotite granodiorite (Rattenbury et al. 2010). In the north, relatively large outcrops of Early Cretaceous biotite – muscovite granites and granodiorites occur in the Arahura and Taramakau river catchments (i.e. Hohonu Ranges) (Cox & Barrell 2007).

3.2.2 Cretaceous to Pliocene Sedimentary Rocks

Outcrops of Cretaceous to Pliocene rocks in SWCM catchments are generally restricted to limited coastal outcrops northwest of the Alpine Fault (Figure 3-3) (Rattenbury et al. 2010). Most notable outcrops occur in the Jackson Bay region, the Moeraki to Paringa River region, and extensively in the lower Grey River catchment. The majority of these rocks are sedimentary, related to the extension and separation of Zealandia from Gondwana (Middle - Late Cretaceous breccias, conglomerates and quartz rich coal measures), its subsequent erosion and extension to a low lying landscape (ca. Eocene – Oligocene calcareous mudstones, muddy limestones, and Brunner coal measures), and the early development of the modern plate boundary (Early Miocene – Pliocene conglomerates, sandstones, and mudstones) (Nathan et al. 1986; Rattenbury et al. 2010). Seismic evidence and petroleum exploration wells (Waiho-1 and Harhari-1exploration wells) indicate the Cretaceous to Pliocene sediments continue offshore, comprising up to 3-5 km of the Western Platform (Rattenbury et al. 2010; Cox & Barrell 2007).

3.3 METHODS

Mineral content was investigated using a combination of binocular examination of loose sand samples (> 63 μm), thin section descriptions of bulk samples, point counts of the sand fractions. Details of the specific sample treatments are provided in Appendix A5. Descriptions of the sand fraction in all shelf and canyon samples was made from the > 63 μm fraction only. This included all samples from the Cascade and Haast shelves. This initial survey provided a means to focus petrographic studies and other analyses such as geochemistry.

Bulk thin section descriptions: Thin sections for bulk sediment descriptions and point counts were made from the loose sediments in epoxy moulds following the methods in Appendix C1. The mineralogy of selected bulk samples from the South, Central, and North shelves and canyon heads were described and modal estimates of mineralogy were made using percentage estimate charts. Thin sections from beaches and rivers were described also but it must be noted these are form the sand fraction only. These descriptions are provided in Appendix C3.

Point counts: All point counts were made on the > 63 μm fraction in shelf and canyon samples. Beach and river samples were sieved for the very fine sand to very coarse sand fraction so as to be comparable to the shelf and canyon point counts. A total of 300 grains per slide were counted on a Prior James Swift point counter. Thin sections for point counting were stained for plagioclase and alkali feldspars using the methods from Lewis & McConchie (1994). This was useful for distinguishing untwinned plagioclase and Quartz. In several cases, the stain was poor or the feldspars were altered, making distinctions between feldspar varieties difficult. Difficult grains were classed as 'undifferentiated' feldspars in point counts. Samples able to be point counted were restricted partly due to a lack of sand sized grains and/or the small sample size of the middle to outer shelf samples. A total of 12 shelf, 9 canyon head, and 10 river and beach thin sections were point counted (Figure 3-1). Point count results are provided in Appendix C4.

Heavy minerals:

The heavy mineral percentage was determined by the liquid separation technique (using lithium heteropolytungstate, LST) from the very fine to fine sand fractions (63 – 250 μm). Restriction to these fractions allowed for comparisons to other heavy mineral studies (i.e. Bradley et al., 2002; Chew, 1981), and removed silts and clays which can clog up the heavy liquids. In addition to the shelf transects, the Haast to Cascade shelves, and beach and river samples were included in the heavy mineral separations. The Heavy mineral separation methods and results are provided in Appendix C10 and C11.

3.4 MINERALOGY

3.4.1 Quartz

Shelves: Quartz is the most common detrital grain in SWCM shelf sediments, averaging 45 % of the sand fraction, and ranging from 32 to 60 % (n=12). Grains are typically sub-angular to sub-rounded (Figure 3-15). Across shelf trends in quartz content are variable on the shelves. The Central Shelf shows little to no decrease in quartz content with depth except on Transect C (Figure 3-5 & Appendix C4). Similarly, on the North Shelf there is little change in quartz content on the inner and middle shelves. The South Shelf (Transect F) displays a stronger across shelf trend, with 60 % quartz in the sand fraction, which is 85 - 95 % of the bulk sediment on the inner shelf, and decreases to 48% at middle shelf depths.

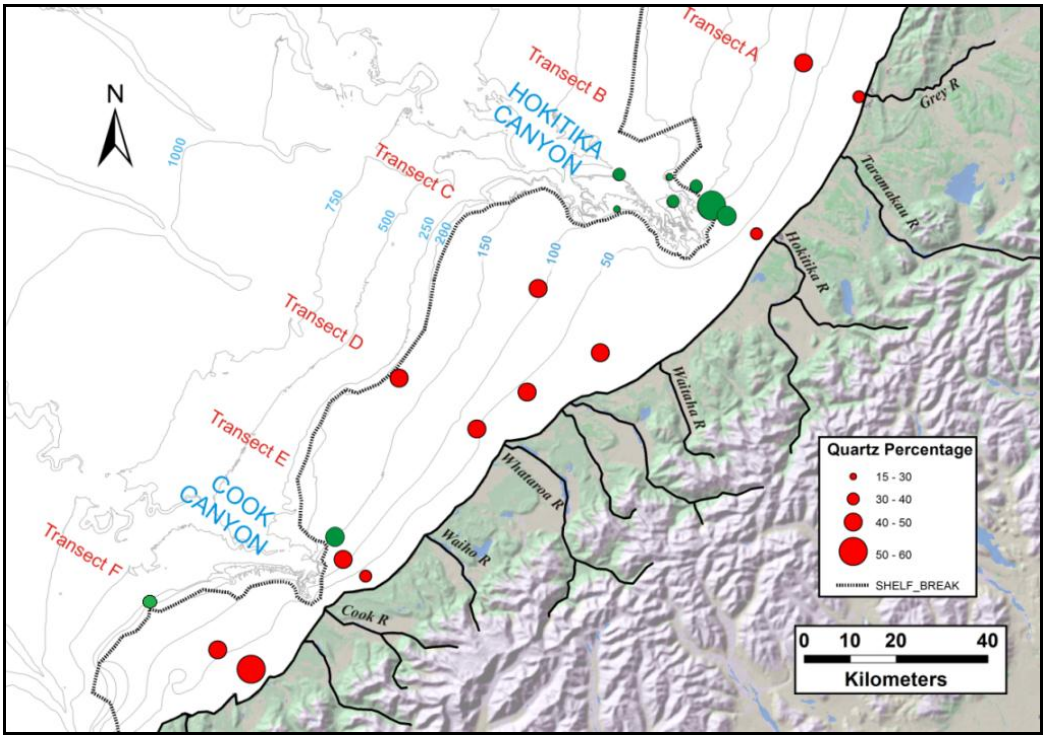

Figure 3-5 Percentage of quartz in the sand fraction of shelf and canyon surface sediments on the SWCM. Expressed as a percentage of 300 grains. Green circles represent canyon head samples.

Straight and undulose extinction quartz grains co-dominate shelf sediments, averaging 44 and 42 % of quartz grains in the sand fraction respectively (Figure 3-6). Polycrystalline quartz is less common, averaging only 13 % quartz in the sand fraction. A weak increase in undulose quartz from the inner to middle shelf is common, especially on the Central and South shelves (Figure 3-6). A weak, along shelf trend in the proportion of undulose vs. straight extinction quartz exists. Here, the North Shelf is dominated by undulose quartz while on the Central and South shelves straight extinction quartz dominates. Polycrystalline quartz is variable with no obvious regional or across shelf trends.

Canyon Heads: In the canyon heads, total quartz content is highly variable ranging from 19 – 53 %, of the sand fraction (Figure 3-5). Quartz grains typically range between 125 – 300 µm in the sand fraction (Figure 3-16 and Appendix C3). Larger quartz grains are common at 94 m water depth in the east of the HCH, with grains are up to 1-2 mm in diametre. In the south of the CCH at 256 m depth, yellow stained quartz grains between 1-3mm in diametre are common. A weak trend in the HCH shows that the quartz % of the sand fraction is higher in the eastern samples (>40%), and lower to the west (<40%). Straight and undulose extinction quartz grains co-dominate in the canyons heads. Within the HCH, undulose quartz tends to be the dominant quartz type, especially in the eastern sediments (Figure 3-6, H848, H850, H851, and B469). In contrast the CCH is predominantly straight extinction quartz grains.

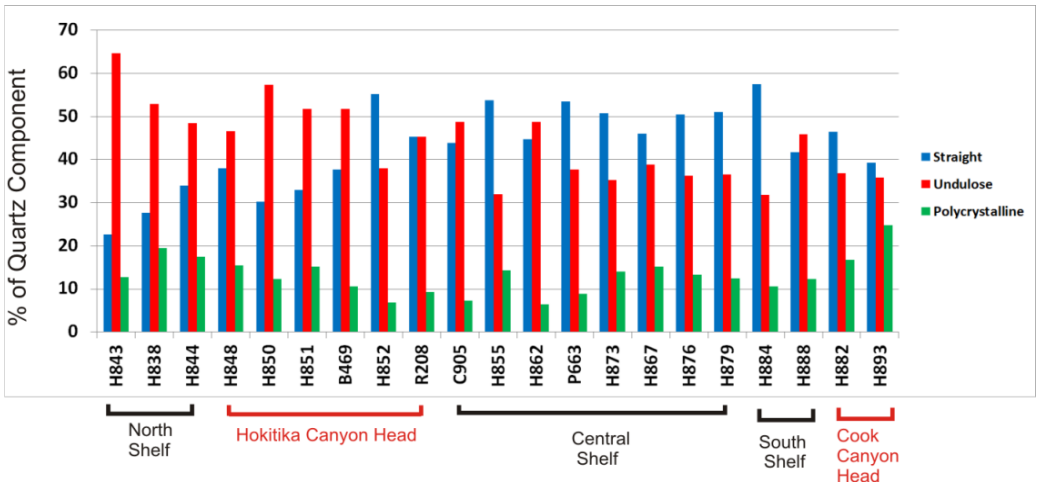

Figure 3-6 Graph showing the percentage of straight, undulose, and polycrystalline quartz varieties in the quartz component of the sand fraction in shelf and canyon head surface sediments.

Beaches and Rivers: Straight and undulatory quartz varieties are typically even in proportion in the North and Central region beaches and rivers (Hokitika beach to Gillespies beach). In the South region (Bruce bay to Jackson Bay beach) these proportions are more variable with polycrystalline quartz more common (Figure 3-7).

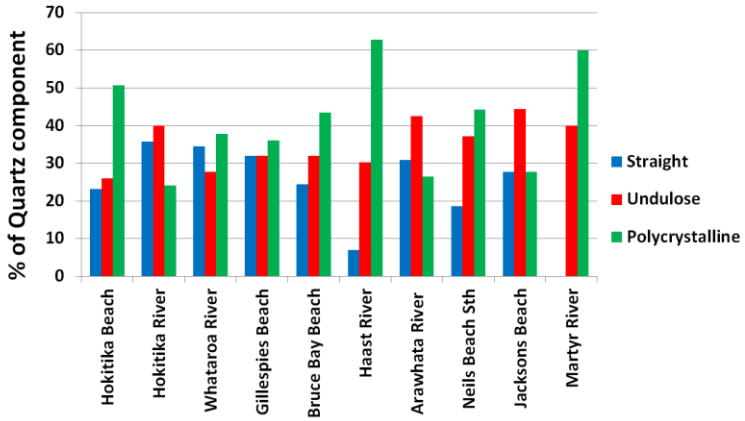

Figure 3-7 Graph showing the percentage of straight, undulose, and polycrystalline quartz varieties in the quartz component of the sand fraction in rivers and beaches from the Westland region.

3.4.2 Feldspars

The average feldspar content in the sand fraction of SWCM shelf sediments is ca. 5 % (Appendix C4). The inner shelf contained 5-10% feldspar compared to the middle shelf sediments with < 5% in the sand fraction. Plagioclase co-dominates with the unidentified feldspars in the sand fraction on the shelf with 2.5 and 2 % respectively. Plagioclase probably comprises most of these unidentified grains. This is supported by XRD results which identify albite (the sodium plagioclase end member) as the main feldspar in bulk samples (Appendix C8). Partial to complete feldspar alteration to clays and sericite is common in many samples.

Feldspar content in canyon head sediments is variable (2- 9 % of the sand fraction) and plagioclase is the dominant variety. A single microcline grain was identified at 188 m depth in the HCH. In Westland River and beach samples, feldspar content is typically < 10 % of the fine sand to coarse sand fraction (Appendix C4). Rivers contained higher feldspar contents than beaches typically and plagioclase was the most common variety observed in both environments.

3.4.3 Lithics

Metamorphic lithics are the most common lithics in the SWCM sediments,. Metamorphic lithics were distinguished in point counts based on the following grain size boundaries; schists had a consistent grain size greater than fine sand (>250 μm), phyllites between fine sand to coarse silt, and slates where foliation was finer than coarse silt (< 31μm). Only the canyon heads contained coarse siliciclastics lithics (medium sand to gravel size) (Appendix C3).

Shelves: Lithics are a common grain type in shelf sediments, averaging 12 % of the shelf sand fraction (Appendix C4). Generally, shelf lithics are sub-rounded to rounded grains that become less common across shelf with increasing depth. All lithics observed on the SWCM shelves were generally medium sand sized or finer. The inner shelf sediments have the highest lithic content, averaging 14% of the sand fraction, while the middle shelf is lower with only 8.5 % (

Figure 3-8). Metamorphic lithics are the dominant lithic on the SWCM, primarily in the form of quartzofeldspathic schists to slates (Figure 3-15, H884). Moderate to strong foliation defined by micas and quartz is clearly present in many clasts. Phyllites are the most common variety, followed by schists and slates (Figure 3-9). The inner shelf is high in schist lithics compared to the middle and outer shelves while slates are more common on the middle shelf (Figure 3-9). Sedimentary lithics were uncommon in shelf sediments and no plutonic or volcanic clasts were observed.

Canyon heads: Canyon head sediments are characterized by more variable and coarser lithics than on the shelves. Within the sand fraction, lithics are usually poorly sorted, sub-rounded to rounded clasts with a modal grain size of 300-500 μm (Appendix C3). Pebble sized lithics were common at H848 and H852 in

the HCH (Figure 3-16, H848). These were dominantly dark grey-black schistose pebbles up to 10mm in length, followed by transparent to yellow quartz-feldspar lithics with minor amounts of dark minerals. South of the CCH, lithics up to 2-3mm in size (granule) are common at 256 m depth (H893). The average lithic content in canyon heads is 13% of the sand fraction (

Figure 3-8 and Appendix C3). Metamorphic lithics are the dominant variety, with quartzofeldspathic phyllites and slates typical (Figure 3-9). Only in sediments at H848 in the HCH, and H893 to the south of the CCH do schists dominate over phyllites.

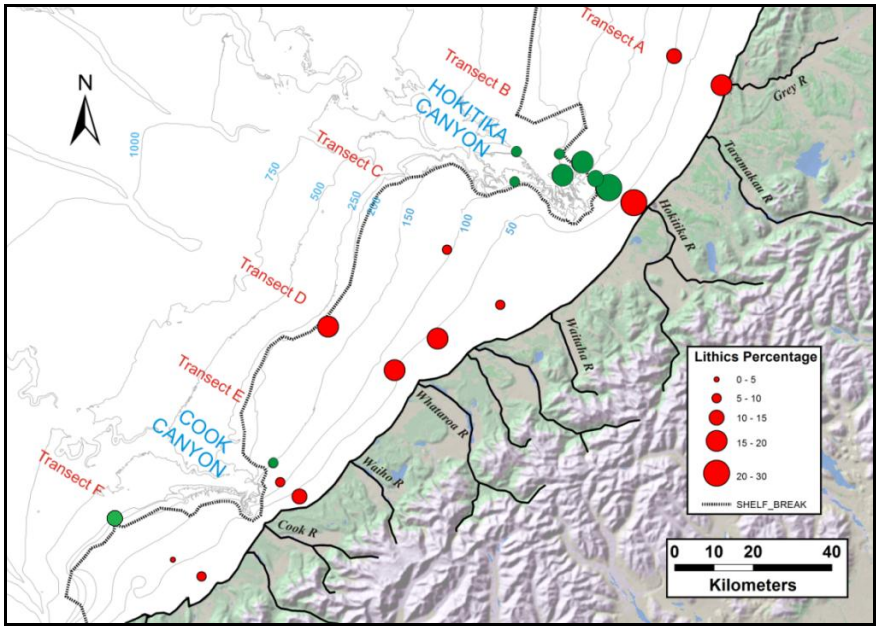

Figure 3-8 Percentage of lithic grains in the sand fraction of SWCM shelf and canyon surface sediments Green circles represent canyon head samples.

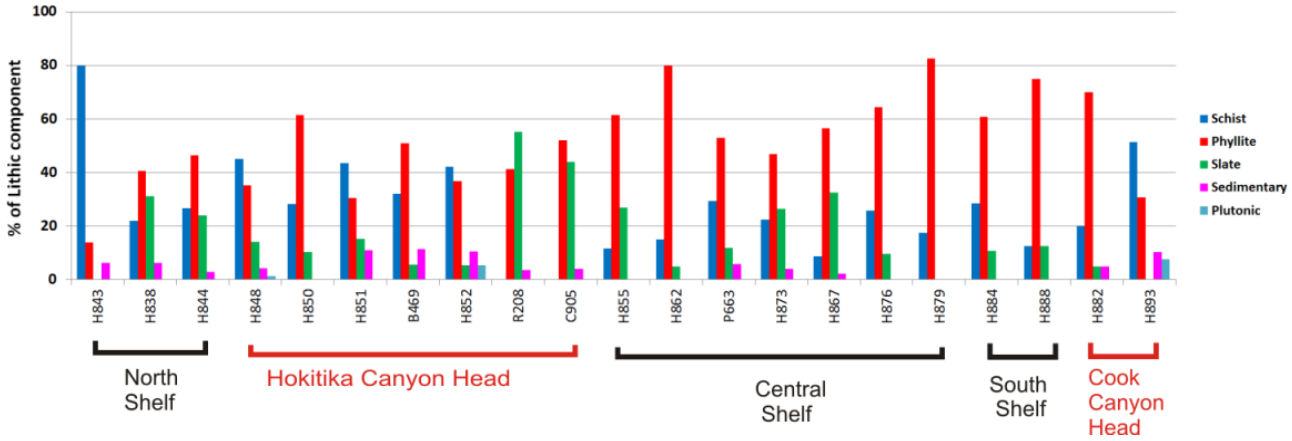

Figure 3-9 Graph showing the percentage of lithic varieties in the lithic fraction of the sand fraction in SWCM shelf and canyon samples. Based on point count data.

The south rim of the HCH contains no schist lithics, in contrast to the northern rim sediments. Slates are common in the HCH (average 2.5%), but rare in the CCH. Plutonic and sedimentary lithics are present in both canyon heads, but are rare (Figure 3-9). A single seperntinised metamorphic lithic was present in the southern CCH sample (H893).

Beaches & Rivers: Lithics in SWCM beaches and rivers are dominated by metamorphic lithics comparable to those described for the shelf and canyon heads (Figure 3-10). No strong regional trend is apparent except for low total lithic counts in the Arawhata River and Neils Beach samples (Appendix C4 & Figure 3-10). Quartzofeldspathic schists and pyhllites are the dominant metamorphic lithic varieties in SWCM .

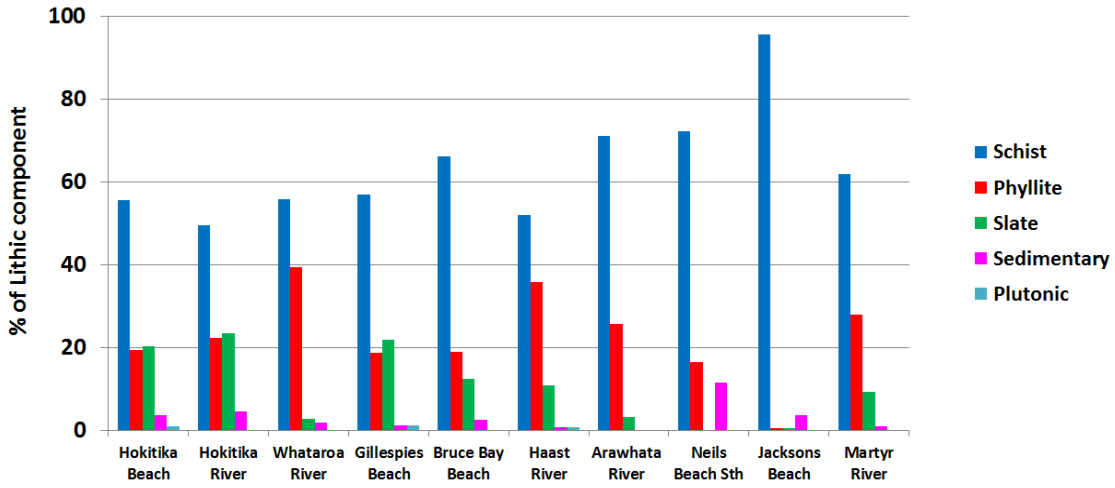

Figure 3-10 Graph showing the percentage of lithic varieties in the lithic fraction of the sand fraction in SWCM beaches and rivers.

At Jacksons and Neils beach, sedimentary lithics become more common (2-3% of the sand fraction). Rare serpentinised metamorphic lithics were identified in the Hokitika River, Bruce Bay beach, and most sediment from the Haast to Cascade region (Appendix C3). Mafic minerals such as olivine and pyroxene were commonly observed in these serpentinised lithics.

3.4.4 Micas

Shelf: Shelf micas are typically tabular, elongate grains, averaging 11.5 % of the sand fraction (Appendix C4). Shelf micas have a modal size of 200-300 µm with a maximum size of 600 µm in the shelf sand fraction. Partial alteration to clay is common, with chlorite alteration of biotite also present. An increase in mica content with water depth exists on most shelf transects, especially on the South and Central shelves (Figure 3-11). The inner shelf sand fraction contains an average of 8% mica while the middle shelf (50 - 150 m depth) averages is 15.5% (Figure 3-15, H862). The middle shelf micas are often more elongate and platy than the inner shelf micas (Appendix C3). No clear overall dominance of biotite or muscovite exists

in SWCM shelf sediments (Figure 3-11). Chlorite is less common in shelf sediments than the other micas (<3 % of sand fraction) and is occasionally observed as an alteration product of amphibole or pyroxenes.

Canyon heads: Mica content in the HCH contrasts between the north and south rims. The north rim sediments (i.e. H848, H850, H851 & H852) have a very low total mica contents in the sand fraction (<6%). Conversely, at 241 m depth on the south rim (C905) and 450 m depth on the canyon floor adjacent to the south rim (R208), mica content is much higher with 26.7 and 16.5 % respectively in the sand fraction (Figure 3-11 & Figure 3-12).

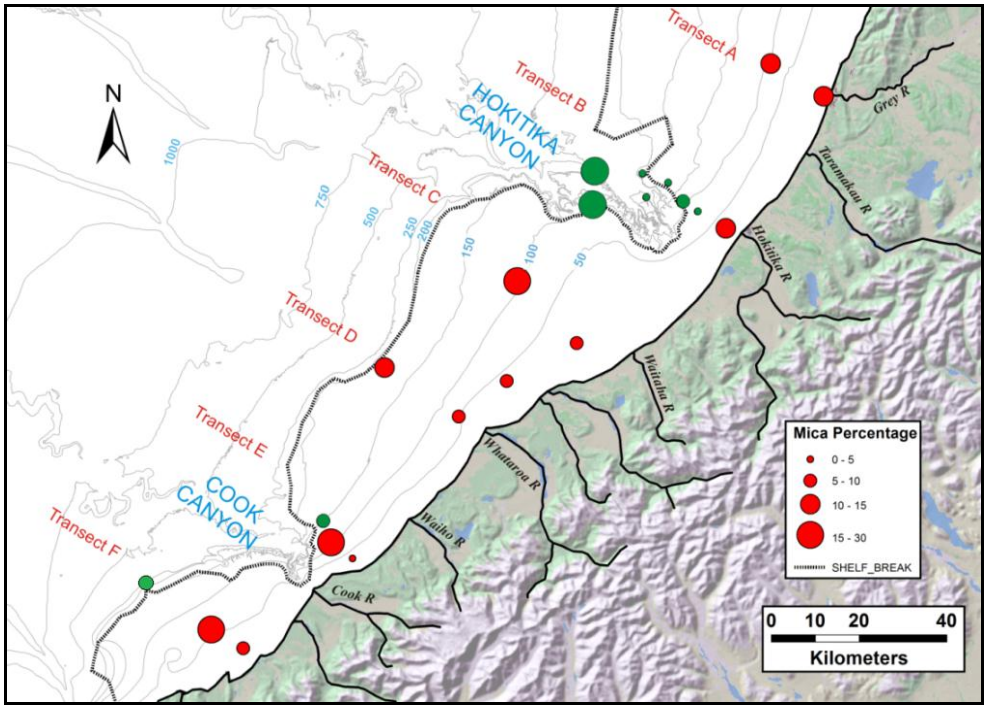

Figure 3-11 Mica percentage (muscovite and biotite) in the sand fraction of SWCM shelf and canyon surface sediments. Green circles represent canyon head samples.

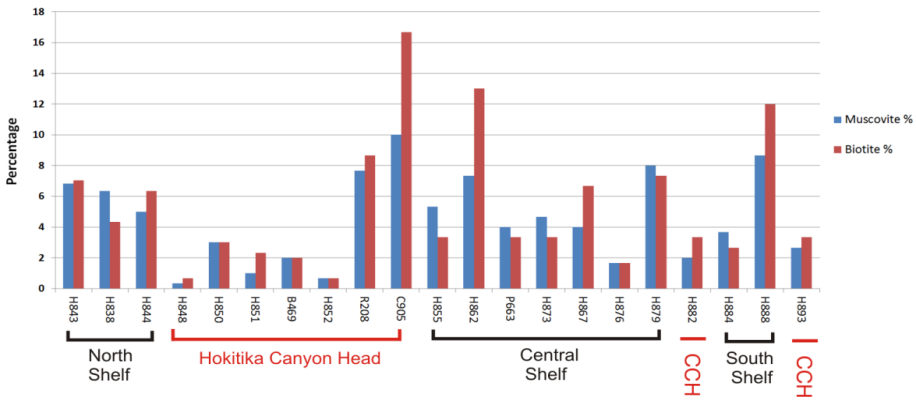

Figure 3-12 Graph showing the percentage of muscovite and biotite in the sand fraction of SWCM shelf and canyon head sediments. CCH = Cook Canyon head.

Like the HCH north rim sediments, CCH mica content is around 5-6%. Neither biotite nor muscovite show any clear dominance in the canyon sediments (Figure 3-11). Chlorite is rare in canyon head samples except in the south HCH rim sample (R208) where up to 2 % chlorite is present (Appendix C4).

Beaches & Rivers: As expected, mica content in beaches is low, typically <4% in the sand fraction (Appendix C4). Neils and Bruce Bay beaches have mica levels over 3 % while other beaches are <1%. Rivers had higher but more variable mica content. The Hokitika, Whataroa and Arawhata rivers had the most mica (9-13%). In most river and beach samples, muscovite is more dominant, except in the Hokitika River where biotite is more common.

3.4.5 Heavy minerals

Heavy minerals are accessory minerals with a specific gravity of >2.9. All heavy mineral contents of the SWCM samples are reported as a percentage of the fine sand to very fine sand fraction. These are displayed in (Figure 3-13). Individual heavy mineral identifications are based on point counts of the thin sections used to identify other minerals in this chapter. Hence, individual heavy mineral varieties are expressed as percentages of the sand fraction (Figure 3-14).

3.4.5.1 Shelf

Heavy mineral percentage: Heavy minerals comprise <10% of the fine to very fine sand fraction in shelf sediments (Figure 3-13 and Appendix C11). A weak to moderate seaward decrease in heavy mineral content is present on the three shelf regions (Figure 3-13). This trend is strongest on the South Shelf (Transect F) and in the south of the Central Shelf (Transect E). Average heavy mineral contents in the fine to very fine sand fraction falls from ~16 % on the inner shelf, to ~7.5 % on the middle shelf (50 -150 m depth), to ~ 4 % on the outer to upper slope samples. At 21 m depth on transect E, sediments contain an exceptionally high level of heavy minerals (~44%). The Haast and Cascade shelves appear more enriched in heavy minerals (Figure 3-13).

Heavy mineral types: Opaque minerals are generally minor, with < 2 % in the shelf sand fraction (Figure 3-14). An exception is on the inner shelf of transects C and E, where 3 and 9 % were identified respectively. Epidote was usually observed as individual grains, but sometimes as granular clusters. Typically < 3 % epidote grains were present in the shelf sands. On the inner shelf of Transects C and E, epidote content was up to 9 %.

Due to the fine grain size of shelf sands (usually very fine – fine sand), distinction between amphiboles and pyroxenes was difficult, thus they were identified as a single group. They typically occur as pale green, pleochroic, individual grains, with partial to extensive alteration to clays and chlorite. In larger grains where cleavage was present, amphibole was commonly identified (Appendix C4). No across shelf trend is present on the North Shelf and transects C and D on the Central Shelf. A weak seaward decrease in amphibole and pyroxene is present on transect E and the South Shelf (Figure 3-14). Garnet was

observed on the shelf but was rare. An exception occurs at 21 m depth on Transect E where colorless to pale pink, sub-angular to sub-rounded grains comprise 2-3 % of the sand fraction.

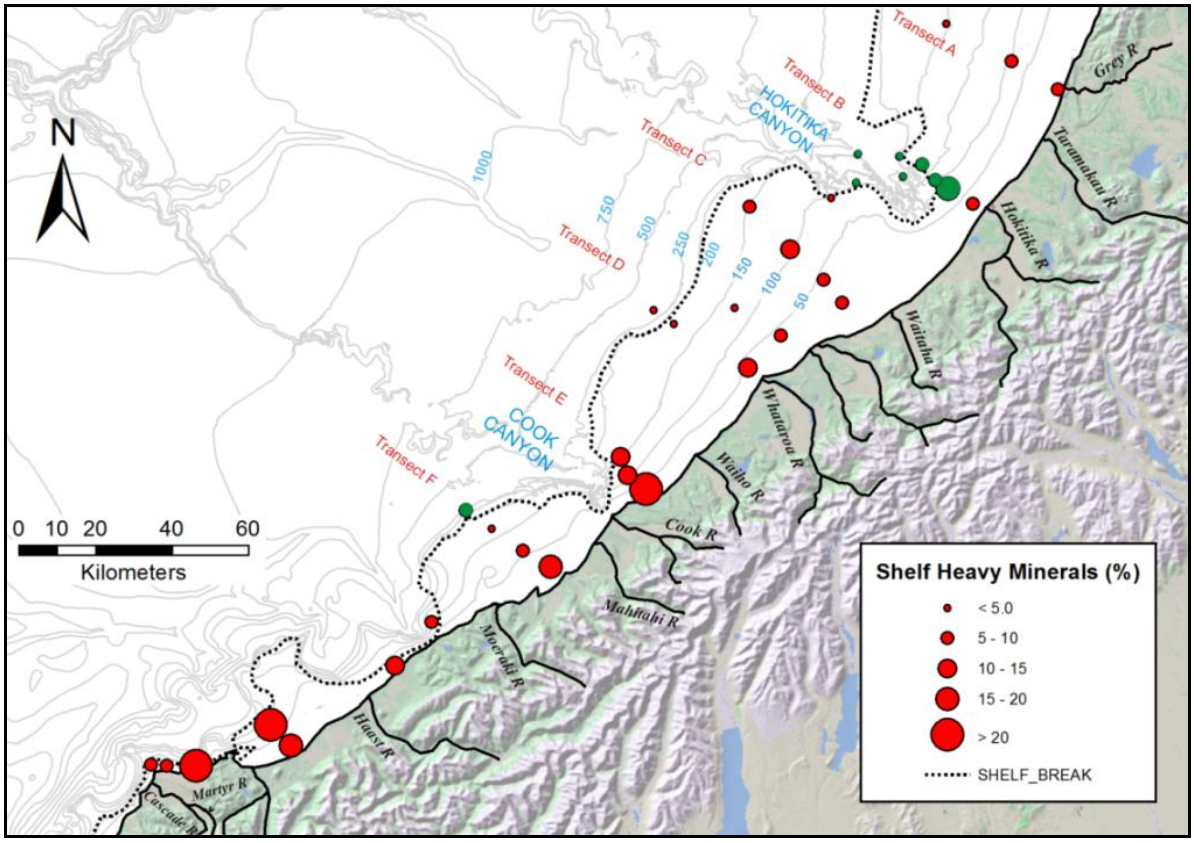

Figure 3-13 Map of heavy mineral percentages in the fine to very fine sand fraction in SWCM shelf and canyon surface sediments. Green circles represent canyon head samples. Determined by the heavy liquid separation technique, see Appendix C11 for results.

3.4.5.2 Canyon heads

Heavy mineral percentage: The average heavy mineral percentage in canyon heads is 7 % (n=10) of the fine to very fine sand fraction (Figure 3-13). In the shallower HCH north rim samples, heavy mineral contents were high (up to 17% of fine to very fine sand fraction). With increasing depth, heavy mineral content on the north HCH rim falls to between 3-6 % (Figure 3-13). In the CCH, heavy mineral content is high, with 13.2 and 9.2 % in the north and south of the canyon.

Heavy mineral types: Opaque grains comprise less than 3% of the sand fraction in canyon point counts, and decrease with increasing water depth in the HCH (Figure 3-14). Epidote and amphiboles/ pyroxenes were uncommon in canyon had sediments, comprising < 1.5 % of the sand fraction. Garnet is present in all canyon head sediments except the deeper HCH north rim locations and all south HCH rim sites (Figure 3-14).Garnets are especially rich at 94 m depth on the HCH north rim (5.5 % of the sand fraction) (Figure

3-16, H848). Garnet content decreases offshore in the HCH. At 182 m depth on the HCH north rim, rare olivine grains up to 100 µm in size were found.

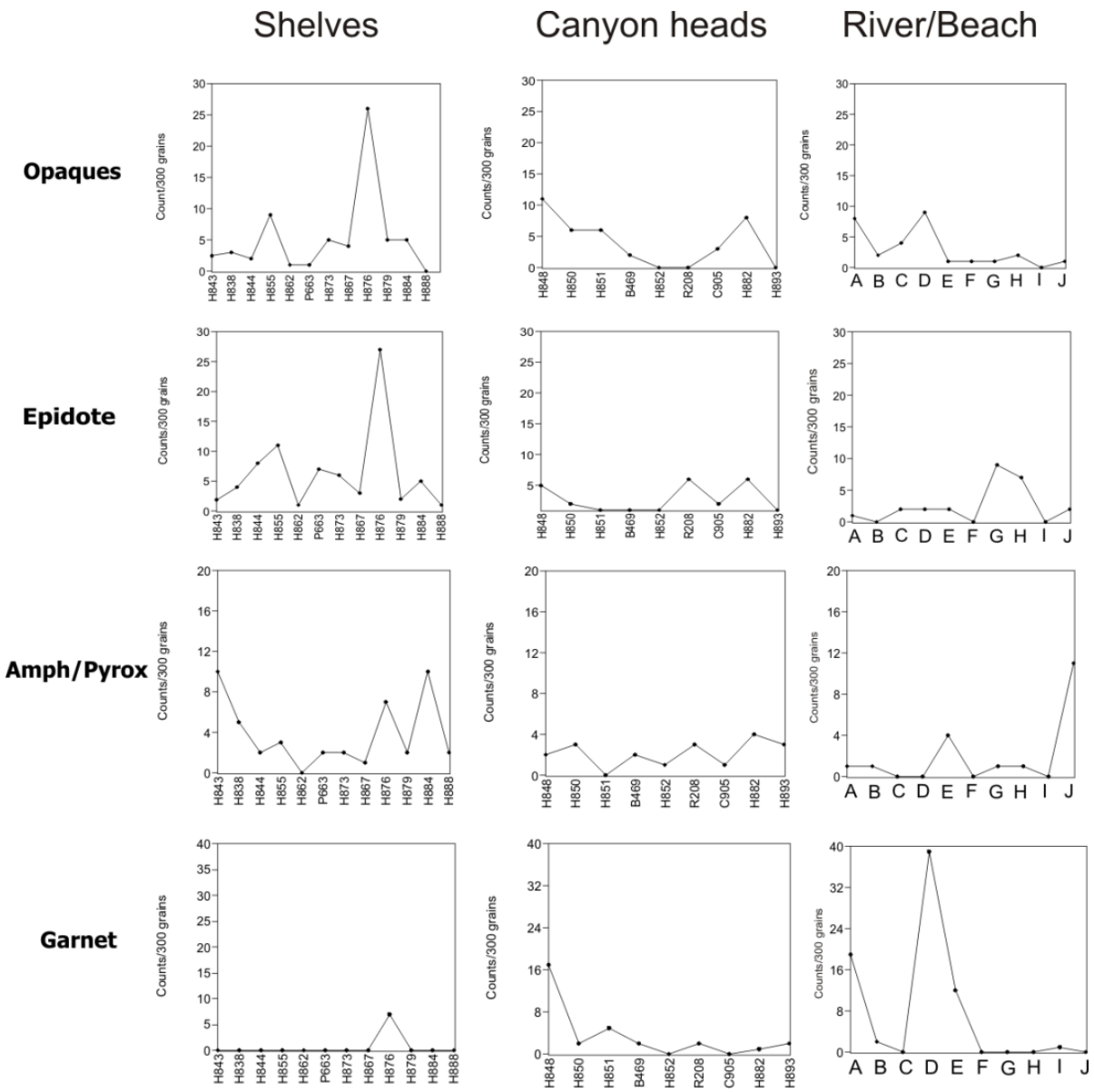

Figure 3-14 Distribution of selected heavy minerals in SWCM shelf, canyon head, and river-beach samples. All samples are plotted as percentage of the sand fraction determined in point counts. Shelf and river-beach samples are ordered approximately north (left) to south (right). For rivers –beaches, A=Hokitika beach, B=Hokitika river, C=Whataroa river, D=Gillespies beach, E=Bruce Bay beach, F=Haast river, G=Arawhata river, H=Neils beach, I=Jacksons beach, and J=Martyr river.

3.4.5.3 Beaches & Rivers

Heavy mineral percentage: Beaches were typically rich in heavy minerals, with an average of 45% in the fine sand to very fine sand fraction (n=6) (Appendix C11). SWCM rivers contained much lower heavy mineral content than beaches, with an average of 14 % in the fine sand to very fine sand fraction (n=6). The Martyr and Waitaha river samples had the highest heavy mineral contents.

Heavy mineral types: Opaque minerals comprise <3% of the sand fraction in point counts, with the highest counts in the Hokitika and Gillespies beach samples. Epidote was very rare in most samples except for the Arawhata River and Neils Beach, with 9 and 7 grains per point count respectively (Figure 3-14). Amphibole/pyroxenes are present in all samples except for the Whataroa river sample. They occur in low quantities usually with < 2% in the sand fraction, except for the Martyr river sample with 3.5%. Garnets in rivers are generally rare, but beach samples were commonly rich in garnets, i.e. (Bruce Bay, Gillespies, and Hokitika beaches). Garnets were typically colorless to pale pink, poikilitic, and sub-rounded to rounded grains. Olivine is present in the Haast – Cascade region beach and river samples, usually as rare fractured, iron oxide altered grains (Appendix C3). The Martyr River has the highest concentration of olivine (1.3% of sand fraction).

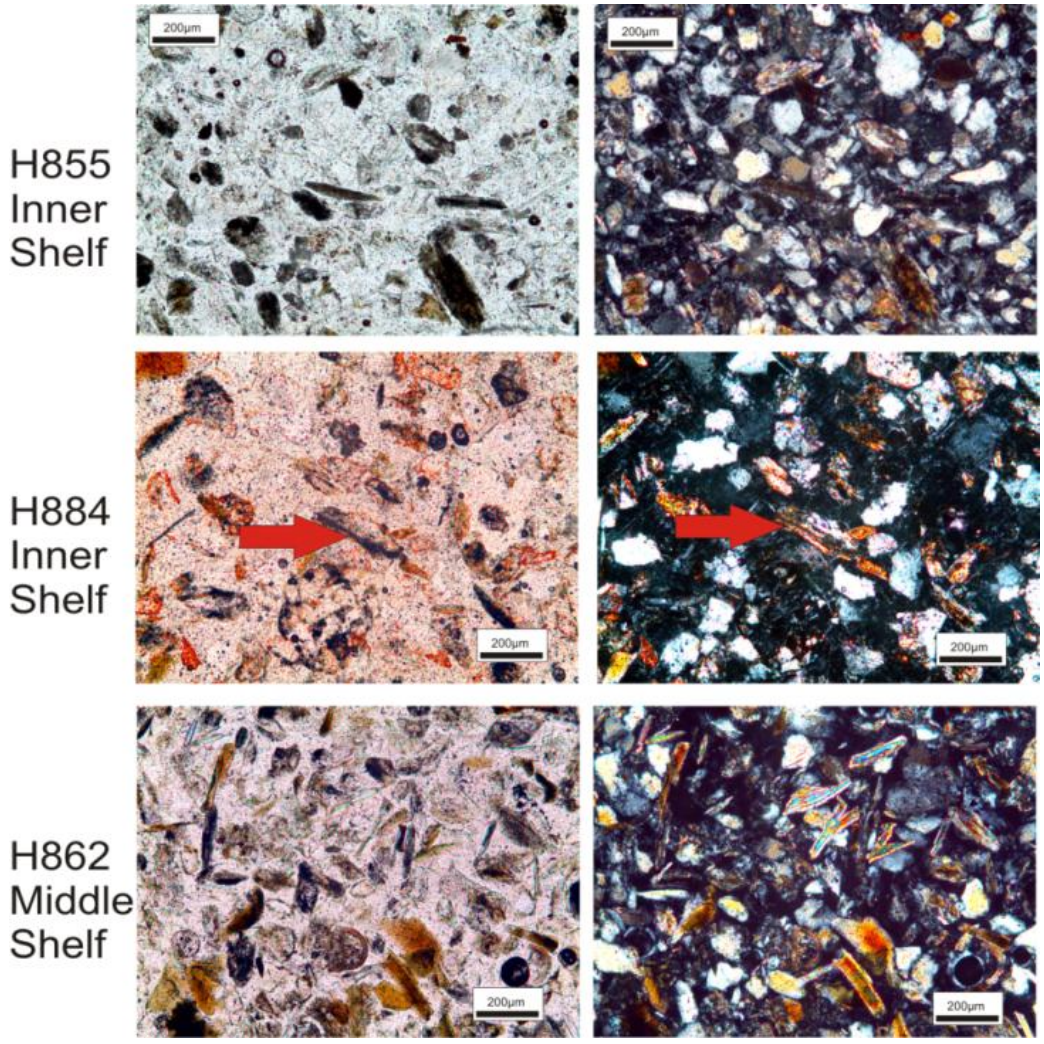

Figure 3-15 Selected photomicrographs from the sand fraction of SWCM shelf sediments. H855 and H884 illustrate the typical mineralogy of the SWCM inner shelf, with quartz, metamorphic lithics, feldspars (not shown) and micas. Red arrow in H884 highlights a typical metamorphic lithic. H862 displays the relative increase in mica content on the middle shelf. All thin sections are from the sand fraction only. Left hand image is plane polarized light, right hand image is under cross polarised light.

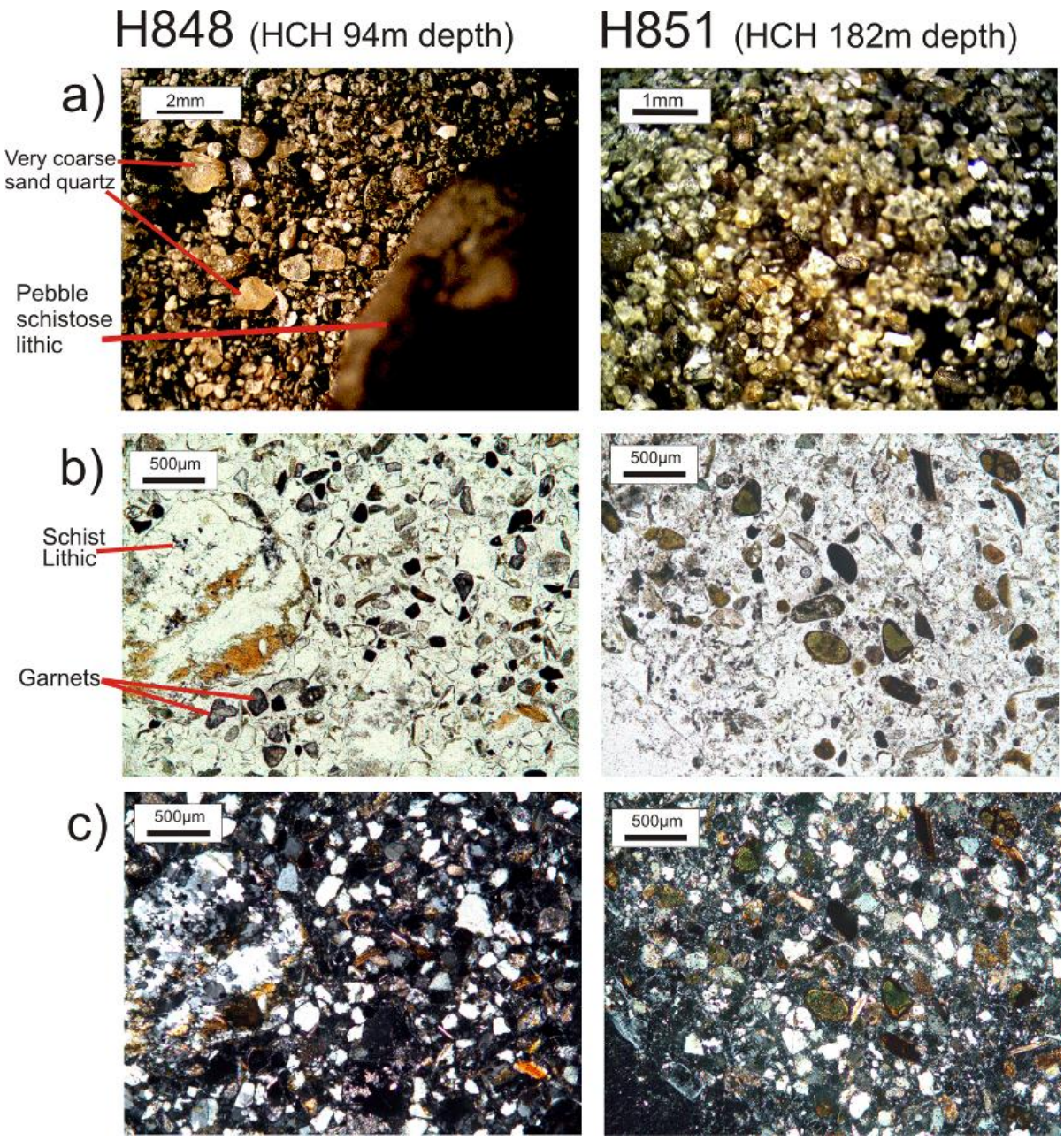

Figure 3-16 Selected photomicrographs from the Hokitika Canyon surface sediments. a) loose sand photos, b) plane polarized light, and c) cross polarized light. *H848 (94 m depth):* Note pebble sized schist lithic, the coarse, poorly sorted quartz grains and abundant garnets in H848. Mica is very rare. *H851 (182 m depth):* Coarse lithics and quartz grains less common, still poorly sorted, appearance of authigenic minerals (Glaucony).

3.4.6 Glaucony

Glaucony is a sensitive indicator of low sedimentation rates in the marine environment (Amorosi 1997; Amorosi 1995) and therefore can provide valuable information about sedimentation and dispersal on the SWCM. Glaucony grains in SWCM sediments are described from the sand fraction only via binocular examination of bulk loose sands and points counts of thin sections (Appendix C3 and C4). Photomicrographs of glaucony types from the SWCM are provided in Figure 3-18 and Figure 3-20.

3.4.6.1 Glaucony Distribution:

Shelf: On the SWCM shelves, glaucony is rare, with grains only identified on the Central Shelf transects (Appendix C3, C4 and C6). Here, they occur in sandy muds between 100 – 180 m water depth. At 173 m depth on transect D, rare glaucony rimmed siliciclastic grains are present.

Canyon heads: Glaucony is a common grain type found in the canyon head surface sediments. Glaucony grains vary in color from shades of brown-red to darker green-black (Figure 3-17 and Appendix C6). In the sand fraction grains are typically between 150 – 300 µm, with a maximum diametre of 700 µm (Appendix C6).

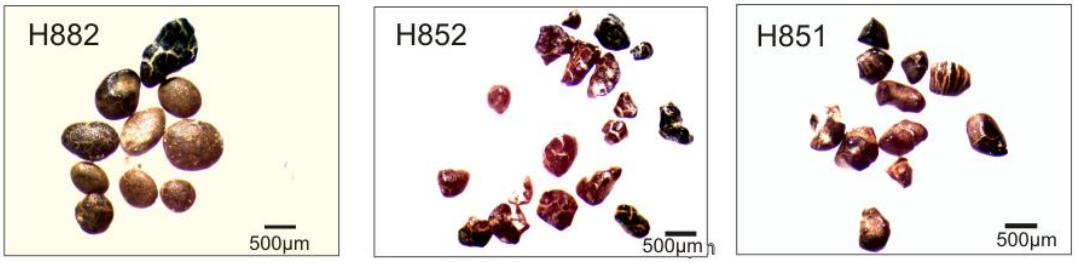

Figure 3-17 Photos of sand sized glaucony from the Hokitika (H852 & H851) and Cook Canyon Head (H882) north rims. In H882 well-rounded brown to dark red grains and dark green to black grains are present. H852 is dominated by dark green to black 'polished' sub-rounded grains. Grains are separated from the sand fraction of canyon surface samples.

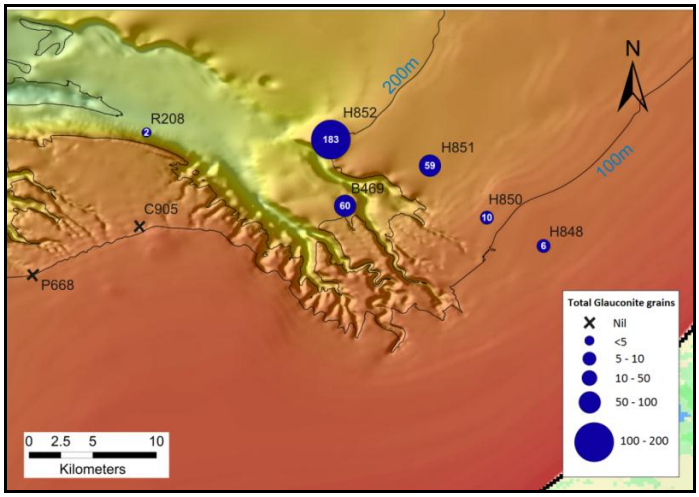

Figure 3-18 Map of glaucony distribution of the Hokitika Canyon Head. White number is the count of glaucony grains per 300 grains in the sand fraction pint counts (out of 300 grains).

Most grains are sub-rounded to well-rounded and moderately sorted. Total glaucony content is not distributed evenly in the canyons. A strong north vs. south canyon rim contrast is present in the HCH. South rim locations and on the canyon floor adjacent to the south rim little to no glaucony is present (Figure 3-18). In contrast, the north rim is far more enriched in glaucony grains (6 - 182 grains per 300 in

the sand fraction) (Figure 3-18). In the HCH, lighter brown-red grains are more common in the shallower, landwards sediments (H851 & B469), while dark green to black grains dominate the deeper, more distal sediments (i.e. H852) . In the CCH, glaucony grains are common in the north of the canyon (182 m depth) where well rounded brown to dark red grains and darker green-black grains are common.

3.4.6.2 Glaucony Types:

Mature: Mature glaucony is the most common grain type found in the canyon heads (Figure 3-19). They are typically light to dark green in thin section with a mottled texture throughout the grain (Figure 3-20). They are larger, more rounded, and more commonly fractured than other grain types. Alteration or replacement with iron oxides is common, usually as a concentric rim or infilling of fractures. Occasionally complete glaucony replacement of the mature grain with iron oxide occurs (Figure 3-20, H851). Limonite is probably the dominant iron oxide involved. The north rim of the HCH between 180 – 200 m depth is rich in mature grains, with up to 160 counted in sediments at 198 m depth (Figure 3-19 & Figure 3-20, H852). In the north of the CCH over 45 mature grains were present at 186 m depth. Rare, mature glaucony occurs on transect C at middle shelf depths on the Central Shelf.

Mixed: Mixed glaucony grains are the second most common type, with up to 25 grains per 300 in canyon head samples (Figure 3-18). They consist of siliciclastic grains (such as quartz, feldspar, mica, and clays) enveloped by glaucony to varying degrees (Figure 3-20, H851). Grains with thin glaucony rims veneering siliciclastic grains were also observed in association with mixed glaucony grains. However, these were not classified under the mixed glaucony group. Mixed glaucony grains have a wider distribution in the canyon heads than mature grains and are the dominant grain in the shallower, eastern sediments of the HCH (H848 & H850) (Figure 3-19). Very rare mixed glaucony-siliciclastic grains and siliciclastics with glaucony rims occur in surface sediment at 116 m depth on transect E.

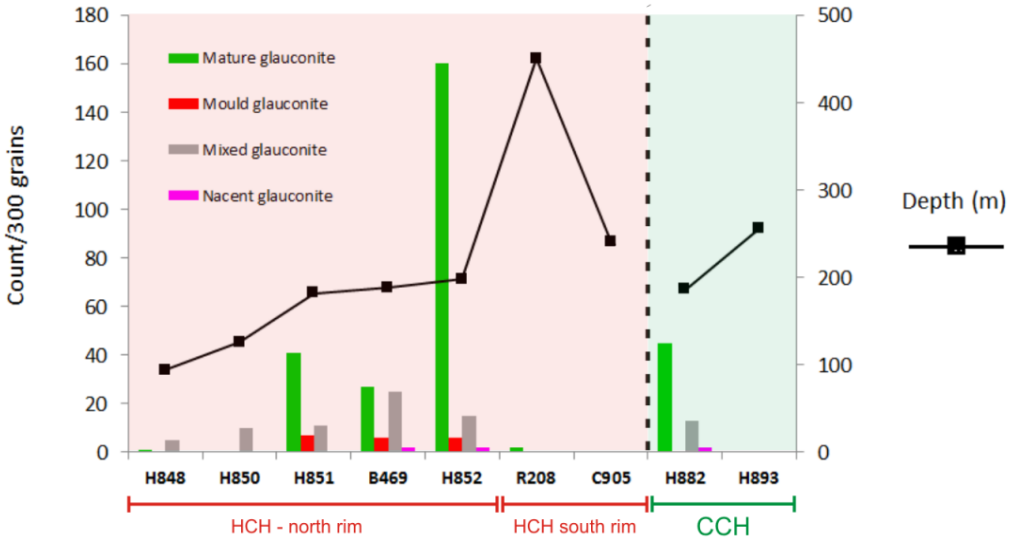

Figure 3-19 Graph showing different glaucony varieties and water depth of canyon head sediments. Based on point count data (Appendix C4). HCH = Hokitika Canyon Head, CCH= Cook Canyon Head.

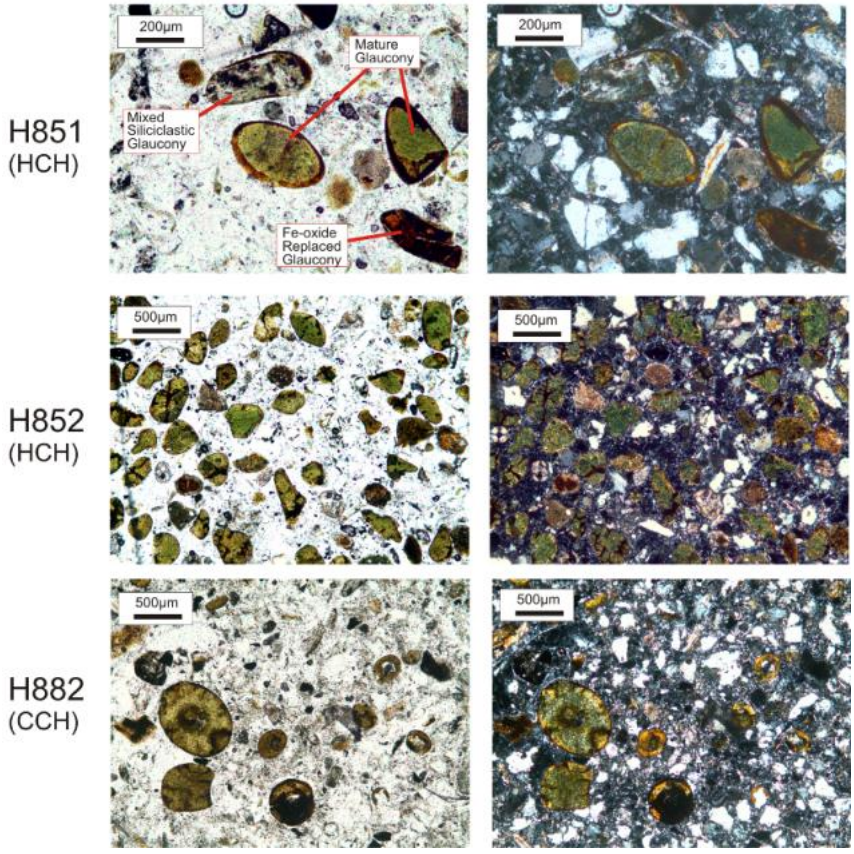

Figure 3-20 Photomicrographs of north canyon rim glaucony grain types. H851 from the HCH displays typical mature and mixed type glaucony grains. H852 is dominated by sub-angular to sub-rounded mature grain types. H882 from the Cook Canyon north rim commonly contains large well rounded grains up to 700 µm in diametre. All thin sections images are from the bulk sediment.

Moulds: Glaucony moulds of canyon head skeletal grains are present in most samples, but more commonly in the deeper locations of north rim sediments (Figure 3-19). Foraminifera (both benthic and planktonic) are the most common skeletal grains filled with glaucony (Figure 3-21). At 256 m depth at the head of a Cook Canyon tributary canyon, numerous planktic foraminifera moulds were observed but not counted in point counts.

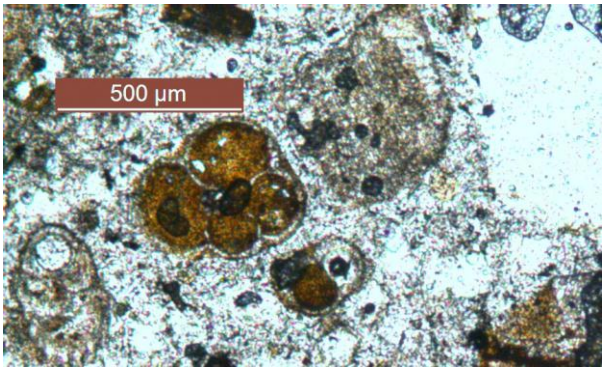

Figure 3-21 Photo of typical glaucony mould. In this case each chamber of a planktic foraminifera is filled. Photo is from a bulk sediment thin section of H893 located at the head of a tributary canyon to the Cook Canyon Head.

Nascent: These grains are very rare in the SWCM canyon heads, with up to 2 grains per 300 observed on the HCH and CCH north rim locations (Figure 3-19).

3.5 INTERPRETATIONS AND DISCUSSION

3.5.1 Provenance Interpretation

The bulk mineralogy of shelf, canyon, river, and beach sediments demonstrate the primary control of the Alpine Schist lithology on SWCM composition. The contribution of other lithologies to the bulk mineralogy of SWCM sediments is relatively localised, with rapid dilution from Alpine Schist derived detritus. In Table 3-1 the important minerals present within the basement geology of the SWCM catchments is displayed.

Table 3-1 Summary of key minerals occurring in SWCM catchments basement rocks. Minerals in bold are the dominant species of the rock unit.

Potential Source Rocks	Mineralogy		Reference (s)
Greenland Group	**Quartz** (30-35%); **Plagioclase** (≤6%);	Variable L_{sed} and $L_{volc.}$ Rare K-feldspar Up to 50% matrix.	Laird (1972) Roser & Nathan (1997)
Alpine Schist **'grey schists'** (i.e. Hokitika & Waiho catchments)	**Quartz** **Muscovite** Ilmenite/Magnetite Chlorite Biotite	Plagioclase (Albite) Epidote Garnet Amphibole K Feldspar	Vry et. al. (2008) Grapes (1995)
Alpine Schist **'green schists'** (i.e. Haast & Arawhata catchments)	**Quartz** **Plagioclase** (av. 20-30%) **Hornblende-Actinolite** (av. 30 %) Chlorite (0-40%; av. 10%)	Biotite (0-40%, highly variable) Epidote (0-17%, highly variable) (Epidote dominates heavy mineral fraction (>90% in Arawhata R))	Cooper (1970) Morton and Smale (1990)
Dun Mountain Ultramafics and Livingston Group. Volcanics (i.e. Cascade/Martyr catchments)	**Diverse ultramafic lithologies containing:** Olivine Orthopyroxene	Clionopyroxene Epidote Amphibole Cr-spinels	Morton and Smale (1990) Sinton (1975)
Granitoids	**<u>Karamea Suite:</u>** **Quartz + orthoclase + plagioclase + biotite +** muscovite+garnet		Rattenbury, Jongens, & Cox, (2010)

Alpine Schists

The mineral assemblage of SWCM shelf and canyon sediments is primarily controlled by the Alpine Schists. In the traditional QFL plot in Figure 3-22, most SWCM sediments plot in the recycled orogeny field, reinforcing the provenance from uplifted metamorphic rocks of the Alpine Schist.

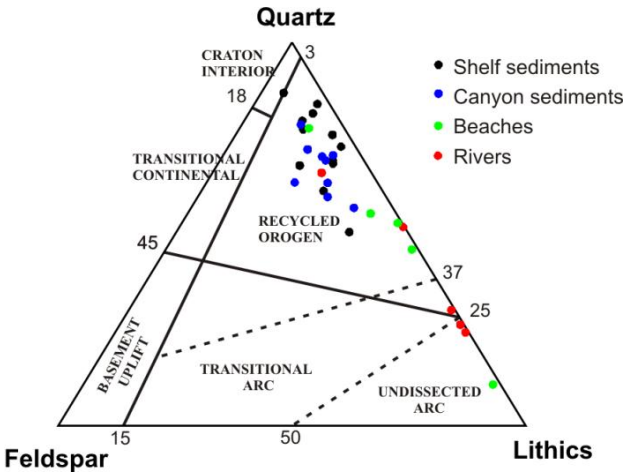

Figure 3-22 Tectonic discrimination diagram plotting SWCM shelf, canyon, beach and river sediments. based on point count data in Appendix C4. After Dickonson (1982)

The abundance of undulatory and polycrystalline quartz reflects a source dominantly from low grade (chlorite and biotite zone) metamorphic rocks (Boggs 2009).

Polycrystalline quartz (especially with 2-3 crystal units) may also indicate a plutonic source (Basu et al. 1975), but the lack of granitic outcrops south of Hokitika and the presence of > 3 crystal unit quartz grains in SWCM sediments precludes a granitic origin (Figure 3-3).

The southward increase in the proportion of straight extinction quartz in SWCM sediments (i.e. Central to Haast shelves and CCH) may reflect the increase in width of higher grade oligoclase-garnet schist zones along the Alpine Fault. Straight extinction quartz is more common in these higher grade metamorphic rocks. Catchments south of the Hokitika River drain increasingly larger areas of higher grade metamorphic rocks (Figure 3-3), resulting in greater proportions of straight extinction quartz transferred to the shelf. However, in southern SWCM rivers and beaches the higher proportions of straight extinction quartz are not seen, indicating increased mechanical breakdown of polycrystalline grains on the shelf.

Plagioclase feldspar, the dominant feldspar variety in the Alpine Schist, is clearly the main feldspar in SWCM sediments also (especially Albite , Appendix C8). Abundant metamorphic lithics and micas in shelf and canyon sediments are clearly from the foliated quartzofeldspathic metamorphic rocks of the Alpine Schist. The high mica concentrations on the middle to outer shelves is primarily due to the export from the energetic inner shelf to more hydrodynamically favorable depths offshore.

The heavy mineral suite of SWCM sediments is controlled largely by the Alpine Schists, with amphiboles and epidote (common low to medium grade metamorphic minerals) widespread on the SWCM. Garnets are present in most SWCM sediments, with the greatest concentrations in the canyon heads and the inner shelf. These colourless to pale red garnets will lmost likely be almandine, a regional metamorphic garnet found in mica schists (Phillips & Griffen 1981). Heavy minerals exhibit a typical decrease offshore due to hydrodynamic sorting (Morton & Hallsworth 1999; Komar 2007).

Ultramafics:

Serpentinised lithics and mafic minerals (particularly olivine) in the rivers and beaches of the Cascade and Haast regions reflect contributions from the Dun Mountain Ultramafics (DMU). The Martry River in particular is heavily influenced by this lithology. Since thin section point counts were focused on the shelf transects between the South – North shelves, no petrological data from the Cascade or Haast shelves was available to verify the ultramafic signal on the shelf. A single serpentinised lithic to the south of the CCH (H893, Transect F) may be from the DMU. Rare serpentinised lithics in the Hokitika River and beach samples are likely associated with the Pounamu Ultramafics of the Hokitika-Waitaha catchments. A single olivine grain in the Hokitika Canyon (H851, Appendix C3) will probably be related the Pounamu Ultramafics also.

Greenland Group Rare, quartz rich sedimentary lithics are probably from the limited outcrops of the Greenland Group west of the Alpine Fault. A slight increase in sedimentary lithics at Neils Beach and Jacksons Bay Beach is probably due to the coastal outcrops of Greenland group in Jackson Bay area (Figure 3-3).

Granitoids Occasional spikes in the proportion of biotite over muscovite on the shelf (i.e. transect C on the Central Shelf) maybe related to plutonic rocks. The Waitaha River catchment contains significant outcrops of the Karamea plutonic suite, a biotite bearing unit (Cox & Barrell 2007), which may be contributing to biotite levels on the middle shelf of Transect C (Figure 3-3). The Hokitika catchment also contains some out crops of Cretaceous granites with notable amounts of biotite in their mineralogy.

3.5.2 Glaucony

Glaucony in the Hokitika and Cook Canyons are dominated by mature grains which represent fecal, siliciclastic, or skeletal carbonate grains completely replaced with glaucony clays (Odin & Fullagar 1988). The less common but more widespread mixed glaucony-siliciclastic grains may represent transitional glaucony grains still actively forming. A common goal of glaucony analysis is to determine whether the grains are *autochthonous* (formed in-situ) or *allochthonous* (transported from the site of formation i.e. detrital). After Amorosi (1997), allochthonous grains are further divided into: a) *Parautochthonous* - grains transported by storm surges, tidal currents, or gravity flows away from their place of origin to a coeval seaward or land ward deposit and b) Detrital – grains undoubtedly reworked from an older deposit (Figure 3-23). Based on the work of Odin and Fullagar (1988) and Amorosi (1997), a number of morphological and internal features can be used to determine glaucony origin. Geochemistry is an additional tool used in determining glaucony origin, but was beyond the scope of this study.

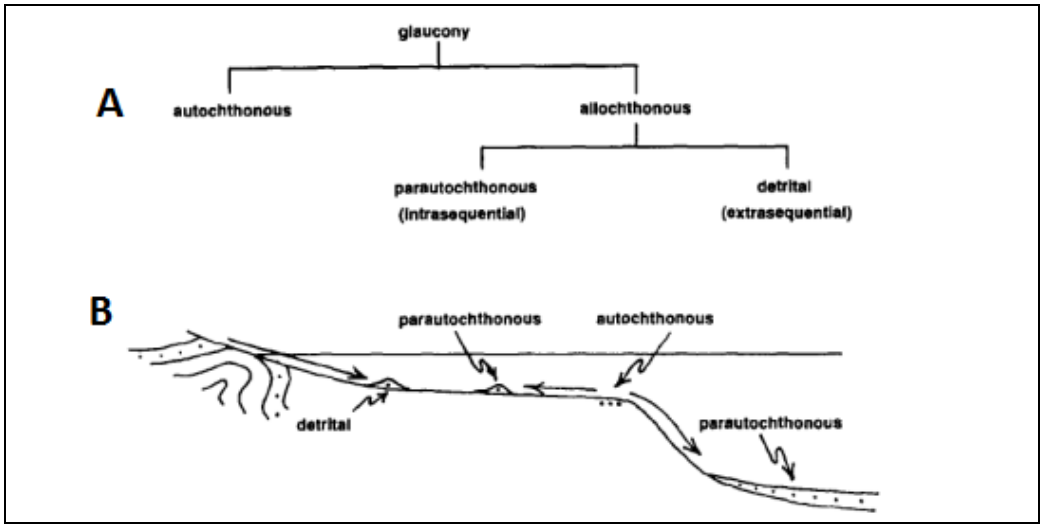

Figure 3-23 (A) Classification of glaucony based on spatial and temporal features. (B) Spatial relationships between different types of glaucony (from Amorosi 1997).

Several features in SWCM canyon glaucony indicate a degree of transport (allochthonous), but it is difficult to evaluate transport distance. Well sorted glaucony grains can be indicative of an allochthonous origin (Amorosi 1997). Generally, the canyon head glaucony is at least moderately sorted, supporting this line of evidence. However, poorly sorted glaucony grains may still be detrital in origin if the original material replaced by glaucony was poorly sorted itself (Amorosi 1997). Rounded to very well rounded (sometimes polished) grains of the HCH and CCH north rims could also be the result of significant transport (Amorosi 1997). The partial to complete replacement of glaucony or the infilling of fractures in many mature glaucony grains with iron oxides suggests there is minimal active glauconitisation occurring today. The lack of nascent grains in canyon sediments also suggests active glaucony formation is minimal, with mature grains potentially formed centuries to thousands of years ago.

Despite the evidence for a detrital origin, other features suggest transport has been limited and the grains are mainly *parautochthonous* . This includes the lack of mechanical breakdown of highly fractured mature gains and the location of the grains at optimal depths for glaucony formation. The preservation of numerous fractures in the HCH and CCH glaucony grains is a good indication that transport has been restricted. Prolonged transport would otherwise breakup grains along these zones of weakness through mechanical fragmentation (Fischer 1990). The optimal depth and location for glaucony formation is near the top of the continental slope, close to 200 m depth (Odin & Fullagar 1988). Canyon head sediments rich in mature glaucony on the HCH and CCH are found close to this depth near the shelf edge, where optimal conditions prevail for glauconitisation. This suggests most of the glaucony of the HCH and CCH has not been transported far from where the grains formed, i.e. they are probably *parautochthonous* grains (Figure 3-23).

CHAPTER 4 : DETRITAL MAGNETITES

4.1 INTRODUCTION

The elemental composition of individual minerals, rather than bulk geochemistry or mineralogy, has proven a useful tool for assessing sediment dispersal and provenance (Grigsby 1990; Bradley et al. 2002; Yang et al. 2009). This is because processes other than source rock composition, such as hydrodynamic sorting and weathering, can alter the final mineralogy and composition of shelf sediments (Grigsby 1990). Previous studies by Ooi (1982) and Bradley et al. (2002) on detrital magnetites in Westland beaches and rivers have identified broad trends related to catchment geology and dispersal patterns. In particular, the Chromium (Cr) content proved the most powerful determinant of magnetite provenance and dispersal in these studies. This is due to the ability of Cr to replace and substitute into the magnetite lattice relatively easily, resulting in highly variable Cr contents in magnetites (and other spinels).

This chapter presents results and discussion of a microprobe study focused on detrital magnetites in South Westland Coastal Margin (SWCM) sediments. Key questions include: Are the patterns identified by Ooi (1982) and Bradley et al. (2002) in beach sediments reflected on the adjacent continental shelves? Can sediment dispersal be traced on the shelf? Can detrital magnetites be used to understand canyon to shelf interactions?

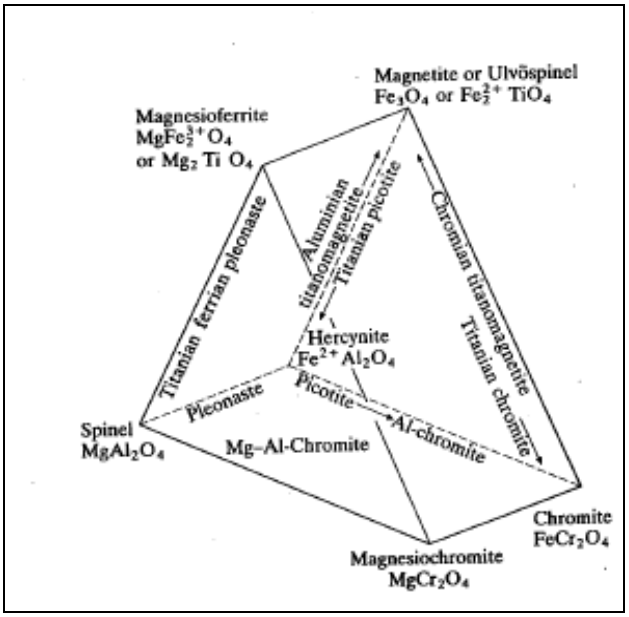

Figure 4-1 The spinel compositional prism showing key end members and solid solution series. From Deer et al. (1992)

The microprobe technique was chosen over other geochemical analyses (i.e. Atomic Absorption or XRF) given the small sample size of shelf sediments available. In this chapter the term "magnetite" refers to all

phases in the magnetite-ulvospinel solid solution series extracted from the heavy mineral fraction (Figure 4-1). The use of "spinel" refers to all mineral species from the spinel group (i.e. Magnetite series and chromite series).

4.2 METHODS

A total of 254 magnetite grains were analysed from 20 shelf and 9 beach and river samples using a JEOL JXA-8230 SuperProbe at Victoria University, Wellington. Details of sample preparation, microprobe procedures, and results are provided in Appendix F. Samples were selected from within canyon heads, the shelf regions, and beaches and rivers to give the best indication of dispersal patterns (Figure 4-2). To be comparable to previous studies on Westland beach and river magnetites, only the 2-4 phi (fine – very fine sand) fraction was processed. This also reduces the effects of composite grains found in coarser size fractions (Bradley et al. 2002).

The weight percentage of Al_2O_3, MgO, TiO_2, V_2O_3, FeO, Cr_2O_3, Fe_2O_3, and MnO was determined for 3 points in each grain and then converted to an average value. FeOT has been recalculated to give FeO and Fe_2O_3 based on the basis of 32 oxygens. Calibration standards and oxide weight percentages are given in Appendix F2. Due to the importance of Cr in the provenance of SWCM spinels, the elemental concentration and parts per million are given in Appendix F2 also.

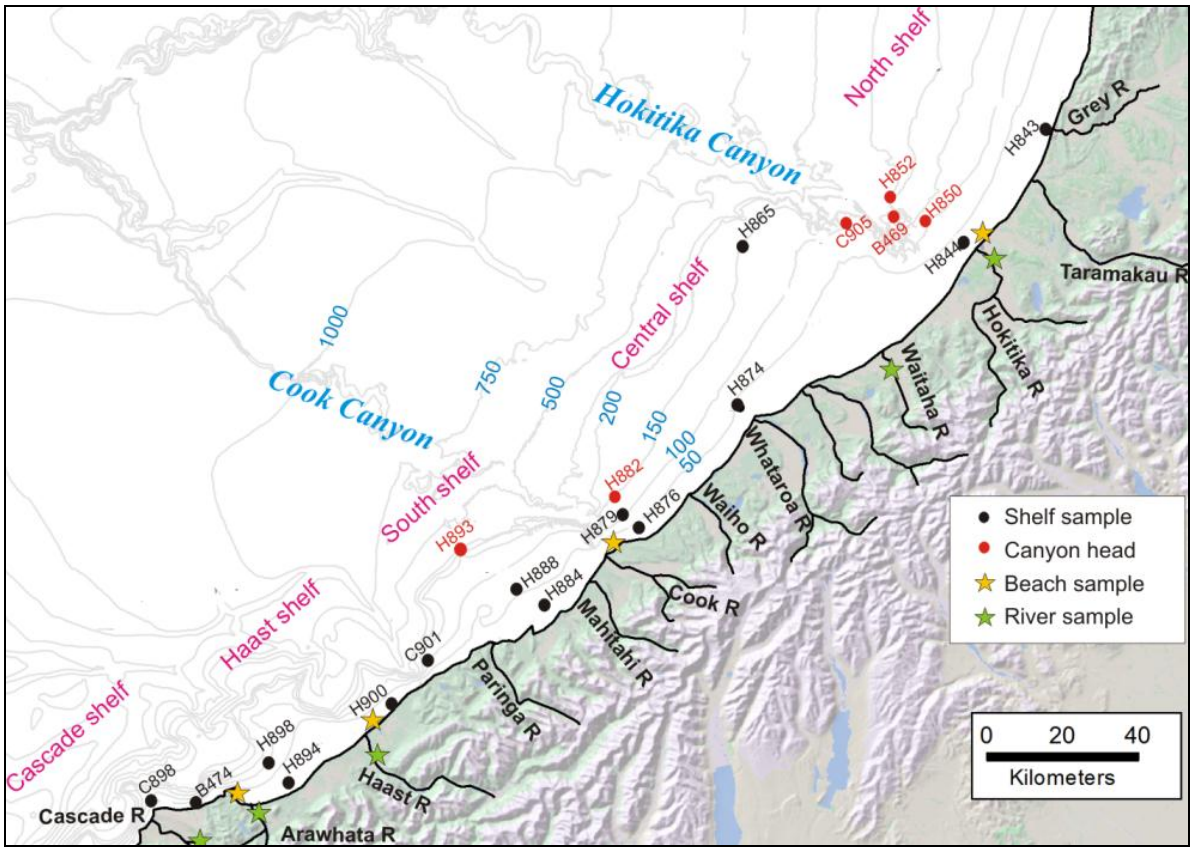

Figure 4-2 Locations of SWCM shelf, beach and river samples used for detrital magnetite analysis.

4.3 RESULTS

4.3.1 General Oxide Results

The overall results for all magnetite grains analysed show considerable variation, especially the chromium, aluminium, magnesium, and iron oxides (Table 4-1). The percent weight TiO_2 is notably low with most grains well below 1%. Combined levels of Ferrous and Ferric oxide are typically over 90 % by weight, typical for grains from the magnetite-ulvospinel series (Deer et al. 1992; Grigsby 1990).

Table 4-1 Descriptive statistics for all magnetite grains (n=254) analysed in this study. All results are in wt. %.

Wt. %	Mean	Min	Max	Median	Std. error	Variance	Std. dev.
MgO	0.39	0.00	13.45	0.01	0.12	3.38	1.84
Al_2O_3	0.53	0.00	21.53	0.04	0.16	6.13	2.48
TiO_2	0.11	0.00	6.27	0.03	0.03	0.28	0.53
V_2O_3	0.10	0.00	0.56	0.08	0.00	0.01	0.08
FeO	44.52	13.93	46.60	45.92	0.34	29.97	5.47
Cr_2O_3	2.54	0.00	59.88	0.03	0.64	103.43	10.17
Fe_2O_3	48.95	5.64	51.83	51.10	0.54	73.72	8.59
MnO	0.12	0.00	2.23	0.05	0.02	0.06	0.25

Plotting FeO, Fe_2O_3 and TiO_2 on a mole % basis after Deer et al. (1992) also confirms the dominance of magnetite, making up >95% of all grains (red dashed circle) in the magnetic fraction (Figure 4-3). A minor outlier grouping of only 9 grains plots in the wustite-magnetite field, this is discussed further in section 4.4. To identify regional differences in magnetite composition, bar charts and descriptive statistics by region are compared to the mean overall oxide values (Appendix F3 and Figure 4-4).

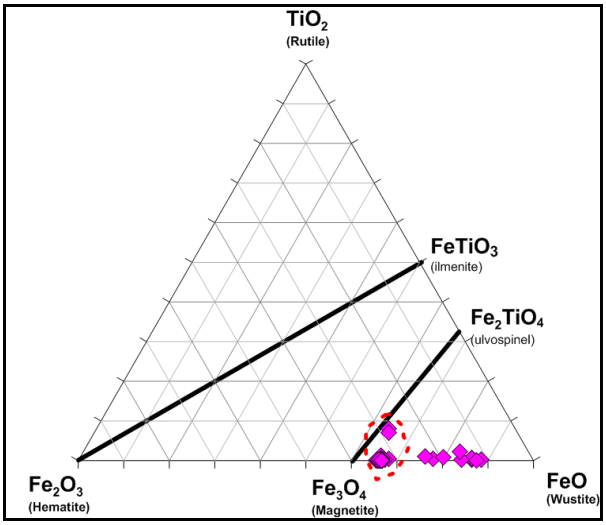

Figure 4-3 Compositional plot of all 254 magnetite grains analysed this study. Red dash circle represents over 95% of all grains. Outlier grouping is mainly from the shelf and catchments of the Cascade region. Ternary diagram plotted on a mole percent basis after Deer et al. (1992, p.563).

4.3.2 Oxide Results by SWCM Regions

For the following sample sites and regions please refer to Figure 4-2 for specific locations and Appendix F3 for regional oxide statistics.

North Shelf & Hokitika Canyon:

A total of 58 magnetite grains from seven sediment samples were analysed in this region (Figure 4-2). Generally, they are slightly enriched in Cr_2O_3 (mean = 0.42 wt.%) but are similar to other shelf regions for the other oxides (Appendix F3). Rare Cr_2O_3 rich grains are present on the inner shelf near the Grey River (H843, up to 10% wt. Cr_2O_3), while on the inner shelf of transect B (H844), no grains with over 0.1 wt. % were found (Figure 4-4). Within the Hokitika Canyon Head (HCH), most magnetite grains are not enriched in Cr_2O_3, MgO or Al_2O_3, however, rare anomalous grains do contain up to 2 % wt. Cr_2O_3 (i.e. H852, Figure 4-4). In the Hokitika River sample, 3 out of the 6 grains were enriched. In particular, grain number 2 contains 52 % wt. Cr_2O_3 (Appendix F2). In the Hokitika Beach sample, 4 out of 13 magnetite grains contain between 1.2 and 19% wt. Cr_2O_3 (Figure 4-4).

Central, South, and Haast Shelves:

Of the 11 shelf samples analysed (103 magnetites in total), very few were enriched in Cr, Mg, or Al oxides (Appendix F3). The mean Cr_2O_3 is generally < 0.1% wt., except for an individual grain in H893 (Figure 4-2, Transect F, 293 m depth). Similarly, most beaches and rivers supplying these shelves are dominated by detrital magnetites not enriched in Cr_2O_3, MgO, and Al2O3. An exception is the Waitaha River where 2 grains contain between 1-2 % wt. Cr_2O_3 (Figure 4-4).

Cascade Region:

The cascade region includes 2 shelf samples south of Jackson Head (Figure 4-2, B474 and C898) and single samples from Neils beach and the Martyr and Arawhata rivers. Fifty grains were analysed in total. Shelf sediments (B474 & C898) are characterized by magnetites highly enriched in Cr_2O_3, MgO, and Al_2O_3 (Figure 4-4 & appendix). The overall means for the Cascade Shelf are 16.5, 3.6, and 3 % wt. for these oxides respectively. At 24 m water depth, 8 grains from sample B474 contained over > 35% wt. Cr_2O_3 and > 8 % wt. MgO (Figure 4-4). The Martyr River contained a single very enriched magnetite grain (49 % wt. Cr_2O_3) but was otherwise characterized by compositions typical for the majority of other regions. Similarly, Neils Beach south of the Arawhata River mouth had a single Cr enriched grain (Figure 4-4).

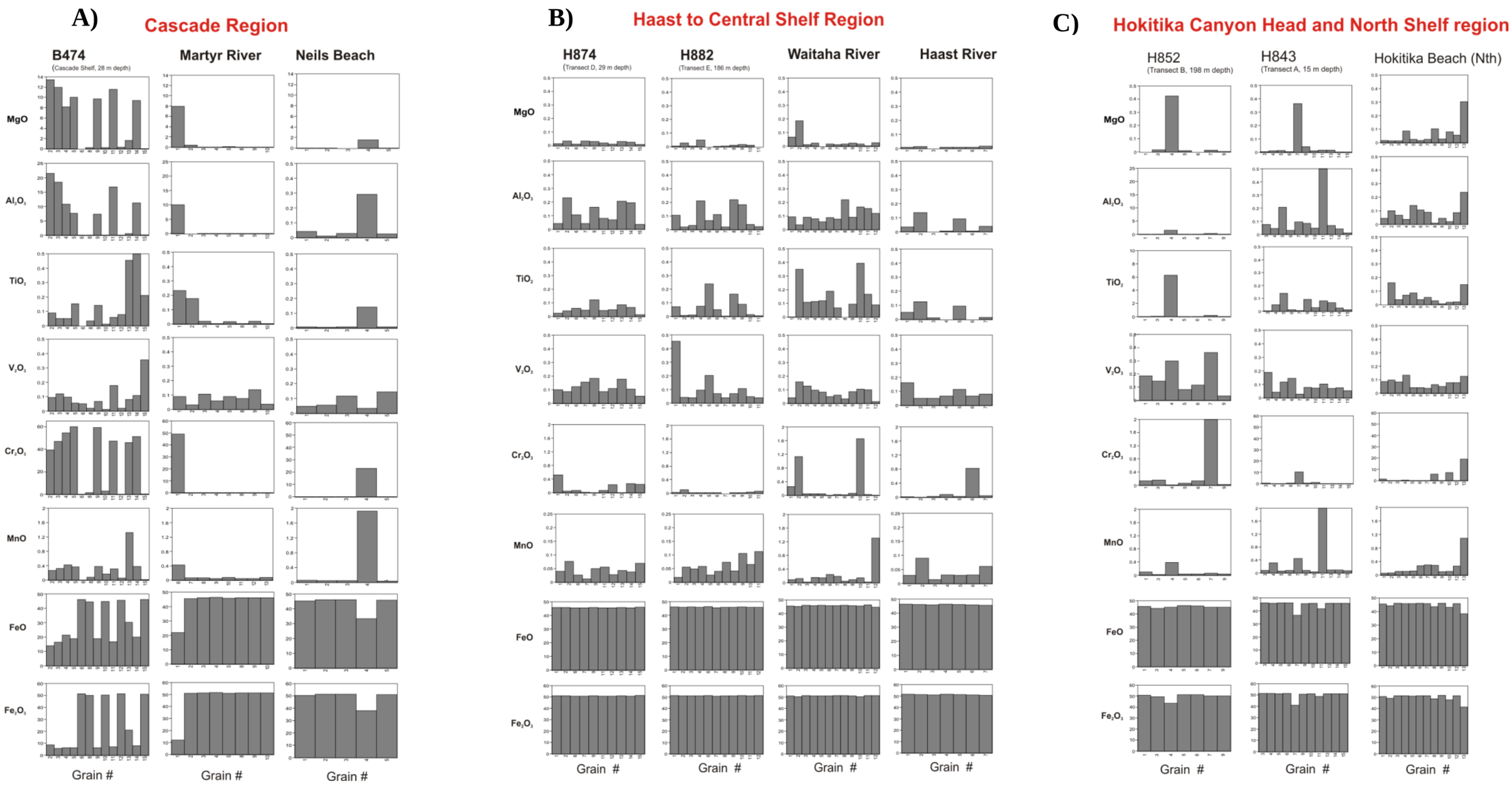

Figure 4-4 Selected bar charts for detrital magnetite oxides from A) Cascade region, B) Haast, South, and Central regions, and C) Hokitika Canyon & North Shelf region (Figure 4-2**). All oxides are in wt. %. Note changes in scale for some oxides.**

4.4 DETRITAL MAGNETITE CLASSIFICATION

From the microprobe results, it is clear there are several geochemically distinct 'magnetite' groups. These have been classified into likely mineral species from within the spinel group based on the criteria outlined in Table 4-2. Classification will further help identify regional patterns of dispersal and may allow interpretations of the provenance of detrital magnetite's. Using oxides displaying the greatest variation in the data set (i.e. Cr_2O_3, MgO, Al_2O_3), 4 groups have been identified based on predefined chemical criteria (Figure 4-5). All data and summary statistics for each group is provided in Appendix F4.

Table 4-2 Criteria used to define compositional groups within magnetites analysed during this study. Var. = Variable, Mg # = Mg/(Mg + Fe^{2+}) , Cr # = Cr/(Cr + Al).

Classification	Cr_2O_3 (wt. %)	Al_2O_3 (wt. %)	MgO (wt. %)	Mg #	Cr #	Total identified
Chromite	> 30.0	> 5.0	> 5.0	> 2.0	> 7.0	9
Ferrian Chromite	> 10.0	< 2.0	< 2.0	Var.	> 7.0	5
Cr - Magnetite	0.5 - 10.0	< 2.0	< 1.0	Var.	> 7.0	21
Low Cr Magnetite (I)	0.1 – 0.5	< 2.0	< 1.0	Var.	Var.	40
Low Cr Magnetite (II)	< 0.1	< 2.0	< 1.0	Var.	Var.	178

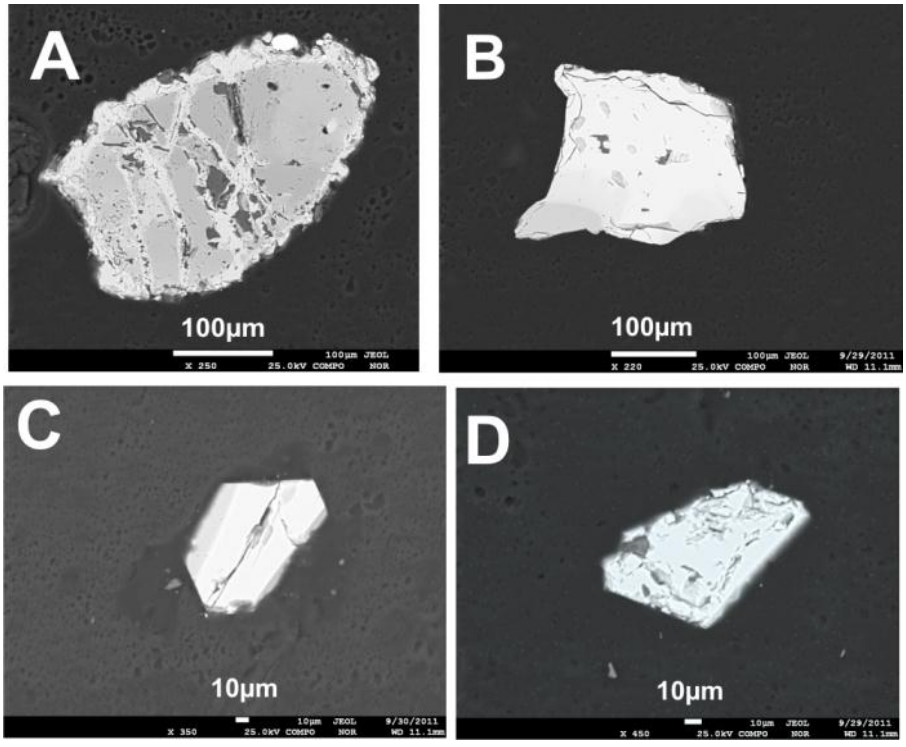

Figure 4-5 Backscatter images of detrital spinels from the SWCM region. A) Chromite grain from the Martyr River (note the contrast between cores and rims) B) Ferrian chromite grain from Hokitika Beach, C) Cr-magnetite from H893 (Cook Canyon tributary, 256m depth), D) Low Cr magnetite grain from H884, South Shelf.

A)

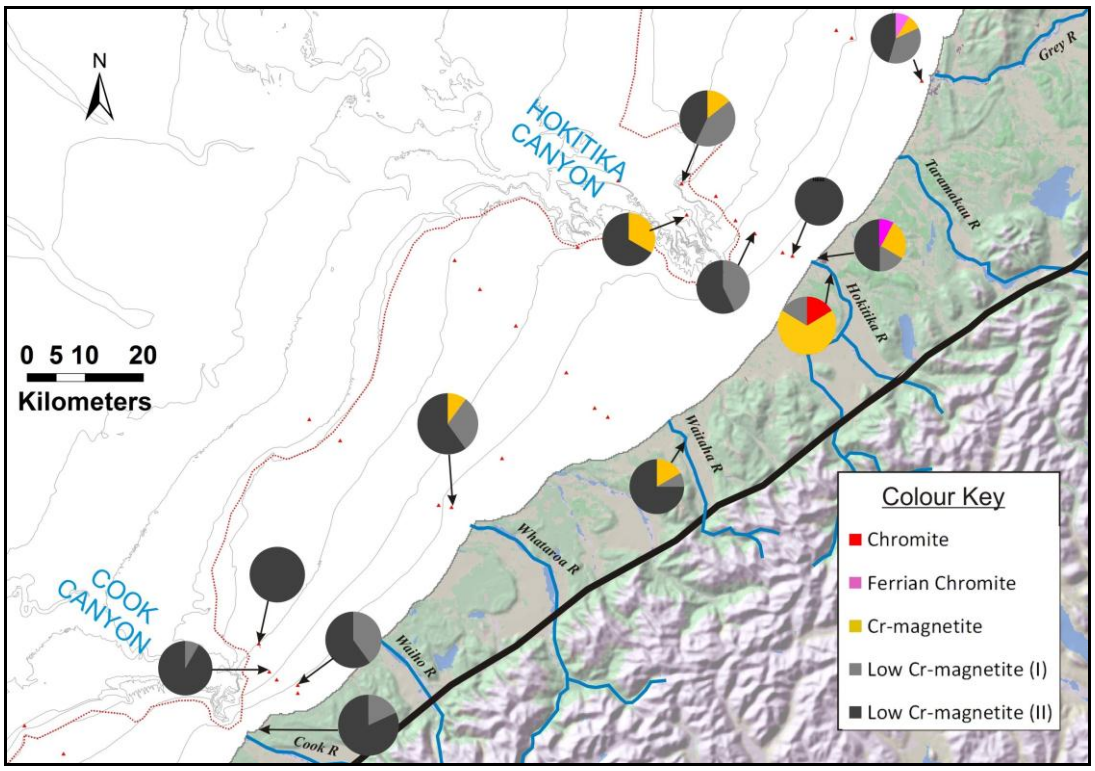

B)

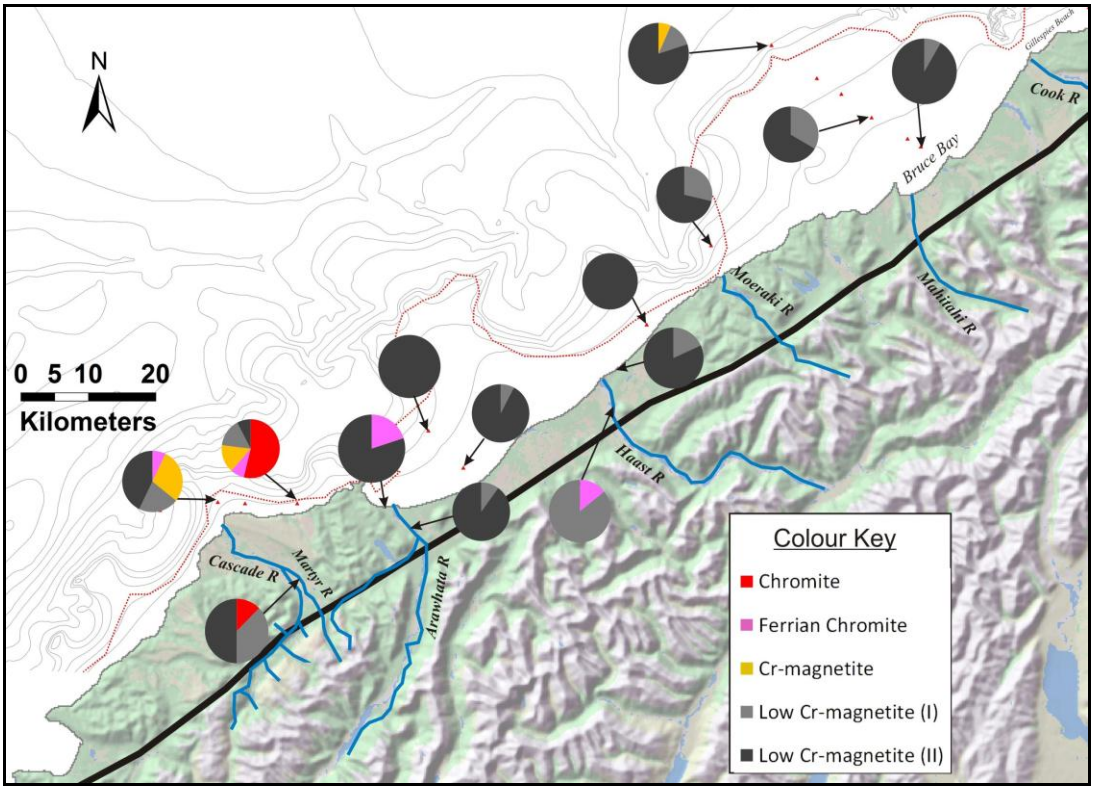

Figure 4-6 Proportions of Chromites and Magnetites found in shelf, river and beach samples in A) northern regions and B) southern regions.

4.4.1 Chromites

These grains form a distinct compositional group with oxide weight percentages ranging from 39.26 - 59.88 Cr_2O_3 , 7.42-21.53 Al_2O_3, 3.02- 13.45 MgO, 13.93 – 28.06 FeO, and 5.64 -11.88 Fe_2O_3 (Appendix F4).The Mg # varies from 0.77-4.28, and Cr # from 0.702-0.912 (Figure 4-7). Nine grains have the chromite group composition, 8 of which are from the Cascade region (Figure 4-6 B). Of these, 7 are from B474, located at 28 metres depth, 10km west southwest of Jackson Head, and 1.4 km offshore (Figure 4-2). Single chromite grains were found in the Martyr River and in the Hokitika River. These compositions are typical of the Chromite series, spinel group minerals associated with ultramafic lithologies (Deer et al. 1992; Uysal et al. 2007). Chemical compositions suggest these grains are dominantly from the Chromite ($FeCr_2O_4$) rather than the Magnesiohromite ($MgCr_2O_4$) end member of the chromite series (Figure 4-7, A). The distinction between a podoform and stratiform origin for the chromites is not entirely clear in Figure 4-7 B. However, the compositional differences between grain types is clearer in Figure 4-7 B, with ferrian chromites clustering widely along the Cr_2O_3 axis and Cr-magnetites tightly grouping near the graph origin.

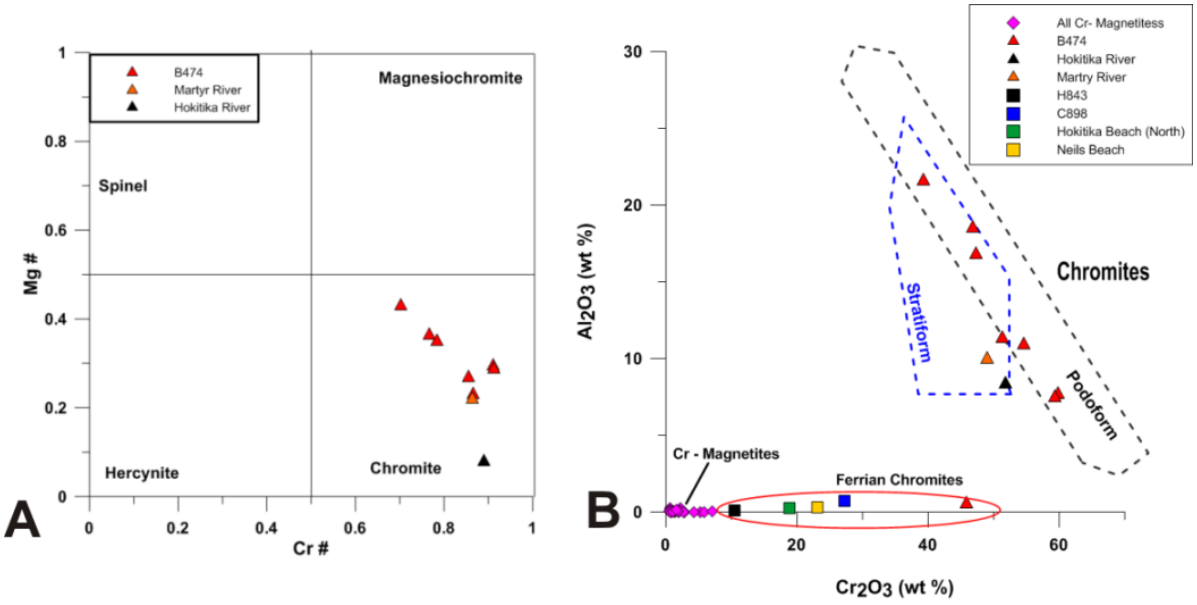

Figure 4-7 A) Compositions of individual Chromite series spinels from the Cascade and Hokitika regions. Mg # = Mg/(Mg + Fe^{2+}) , Cr # = Cr/(Cr + Al) after Uysal et al. (2007). B) Al_2O_3 vs. Cr_2O_3 for individual chromite, ferrian chromite and Cr-Magnetite grains. Modified from Uysal et al. (2007).

4.4.2 Ferrian Chromites

Five grains analysed fall within the Ferrian chromite category. Here, weight percentages range from 10.52 – 45.79 Cr_2O_3, 0.1 – 0.73 Al_2O_3, 0.3 – 1.76 MgO, 30.4 – 38.43 FeO, and 20.87 – 41.38 Fe_2O_3 (Appendix F4). While Cr_2O_3 remains high, Al and Mg oxide levels are well below those seen in the chromite group grains (Figure 4-7 B). A single grain was found in 3 sites from the Cascade region (B474, C898, and Neils Beach) and 2 grains from the North Shelf region (H843 and Hokitika Beach) (Figure 4-6, B). Between the Haast and Hokitika Rivers, no Ferrian Chromites were identified in shelf, beach or river sediments.

4.4.3 Cr-Magnetites

A total of 21 grains are Cr – magnetites, plotting distinctly from chromites, ferrian chromites, and low Cr-magnetites (Figure 4-7, B). Chemical compositions range from 0.52 – 7.08 Cr_2O_3 wt.%, 0.0 – 0.27 Al_2O_3 wt. %, 0.0 – 0.88 MgO wt. %, 43.13-45.93 FeO wt. %, and 47.79 – 51.09 Fe_2O_3 wt.% (Appendix F4). Between Jackson Head and the Waitaha River, Cr- magnetites were rare in all sampling environments. The exception was a single grain found at upper slope depths on Transect E (H893) and the inner shelf of Transect D (H874). Cr-magnetites are common in Hokitika beaches and river sediments, with grains also present in Hokitika Canyon Head (Figure 4-6 A).

4.4.4 Low Cr-Magnetites

The majority of magnetites belong to the low Cr magnetite group (218 of 254 grains). They are geochemically similar to Cr – magnetites except for lower Cr_2O_3 wt.% (<0.5 %) and a much more variable Cr # (Appendix F4). This group is further divided into magnetites with 0.1 - 0.5 Cr_2O_3 wt.% (Type I) and those with <0.1 Cr_2O_3 wt.% (Type II). Low Cr magnetites are ubiquitous in most environments sampled, comprising over 85% of all grains analysed (Figure 4-8). Their dominance is most pronounced between Jackson Head and the Waitaha River.

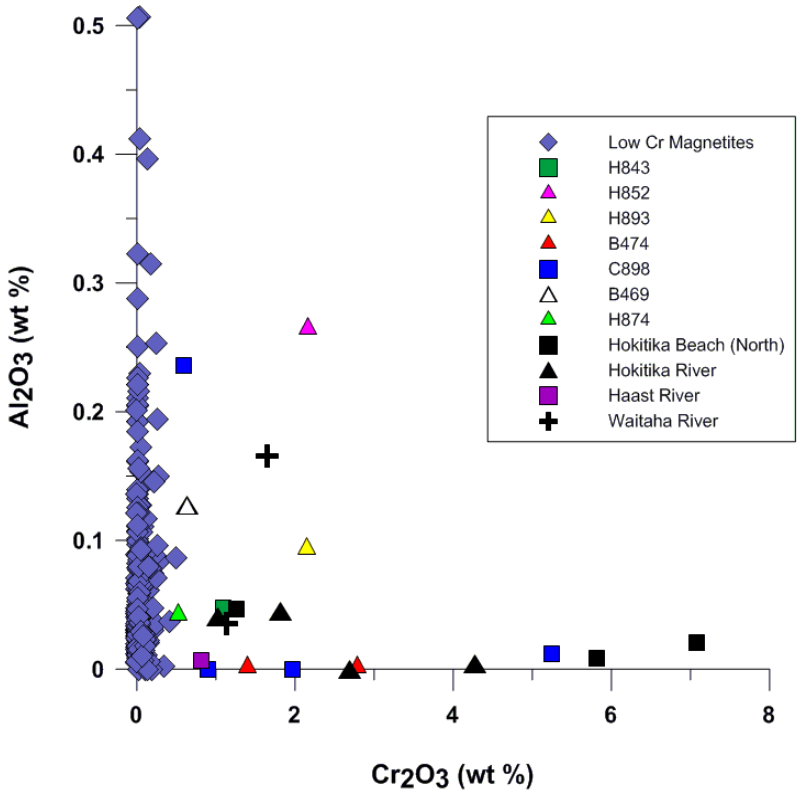

Figure 4-8 Discrimination between Low Cr magnetites (purple) and Cr magnetites by location.

4.5 CHROMIUM CONCENTRATION BY REGION

Chromium concentration in detrital magnetites, expressed as parts per million (ppm), is used in previous studies by Ooi (1982)and Bradley et al. (2002) for Westland beaches and rivers. Data from Ooi (1982) is most directly comparable for the shelf samples in this study since a microprobe was used on individual magnetite grains rather than "bulk magnetite samples" as used by Bradley et al. (2002). Several rivers and beaches not sampled in this study have been supplemented by data from Ooi (1982). All ppm values are an average of all detrital spinel grains within each sample.

North Shelf, Hokitika Canyon, and Hokitika River:

Very high Cr levels (average Cr of up to 35000 ppm) are present in magnetites from the Hokitika River and the Hokitika beach north of the river mouth as identified by Ooi (1982) (Figure 4-9, A). In contrast, the inner to middle shelf magnetites east of the HCH are depleted in Cr, with average Cr at less than 700 ppm. Within the HCH, Cr levels are an order of magnitude higher (1600-2700ppm Cr) than the shelf samples to the east (200-700ppm Cr), but still markedly less than the Hokitika River.

Central, South, and Haast regions:

The continental shelves, rivers, and beaches in the Central, South, and Haast Shelf regions show distinctly low Cr levels with most samples averaging <500 ppm Cr (Figure 4-9, A & B). An exception is the Waitaha River where 1878 ppm Cr was measured, or in the case of Ooi's (1982) samples, 57,000 ppm Cr.

Cascade Region:

In the Cascade region both continental shelf, beach and river magnetites and spinels show high Cr levels (Figure 4-9, B). In particular, B474 has the highest measured Cr content of all samples with 215,000 ppm. Between Jackson Head and the Arawhata River beach, samples were at least 20,000 ppm. The Arawhata river sample was notably low (124 ppm) compared to the value obtained by Ooi (1982) (24,000 ppm).

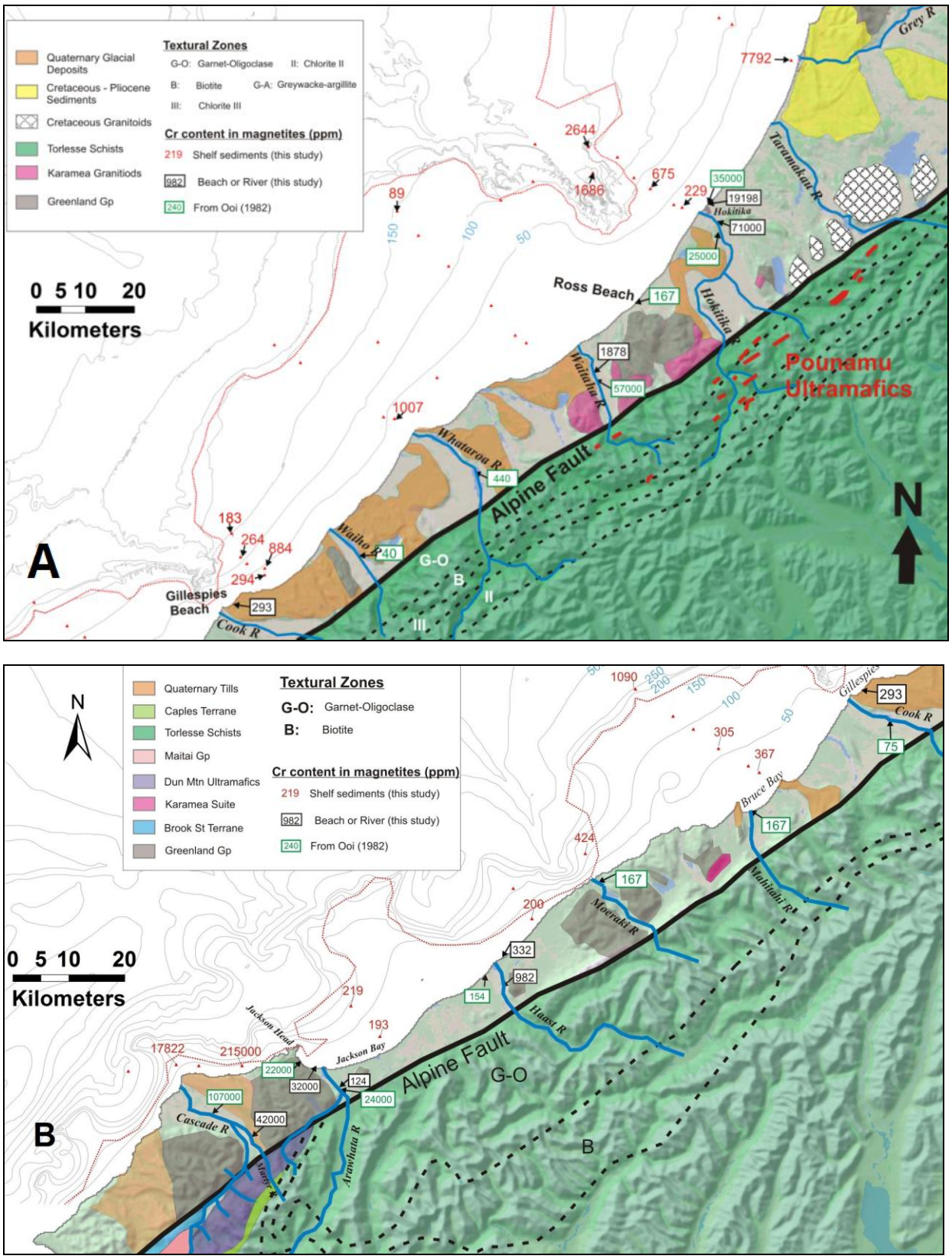

Figure 4-9 Regional geology and average Cr content (ppm) in detrital magnetites from sample sites for A) North Westland and B) South Westland. Data in green boxes from Ooi (1982), black boxes from this study.

4.6 INTERPRETATIONS AND DISCUSSION

4.6.1 Spinel Provenance

The provenance of detrital grains in SWCM shelf, beach and river sediments is based on detrital magnetite oxides, grain classifications, and comparisons to Westland regional geology.

a) Chromites: Chromium rich spinels are common accessory minerals in ultramafic plutonic rocks (i.e. Dunite or Peridotite) and their serpentinised equivalents (Phillips & Griffen 1981). These grains exhibit the 'unaltered' chemistry of chromite. The content of MgO in these chromites (appendix F2 & F4) is typical of natural chromites where significant amounts of Mg replaces Fe^{2+} during petrogenesis (Deer et al. 1992). The spatial association of Cascade Shelf detrital spinels with the Cascade-Martyr catchments emphasizes that these chromites are probably derived from the Dun Mountain Ultramafic Group (DMU). The DMU is characterized by variants of chromite bearing peridotites and dunites which crop out in the Cascade and Martyr river catchments (Coombs et al., 1976; Morton & Smale, 1990; Smale, 1991; Rattenbury et al. 2010). These rivers eventually supply the Cascade continental shelf as Bradley et al. (2002) notes for beach coastal cliff sediments near the Cascade River mouth. In the Hokitika River, the single chromite identified is likely related to the Ultramafic Pounamu pods which feature in the upper catchment (Figure 4-9, A). Chromium content for SWCM chromites ranged from 268,000 – 410, 000 ppm. Hence, a single chromite has dramatic effects on the average Cr content in samples otherwise dominated by less Cr enriched magnetite (i.e. Hokitika and Martyr Rivers). Bradley et al. (2002) and Ooi (1982) note comparably high Cr contents in magnetite grains from the Hokitika River.

b) ***Ferrian chromites:*** These share a close relationship with chromites by being serpentinisation alteration products of chromite (Uysal et al. 2007). Metamorhpic grade can be a key factor in the compositional variation in chromites and magnetites (Evans & Frost 1975). The varying metamorphic grade of the DMU (Coombs et al. 1976) may explain the origin of the ferrian chromites, which may represent armoring surrounding a chromite core in many grains (Uysal et al. 2007). Because of this, some analyses may not be representative of the mean grain chemistry. Despite probing three random points per grain, the chromite core may have been missed. The likely origin of ferrian chromites is similar to chromites with the DMU in the Cascade region and Ultramafic Pounamu of the Hokitika catchments providing the likely sources (Figure 4-6 A & B).

c) ***Cr – magnetites***: These magnetite's, while low in Cr compared to ferrian chromite and chromite, are indicative of a similar Cr-rich source. The distribution of Cr – magnetites reflect this, with most grains found in the Cascade and Waitaha to Hokitika shelf regions, areas with Ultramafic lithologies within river catchments supplying these shelves (DMU and Pounamu Ultramafics) (Figure 4-6 and Figure 4-9).

d) ***Low Cr magnetites:*** These have been identified in beach and river sediments by Bradley et al. (2002) as characteristic of the schist draining rivers of Westland. These magnetites are low in Cr since

they are associated with quartzofeldspathic and pelitic Alpine Schists which are naturally depleted in Cr (Bradley et al. 2002). The extensive distribution of these grains on the shelf is reinforced by results in this study. Shelf, beach, and river samples are mostly dominated by low-Cr magnetite grains which represent the "background" magnetite composition. There is probably only a minor input of low Cr magnetites from granitoids northwards from the Waitaha River (Figure 4-9 A).

4.6.2 Dispersal

Interpretation of shelf sediment dispersal are based on observed relationships between Cr ppm, spinel grain type, and regional geology.

Cascade region: Chromium rich magnetite and chromite supplied to the Cascade Shelf from the Cascade-Martyr river system provide a potential tracer for marine sediment dispersal. The inner to middle Cascade Shelf is clearly nourished by this fluvial supply to at least 95 metres depth (C898). Erosion of Quaternary glacial moraine cliffs supply a significant portion of Cr enriched magnetite to beaches (Bradley et al. 2002), and likely further offshore on the shelf (Figure 4-9, B). The presence of a ferrian chromite grains at Neils Beach may be evidence for littoral transport of material from the Cascade Shelf northwards around Jackson Head, driven by predominant South westerly swells. Alternatively, this may be from the Arawahta River which is fed by the DMU draining Jackson River (Figure 4-9, B). The lack of Cr-bearing spinels in the Arawhata river sample compared to data from Ooi (1982) suggests this study's sample was taken from a site unfavorable for heavy mineral deposition.

Haast, South, and Central Shelves: The influence of Cr-rich spinels from the Cascade region decreases rapidly north of the Arawhata River mouth. The Haast Shelf samples contain a mean Cr content of < 300 ppm, suggesting dilution of Cascade spinels with large volumes of low Cr magnetites from Alpine Schist dominated rivers (i.e. Haast River) (Figure 4-9, B). This dilution effect was demonstrated by Bradley et al. (2002) for beaches in these regions. The South and Central shelves similarly demonstrate the overwhelming influx of Alpine Schist derived sediment, with low Cr values and very few Cr rich magnetites. Not until the Waitaha River do fluvial sediments begin to reintroduce Cr rich magnetites (or chromites). Unfortunately, no shelf samples near the Waitaha River were analysed to detect their arrival on the shelf.

North Shelf and Hokitika Canyon Head (HCH): Chromium enriched magnetites and chromites observed in the Hokitika River and beach were not observed on the inner to middle shelf west of the Hokitika River mouth (Figure 4-9, A). Two possibilities may be causing this. Firstly, the two sample sites (H844 and H850) could be slightly too far south of the Hokitika River mouth to receive fluvial material before it is transported northwards by littoral transport. Secondly, and more plausibly, Hokitika River material is reaching the sample sites but is rapidly diluted by northwards transported low Cr magnetite bearing sediments on the inner to middle shelf.

Due to the lack of Cr - enriched magnetite between the HCH and the coast, Cr enriched magnetites in the HCH may have been deposited during sea level lowstands, when a more direct connection to the canyon system prevailed.

From a stratigraphic perspective, sea level fluctuations may influence not only the proportion of terrigenous material in the Hokitika Canyon strata, but also the proportion of Cr-enriched magnetites present. During low stands, direct connectivity of the Hokitika River would export more Cr-rich magnetites into the canyon system strata. During highstands, i.e. today, the shelf width between the canyon head and river mouth creates a more disconnected system, with a lower influx of high Cr magnetite bearing sediments. This potential contrast in lowstand vs. highstand Cr content in canyon stratigraphy is investigated in more detail in Chapter 7.

4.7 SUMMARY AND CONCLUSIONS

- SWCM shelf detrital magnetites are dominated by low Cr magnetites (<0.5 % wt.), mainly derived from catchments draining the Alpine Schist. These grains constitute the "background" detrital magnetite composition of the SWCM.
- Shelf sediments between the Haast and Central shelves are characterized by low Cr magnetites sourced from numerous rivers draining Alpine Schist dominated catchments.
- Chromites, Ferrian chromites, and Cr-magnetites in shelf sediments are derived from either:

  a) The Dun Mountain Ultramafic Group (i.e. Cascade Shelf sediments)

  b) Ultramafic Pounamu pods (i.e. Hokitika River and Hokitika Canyon Head)
- The dispersal of Cr-rich spinel's is generally limited to shelf areas adjacent to source areas. Subsequent dilution with low Cr-magnetites from rivers and littoral sediments probably limits the influence of Cr-rich spinels.
- Cr-magnetites present in Hokitika Canyon sediments may reflect a relict origin from when sea levels permitted strong connectivity between the Hokitika River and Canyon system.

CHAPTER 5 : GEOCHEMISTRY, PROVENANCE, AND RELICT SEDIMENTS

5.1 INTRODUCTION

Geochemical data are used here to investigate the influence of different source materials (both detrital and authigenic) on the bulk composition of shelf and canyon head surface sediments. Previous work by Stoffers et al. (1984) on Westland shelf geochemistry between the Whataroa and Karamea Rivers provided a general depiction of across and along shelf trends in geochemistry. Building on this work, and using shelf and canyon head geochemical analyses this study, the nature of canyon head sediments and their relationship to the shelves is examined. These results will contribute to the primary aim of this study to examine the nature of Westland shelf-canyon interactions and related sediment dispersal. Particular questions include: what dispersal patterns are identifiable and are there contrasts between the shelf regions as a consequence changes in regional geology? How is geochemistry varying in the canyon heads and what does it indicate in terms of sediment mixing?

5.2 METHODS

5.2.1 X-ray Fluorescence (XRF)

Bulk samples from shelf, canyon head, beach, and rivers locations were analysed using X-ray Fluorescence (XRF) techniques at the University of Canterbury. Details of sample preparation and XRF analyses are in Appendix E1. A total of 46 shelf/canyon head, and 17 beach and river samples were analysed for major and trace elements. Major elements were normalised to 100% for LOI's and iron content is reported as total Fe_2O_3. Raw XRF results and descriptive statistics and ratios are provided in appendix E2 – E8. Margins or error are reported to 1 standard deviation

5.2.2 Carbonate Analysis and Skeletal Components

The bulk carbonate percentage of 44 shelf samples was determined at NIWA (Wellington) using the gasometric quantitative analysis after acidification method. A detailed description of this technique is in Appendix D1 and Jones & Kaiteris (1983). This technique provides rapid, relatively precise (± 2% accuracy) results from only small sample sizes (~ 0.333g). All SWCM carbonate analysis results are found in Appendix D3. Skeletal components were investigated using a combination of binocular examination of loose sand samples (>63 μm only), and thin section point counts of the sand fractions. The total percentage of skeletal grains present in this sand fraction and the dominant skeletal types were estimated also. Binocular skeletal component results are provided in Appendix C5 and C6. Skeletal component data from point counts are in Appendix C4.

5.2.3 X-ray Diffraction (XRD)

X-ray diffraction analysis was used to supplement the petrological studies of the bulk mineralogy in SWCM sediments. Sample preparation and details of the XRD method is provided in Appendix C7.

5.3 SWCM MAJOR AND TRACE GEOCHEMISTRY

Major element geochemistry is summarized in Table 5-1 for all marine surface samples. Detailed results and statistics for each shelf region are located in appendix E4 and E5. The most common oxides are SiO_2 and Al_2O_3 with 69.17 ± 4.9 % and 14.13 ± 2.79 % respectively. The mean content for MgO, CaO, Na_2O, and K_2O is typically between 1-5 %. For TiO_2, MnO, P_2O_5 the average is less than 1%. A significant amount of variation exists among marine samples, especially with SiO_2, Al_2O_3, Fe_2O_3T, CaO, Na_2O, and K_2O (Table 5-1).

Table 5-1 Summary statistics for all 46 shelf and canyon head surface sediment samples (in wt. %).

	SiO_2	TiO_2	Al_2O_3	Fe_2O_3T	MnO	MgO	CaO	Na_2O	K_2O	P_2O_5
Mean	69.17	0.91	14.13	5.48	0.08	1.74	2.57	3.39	2.31	0.23
Min	59.55	0.50	9.04	3.15	0.05	1.02	1.59	1.62	0.93	0.13
Max	77.45	6.61	18.69	16.94	0.38	2.93	6.54	4.75	4.23	0.76
Std. error	0.72	0.13	0.41	0.42	0.01	0.07	0.12	0.11	0.11	0.02
Variance	24.01	0.79	7.79	8.00	0.00	0.22	0.71	0.56	0.58	0.01
Stand. dev.	4.90	0.89	2.79	2.83	0.05	0.47	0.84	0.75	0.76	0.11

Correlations: A Pearson correlation analysis was used to highlight significant correlations between all elements, water depth, and mean grain size of all marine samples (significance level > 99%) (Appendix E7). For SiO_2, strong to moderate negative correlations exist with Al_2O_3 (-0.61), K_2O (-0.77), V (-0.81), Zn (-0.79), Ga (-0.73), and Rb (-0.69). Moderate to strong positive correlations of Al_2O_3 with MgO (0.65), Na_2O (0.75), K_2O (0.58), and Ba (0.87) also occur. Moderate to strong positive correlations of K_2O with Zn (0.91), Ba (0.67), and Rb (0.93) exist. Positive correlations of Fe_2O_3T with P_2O_5 (0.85), V (0.69), and Pb (0.87) are also present. Notable mean grain size correlations include a strong negative correlation with Al_2O_3 (-0.85), and a weak negative correlation with K_2O (-0.57).

5.3.1 Major Elements

The relationships between bulk major element chemistry, water depth, and mean grain size are displayed in Figures 5-1 (A & B) and 5-2 to 5-4. In addition, the SiO_2/Al_2O_3 ratio is employed as a useful maturity index, reflecting the abundance of either silica (high ratios) or clays and feldspars (low ratios) (Figure 5-5) (Rollinston 1993). Major elements in the marine samples show typical continental shelf trends, with Al_2O_3, K_2O, Na_2O, and MgO increasing towards the middle shelf, until leveling off close to 100 m depth (Figure 5-1 A). Silica content shows a typical decrease with water depth. These depth trends are reinforced by major element variations with mean grain size. Here, Al_2O_3, K_2O, Na_2O, and MgO concentrate in the finer grain sizes common at depths of greater than 50 m (Figure 5-1 B). Silica content is strongly controlled by grain size, showing higher levels at shallower depths where mean grain size is greatest.

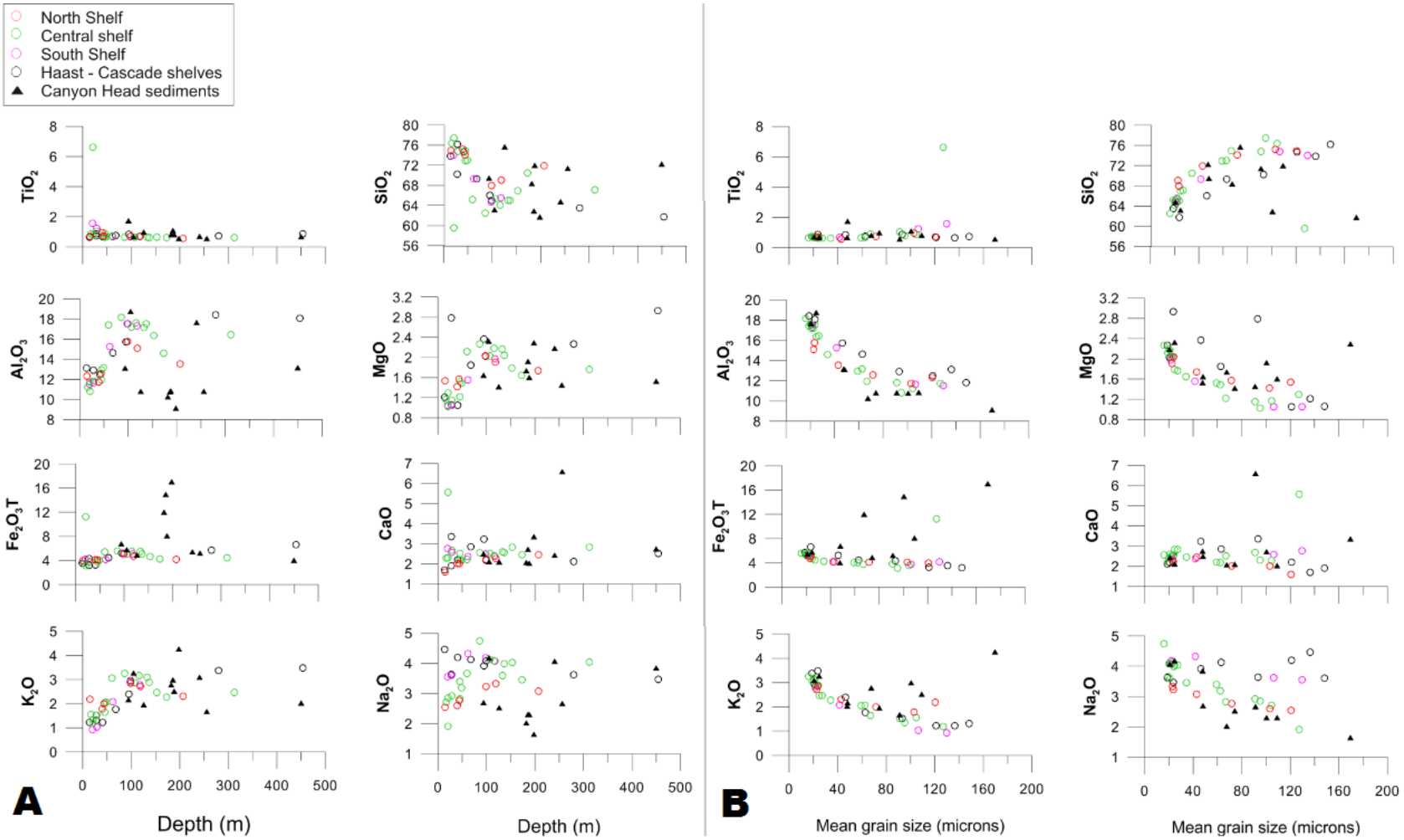

Figure 5-1 Major element variations against A) water depth and B) mean grain size, for all shelf and canyon head surface sediments samples from the South Westland region

a) Inner Shelf (< 50 m depth)

The inner shelf surface sediments contain the highest SiO_2 ($\bar{x}$ =73.5 ± 4.07 %) (Figure 5-1A & Figure 5-2). At depths of less than 30 m, SiO_2 content is often greater than 75 % (Figure 5-2). On transects C and D of the Central Shelf, SiO_2 is slightly more enriched. At 21 m depth on transect E (3-4 km offshore from Gillespies Beach) silica is abnormally low (59.5). The Al_2O_3 content is low ($\bar{x}$ =12.12 ± 0.7 %) and maintains a narrow range (11.5 – 13.1 %). A wide zone of low Al_2O_3 sediment extends from 15 km offshore to at least upper slope depths on the broad Central Shelf (Figure 5-3). The Fe_2O_3T content at inner shelf depths is typically < 4 % with a notable spike of 11.3 % at 21 m depth on Transect E (Figure 5-4). Low K_2O is characteristic on the inner shelf, especially at depths of less than 30 m (Figure 5-1 A). The inner shelf is characterized by high TiO_2 levels and high SiO_2/Al_2O_3 and Na_2O/K_2O ratios (Figure 5-5 and appendix D5). Regional variations of the inner shelf SiO_2/Al_2O_3 ratio are minor, while the Na_2O/K_2O ratio is markedly higher on the South to Cascade inner shelves.

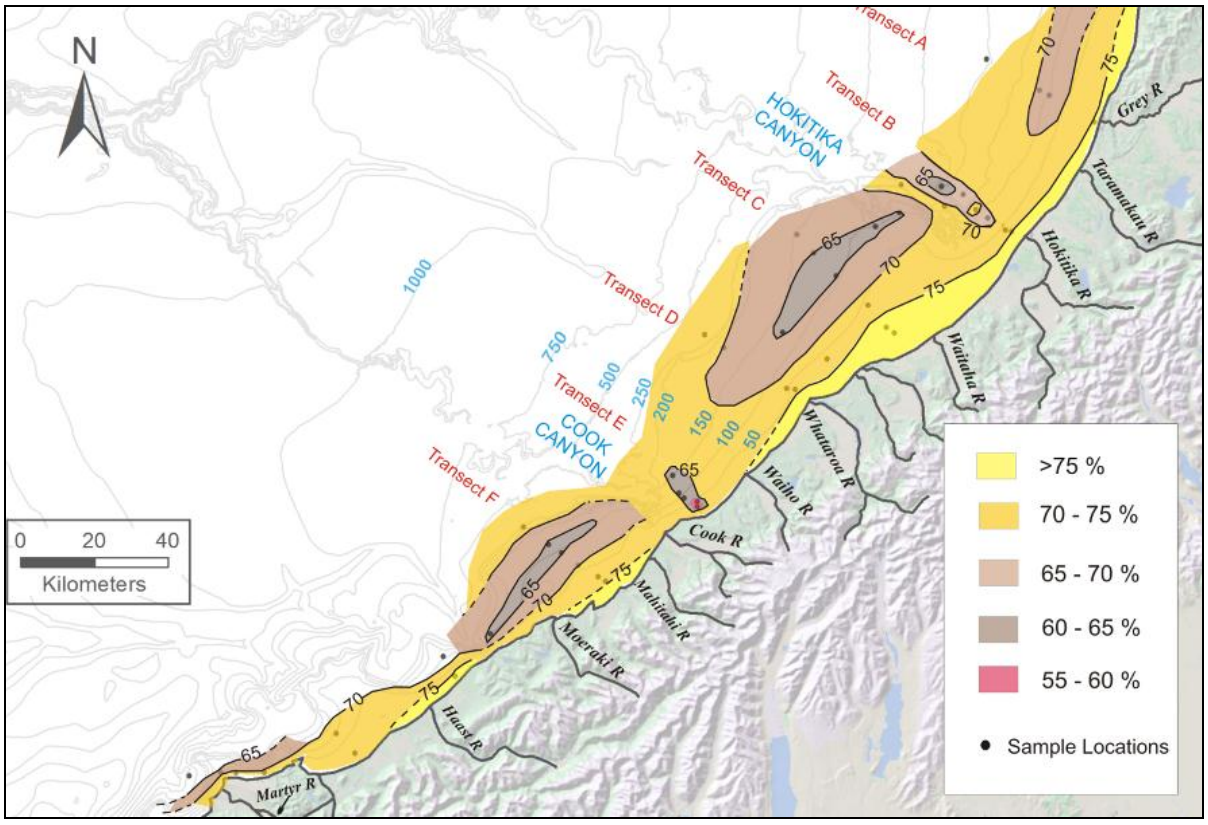

Figure 5-2 Map of SiO_2 content in South Westland shelf and canyon head samples. All data in weight %.

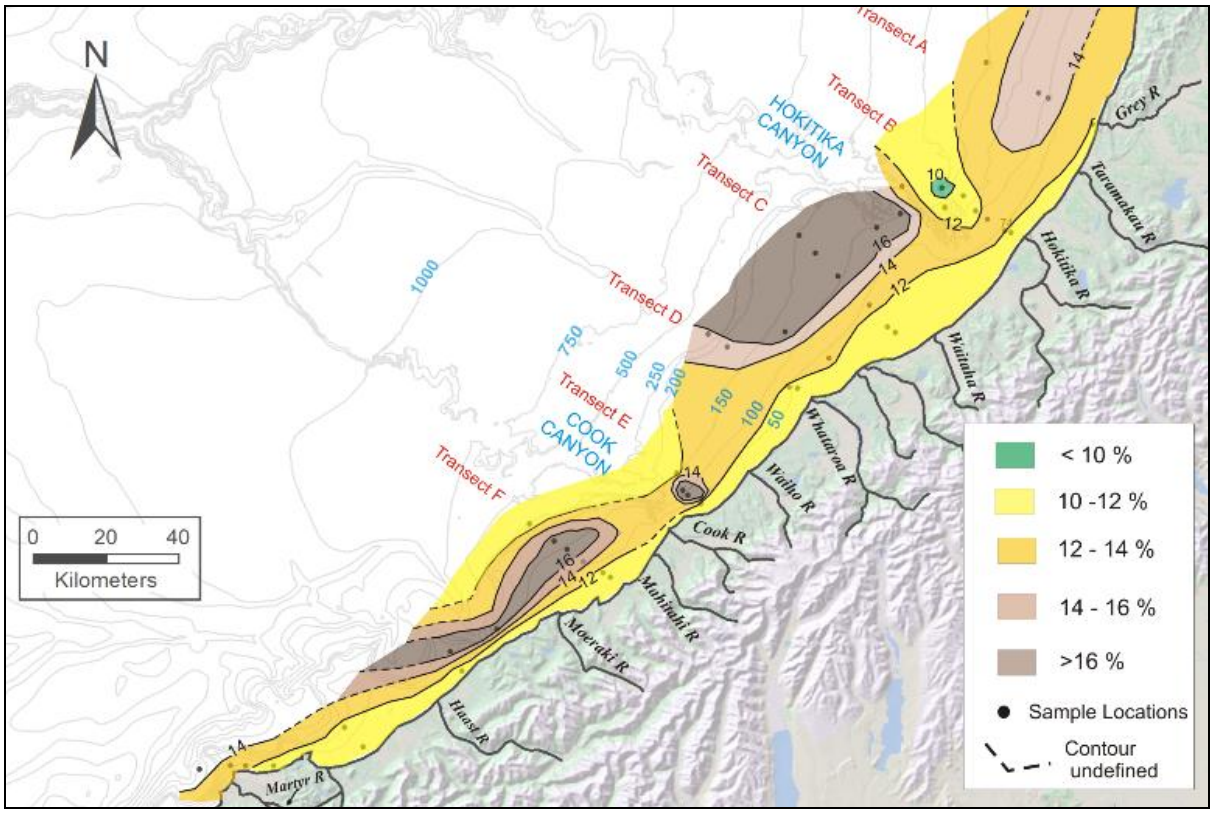

Figure 5-3 Map of Al_2O_3 content in SWCM shelf and canyon head samples. All data is the bulk weight %.

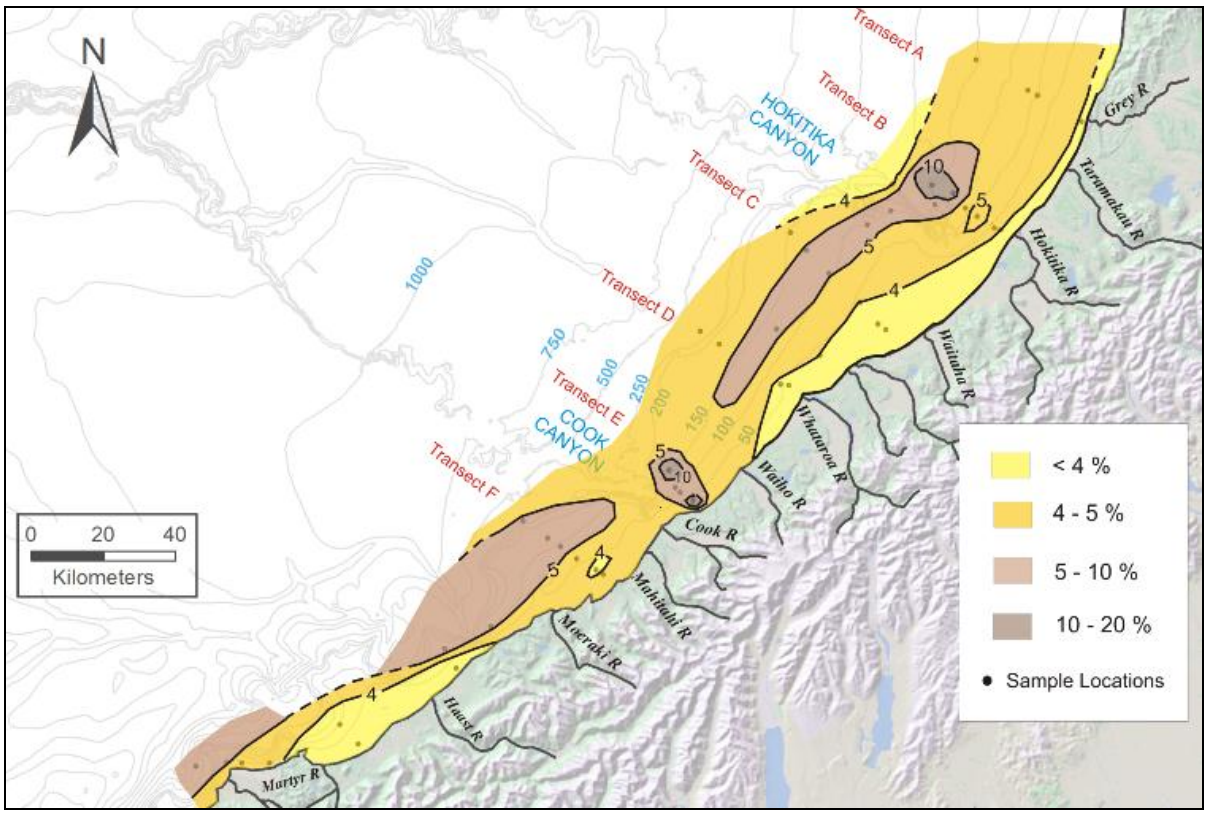

Figure 5-4 Map of total Fe_2O_3 content in SWCM shelf and canyon head samples. All data is the bulk weight %.

b) Middle Shelf (50 – 150 m depth)

On the middle shelf, SiO_2 is low ($\bar{x}$ =66.0 ± 2.0 %), especially between 85 and 115 m depth (Figure 5-1 A & Figure 5-2). This forms a rough belt of SiO_2 depleted sediments eventually increasing to 65 - 70 % SiO_2 to the west and east. On the North Shelf this belt is slightly richer in SiO_2. The Central Shelf has much broader zones of low SiO_2 than the South Shelf (Figure 5-2). As expected, the middle shelf Al_2O_3 content is high ($\bar{x}$ =16.72 ± 1.15 %), defining approximate belts of elevated Al_2O_3 on the North to South shelves (Figure 5-3). No seaward decrease in Al_2O_3 content towards outer shelf depths on the Central Shelf is apparent. The average Fe_2O_3T and MgO content is slightly higher in middle shelf sediments (Figure 5-1 A and Figure 5-4). A weakly defined belt of higher Fe_2O_3T content (5-6 %) occurs on the Central Shelf between 100 – 150 m depth (Transect C and D). Average Na_2O and K_2O content is higher than the inner shelf sediments ($\bar{x}$ =3.96 ± 0.4 & 2.77 ± 0.41 respectively) (Appendix E5). Middle shelf SiO_2/Al_2O_3 and Na_2O/K_2O ratios are lower than the inner shelf, with the SiO_2/Al_2O_3 ratio almost half of that in inner shelf sediments (Figure 5-5). The middle North Shelf is more enriched in the SiO_2/Al_2O_3 ratio at middle shelf depths.

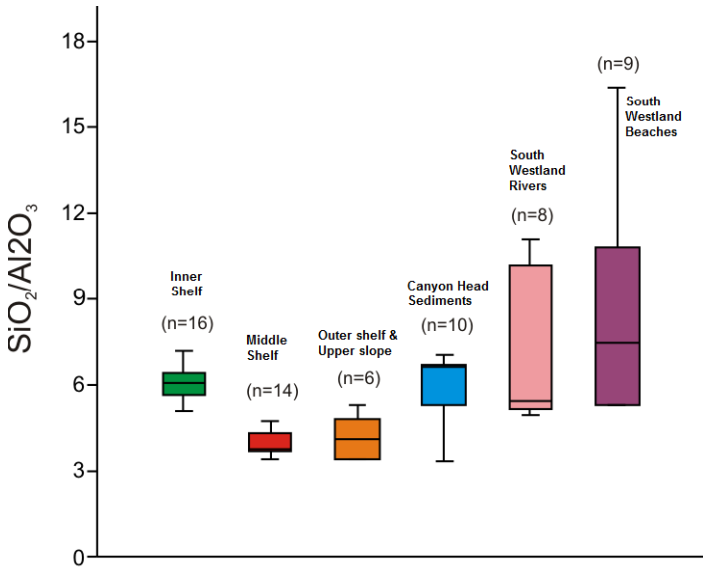

Figure 5-5 The SiO_2/Al_2O_3 ratio for the various SWCM depositional environments.

c) Outer Shelf to Upper slope (>150 m depth)

Beyond 150 metres depth, SiO_2 content increases slightly ($\bar{x}$ = 66.95 ± 3.90 %) from the middle shelf and is more variable (61.7 – 71.9 %) (Figure 5-1 A and Figure 5-2). This increase is not as pronounced on transects C and D of the Central Shelf. The Al_2O_3 content remains high, but decreases slightly to define the seaward boundary of the middle shelf Al_2O_3 rich belts (Figure 5-3). The Fe_2O_3T content is similar to the middle shelf except for a notable decrease (< 4.5 %) on transect D (Figure 5-4). The SiO_2/Al_2O ratio is slightly higher and more variable than the middle shelf sediments (average 4.2 ± 0.75) (Figure 5-5).

d) Canyon Heads

The major element composition of canyon head sediments is characterised by high spatial variability, and a distinct contrast between the north and south rim geochemistry (especially in the HCH).

Overall, SiO_2 content is relatively low ($\bar{x}$ = 68.0 ± 4.8 %) and more variable compared to the other shelf environments (Figure 5-1 A and Figure 5-2). The south rim of the HCH is notably lower in SiO_2 (<65%), while the north rim sediments contain 65 – 75 % (Figure 5-2) An exception is at 198 m depth on the north rim where sediment contained 61.5 % SiO_2.

While highly variable, the mean Al_2O_3 content is similar to inner shelf levels ($\bar{x}$ =12.46 ± 3.24 %). A number of north HCH rim locations contain the lowest levels of Al_2O_3 for all marine sediments (9 - 13 %). Highly enriched south rim samples containing 13 – 18 % Al_2O_3 contrast with these north rim values (i.e. C905 & P668, Appendix E2). This contrast is less apparent in the two CCH locations.

The canyon heads display the greatest variation and highest average Fe_2O_3T content for all marine environments (3.92 – 16.90 % and $\bar{x}$ = 8.29 ± 4.60 %). On the HCH north rim, Fe_2O_3T increases from 4 - 6 % at 100 m depth to 16.9 % at 198 m in the west. Several north HCH rim samples contain 3 times the iron content of the south rim sediments, with a similar contrast in the CCH (Figure 5-4 and Appendix E2).

On the HCH south rim, Na_2O and K_2O are more concentrated (i.e. Na_2O > 4.0 % & K_2O > 3.0 %) than other areas in the canyons (Appendix E2). An anomalous spike of 4.23 % K_2O occurs in the HCH north rim sediments (198 m depth).

The TiO_2 content in canyon head sediments decreases with depth on the HCH north rim, from 1.7 % at 94 m to 0.5 % at 198 m depth. The highest marine P_2O_5 levels are found in canyon head sediments ($\bar{x}$ = 0.3 ± 1.9). These P_2O_5 levels are most elevated in the deeper north rim locations of the HCH and CCH.

A high SiO_2/Al_2O_3 ratio is typical of the canyon head sediments ($\bar{x}$ =5.76 ± 1.3) and is similar to the inner shelf ratios (Figure 5-5). In the HCH, a strong north vs. south rim contrast exists, with ratios > 6.0 in the north compared to < 4.0 on the south rim.

e) Beaches

A silica rich, quartzofeldspathic geochemistry is typical of beach samples. Between the Haast River mouth and Jackson bay average silica content is higher compared to the northern beaches (Appendix E2). Beach sediments contain more variable Fe_2O_3T and TiO_2 content than the river samples, with notable spikes at Hokitika and Gillespies beaches (up to 10.61 % Fe_2O_3T and 3.10 % TiO_2 respectively) (Appendix E2). Compared to marine and river samples, the SiO_2/Al_2O_3 ratio is highest in beach sediments, particularly on the Haast region beaches ($\bar{x}$ =8.53 ± 3.5 %) (Figure 5-5).

f) Rivers

In the river samples, SiO_2 is relatively high ($\bar{x}$ =74.04 ± 7.64) and variable (69.72 – 85.0 %). The highest SiO_2 contents occur in the Haast and Arawhata River samples which contained over 80 % SiO_2. The rivers discharging to the Central and South shelves (Waitaha, Whataroa, Cook, and Paringa rivers) contain between 13-14 % Al_2O_3, relatively high compared to the overall average (11.60 ± 2.55 %). In the Martyr River, anomalously high Fe_2O_3T and MgO contents were found (7.03 & 14.44 % respectively). A high SiO_2/Al_2O_3 ratio (6.18 ± 2.4) is evident in the river sediments (Figure 5-5). This ratio is similar to the inner shelf sediments, but shows more variation. Very high SiO_2/Al_2O_3 ratios were found in the Haast and Arawhata rivers (>10.0).

5.3.2 Geochemical Classification of Modern SWCM Sediments

Major element ratios in sediments have been used by several authors to classify terrigenous sediments, and in some cases discriminate between tectonic settings (Roser & Korsch 1986, 1988; Bhuiyan et al. 2011). The SiO_2/Al_2O_3 and Na_2O/K_2O ratios are used primarily here after Rollinston (1993) and Herron (1988) to distinguish between depositional environments on the South Westland region (Figure 5-6 A-C).

Shelf sediments: All shelf and canyon head surface sediments from the SWCM plot within either the Greywacke or Litharenite fields, typically close to the boundary between these fields (Figure 5-6 A). The Greywacke field in Figure 5-6 represent sediments rich in clays in silts (Boggs 2009). Inner shelf sediments (green squares) plot mostly as a separate group towards the litharenite field, reflecting a slightly more silica enriched (‘mature’) geochemistry. The middle to outer shelf sediments (red triangles) plot further into the Greywacke field, reflecting a more silica-depleted composition and enrichment in clays and feldspars.

Canyon head sediments: The canyon head sediments reveal a more diverse range of compositions, plotting in both the middle - outer shelf and inner shelf fields. Several samples plot outside the typical shelf sediment groupings as litharenites more towards the Arkose field (Figure 5-6 A). The distinction between canyon head environments and the two main shelf compositions are displayed in (Figure 5-6 B). The HCH south rim sediments show a strong association with the middle - outer shelf geochemistry (particularly C905 and P688). In contrast, the HCH north rim sediments plot exclusively in the litharenite field, indicating higher silica levels.

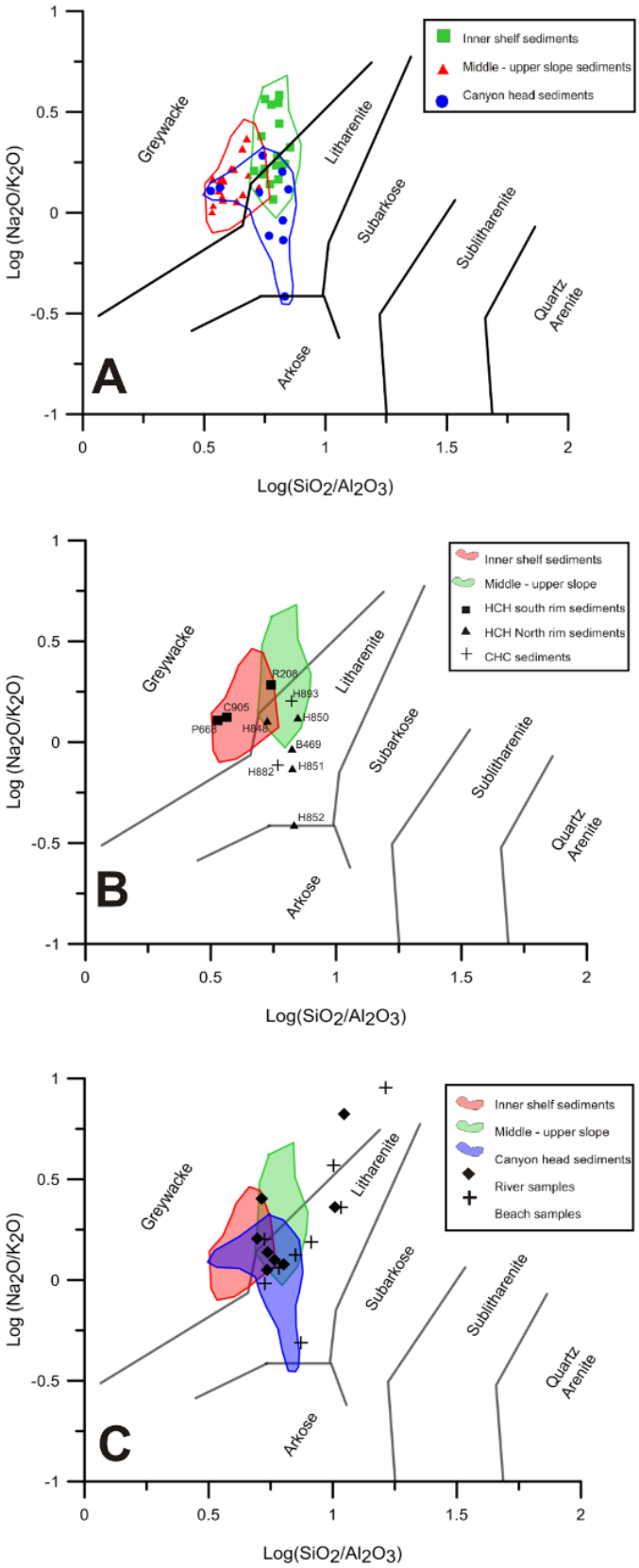

Figure 5-6 Geochemical sediment classification plots for A) all shelf and canyon samples. B) All shelf samples with canyon head 'sub'-environments, C) river and beach samples. After Rollinston (1993) and Herron (1988).

The Na_2O/K_2O ratio decreases progressively with depth on the north rim, with the deepest sediments plotting on the Litharenite – Arkose boundary (Figure 5-6 B , H852). This north versus south contrast is also indicated in the two CCH samples. Here, the northern CCH (H882) plots with the other outlier samples from the HCH north rim.

Rivers and beaches: The majority of river sediments overlap the litharenite – greywacke boundary and the region of overlap between the inner and middle - outer shelf groups (Figure 5-6 C). The Arawhata and Haast rivers are the only outliers, with a more silica enriched chemistry. Beach samples display more variation than the rivers but still maintain a grouping in the inner and middle – outer shelf overlap region. All beaches outlying this overlap region are from the Haast Shelf region.

Most of the beaches and rivers associated with the North to South Shelf regions plot within the overlap between the inner and middle - outer shelf groups (Figure 5-6 C).This indicates the general connection between rivers supplying these shelves and shelf sediment geochemistry.

5.3.3 Trace Elements

Trace element data for all marine sediments are presented in Figure 5-7 and Figure 5-8 to show variations with mean grain size and water depth. Trace element variation diagrams in Figures 5-9 and 5-10 provide regional comparisons. Descriptive statistics for trace elements by region and depositional environment are provided in appendix E4 and E5.

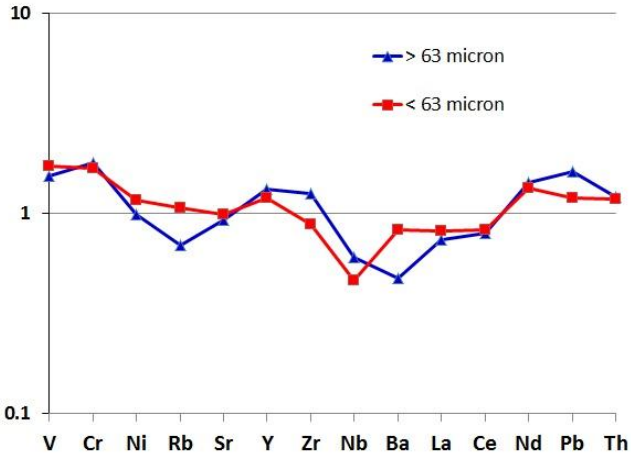

Figure 5-7 Average South Westland shelf and canyon head trace element distributions for mean grain sizes greater than and less than 63 microns. Trace elements are normalised to the upper continentsal crust (UCC) after Taylor & McLennan (1985).

Trace elements such as Rb, Ba, Zn, and to a lesser extent Ni and V, display a tendency to concentrate in the finer grain sizes, mostly between 20 – 80 µm (Figure 5-7 and Figure 5-8 B). Generally, the coarser inner shelf sediments display more variation compared to the finer grained middle to outer shelf sediments (i.e. Ba, Zn, and Rb). Variations with water depth demonstrate a typical continental shelf trend where elements such as V, Rb, or Ba concentrate in sediments beyond the inner shelf (Figure 5-8 A).

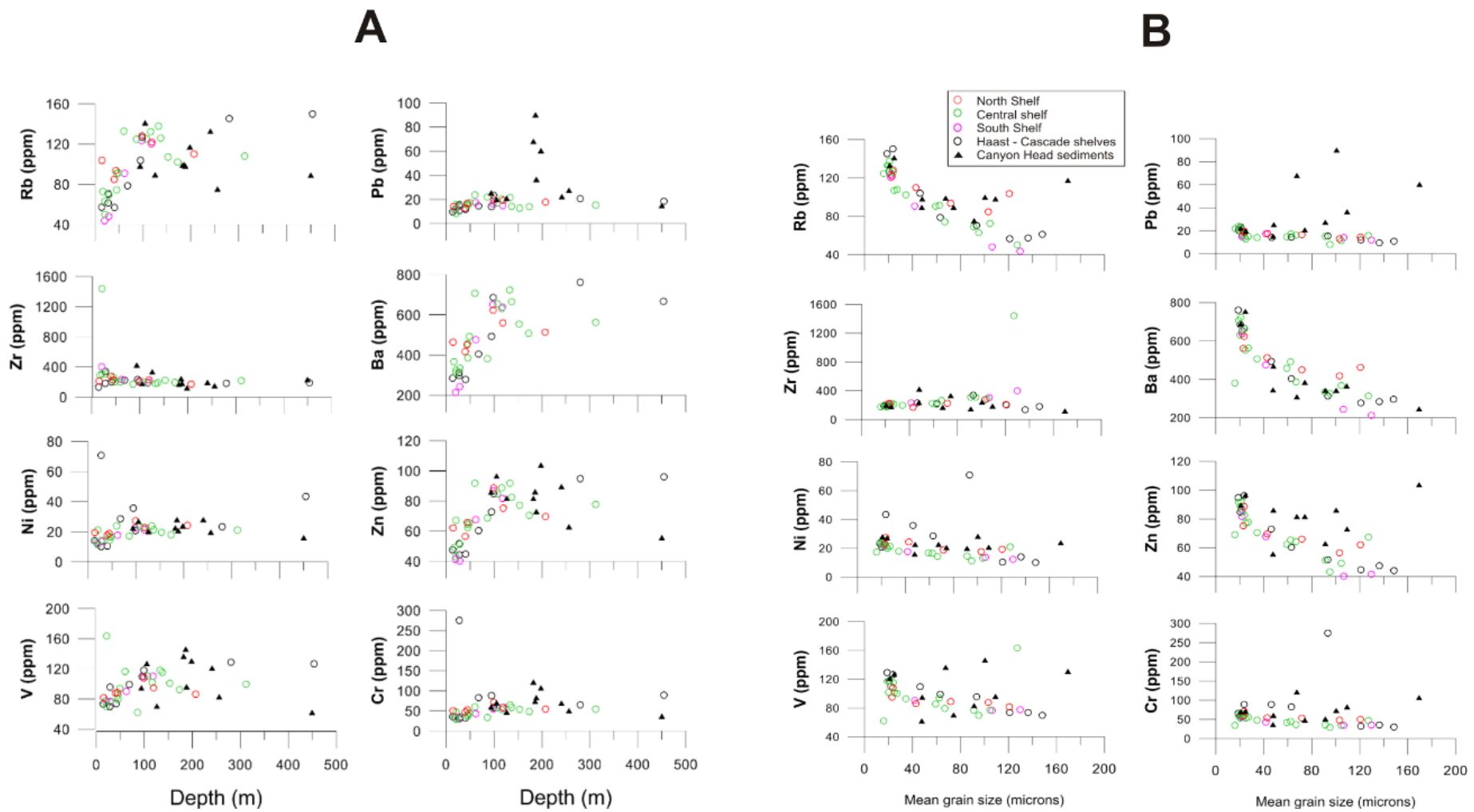

Figure 5-8 Bulk trace element variations against A) water depth and B) mean grain size, for all shelf and canyon head surface sediments samples from the SWCM region.

Trace elements variations with silica are broadly similar to the variations with mean grain size. This probably reflects the higher quartz content of the coarser, inner shelf sediments. The strength of correlations with silica appear stronger than with mean grain size, especially for V. Several trace elements concentrate in the inner shelf. In particular, Zr is high on the inner shelf with an average of 333 ppm, decreasing to 204 and 197 ppm on the middle and outer shelves respectively (Figure 5-8 A and Appendix E5).

Some regional trends are apparent in the trace element data. Several of the canyon head samples are enriched in trace elements relative to shelf sediments of similar grain size, silica content or depth. In particular, Pb, Zn, V and Cr show canyon head enrichments. A weak north to south decrease in the content of Rb, Ba and possibly Zn is also apparent (Appendix E4). In some of the Haast to Cascade Shelf sediments, enrichments in Ni and Cr are present (Figure 5-8 A and B).

In Figure 5-9 and 5-10, multi element plots are used to compare the trace element chemistry of shelf, river, beach, and typical Alpine Schist compositions. The North, Central, and South Shelf regions show similar trends, with most variation due to grain size effects as demonstrated in Figure 5-7. These shelves, as expected, reflect an overall common source from the Alpine Schists of the Southern Alps (Figure 5-9 and 5-10). An anomalous trend with Zr highly enriched on the inner Central Shelf indicates a localized concentration of heavy minerals, in particular, zircon. More diverse trace element patterns occur in the Haast – Cascade Shelf sediments, particularly the Cr and Ni levels further south in the Cascade Shelf sediments.

Canyon head trace element patterns highlight the diversity of materials forming the bulk sediment geochemistry here. The South rim sediments (R208, C905, & P668) follow the typical modern North to South Shelf region trends (Figure 5-10). Elevated Cr levels on the deeper north HCH locations (H852 & H851), and high Zr and Y on the shallower North rim locations (H848 & H850) contrast with the south rim.

River and beach plots broadly reflect the Alpine Schist influence in most South Westland catchments (Figure 5-10). The Haast region rivers and beaches (i.e. Arawhata River and Neils Beach) have slightly more depleted trace element patterns. The Martyr River in the Cascade region is highly enriched in Cr and Ni, reflecting the influence of Dun Mountain Ultramafic exposures in the Martyr catchment (Morton & Smale 1990). Similarly, the Cr enrichments in the Hokitika Beach trace element pattern also reflect an ultramafic influence. This enrichment at Hokitika beach is probably from Cr rich spinels, which Bradley et al. (2002) have associated with ultramafic Pounamu pods in the upper Hokitika catchment.

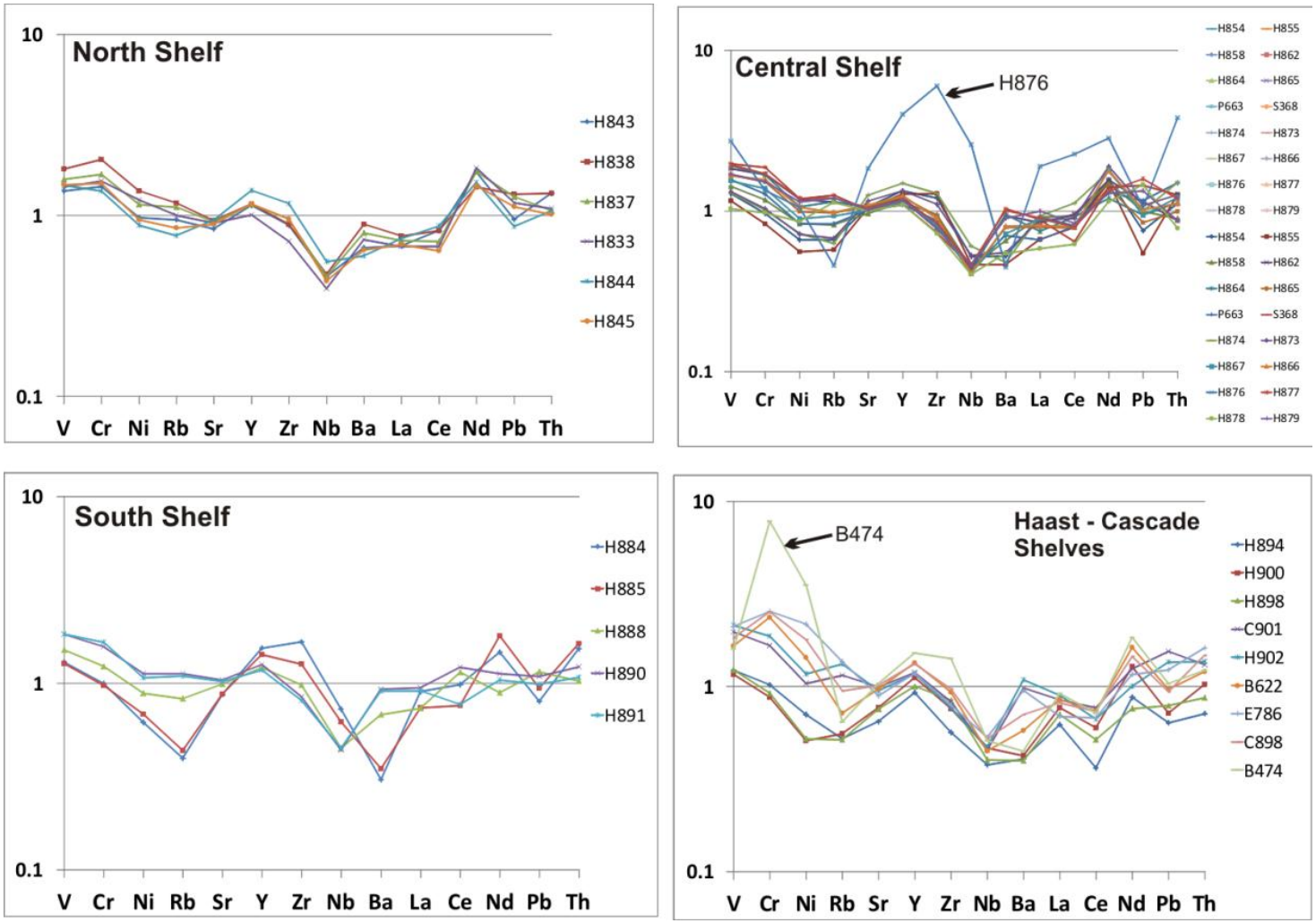

Figure 5-9 Trace element multi-plots for SWCM shelf sediments from. Note change in scale for river and beach multi-plot. Representative Alpine Schist data are for the Franz Josef-Fox Glacier area schists in Grapes et. al. (1982).Trace elements are normalised to the upper continentsal crust (UCC) after Taylor and McLennan (1985).

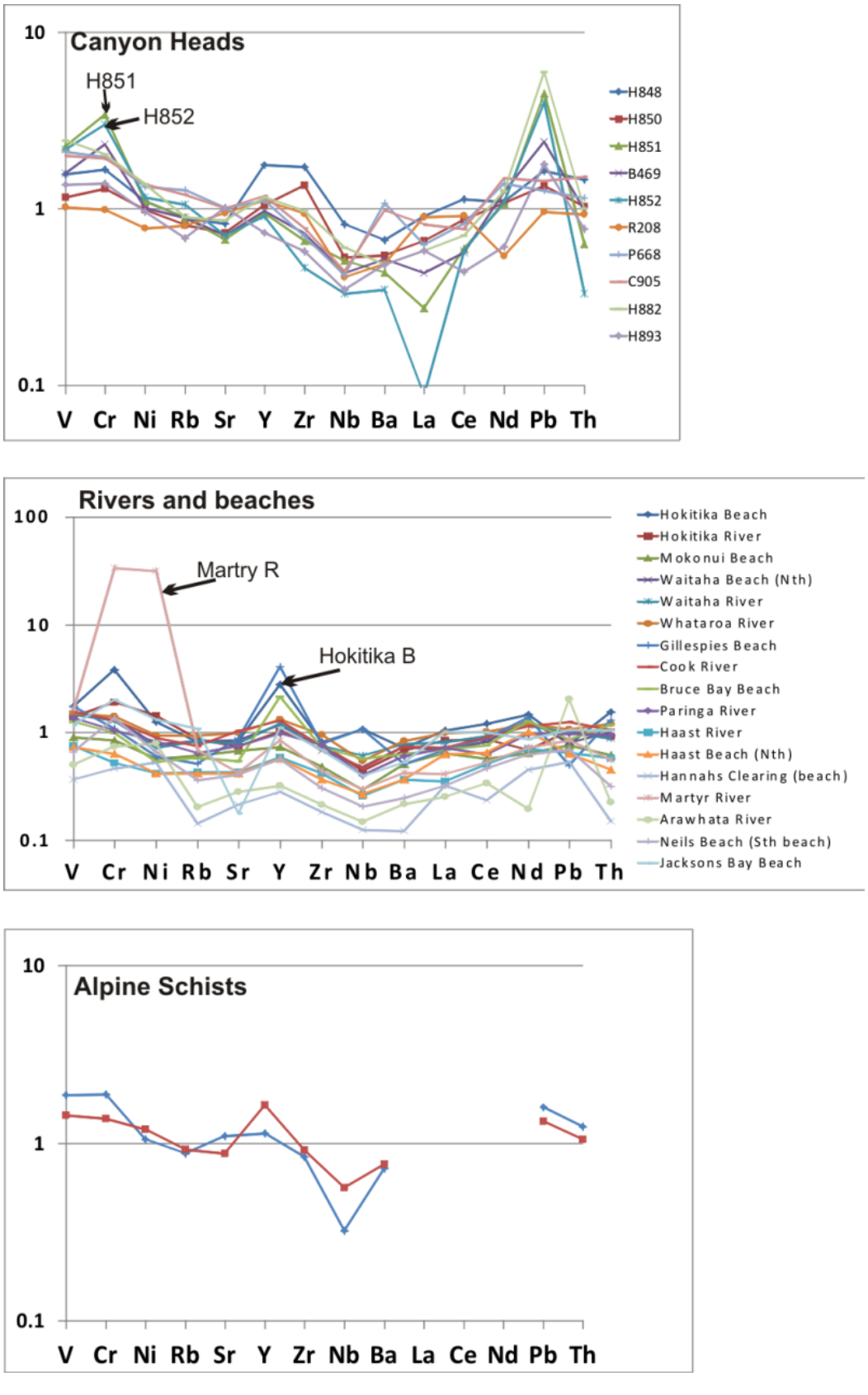

Figure 5-10 Bulk trace element multi-plots for SWCM canyon head and terrestrial sediments from the SWCM region. Note change in scale for the river and beach multi-plot. Representative Alpine Schist data are for Franz Josef-Fox Glacier area schists from Grapes et al. (1982).Trace elements are normalised to the upper continentsal crust (UCC) after Taylor and McLennan (1985).

Trace element ratios:

Trace element ratios are very applicable to tracing the dispersal and provenance of marine sediments because they are less affected by grain size differences or carbonate dilution than bulk geochemistry (Rollinston 1993). The Cr/V and Y/Ni ratios (Figure 5-11 & Appendix E8) are the most useful dispersal indicators for SWCM sediments. The Cr/V ratio reflects the enrichment of Cr over other ferromagnesian minerals, while the Y/Ni ratio indicates the general level of ferromagnesian minerals present (McLennan et al. 1993). Sediments sourced from mafic and ultramafic rocks with abundant ferromagnesian minerals will have a low Y/Ni ratio, while a high Cr/V ratio is typical of sediments derived from Cr-mineral bearing rocks (i.e. Ophiolites).

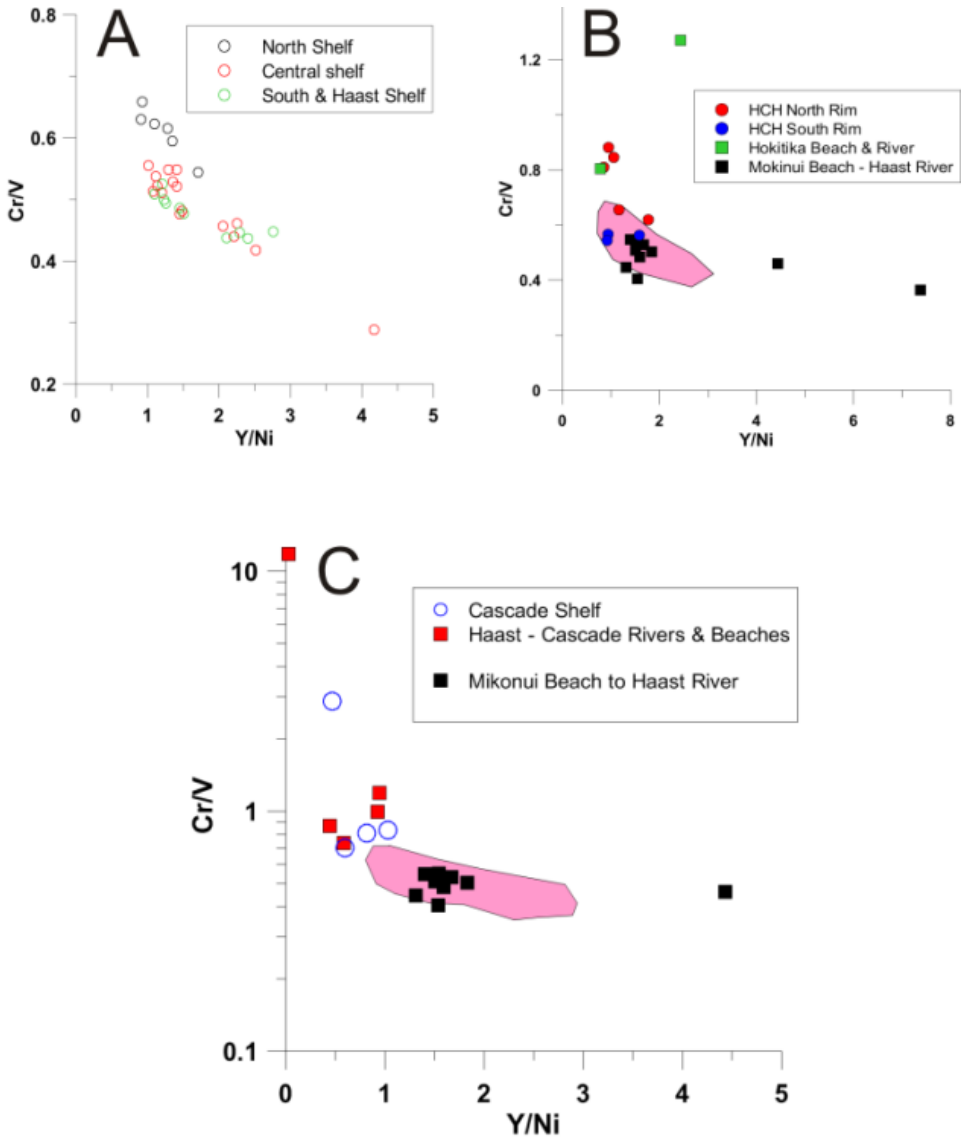

Figure 5-11 Graphs of the Cr/V vs. Y/Ni ratios for A) North to Haast Shelf sediments, B) North to Haast Shelf sediments (pink area), Hokitika Canyon Head samples, and terrestrial samples between Hokitika River to Haast river, and C) Cascade region shelf and terrestrial samples, and North to Haast Shelf samples (pink area). Note logarithmic scale in C. Graphs based on McLennan et al. (1993).

In Figure 5-11 A, the North Shelf samples (black circles) show a slight enrichment in Cr over other shelf sediments between the Haast River and the Hokitika Canyon Head (HCH). A strong association

between the HCH north rim sediments and Hokitika beach and river sediments is clear in the Cr enrichments in Figure 5-11 B. By far the most Cr enriched sediments are from the Cascade Shelf and terrestrial sediments Figure 5-11 C. The extremely enriched sample in Figure 5-11 C is from the Martyr River sample, where the ratios suggest high concentrations of Cr and ferromagnesian minerals (Cr/V > 10.0 and Y/Ni < 0.05) (Appendix E8).

5.4 CARBONATE AND SKELETAL CONTENT ON THE SWCM

Carbonate content and the skeletal composition of SWCM sediments are presented in this section. Skeletal content is based on thin section point counts (Appendix C4), bulk thin section descriptions (Appendix C3), and binocular microscope work on the loose sand fractions (Appendix C6).

5.4.1 Carbonate Content

The bulk carbonate content in shelf and canyon head surface sediments is generally low (Figure 5-12 and Appendix D3). The average percentage was 0.6 % (n=41) and ranged between 0 to 9.2 %. Despite carbonate values being small, across shelf trends are observed. On the inner shelf (<50 m depth), carbonates generally comprise less than 1 % of sediments. Beyond the 100 m isobath, carbonate content increases slightly to 1-3 % of shelf surface sediments. On the Central Shelf no carbonate occurs except in the northern end of this shelf (transect C). The most distinct across shelf increase occurs on the South Shelf (transect F), with the highest carbonate percentage (9.2%) on the upper slope at 256 m depth (Figure 5-12).

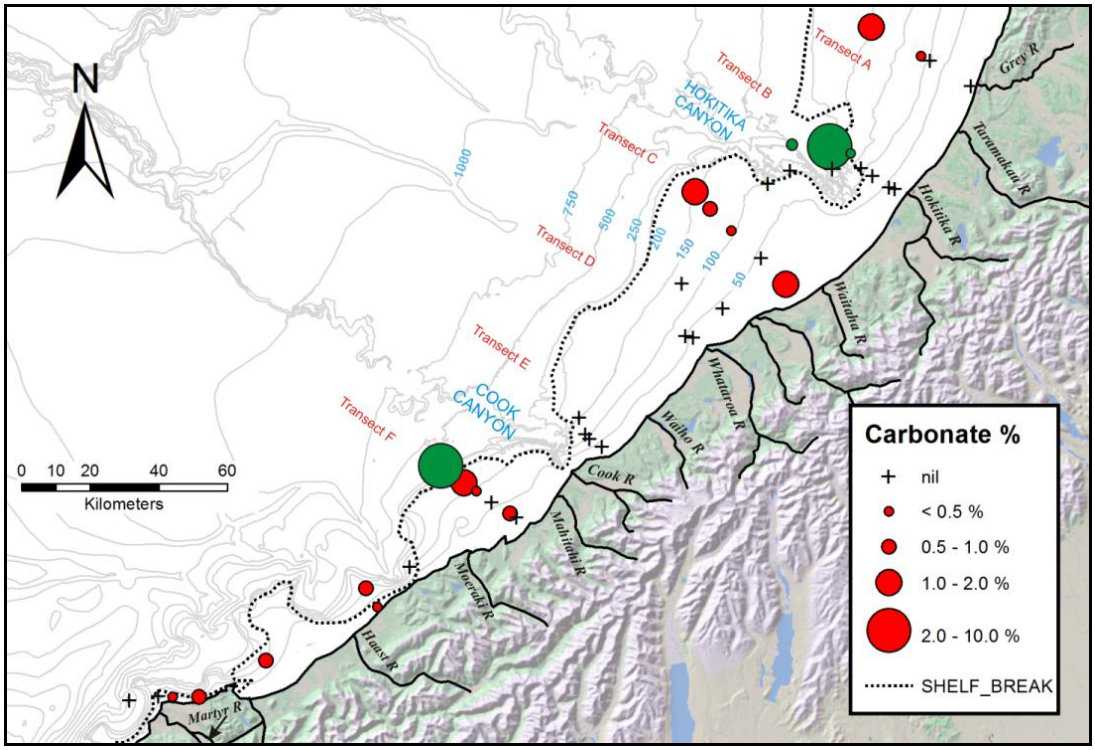

Figure 5-12 Map showing the bulk carbonate percentage in shelf and canyon head surface sediments of the SWCM. Determined by gasometric quantitative analysis of bulk sediments. Green circles represent canyon head samples.

Southwards towards the Haast and Cascade shelves, less than 1 % carbonate is common. From the coastline out to the Hokitika Canyon Head (transect B), carbonate values are negligible until a spike of 6% at 200 m depth on the north canyon head rim (Figure 5-12).

5.4.2 Skeletal Percentage and Varieties in the Sand Fraction

While the classification of individual species was not the aim of this study, some foraminifera and bivalves were identified. Common skeletal grains are displayed in photos and photomicrographs in Figure 5-13 and Figure 5-14. The dominant skeletal component in the sand fraction was estimated under the binocular microscope (Figure 15 and Appendix C6). An estimate of planktic vs. benthic was possible where enough foraminifera were present in loose sands (Figure 5-16 and Appendix C5). Foraminifera identifications were assisted with reference to Hayward et al. (1999).

Shelves

Skeletal percentage: Skeletal grains are rare on the SWCM shelves, comprising less than 4 percent of shelf sediments (Appendix C6). In point counts, shelf skeletal components averaged 1.9% of all grains in the sand fraction (n=12). No notable regional trends are evident. A weak across shelf increase in skeletal content with depth occurs on most shelf regions. The inner shelf averages ~1.5% in the sand fraction and increases to 2 - 4 % at middle to outer shelf depths (Appendix C4).

Foraminifera: Foraminifera are the dominant skeletal type on most of the SWCM shelves, except for the narrow Haast and Cascade shelves (Figure 5-15). At inner shelf depths (< 50 m) foraminifera are very rare, while at middle to outer shelf depths (50 – 220 m) foraminifera typically comprise 1-2 % of the sand fraction (Figure 5-16). Planktonic species (mainly *Globigerina*) are the most common foraminifera, particularly on the middle to outer shelves (Figure 5-13 and Figure 5-16). Benthic species are dominant in several middle shelf locations, such as on the North Shelf and transect E on the Central Shelf (Figure 5-13 and Figure 5-16). Benthic varieties identified include: *Elphidium, Bolivina, Cibicides, Uvigerina,* and *Saidovina*.

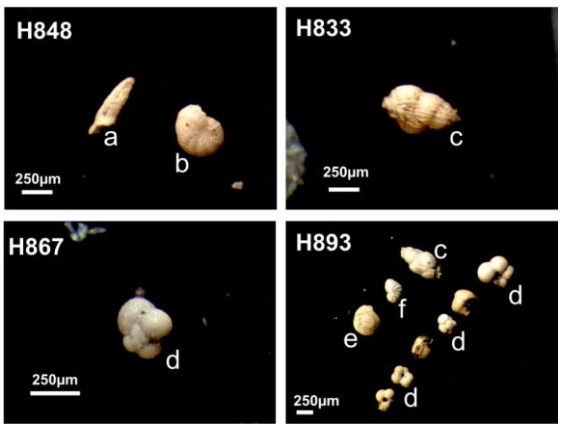

Figure 5-13 Selected foraminifera common in the sand fraction of SWCM surface sediments. a) Unidentified uniserial benthic, b) *Elphidium, c) Bulimina, d) Globigerina,* e) *Cibicides,* f) Unidentified benthic.

Bivalves: Bivalves are the second most abundant skeletal type present on the Westland shelves (Figure 5-14 and Appendix C6). Fragmented bivalves are most common, with rare whole bivalves ranging up to 15mm in length (Figure 5-14). On the inner Central Shelf bivalves are present, especially at 45 m depth on Transect D (Figure 5-15). No bivalves were identified on the North or South shelves in thin section or in loose sand samples, while the Haast to Cascade shelves are rich in bivalves. The most common species present is *Scalpomactra scalpellum,* no other species were identified given the highly fragmented nature of other bivalves.

Other skeletal components: No gastropods are present in surface sediments between the South and North shelves. Only on the Haast and Cascade shelves were gastropods up to 4mm in size observed (Appendix C6). Other skeletal grains on the shelf include rare, echinoid spines up to 10mm in length, and very rare worm tubes up to 20mm in length (B622, Cascade Shelf), and sponges.

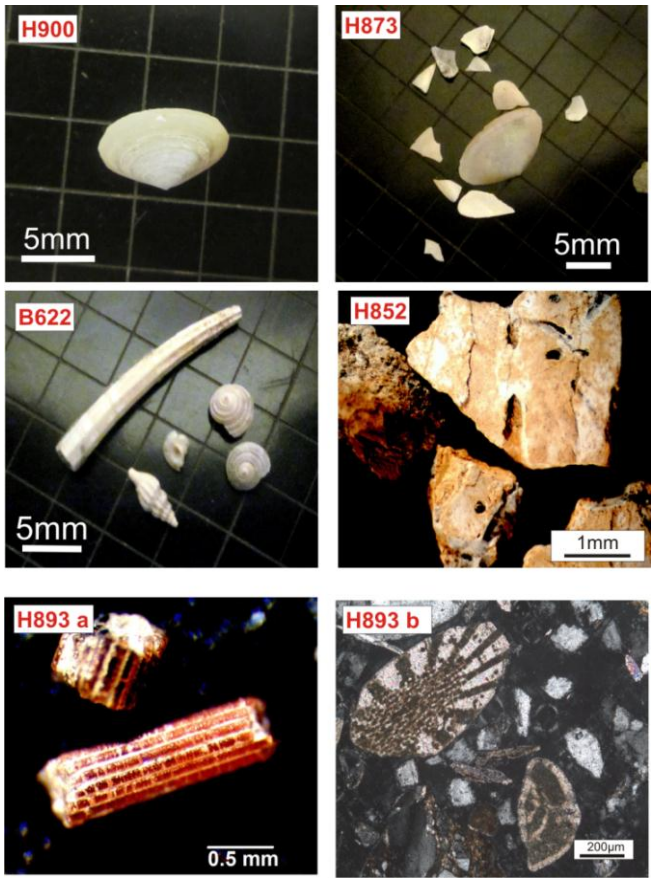

Figure 5-14 Images of skeletal grains in SWCM shelf and canyon surface sediments. H900 and H873 are of *Scalpomactra scalpellum* and other bivalve fragments from the inner shelf. B622 displays various gastropods and a large, elongate Scaphopod. H852 displays bored and iron stained shelf fragments from 198 m depth on the Hokitika Canyon north rim. H893a) shows echinoid spine fragments, a very common skeletal grain at this location. H893b) is a photomicrograph with a large echinoid in the upper left.

Canyon Heads:

Skeletal percentage: Skeletal content is highly variable in the canyon heads, ranging from 0.7 to 28 % in the sand fraction. Typically, HCH surface sediments range from 2 – 6 %. In the south of the CCH, sediments with very high skeletal content (28%) occur at the head of a Cook Canyon tributary (Transect F).

Foraminifera: Canyon head skeletal grains are primarily foraminifera, with planktonic species most common (Figure 5-16). A less numerous but diverse array of benthic species is also present. Binocular inspection of loose sand samples indicates benthic species decrease to the west, in the deeper HCH sites (H852 & R208) (Appendix C6). On the North rim of the CCH, foraminifera are rare, while at the head of the tributary canyon to the CCH, planktic foraminifera are very abundant (~ 7 % of the sand fraction) (Figure 5-16, H893).

Bivalves: Bivalves are the second most common skeletal component observed in the canyon head sand fraction, especially on the northern rims of both canyons (Figure 5-15). They are usually fragments up to 5mm in size. At 198 m depth on the HCH north rim, Fe-stained bivalve fragments with worm borings are present (Figure 5-14).

Other skeletal components: No gastropods or sponges were observed in the canyon head sediments. Echinoid spines occur as rare fragments in most canyon sediments except at H893 where they are a major component of the sand fraction (Appendix C6).

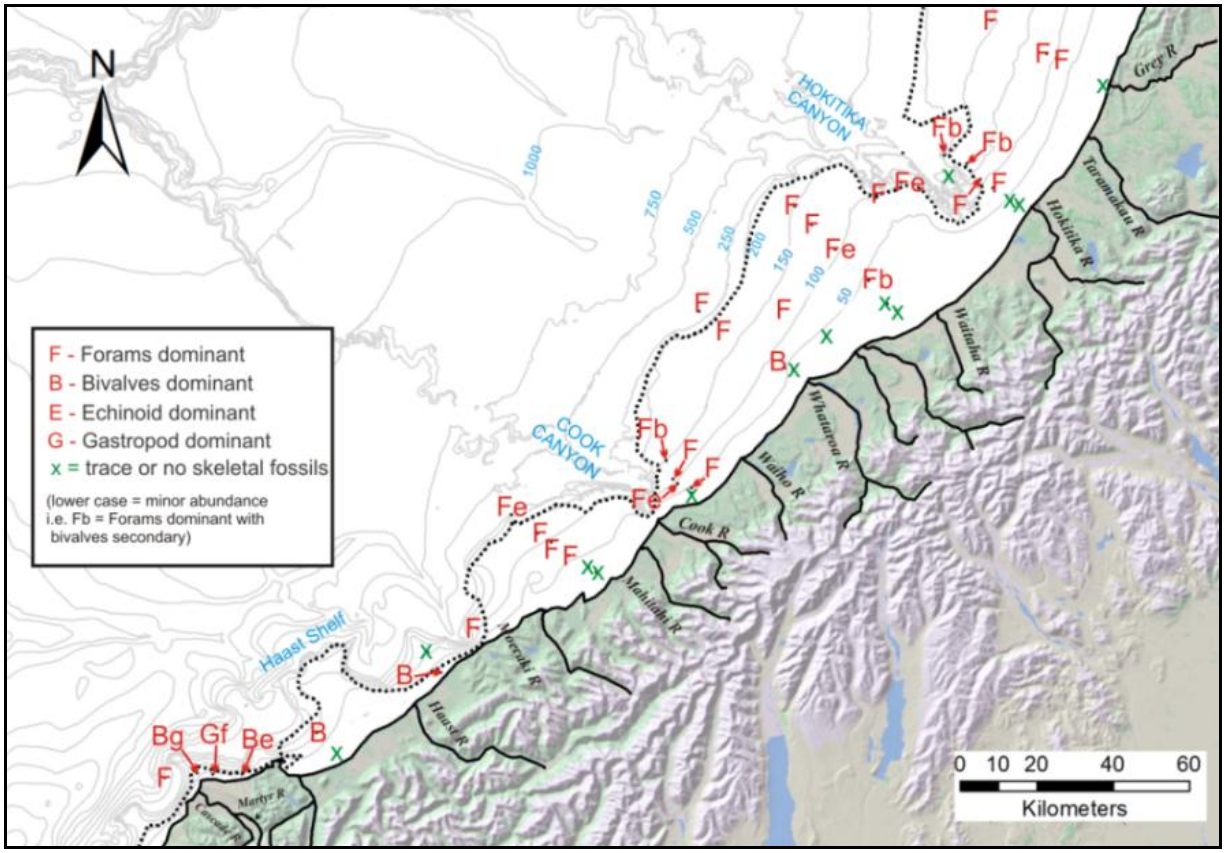

Figure 5-15 Map of the dominant skeletal types found in SWCM shelf and canyon surface sediments. Based on binocular microscope examination of > 63 µm sediments (Appendix C6).

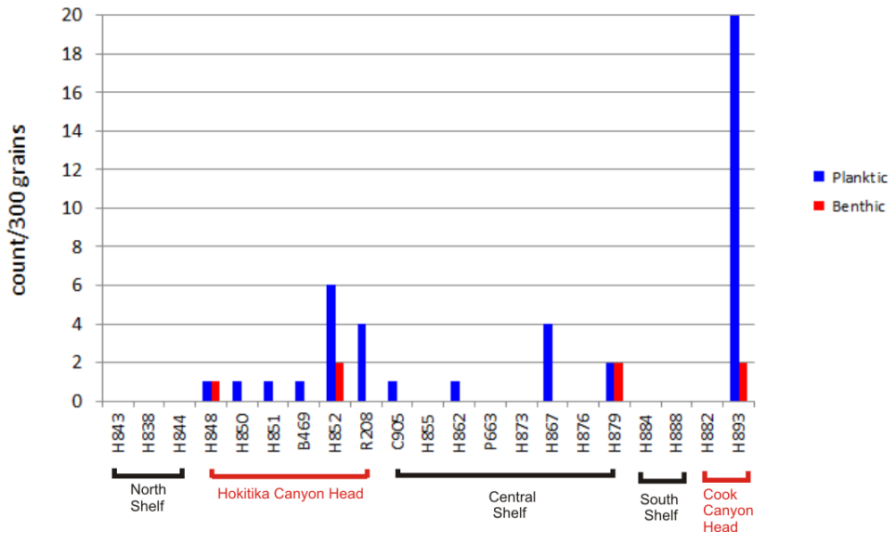

Figure 5-16 Graph of planktic and benthic foraminifera identified in shelf and canyon thin section point counts from the SWCM.

5.5 HYDRODYNAMIC CONTROL ON SWCM COMPOSITION

Hydraulic processes during the transport and deposition of shelf sediments can have powerful effects on the relative abundance of minerals and hence the geochemistry of different shelf environments (Johnsson 1993;Morton & Hallsworth 1999). Different hydraulic behaviors between mineral grains may be due to differences in density, grain size, and grain shape (or a combination of these). Geochemical results in this study reiterate the strong role hydrodynamics play in shelf sediment composition. On the SWCM shelves, this has been demonstrated by Stoffers et al. (1984) north of the Whataroa River. South of the Whataroa River on the Central, South, and Haast-Cascade shelves, this hydrodynamic control is highlighted in this study.

5.5.1 Hydrodynamic Controls on Silicilastic Mineralogy and Geochemistry

The high silica content of the inner shelf reflects the resistance of quartz to abrasion and weathering, resulting in larger grains concentrated on the inner shelf. The high SiO_2/Al_2O_3 ratio also reinforces the partitioning of clays and micas out from the turbulent inner shelf to more hydrodynamically favourable conditions over 50 m depth. Shelf Al_2O_3 content clearly indicates that naturally platy micas are a key factor raising Al_2O_3 levels at middle shelf depths (Figure 5-17 A). The negative correlation of Al with mean grain size also points to the concentration of Al in clays and monomineralic silts (Appendix E7). Muscovite, which contains appreciable amounts of K_2O, shows a strong control on bulk K_2O content of sediments, especially at middle and outer shelf depths (Figure 5-17 B).

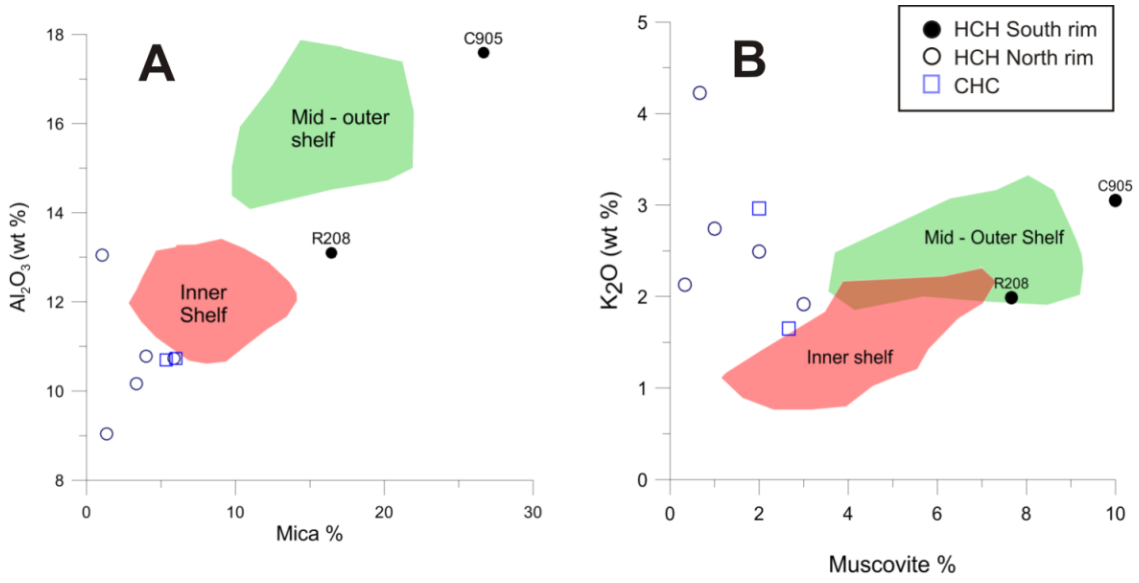

Figure 5-17 Comparisons between shelf and canyon head surface sediments for A) total mica content vs. Al_2O_3 and B) Muscovite content vs. K_2O. Total mica and muscovite contents are determined from point counts of the > 63 µm fraction only (Appendix C4). (Pink area = inner shelf samples; Green= Mid – outer shelf samples)

The resultant clay minerals delivered to the South Westland shelves are most likely from the illite, smectite, and chlorite groups. These groups would contribute to the elevated levels of Al_2O_3 (smectite and chlorite), K_2O (illite), and total iron (chlorite) on the middle to outer shelves (Griffin et al. 1968). High precipitation and well vegetated SWCM catchments are likely to create acidic groundwater which can produce considerable dissolution of unstable minerals, in particular, feldspars and ultramafic minerals. Despite SWCM catchments being well vegetated and characterised by high rainfall, high physical weathering and erosion rates in the Southern Alps are sufficiently high that silicate chemical weathering is low (Kautz & Martin 2007). Chlorite and illite group clays are typical where chemical weathering is moderate to low in river catchments with low grade metamorphic and argillaceous sedimentary rocks (Griffin et al. 1968).

5.5.2 Effects of Hydrodynamics and Sediment Supply on Carbonate Content

The low carbonate and skeletal content in SWCM surface sediments is typical of high energy, open shelves, with large terrestrial siliciclastic input (Carter 1975). High input of siliciclastics on continental shelves has a hindering effect on the productivity of carbonate-secreting organisms (Mount 1984). Carter (1975) points out that narrow shelves with high terrigenous sediment input are commonly blanketed with terrigenous sediment towards upper slope depths. The high fluvial input to the SWCM was emphasised in Chapter 1, Table 1-1. Hence, high sedimentation rates on the SWCM will be a main reason for the lack of carbonate organisms on the Westland shelves.

An energetic hydraulic regime can also limit carbonate productivity, particularly on the inner shelf (Boggs 2001). Wave orbitals from ocean swells incident on the SWCM are capable of frequently stirring and resuspending shelf sediments shallower than 50 m depth, and over 100 m depth during large storm events (Chapter 3 this study and Heath (1985)). In addition, wind drift, the Westland

Current, and tides can further inhibit carbonate productivity with near bed unidirectional velocities reaching up to and over 15 cm/s (Carter 1980). The inner shelf (< 50 m) is clearly the most carbonate poor area of the SWCM. In addition to high sedimentation rates, the high energy hydraulic conditions constantly stir and distribute suspended and bed load sediments here. This high energy on inner shelves contributes to a limited diversity of organisms i.e. bivalves and gastropods.

Beyond fair-weather wave base, carbonate organisms are typically more abundant on the lower energy middle shelf (Boggs 2001). However, the large volumes of terrigenous sediment, highlighted by the presence of middle shelf terrigenous silts and clays, is probably a major limiting factor (refer to Section 2.3). Toward the outer shelf, carbonate content increases as the influence of wave stirring during storms declines, and lower sedimentation rates permit more biological activity. The composition of outer shelf sediments show carbonate organisms in more abundance (particularly Foraminifera), corresponding to a higher carbonate percentage here. Carbonate content in the canyon heads suggest the activity of carbonate secreting organisms is highly variable. This is possibly the result of the varied bathymetry creating more favorable and less favorable habitats for organisms.

Carbonate and skeletal results in this study for the SWCM sediments broadly agree with previous work by Stoffers et al. (1984) and Probert and Swanson (1985) north of the Whataroa River. However, the north to south decrease in carbonate content observed by Probert and Swanson (1985) is not clear further south on the Central, South, and Haast shelves. This is largely because carbonate content is so low south of the Whataroa River that it becomes difficult to detect such change.

5.6 CONTRASTING NORTH VS. SOUTH CANYON RIM COMPOSITIONS

The bulk geochemistry of canyon head sediments reveal very contrasting compositions, particularly in the Hokitika Canyon Head (HCH).

5.6.1 South Rim ‘Modern’ Composition

Geochemically the south HCH rim sediments are very similar to the bulk chemistry of the middle to outer shelf surface sediments. The high Al_2O_3, K_2O, and low SiO_2/Al_2O_3 ratios all suggest finer grained compositions rich in clays and micas like the middle to outer shelves (Figure 5-17 & Figure 5-18 A).

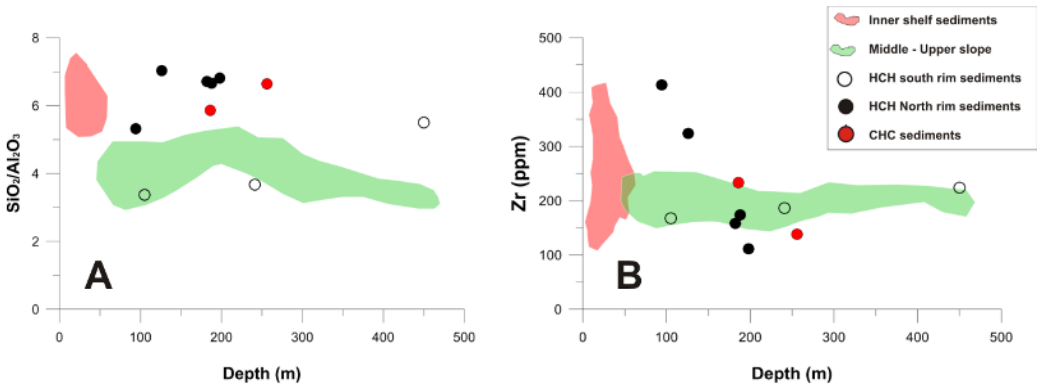

Figure 5-18 Comparisons between shelf and canyon head surface sediments for A) SiO_2/Al_2O_3 vs. water depth and B) Zr vs. water depth. An extreme Zr value of 1441 ppm for H876 has been omitted from B to improve clarity.

South rim trace element patterns are also akin to the middle-outer shelf patterns (Figure 5-9 & Figure 5-10). These similarities suggest the southern HCH rim sediments are an extension of the middle to outer shelf sediments blanketing the Central Shelf further south. The bulk geochemistry of the HCH north rim sediments differ from the typical middle to outer shelf composition (Figure 5-17 & 5-11). These differences include contrasting trace element patterns, much higher SiO_2 content and SiO_2/Al_2O_3 ratios, and low Al_2O_3 and K_2O levels. This indicates that shelf sediments, derived from either the North or Central shelves, contribute less to the bulk composition on the HCH north rim.

5.6.2 Evidence for Relict Sediments on the HCH North Rim

Enrichments in Zr and Y at 94 and Zr at 126 m depth on the HCH north rim (Figure 5-9) suggest a relict contribution to these sediments. These incompatible trace elements are commonly partitioned into the heavy minerals zircon (Zr) and garnet (Y) (Winter 2001). Zircon and garnet are more concentrated on beaches and the inner shelf due to their higher densities than lighter minerals such as quartz and feldspar (Komar 2007). Some north HCH rim sediments may have formed in shallower, more energetic hydraulic conditions to concentrate these elements (Figure 5-18 A & B). In section 3.4, abundant garnets and other heavy minerals were common in the sand fraction of the shallower HCH north rim sediments.

The origin of the Cr-enriched signature in deep water (180 – 220m) northern rim sediments is problematic since the shallower north rim HCH and inner shelf sediments to the east show no Cr-enrichments. It is not until Hokitika beach, up to 20 km to the east, do Cr – enriched sediments occur. Bradley et al. (2002) have stressed that Ultramafic Pounamu pods in the Hokitika catchment are the primary source for Cr- rich detritus in local beaches. This may suggest a relict origin for the ultramafic material in HCH, when the Hokitika River had a more direct connection to the HCH during sea level low stands. The presence of Cr-magnetite grains in the north rim sediments (Chapter 4) would probably produce the Cr-enriched geochemistry here. The association of iron stained, bored shell fragments with the Cr-enriched sediments on the HCH north rim provides further evidence for a relict origin (Figure 5-14, H852). In the Cook Canyon Head sediments, no Cr enrichments were found to indicate an influence from the Cascade region ultramafics.

5.6.3 Effects of Glaucony on Canyon Head Sediment Composition

Another difference between the south and north rim sediments is the effect of glaucony on the bulk composition of north rim sediments. In particular, the proportion of mature glaucony grains have contributed to elevated levels of Fe_2O_3T, K_2O, and P_2O_5 (Figure 5-19). This is because the progressive evolution from nascent to mature glaucony results in increases in these oxides within the smectite structure (Amorosi 1997; Odin & Fullagar 1988). Commonly, mature glaucony grains contain 20 – 30 % ferric iron and 8 – 10 % K_2O (Amorosi 1997). Total iron clearly correlates well with glaucony, with both progressively increasing with depth towards H852 at 198 m on the HCH north rim. In addition, the common replacement of glaucony with iron oxides observed in section 4.3.6 will also contribute to

the bulk iron content. Similarly, K_2O and P_2O_5 display this progressive increase with glaucony (Figure 5-19 B & C). Despite varying levels of dilution with terrigenous sediments, these glaucony grains exert a major influence on the final sediment composition on the north rim, particularly beyond 100 m depth. The association of high P_2O_5 levels with glaucony on the north HCH rim may indicate that minor amounts of authigenic phosphorites have formed in these sediments. Elevated levels of P_2O_5 ~ 30 km north of the HCH were suggested by Stoffers et al. (1984) as evidence for phosphorites.

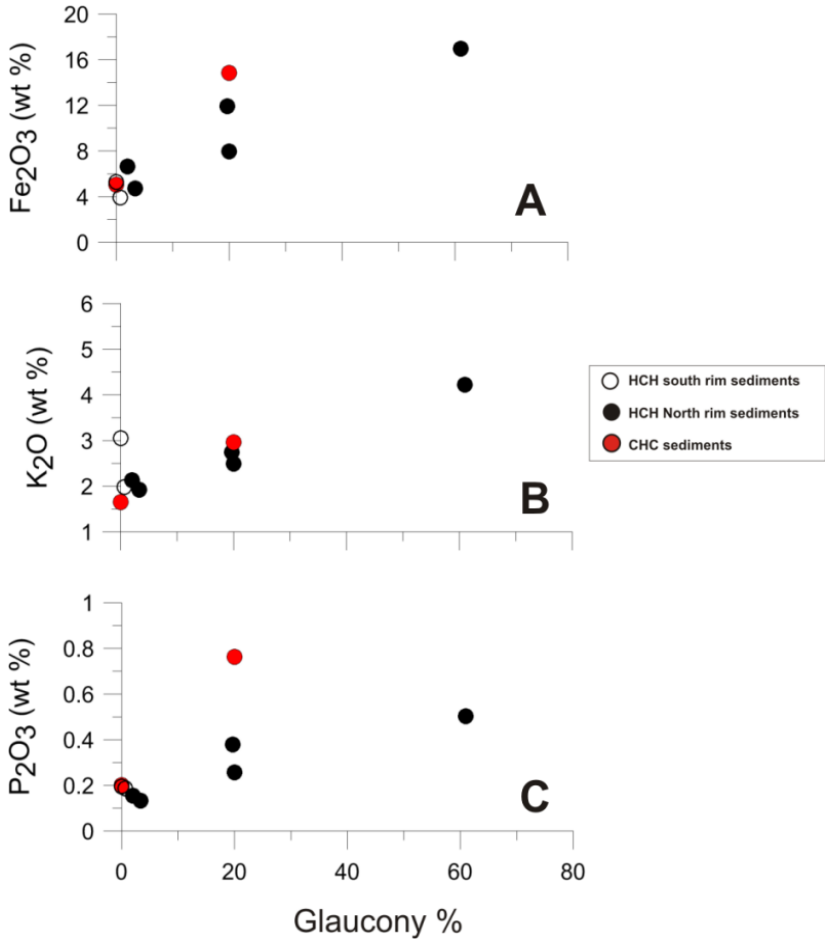

Figure 5-19 Graphs of canyon head surface sediment glaucony content vs. A) Total Fe_2O_3, B) K_2O and C) P_2O_5. Glaucony content is based on point count data from the >63µm fraction only (appendix C3).

Ultimately, the canyon head sediments, particularly on the north rim of the HCH, reflect a bulk geochemical signature influenced to varying degrees by different sources. These include modern shelf sediments, glaucony, and probably relict Cr- enrichments from Pounamu ultramafics, and Zr and Y enrichments from heavy minerals concentrated during lower sea levels.

5.7 DISPERSAL AND COMPARISONS TO REGIONAL GEOLOGY

The SiO_2 content and K_2O/Na_2O ratio in sandstones have been used by several authors to interpret tectonic setting (Roser & Korsch 1986; Roser & Korsch 1988; Bhuiyan et al. 2011) and are used here to identify possible patterns of shelf sediment dispersal in Figure 5-20. The K_2O/Na_2O-SiO_2 model has demonstrated its usefulness in finer grain sizes (Roser & Korsch 1986), like the SWCM shelf sediments. The discrimination diagrams show a clear, mostly felsic active margin source in most shelf,

river, and beach sediments (Figure 5-20 A & B). This reinforces the dominance of quartzofeldspathic Alpine Schists as the main contributor to shelf sediment composition (Figure 5-20 C).

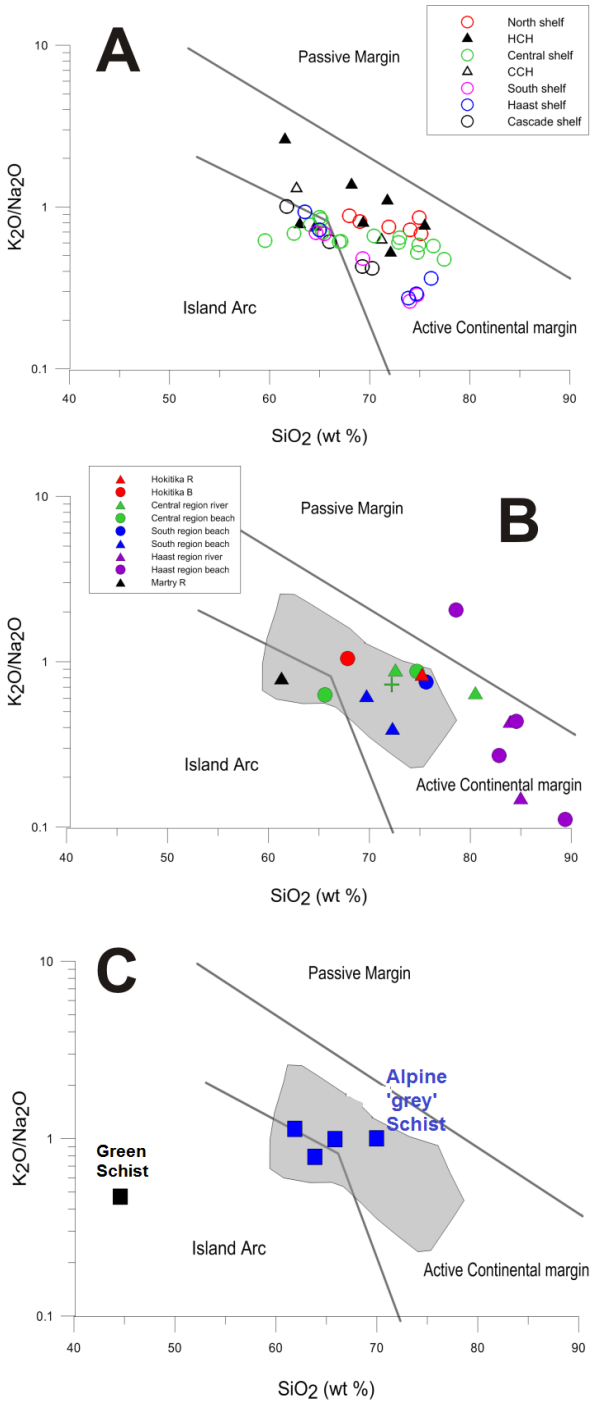

Figure 5-20 K2O/Na2O vs. SiO2 discrimination diagrams showing A) all shelf and canyon head sediments B) SWCM beach and river localities, and C) typical Alpine Schist, Green schist and SWCM shelf and canyon compositions. Gray shaded area in B & C is all shelf and canyon head sediments. Green schist composition is the average composition (n=10) from Cooper & Lovering (1970) in the Haast catchment. Alpine schist compositions are the average compositions from the McArthur Mtns near Hokitika in Vry et al. (2008) and from the Franz Josef-Fox Glacier region in Grapes et al. (1982). Graphs based on Bhatia (1983). are after Roser & Korsch (1986).

In Figure 5-20 A, weak to moderate linear trends are defined by each shelf region respectively. Particularly in Figure 5-20 A, these trends reinforce the effects of grain size, where low K_2O/Na_2O, high silica sands progressively increase in K_2O levels as finer grained phyllosilicates are introduced. Bulk geochemistry on the Cascade to Haast shelves, and possibly the South Shelf, show slight tendencies towards the island arc field in Figure 5-20 A. This may suggest some influence from green schist source rocks (Figure 5-20 C) which become more abundant in catchments south of the Paringa River.

Generally, the bulk shelf and canyon head geochemistry comprise a coherent grouping with internal variations mainly a function of grain size. On the North, Central, and South shelves, apart from hydrodynamic sorting effects, it is difficult to infer dispersal patterns from the bulk geochemistry presented here.

Ultramafic lithologies in catchments supplying the SWCM exert an influence on modern shelf surface sediment composition. The Pounamu Ultramafics in the Hokitika-Waitaha catchments for example produce a slight enrichment of Cr on the North Shelf sediments (Cr/V ratio, Figure 5-11). Further south, the high Cr and Ni contents in the Martyr River (a major tributary to the Cascade River) sediments have a clear influence on the Cascade Shelf surface sediments. The Martyr and Cascade rivers, which drain major outcrops of the Dun Mountain Ultramafics (Figure 3-3), are well known to supply Cascade region beaches with detritus rich in olivine, orthopyroxene, clinopyroxene, and chrome spinel (Morton & Smale 1990; Bradley et al. 2002). These minerals, particularly chrome spinel and olivine, can elevate Cr and Ni levels on the shelf. The northwards dispersal of Cr-enriched Cascade River sediments is evident to at least 14 km along the inner shelf (B474), and at least 9km directly offshore from the Cascade River mouth. The contribution of Cr enriched sediments further north past Jackson Head onto the Haast Shelf (suggested by Bradley et al. 2002) was not detected. This is a testament to the dilution effects of rivers North of the Cascade River, where catchments become increasingly dominated by Alpine Schists.

5.8 SUMMARY AND CONCLUSIONS

- A strong north vs. south rim contrast exists in the Hokitika Canyon Head sediments. The south rim is heavily influenced by modern terrigenous middle to outer shelf sediments, probably derived from the Central Shelf. North rim sediments are geochemically much more diverse, with varying influences from modern and relict terrigenous sediment, glaucony, and possibly phosphorites.
- The presence of high Zr, Y and Cr levels, and elevated SiO_2/Al_2O_3 ratios, and relict shell fragments suggest the north HCH sediments are strongly influenced by relict terrigenous material. Elevated Cr levels mainly on the deeper HCH north rim are most likely derived from the Ultramafic Pounamu outcrops in the Hokitika region catchments during sea level low stands.
- Glaucony has a major influence on the bulk iron and K_2O content in sediments found on the north rim.

- SWCM shelf geochemistry is controlled mainly by the hydrodynamic sorting of Alpine Schist derived sourced material. Major and trace element patterns for most of the shelf surface sediments match closely to those of the Alpine Schists.
- Regional changes in catchment geology are identified in modern SWCM shelf sediments with Ultramafic signals (enriched Cr/V and Ni/Y ratios) well developed on the North Shelf and the Cascade shelves which contrast with the Haast to Central Shelf compositions.
- The low carbonate and skeletal content on the SWCM is restricted by the energetic wave climate and high fluvial supply on the shelves.

CHAPTER 6 : LATE QUATERNARY SHELF HISTORY AND CORE STRATIGRAPHY

Variations in sea level have had major effects on the interaction between Westland submarine canyons and the surrounding continental shelves (Carter 1975; Norris 1978; Carter et al. 1986). Lowstand periods would have been characterized by the direct input of littoral and fluvial sediments into the South Westland canyons. In contrast, highstands like the present day represent periods of decreased terrigenous sediment supply into these canyons (Carter 1975; Carter 1980). This chapter focusses on the effects of the Last Glacial Cold Period (LGCP) between ca.28ka and 18ka (Alloway et al. 2007) on terrigenous sediment supplies to the Hokitika Canyon Head (HCH), and the response when sea levels transgressed after ca. 18ka.

6.1 QUATERNARY HISTORY

In the Early Quaternary tectonic uplift increased abruptly in the Southern Alps; these high rates of uplift continue today. Raised Late Quaternary marine terraces and shorelines along the Westland coast are a testament to this uplift (Nathan et al. 1986; Youngson 2006). In contrast, the offshore Western Platform has been subsiding on the downthrown sides of the South Westland Fault Zone and Cape Foulwind Fault Zone throughout the quaternary until the present (Nathan et al. 1986). Glacial to interglacial deposits are a significant feature on-land and offshore in the SWCM region. Quaternary deposits are widespread on valley floors and vast areas of the Westland coastal plains. These include various forms of alluvium, glacial tills, landslide deposits, and beach and dune complexes (Figure 3-3) (Rattenbury et al. 2010; Cox & Barrell 2007).

Glacio-eustatic sea level change due to varying global ice volume is a major regional factor affecting submarine canyon and shelf development on active coastal margins (Mountjoy 2009; Schattner et al. 2010). Sea levels have fluctuated over the last 900 000 years on 100 000 year cycles, driven by earth's orbital parametres. During the Last Glacial Cold Period (LGCP, ca. 28 – 18ka) (Alloway et al. 2007), a lowstand persisted with sea levels up to 120 m below present, increasing the subaerial extent of the New Zealand landmass dramatically (Carter 1980). The North and South islands were connected, and vast areas of the SWCM were subaerially exposed (Figure 6-1). In marine stratigraphic records, low stand periods are associated with increased terrigenous inputs due to rivers discharging at the shelf edge or directly into submarine canyons, higher precipitation, increased glacial activity, and heavily reduced vegetation cover (Carter et al. 2002; Hoogakker et al. 2004).

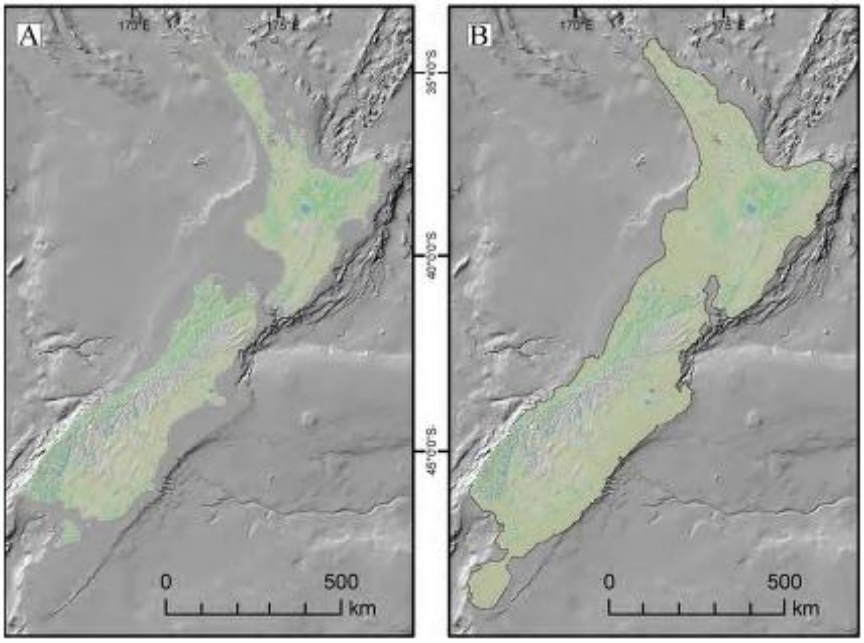

Figure 6-1 The extent of the New Zealand coastline during sea level highstands and lowstands. A) Todays modern sea level highstand and B) New Zealand during the sea level lowstand at the last glacial cold period (LGCP c. 28 - 18ka) with sea level -120 m below present levels. From Mountjoy (2009).

A succession of glacial episodes transported large quantities of sediment to the lowlands and continental shelf in the SWCM region (Table 6-1). Late Pliocene to Pleistocene stratigraphy on the SWCM shelves is dominated by prograding clinoforms related to these glacial-interglacial fluctuations and thicken shorewards due to crustal flexure and high sedimentation from the Southern Alps (Rattenbury et al. 2010; Nathan et al. 1986). On land and in offshore seismic studies, the Late Pliocene to Middle Quaternary glacial advances are poorly preserved due to uplift, erosion, and destruction by later glaciations (Youngson 2006; Norris 1978). The last four glacial advances (Nemona to Otira) are preserved best in the Westland lowlands (Table 6-1).

Table 6-1 Quaternary glacial and interglacial deposits in the Westland region. From Youngson (2006).

O Isotope Stage	Age (Ka)	Glaciation	Advance	Glacial Formation	Interglacial Period	Shoreline Formation
1	<18				Aranui	Nine Mile
2			Otira 3	Moana		
3	18 – c.80	Otira	Otira 2	Larrikins		
4			Otira 1	Loopline		
5c	c.100				Kaihinu	Awatuna
5e	c.125-115					Rutherglen
6	130 – 190	Waimea		Waimea		
7	c.198 c.240				Karoro	Karoro, Scandinavia
8	248 – 300	Waimaunga	Hohonu 2 Hohonu 1	Tansey		
9	300 – 340				*Un-named*	Addison
10	c.360	Nemona		Cockeye		
11	c.400				*Un-named*	Whisky
12?	c.450	Kawhaka		Mudgie Ridge		
13	500 – 485				*Un-named*	Candlelight
15	c.580				*Un-named*	Caledonian
	2.1 – 2.2 Ma	Porika				
	2.4 – 2.6 Ma	Ross		Donnelly Jones		

The ice limit during each glaciation (or glacier termini) varied from north to south along the Westland coast and had important implications for sediment supply to the SWCM. During the earlier glacials, termini extended further west than the most recent Otira advance (Suggate 1990). During the Otira glaciation, North Westland (Grey to Buller rivers) glacier termini occurred well inland, but towards the south (i.e. Wanganui River) glacier termini were at the present day coastline (Figure 6-2) (Youngson 2006). Continuing further south, glacier termini extended west of the present coastline during the Otira advance. Norris (1978) has identified numerous glacial moraine features up to 7.5 km offshore in seismic profiles south of Hokitika River. The net result is a north to south contrast in sediment storage during glaciations (Youngson 2006). In northern Westland on land sediment storage was higher, while further south glacial moraine and fluvio-glacial material was deposited more directly on the SWCM shelves.

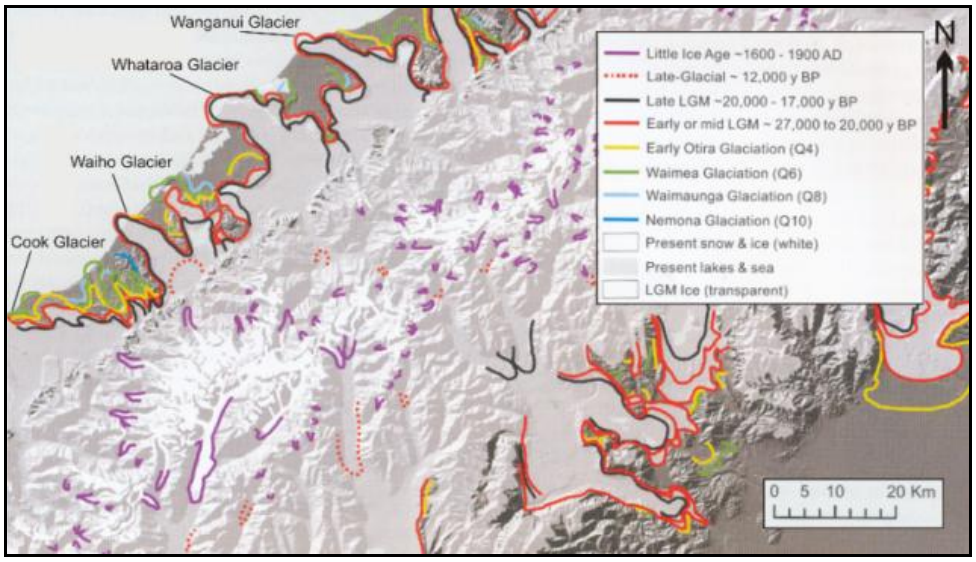

Figure 6-2 Mid to Late Quaternary limits of ice advances in South Westland. Note the more extensive ice coverage during earlier glaciations. Modified from Cox & Barrell (2007).

The influence of glacial – interglacial fluctuations have been significant in the Quaternary, resulting in high volumes of coarse terrigenous material deposited on the shelf and exported to ocean basins during glacials, while interglacial highstands were characterized by fine grained shelf deposition like the present day. The Hawea Series represents the 'modern' highstand sediments that have blanketed the SWCM under the modern hydraulic regime.

6.2 LATE QUATERNARY SOUTH WESTLAND PALEOSHORELINES

Towards the end of the LGCP ca. 20ka, sea levels were up to 120 m below modern levels. An episodic, rapid marine transgression followed (rising 10 -12 m $kyrs^{-1}$), reaching the present day shore line at 6.5ka (Figure 6-3)(Carter 1975; Carter et al. 1986; Schattner et al. 2010). This shift in shoreline position on the Westland shelf has had major effects on the level of interception of terrigenous sediments by canyons (Carter 1980).

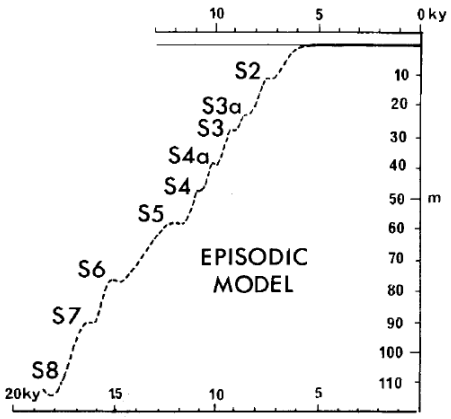

Figure 6-3 Late Quaternary sea level curves from Carter et al. (1986) based on data from the eastern South Island of New Zealand. Stillstands are numbered from S8 – S2 and represent periods of relatively stable sea level (up to several centuries long).

The sea level curve of Carter et al. (1986) is based on the seismic stratigraphy of the eastern South Island shelves. Tectonic uplift is relatively low to stable on the South Island's eastern shelves compared to areas closer to the Alpine Fault; therefore this curve approximates eustatic sea level change. The episodic nature of post glacial sea level rise is largely due to pauses in ice sheet melting Carter et al. (1986).

A series of SWCM paleoshoreline maps created for 20ka, 16ka, 11.5ka, and 8ka are based on the sea level curve of Carter et al. (1986) and follow the method of Payne (2008) (Figure 6-3 and Figure 6-4). These maps are only approximate since the bathymetry prior to 6.5 ka probably differed to that developed from sedimentation after sea levels stabilised 6.5 ka. In addition, these maps do not take into account tectonic uplift or subsidence. An attempt to infer the geomorphic trace of the paleoshorelines from bathymetry and digital elevation models is made in this study. However, these are also only approximate since breaks in slope can be produced by other processes, or conversely, paleoshorelines sometimes do not produce breaks in slope (Carter et al. 1986).

6.2.1 20 ka Paleo-shoreline

Towards the end of the LGCP ca. 20 ka, sea levels were between 113 – 120 m below present levels. Much of the Westland shelf was exposed, with extensive fluvio-glacial outwash systems extending towards the shelf edge (Carter 1980; Rattenbury et al. 2010). Over half of the modern South Westland shelves were subaerially exposed, including most middle and all inner shelf sample sites (Figure 6-4 A). Almost all the remaining sample sites were within 100 m depth of the 20 ka shore line, exposed to the stirring effects of ocean swells. A prominent westward bulge in the shoreline south of the HCH persisted.

The colder LGCP climate and higher precipitation resulted in significant glacial activity, a reduction in vegetation cover, widespread erosion in catchments, and substantial deposition in South Westland valleys and alluvial plains (Rattenbury et al. 2010). Consequently, the supply of coarse terrigenous material to the shelf was higher than the present day.

The 20 ka shoreline ran below and edge of the Hokitika Canyon Head rim, particularly along the south rim and eastern canyon head (Figure 6-4 A and Figure 6-5). While much of the south HCH rim was subaerially exposed, most of the north rim was submerged up to 100 m depth. Sample sites rich in polished mature glaucony and rounded coarse terrigenous grains were well within the reach of ocean storm swells. Such swells could rework these grains, giving them their rounded or polished surfaces. The north HCH rim sample sites H848 and H850, characterised by relict features typical of beach or littoral zones, were subaerially exposed in areas where coarse, terrigenous beaches would have prevailed.

With the extent of shelf exposed at 20 ka, the Hokitika River would have had a strong connection to the Hokitika Canyon system. The Hokitika River probably delivered most of its sediment load into the canyon head during this period. This may have been via the present position of the Totara River mouth ca. 20km to the south as Norris (1978) has noted. A weak, linear feature visible on the HCH north rim 500 – 1000 m west of H850 may be a relict 20ka shoreline (Figure 6-5 A). The episodic nature of Late Quaternary sea level rise commonly left remnant shorelines, developed during brief, several century long still stands (Carter et al. 1986; Payne 2008).

A similar scenario prevailed in the Cook Canyon Head (CCH), with the 20 ka shoreline often running below the edges of the south and eastern rim edges (Figure 6-4A and Figure 6-6).The glaucony rich sample at H882 is well within the energetic inner shelf depths during this time. This may have exposed the glaucony grains to frequent reworking, giving them their often polished surfaces (Payne 2008). The Cook River, and possibly the Karangarua River, had a very direct connection with the CCH, feeding most of their sediments directly into the canyon system (Figure 6-6).

The role the HCH and CCH played in intercepting northward transported littoral sediments at 20 ka is considered significant (Carter 1975; Norris 1978; Carter 1980). The 20 ka shoreline maps illustrate this interception of littoral sediments by both canyon systems, mainly along their south and eastern rims. This would have drastically reduced the supply of terrigenous sediment immediately north of the canyon heads and to the remainder of the Westland shelf north of the HCH (Carter 1980).

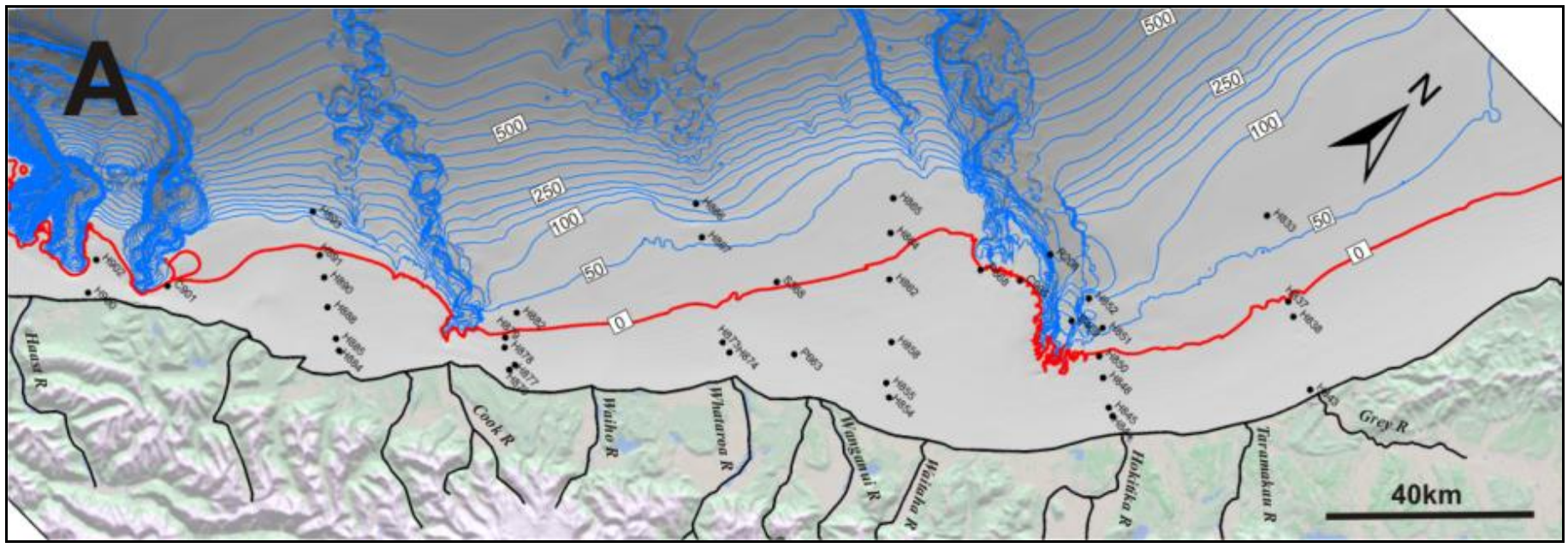

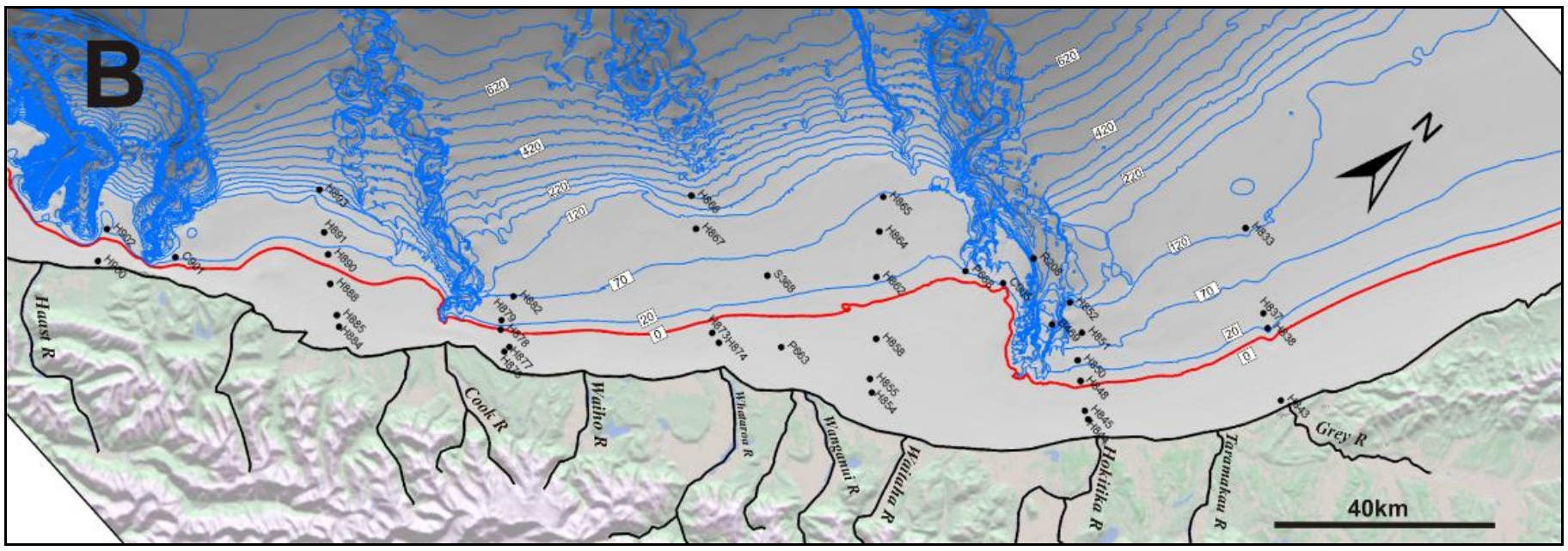

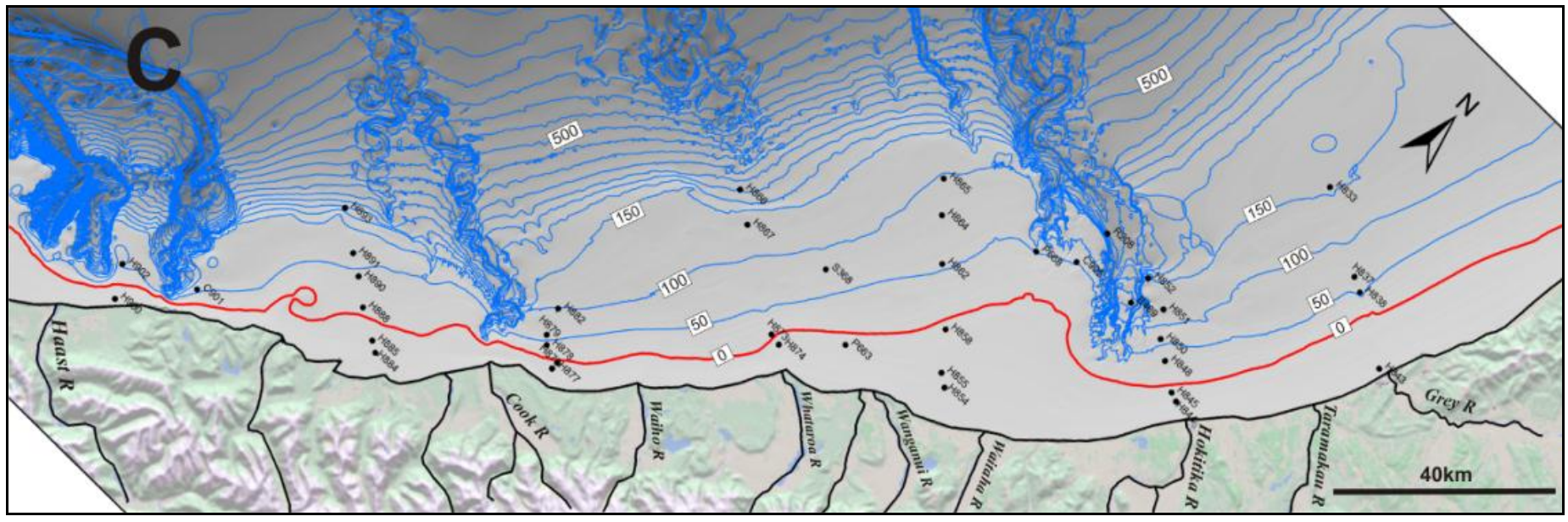

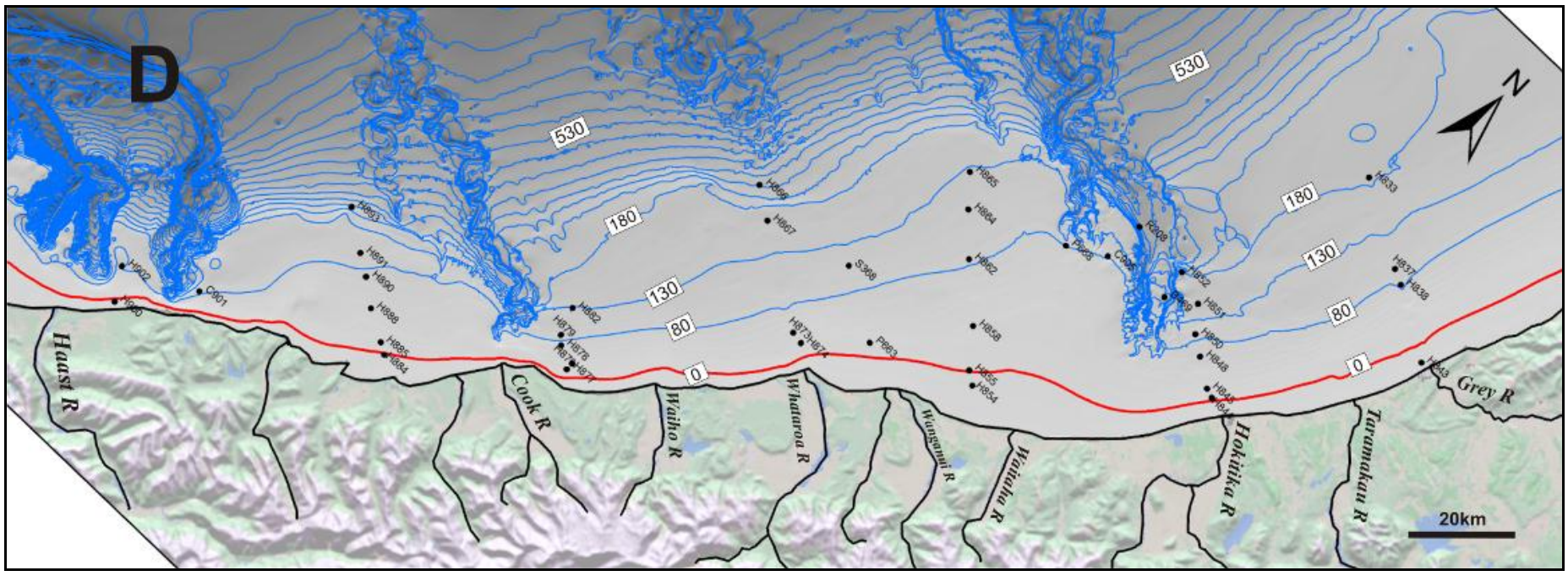

Figure 6-4 Westland paleoshoreline maps for A) 20 ka (-120m) , B) 16 ka (-80m), C) 11.5 ka(-50m), and D) 8 ka(-20m). Based on the 'episodic' sea level curve of (Carter et al. 1986)

6.2.2 16 ka Paleo-shoreline

Approximately 16 000 years ago, sea levels were 80 m below the present level (Carter et al. 1986). Based on the modern South Westland shelf bathymetry, shorelines shifted up to 10 km inland on the gentler sloping shelves by 16 ka. Less than half the modern shelf area was now subaerially exposed (Figure 6-4 B). Many samples sites were submerged at this time (18 in total). The prominent bulge in the shoreline south of the HCH still persisted.

In the HCH, the 40 m of sea level rise meant the shoreline no longer dipped below the canyon rims like the 20 ka shoreline (Figure 6-5). All the HCH sample sites became submerged, with the coarse, relict samples at H848 and H850 within the energetic inner shelf zone. The deeper north HCH samples (i.e. H852) deepened to 120 m depth, beyond the reach of most shoaling storm swells. With the shoreline still close to the edges of the HCH south rim and east lobe, the Hokitika River would still have been strongly connected to the canyon system.

In contrast to the HCH, the CCH shoreline still dipped below the canyon head rims, especially on the south and eastern rims. Consequently, little reduction in the connectivity of the Cook River with the canyon head occurred with the 40 m sea level rise. A submerged shoreline visibly running between H879 and H878 most likely corresponds to the 16 ka shoreline, the S6 still stand of Carter et al. (1986) (Figure 6-6). The interception of littoral transport paths by the HCH and CCH probably experienced little change from the interception occurring at 20 ka. However, since the HCH is a less deeply incised canyon, 40 metres of sea level rise did expose small tracts of shallow sloping shelf where some littoral sediment could bypass the HCH.

6.2.3 11.5 ka Paleo-shoreline

Sea levels were close to 50 m below present 11 500 years ago (Carter et al. 1986). From 16 ka, the South Westland shore line transgressed the shelves by between 2 – 6 km, depending on shelf gradients (Figure 6-4 C). The bulge in the shoreline south of the HCH became less pronounced than in earlier shore line positions. Up to three quarters of the shelf was submerged at 11.5 ka, with only 13 from 46 sample sites subaerially exposed. Due to the expansion of vegetation cover (Alloway et al. 2007), a reduction in the flux of sediment to ocean basins probably reduced sediment supplies to the South Westland shelves (Carter et al. 2002).

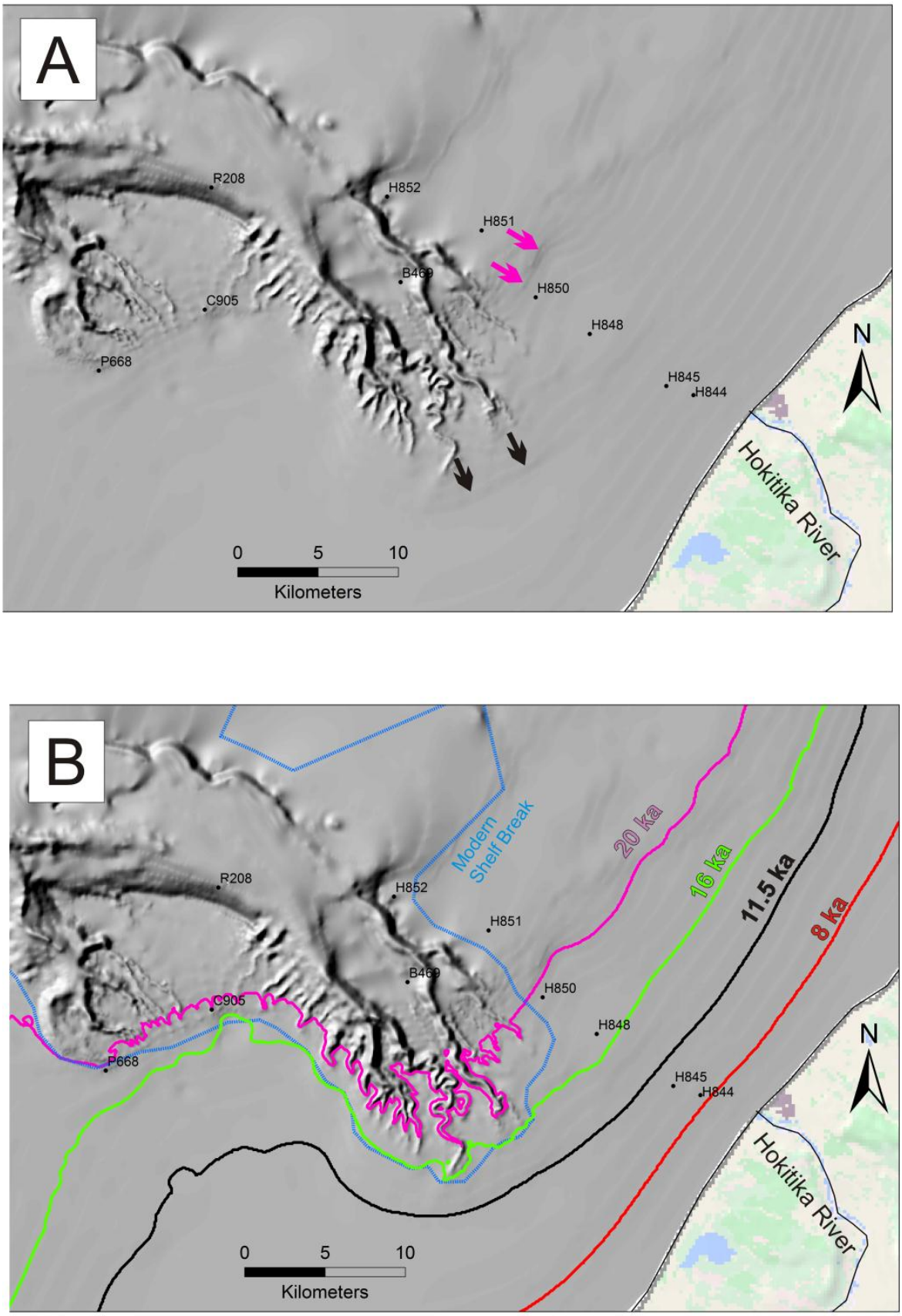

Figure 6-5 Paleoshorelines near the Hokitika Canyon Head (HCH) based on the sea level curve of Carter et al. (1986). A) Bare hillshade image with possible geomorphic features related to the 20 ka shoreline (purple arrows) and 11.5 ka shoreline (black arrows). B) 20 ka to 8 ka paleoshorelines overlaid onto the HCH hillshade.

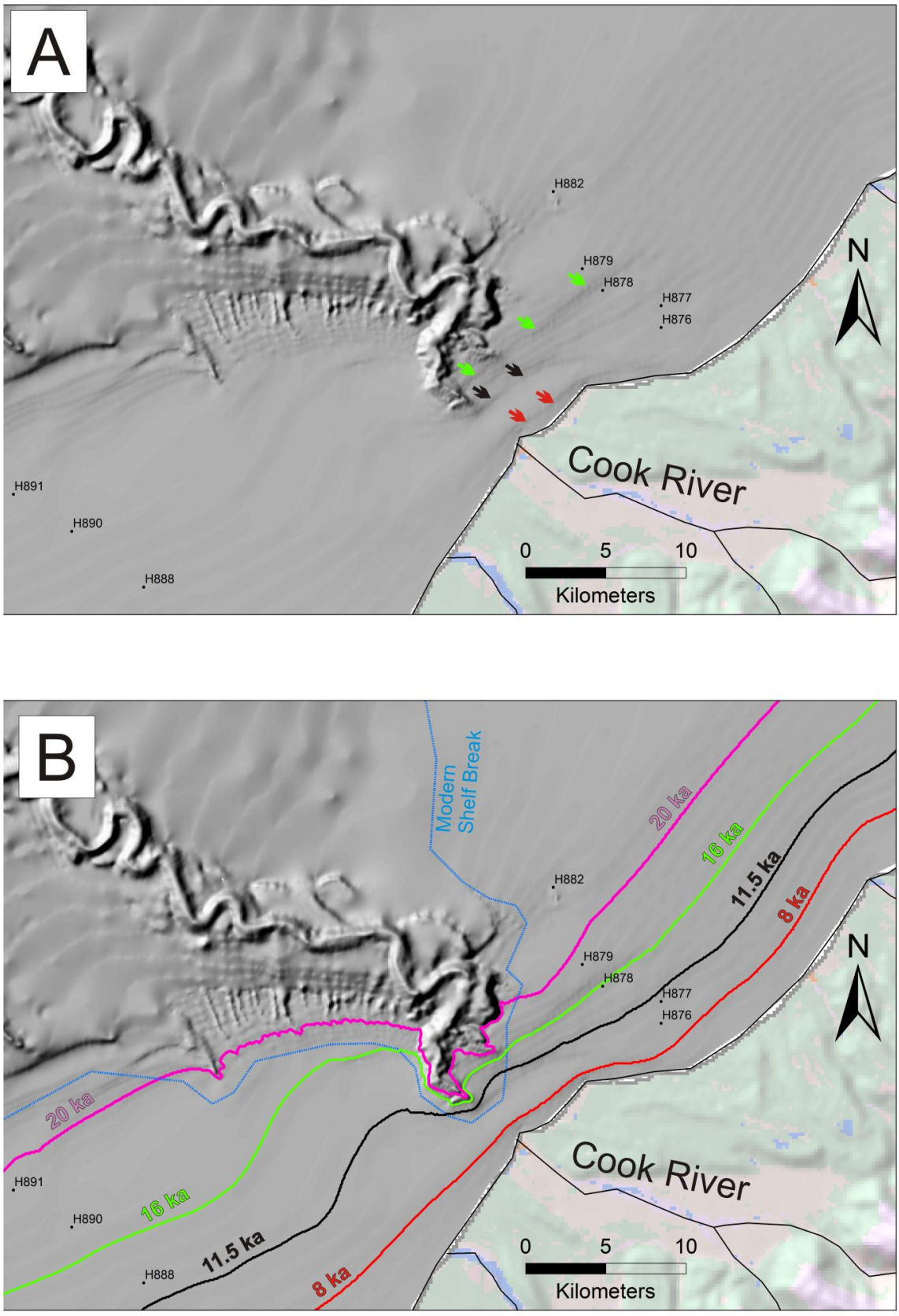

Figure 6-6 Paleoshorelines near the Cook Canyon Head (CCH) based on the sea level curve of Carter et al. (1986). A) Bare hillshade image with possible geomorphic features related to the 16 ka, 11.5 ka and 8 ka shorelines. B) 20 ka to 8 ka paleoshorelines overlaid onto the CCH hillshade.

The shoreline retreated from the edges of the HCH south and eastern rims by 3-6 km between 16 ka and 11.5 ka. This constrained the 11.5 ka shoreline entirely on the gentler sloping shelf east of the HCH (Figure 6-5 B). Only sample H848 with relict textures remained at inner shelf depths, with increasing areas of the north HCH sediments beyond the stirring depths of most storm waves (>100 m). Most of the south and east rims were close to the transition depth between the inner and middle shelves (~50 m water depth). With a gently sloping inner shelf at 11.5 ka, the connection of the Hokitika River to the HCH would have become less robust. Hokitika River sediments at the shoreline would have become increasingly entrained in northward littoral transport paths which operated on the shallower, low gradient inner shelf east of the HCH.

In the CCH, the 11.5 ka shoreline pulled back from the south rim but still remained below or very close to the eastern rim (Figure 6-6 B).This is due to the deep incision of the eastern lobe of the CCH. A paleoshoreline is visible as a break in slope running from the CCH lobe north to sample site H877 (Figure 6-6 A and B). This could represent the S5 shoreline identified in the eastern South Island by Carter et al. (1986) (Figure 6-3).

The contrast in the level of littoral sediments intercepted by the HCH and CCH becomes more pronounced at 11.5 ka. With 2 to 3 km of gently sloping (2-3˚) shelf heavily influenced by shoaling waves, larger volumes of sediment from the Central Shelf would have begun to bypass the HCH (Figure 6-5). Meanwhile, the CCH continued to intercept most littoral sediments and maintained a robust connection with the Cook River (Figure 6-6 B).

6.2.4 8 ka Paleo-shoreline

By 8 000 years ago, sea levels were only 20 m below modern levels (Carter et al. 1986), submerging almost all sample sites on the South Westland shelf areas (Figure 6-4 D). Sample sites from the modern inner shelf were located at or close to the 8 ka shoreline.

The shoreline was separated from the eastern most extent of the HCH by 8-10 km of gently sloping shelf. All HCH samples were beyond the energetic inner shelf depths (>50 m). While shelf sediments would have been exported into the HCH system from the middle shelf, much of the inner shelf could now bypass the HCH. In addition, the contribution of sediments from the Hokitika River into the HCH was reduced further by the level of disconnection of the 8ka shoreline.

Adjacent to the CCH eastern rim, the shoreline transgressed 2-3 km inland from the old 11.5ka position within the CCH rim (Figure 6-6 B). This transgression submerged up to 2 km of the shelf between the CCH and the Cook River. Consequently, for the first time the Cook River became partly disconnected from the canyon system between 11.5ka – 8ka. The partial inundation of the continental shelf would have resulted in littoral bypassing of material from the South Shelf onto the Central Shelf. A visible break in slope offshore from the Cook River mouth and Gillespies beach is probably the trace of the 8 000 year old shoreline (Figure 6-6 A & B). This could be either the S3 or S3a still stand of Carter et al. (1986).

6.3 HOKITIKA CANYON CORE STRATIGRAPHY

A selection of Hokitika Canyon cores, provided by the National Institute of Water and Atmosphere (NIWA), were analysed to identify textural and compositional trends which may reflect glacial-interglacial cycling. Key questions include: To what degree is the 'switching on and off' of high terrigenous inputs to the HCH visible in core stratigraphy? Is there a change in terrigenous composition of core sediments between the LGCP and interglacial periods? How does Hokitika Canyon sediment composition compare to other South Westland canyons? Or to the surrounding shelf regions?

6.3.1 Methods

Three kasten cores from the Hokitika Canyon, TAN 0513-15, 19, and 21 are the focus of this stratigraphic study (see Figure 1-11 for core locations). Five samples per core were supplied by NIWA, with each sample representing a 5cm interval taken from the core depths provided in Appendix A4. All data are plotted as the mid-point of this sampling interval. As a result, a depth error of up to 2-3 cm for each data point must be acknowledged. Grain size parametres were determined by a laser particle sizer at NIWA, with details of this technique and results provided in Appendix B. X-ray diffraction (XRD) was used to obtain the bulk mineralogy of the core sediments, the XRD method and raw results are provided in Appendix C7 & C9. The bulk major and trace element chemistry was determined for core samples using X-ray Fluorescence (XRF). The upper most sample in each core was not analysed with XRF due to insufficient sample volume. Raw XRF results are located in Appendix E6. Magnetic susceptibility, a measure of the 'magnetisability' of sediments, were provided by NIWA, and offer a useful tool for interpreting the textural and compositional changes in the core samples.

6.3.2 Temporal Constraints

Age correlations between the Hokitika cores in this study are based on the age model of Ryan, (2010) This age model is based on the $\delta^{18}O$ chronology of *G. bulloides* and magnetic susceptibility in TAN0513-14, a core adjacent to TAN0513-15 used in this study. Magnetic susceptibility measurements on TAN0513-14 were correlated with magnetic susceptibility measurements in the other Hokitika Canyon cores, with marker horizons picked at 25 ka, 64 ka, and 128 ka (Figure 6-7). These marker horizons form the basis for interpretations of textural and geochemical results herein. The only change to correlations made by Ryan, (2010) is in TAN0513-15 where the 64 ka marker is picked approximately 30 cm further up core.

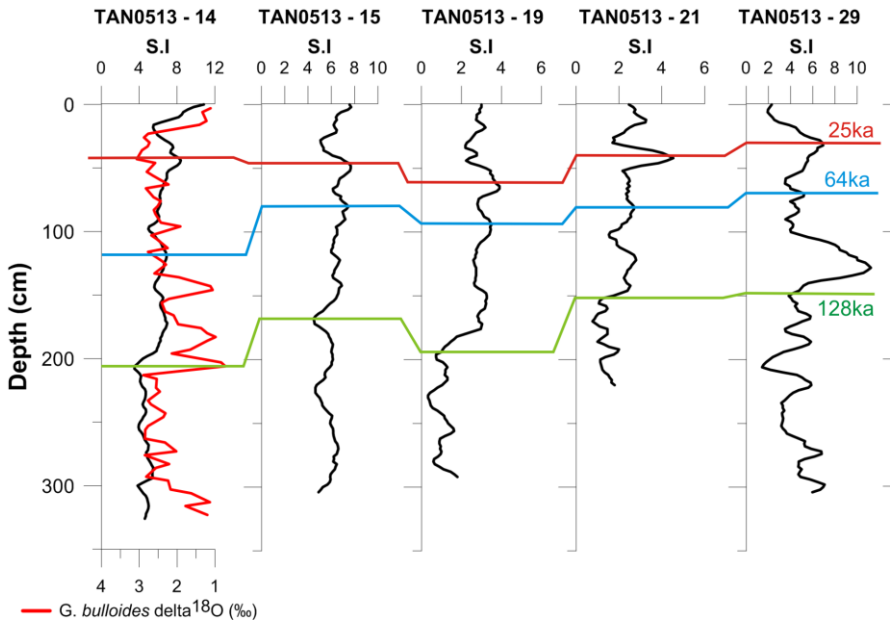

Figure 6-7 Hokitika Canyon core correlations based on the δ ^{18}O chronology from *G. bulloides* in TAN0513-14 (red line) and picked in the other cores using magnetic susceptibility (S.I) (black line). All graphs were constructed using magnetic susceptibility and δ ^{18}O data provided by NIWA and work from Ryan, (2010).

Approximate depths for the marker horizons and linear sediment accumulation rates for the last 128ka in the three Hokitika cores are provided in Table 6-2. Based on linear accumulation rates, an approximate depth range was estimated for the Last Glacial Cold Period (LGCP), a period of erratic, colder global climate between ca. 28 ka to ca. 18 ka (Alloway et al. 2007). The LGCP is projected onto subsequent figures of core textures and geochemistry.

Table 6-2 Depths for key marker horizons and linear sediment accumulation rates for the Hokitika Canyon cores.

Core ID	25ka (cm)	64ka (cm)	128ka (cm)	128ka to present accumulation rate *	LGCP Depth Range (cm)
TAN0513-15	47	80	167.5	1.31 cm kyr^{-1}	38 - 51
TAN0513-19	64	94	198	1.55 cm kyr^{-1}	53 - 69
TAN0513-21	42	79	153	1.20 cm kyr^{-1}	34 - 46

6.3.3 Hokitika Canyon Textures

Textural variations in marine sediments with glacial-interglacial fluctuations are well documented in the literature (Hoogakker et al 2004; Neil et al. 2004; Carter et al. 2006). Despite a low sampling resolution (5 samples per core), the Hokitika cores reveal textural changes near or within the LGCP which contrast with interglacial sediments further up core (Figure 6-8).

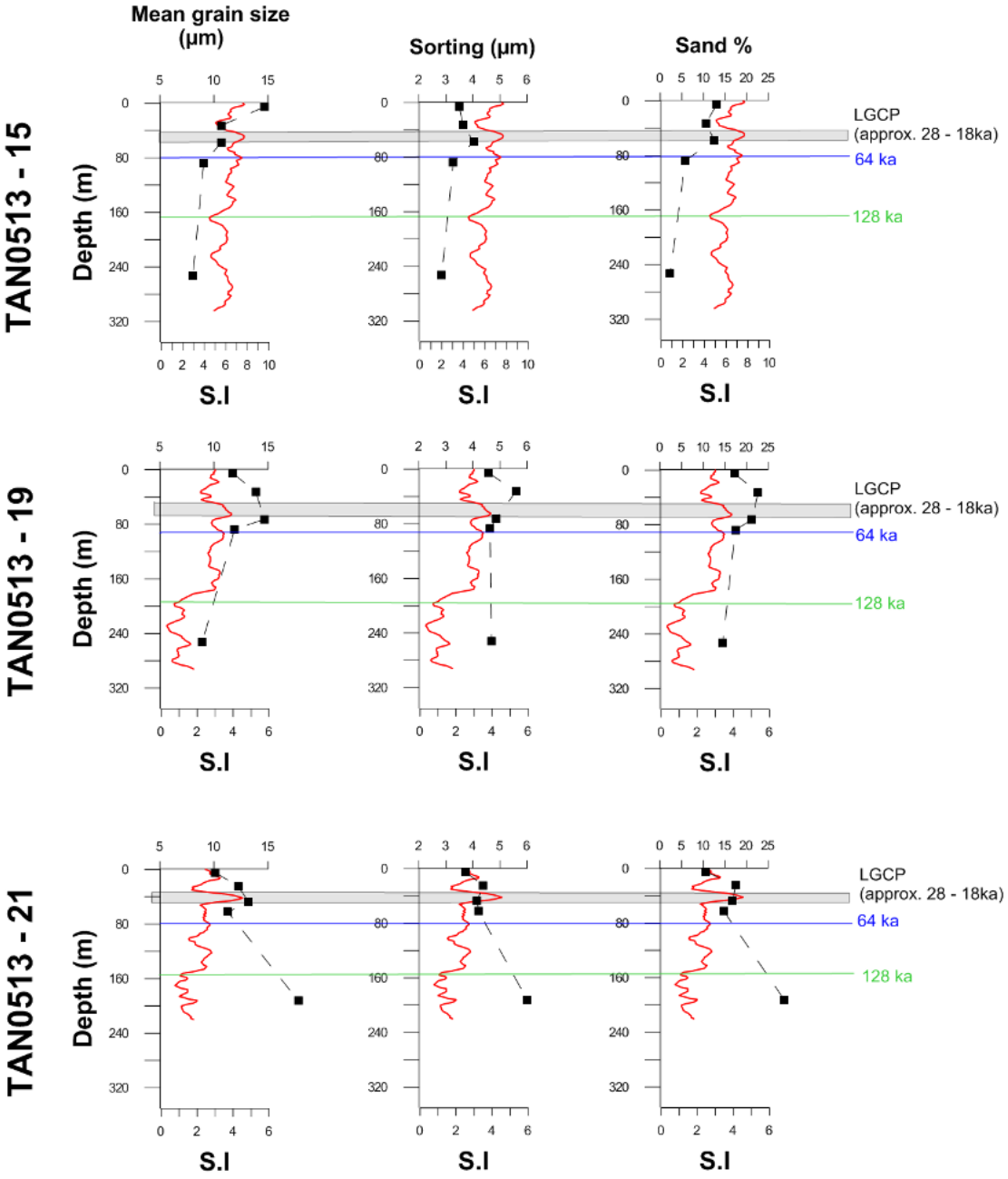

Figure 6-8 Mean grain size, sorting and sand percentages for the Hokitika core samples (black squares). Red line is magnetic susceptibility results courtesy of NIWA.

Increases in mean grain size of 3-4 µm occur in samples plotting near the LGCP, particularly in TAN0513-19 and 21. Further up core from the LGCP, the mean grain size fines up except in TAN0513-15 which coarsens. Fluctuations in sorting show slight reductions at LGCP core depths (increasing values of µm correspond to decreasing sorting) compared to the interglacial samples further up core. The core TAN0513-15 is more sorted overall (2-4 µm) compared to the more distal cores (>4µm). Weak to moderate increases in sand percentage (2-5%) near the LGCP occur in each core respectively (Figure 6-8). These 'spikes' in sand percentage are strongest in TAN0513-19 and 21 and are followed by a reduction (5 %) in the upper most sediments (interglacial).

Mean grain size and sand percentage provide stronger signals compared to sorting values. Textures in the three Hokitika cores display fluctuations generally correlating with glacial (LGCP) and interglacial periods. An increase in carbonate productivity could also increase the mean grain size or reduce the level of sorting (Hoogakker et al. 2004). However, the correlation of periods of enhanced magnetic susceptibility (i.e. more ferromagnesian minerals) with the textural spikes suggests an increased flux of coarser, terrigenous sediment is driving these textural changes.

6.3.4 Composition

Bulk mineralogy (XRD)

The bulk mineralogy of the Hokitika core samples was determined for calcite, quartz, albite, muscovite and kaolinite by XRD (Figure 6-9 & Appendix C9). Samples containing less than 5 % of any of the above minerals are interpreted as only a 'trace' amount.

The Hokitika Canyon mineralogy is controlled primarily by the proximity of the cores to the Hokitika Canyon Head. A change in mineralogy is clear as distance increases from the Hokitika Canyon Head. The more proximal TAN0513-15 (ca. 90 km from HCH eastern rim) is dominated by quartz and feldspar (35 – 75 % collectively), followed by calcite, kaolinite and traces of muscovite. The more distal cores TAN0513-19 and 21 (ca. 170km and ca. 270km down canyon respectively) are dominated by calcite (80 -95%). Due to the abundance of calcite and lack of siliciclastic minerals in these distal cores, down core mineral variations were not readily observed.

However, at 50-55 cm depth in core TAN0513-15, higher quartz and albite contents (a combined total of 60%) correlate with enhanced magnetic susceptibility and the LGCP. This is much higher than the shallower sample at 30-35 cm depth (a combined total of 35%) which correlates with a trough of low magnetic susceptibility (Figure 6-9). This increase in siliciclastic grains in TAN0513-15 suggests either a pulse of terrigenous material or a decrease in carbonate productivity during the LGCP.

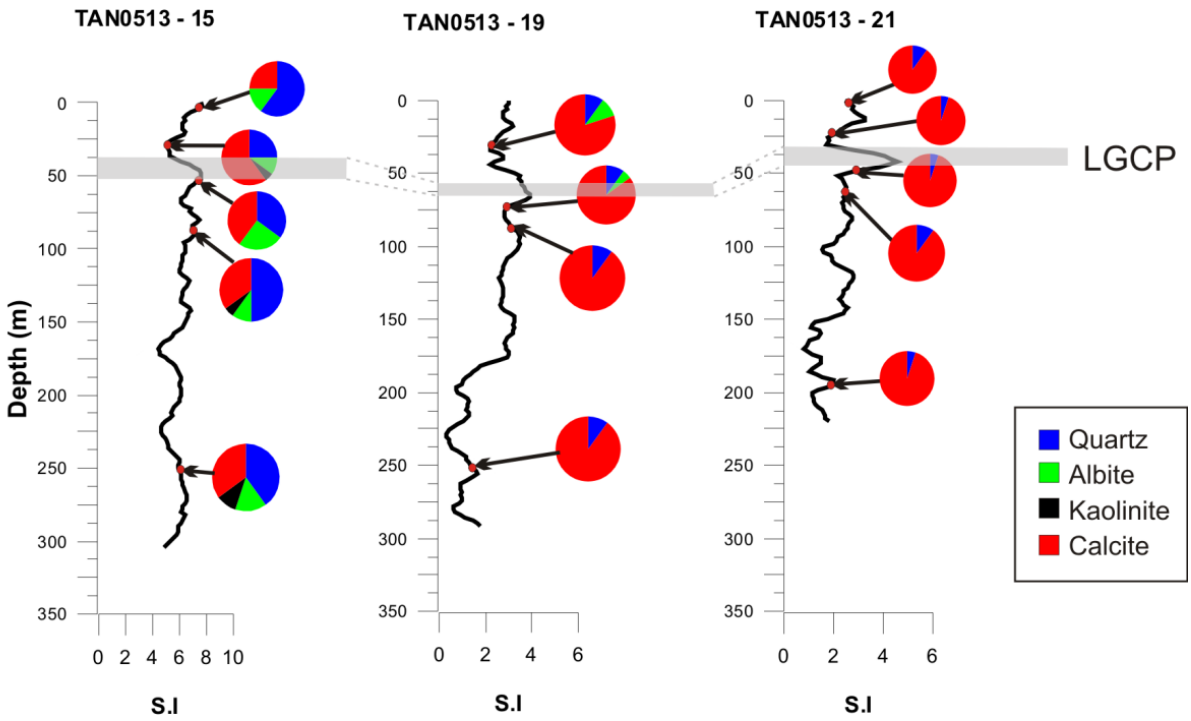

Figure 6-9 Down core variations in bulk mineralogy as determined by X-ray diffraction (XRD) for the Hokitika Canyon core samples. Black line is variations in magnetic susceptibility courtesy of NIWA. LGCP = Last Glacial Cold Period (ca. 28ka to ca. 18ka).

Hokitika core geochemistry

Hokitika Canyon geochemical results were determined by XRF and are presented in Figure 6-10. In TAN0513-21 only 3 samples were analysed and consequently no post-LGCP sample was compared to. Elemental ratios were relied on to minimize the effects of grain size and carbonate dilution, allowing comparisons to be made between cores sites and with the shelf geochemistry. The CaO percentage is assumed to reflect mainly the carbonate content of core sediments. This is especially so in the more distal cores where feldspar, a potential Ca-bearing mineral, is rarer. Even where feldspars are more common (i.e. 10 - 25 % in TAN0513-15) the dominant phase is albite, a Na rich plagioclase with low Ca content.

Silica and CaO show clear increases and decreases during the LGCP respectively (Figure 6-10). In TAN0513-15, SiO_2 increases ca. 6 % wt. while CaO falls by ca. 5 % wt. in the LGCP sample compared to the younger sample at 30 - 35 cm depth. In TAN0513-19, similar fluctuations in SiO_2 and CaO occur during the LGCP but they are less profound. Like silica, Zr shows slight increases in TAN0513-15 and 19 during the LGCP.

The trace element ratios Cr/V and Y/Ni display variations between LGCP and interglacial sediments. The Cr/V ratio reflects the enrichment of Cr over other ferromagnesian minerals, while the Y/Ni ratio indicates the general level of ferromagnesian minerals present (McLennan et al. 1993). Sediments

sourced from mafic and ultramafic rocks with abundant Cr-rich and ferromagnesian minerals will have low Y/Ni and high Cr/V ratios. The LGCP samples from TAN0513-15 and 19 suggest an increased influx of ferromagnesian minerals (drop in Y/Ni) and more Cr-rich material (spike in Cr/V) (Figure 6-10). Further up core in the post LGCP samples there is less enrichment indicated by these ratios.

Geochemical differences between the Hokitika cores reinforce the control that proximity to the Hokitika Canyon Head plays. The proximal core TAN0513-15 has notably higher SiO2, SiO2/Al2O3 ratios, and Zr, and lower CaO compared to the more distal cores. Increasing dilution of terrigenous material down canyon with carbonates would be a key factor driving this.

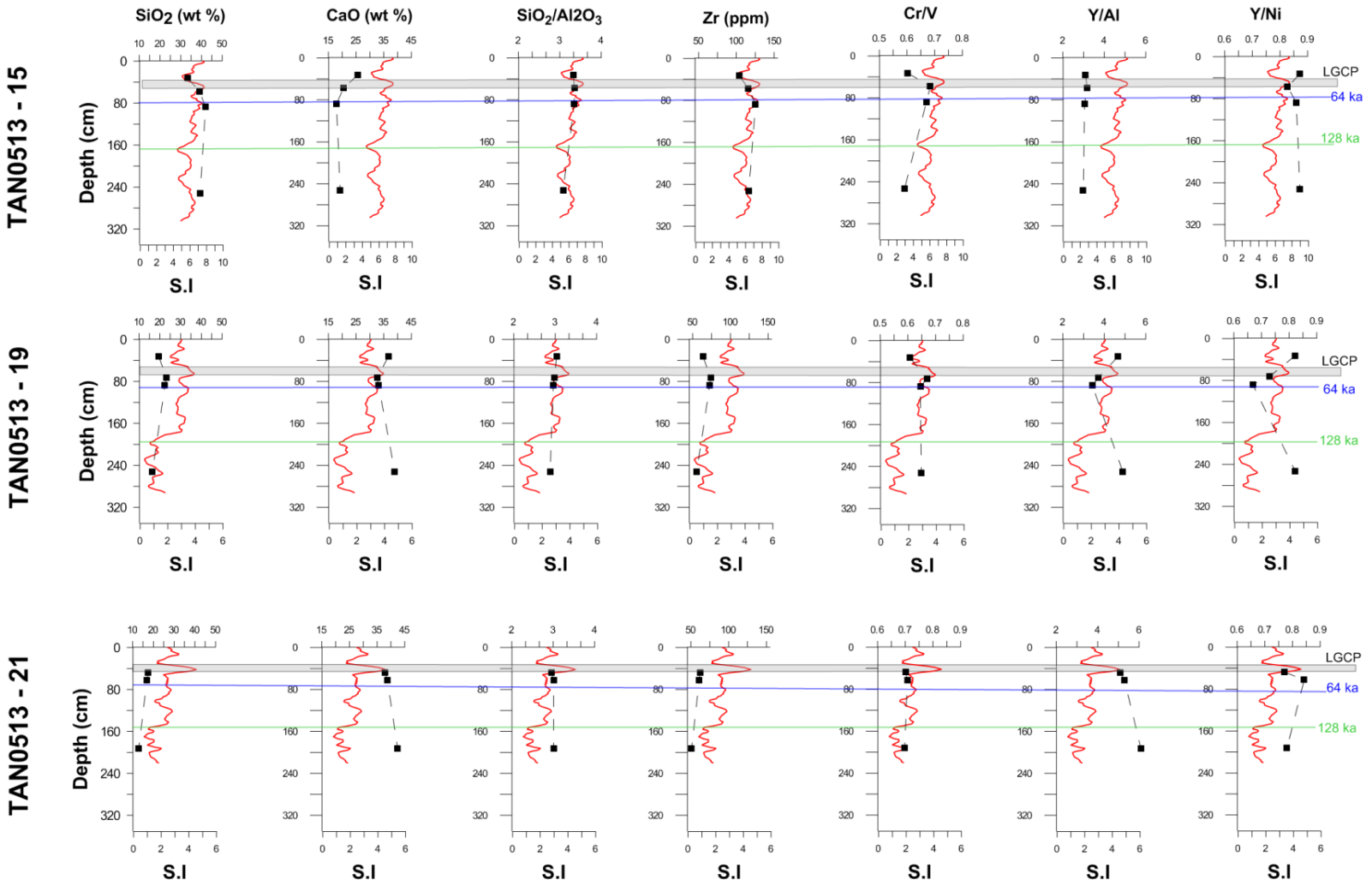

Figure 6-10 Selected major and trace element concentrations and ratios in Hokitika core sediments determined by X-ray fluorescence (XRF). Sample points are represented by black squares. Red line is magnetic susceptibility courtesy of NIWA. LGCP = Last Glacial Cold Period (ca. 28ka to ca. 18ka). Trace element ratios are calculated from ppm.

6.4 INTERPRETATIONS

6.4.1 Evidence for Glacial-interglacial Controls on Terrigenous Sediment Supply

Textural and geochemical results for the Hokitika Canyon cores suggest a strong control from glacial-interglacial cycling. In particular, the difference in texture and composition between LGCP samples (ca. 28ka to ca. 18ka) and younger interglacial sediments is often marked. The primary driver of this is likely to be variations in the flux of terrigenous sediment with changes in sea level (Carter 1975; Carter 1980; Carter et al. 1986; Hoogakker et al. 2004). In addition to sea level change, erosion rates were higher with the reduction in vegetation cover and the intensity of glacial activity in this region. The paleoshoreline maps illustrate for the South Westland region how shelf surface area and the level of connectivity between the canyons and local rivers is dictated by sea level (Figure 6-4). Local rivers such as the Hokitika and Cook rivers exported most of their sediment directly into the canyon systems during the LGCP. With shorelines at the edge of the Hokitika Canyon rims, coarse littoral sediments (<30 m water depth) were exported directly into the canyon system also. The combined export of Hokitika River and Central Shelf littoral sediments into the Hokitika Canyon would explain the spikes in mean grain size, poorer sorting, and higher sand percentages in the LGCP samples. This pulse in terrigenous material is also reflected in compositional data, where higher levels of siliciclastic minerals, SiO_2, and Zr, and lower CaO correlate with enhanced magnetic susceptibility during the LGCP. These interpretations of textural and compositional features during the LGCP assume that major reductions in carbonate productivity or carbonate dissolution (Hoogakker et al. 2004) did not cause the elevated terrigenous signal.

As sea levels increased after ca. 18 ka, the amount of canyon head bypassing of coarse littoral sediments increased as the shoreline migrated east of the HCH until its present position at ca. 6.5 ka. The Hokitika Canyon would have lost its major littoral contributions of terrigenous material earlier than the Cook Canyon due to its less incised morphology (between 16ka to 11.5ka compared to after 11.5ka for the Cook Canyon). The Hokitika River became increasingly disconnected from the HCH as shorelines transgressed. More fluvial sediments became transferred via littoral transport to the northern shelf region. These effects are reflected in the Hokitika core sediments, which show clear increases in CaO, and declines in mean grain size, sand percentage, SiO_2, and Zr as terrigenous sediment supply fell in the post-LGCP sediment samples.

6.4.2 Evidence for Changes in the Composition of Terrigenous Canyon Sediments during the LGCP

In addition to high fluxes of terrigenous sediments, there is evidence for increased proportions of ferromagnesian and Cr-rich minerals in the Hokitika Canyon during the LGCP. This is suggested by the higher Cr/V and lower Y/Ni ratios relative to the younger, post-LGCP sediments. The Hokitika catchment contains numerous lenses of Pounamu Ultramafics (including serpentinite, gabbro and metabasite) hosted within the Alpine Schist (Nathan et al. 2002). These lenses continue to shed

ferromagnesian minerals and numerous Cr-spinels to the Hokitika river sediments and ultimately, local beaches today (section 4.5 this study & Bradley et al. 2002). With a more direct connection to the Hokitika Canyon during the LGCP, Cr - spinel and ferromagnesian bearing Hokitika River sediments were exported directly in the canyon system. Higher rates of erosion could also have elevated the flux of these minerals into the canyon system. The Waitaha River, ca. 50km south of Hokitika, also contains Cr- enriched sediments which elevate Cr levels in modern beaches to the north (Bradley et al. 2002). Consequently, Cr enriched Central Shelf sediments exported into the HCH during low stands, could have contributed to the ferromagnesian and Cr rich signal during the LGCP. In surface sediments on the north rim of the HCH, Cr-spinels are present in relict sediments (Chapter 4.0). These were probably deposited during sea level lowstands by the Hokitika River. During sea level highstands, the disconnection of the Hokitika River and lack of littoral sediment input into the HCH probably decreased the flux of Cr-rich and ferromagnesian minerals into the canyon system. This could explain the more Cr and ferromagnesian mineral 'depleted' terrigenous composition during interglacial periods.

The Cr/V ratio in particular has demonstrated its effectiveness as a proxy for interglacial – glacial change in submarine canyon stratigraphy. Increases and decreases in the connectivity of Cr-bearing fluvial systems during lowstands and highstands respectively can be observed with the Cr/V ratio.

6.4.3 Comparison to other Westland Shelves and Canyons

The Cr/V and Y/Ni ratios for the Hokitika Canyon sediments are compared to the modern shelf sediments studied in previous chapters, and two Haast canyon core samples (Figure 6-11). The distinct groupings of the shelf regions probably reflect trends in regional geology. The North Shelf and the Hokitika Canyon core sediments share similar Cr/V values (0.6 – 0.7), probably due to the influence of the Cr-spinels in Hokitika River sediments.

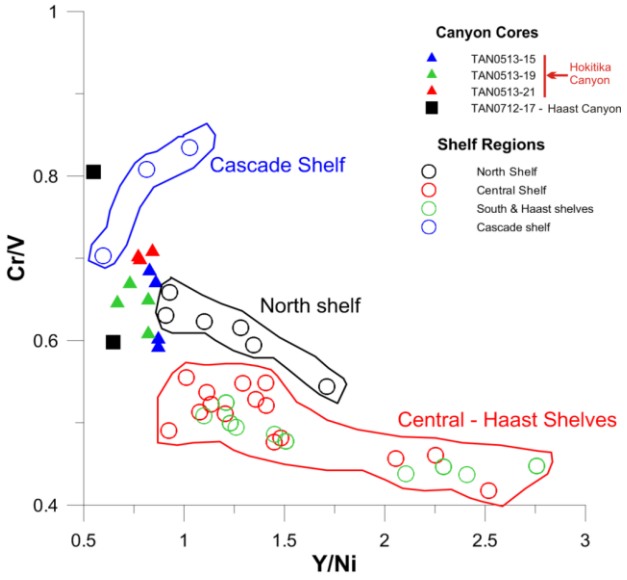

Figure 6-11 Graph of Y/Ni and Cr/V ratios for various Westland shelf regions and the Hokitika and Haast core samples.

The Central to Haast shelves are more depleted in Cr and often richer in Y due to less ferromagnesian minerals in the predominantly Alpine Schist catchments of these regions. The Haast canyon core samples (TAN0712-17) display a strong association with the Cascade Shelf chemistry (especially at core depth 120-125 cm). The Cascade Shelf is supplied with Cascade River Cr-spinel and ferromagnesian rich sediments from the Dun Mountain Ultramafics (sections 4.4 and 3.4) which would enrich the Haast canyon terrigenous fraction.

6.5 SUMMARY

- Paleoshorelines at 20, 16, 11.5, and 8ka reveal dramatic changes in the interactions between SWCM canyon heads, continental shelves, and fluvial systems.
- During sea level lowstands (i.e. the LGCP), the HCH and CCH intercepted littoral transport paths, were strongly connected to local rivers, and inter-canyon shelves became compartmentalised (i.e. the Central Shelf). The net result was elevated terrigenous export into the canyon heads. Hokitika Canyon cores reflect these effects with textural and compositional 'spikes' indicating higher terrigenous input during the LGCP.
- The less deeply incised Hokitika Canyon became disconnected from local rivers and littoral sediment supplies significantly earlier than the Cook Canyon (16ka to 11.5ka and <11.5ka respectively).
- Interglacials are characterised by canyon head bypassing of shelf sediments and reduced connectivity to fluvial systems. This reduces the amount of terrigenous sediment export into canyon heads and is illustrated in the Hokitika Canyon cores with decreased siliciclastic content and increases carbonate.
- The geochemistry of the terrigenous fraction in the Hokitika Canyon provides evidence for more enrichment in ferromagnesian and Cr-rich minerals during the LGCP than the warmer interglacial periods. This is probably due to the increased connectivity of the Hokitika River which more directly fed Cr spinel and ferromagnesian minerals to the HCH during lowstands.
- The Cr level (i.e. Cr/V ratio) in the terrigenous fraction differs between the Haast and Hokitika Canyons, as well as the Westland shelves due to changes in regional geology. The extent of ultramafic outcrop in Westland catchments is probably the primary control of this.

CHAPTER 7 : SEDIMENTARY FACIES, INTERPRETATIONS, AND CONCLUSIONS

This chapter brings together results and interpretations of South Westland Continental Margin (SWCM) surface textures and compositions, shelf and canyon geomorphology, and canyon stratigraphy to provide a comprehensive picture of SWCM sedimentation and the interaction of submarine canyons with the shelves today and during glacial lowstands. In sections 7.1 to 7.4, interpretations and conclusions are specific to the SWCM shelf and canyons. In section 7.5, comparisons of the SWCM with other shelves in New Zealand and overseas are made.

7.1 MODERN FACIES OF THE SWCM

Modern surface sediment facies of the SWCM have been developed from textural and compositional results presented and discussed in Chapters 2, 3, 4, and 5. Textural and compositional characteristics of these facies are presented in Table 7-1, and their spatial distributions on the SWCM are displayed in Figure 7-1.

7.1.1 Inner Shelf Facies (1a and 1b)

Description

The inner shelf facies are comprised of unimodal, moderate to well sorted, very fine to fine sands of inner SWCM shelves. This facies is sub-divided into facies 1a and 1b based mainly on textural differences. Facies 1a is restricted to the Haast and South shelves, and occurs at less than 30 m water depth. It is coarser, better sorted, and more sand and quartz rich than 1b (Figure 7-1). Facies 1b occurs on most of the inner North and Central shelves and the deeper portions (> 30m) of the South and Haast shelves.

Interpretation

Facies 1a and 1b reflect environments where constant agitation and resuspension via waves and currents occur. With a mean H_{sig} wave base of ~ 48 m (Chapter 3), these facies correlate well with a high energy, active environment generated by ocean swells incident on the SWCM. The inner shelf sand facies is typical of active margin shelves exposed to a high energy wave climate (Carter et al.,2010; Edwards, 2002; Puig et al., 2003). Sediment accumulation rates will be low due to the rapid bypassing of silts and clays to the middle and outer shelves (Carter et al. 2010). The lack of benthic organisms in facies 1a and 1b is due to the high bed shear stresses from waves and currents (Rose & Kuehl 2010). The composition of facies 1a and 1b is typical of modern inner shelfs, with dominantly sand sized quartz, metamorphic lithics, and feldspar. High SiO_2 content and SiO_2/Al_2O_3 ratios, and low Al_2O_3 reflect the bypassing of silts, clays, and sand sized micas further offshore.

Table 7-1 Properties of the modern surficial facies of the SWCM.

Facies	Water Depth	Texture[a] and Grain Size	Sorting	Mineralogy [b c]	Geochemistry[d]	Skeletal Components[e]
1a. Inner sand Facies	< 30 m Haast & South shelves	Sand $\bar{x}$ = Fine sand (> 95% sand) < 0.5 % clay	Well Sorted	Quartz >50% Mica <10 % HM% = c. 10-20% (max HM 50%)	SiO_2 70-80% SiO_2/Al_2O_3 5-7 Al_2O_3 10-13% Y/Ni 1.5-4.0	Rare Bivalves (< 1%)
1b. Inner sand Facies	< 50 m	Muddy Sand $\bar{x}$ =very fine sand 75-90% sand <1% clay	Moderate to moderately well sorted	Quartz 30 - 50% Feldspar 5 - 10% Lithics 8-25% HM% = c.5-20%	SiO_2 70-80% SiO_2/Al_2O_3 5-7 Al_2O_3 10-13% Y/Ni 1.0-2.5	Rare Bivalves (< 2 %)
2. Transitional Sandy Mud Facies	Variable. (40-70 m typical, also on outer shelf)	Sandy Mud to Muddy Sand 30 – 70% sand <5 % clay	Poorly Sorted	Quartz 30 - 50% Feldspar < 5% Mica 10 – 20% Lithics 2 – 17% HM% <10% Rare glaucony	SiO_2 65-75% SiO_2/Al_2O_3 4-6 Al_2O_3 12-16% Y/Ni 1.0-2.0	<1 % Foraminifera. Rare Gastropods Bivalves
3. Mud Facies	60 – 150 m	Sandy Mud & Mud $\bar{x}$ =medium silt 80-90 % mud 7-9 % clay	Poorly Sorted	Quartz 25 – 45% Feldspar < 5% Mica 15 – 30% Lithics < 10% HM% <10% Rare glaucony	SiO_2 60-70% SiO_2/Al_2O_3 < 4 Al_2O_3 >17 % Y/Ni 0.5-1.5	1 - 4 % Foraminifera
4a. Mixed Glaucony-Siliciclastic Facies	c. 180-200m (canyon head north rims only)	Slightly Gravelly Sands 0-3% gravel (terrigenous) 15 -35% mud	Poor to Very Poor	Quartz 20 – 40% Feldspar < 10% Mica < 5% Lithics 5-20% HM% <5% (ex CCH) Glaucony 20 – 60% (mature glaucony type mainly)	SiO_2 60-75% SiO_2/Al_2O_3 5-7 Fe_2O_3 8-17% P_2O_3 0.25-0.8% Y/Ni < 1.0	< 3% Foraminifera Rare bored shelf fragments
4b. Mixed Relict-modern siliciclastic facies	Various. (90-125m on HCH, c. 250m on CCH)	Gravelly Mud & Muddy Sands 0 -10% gravel (terrigenous) 30-50% mud	Poor to Very poor	Quartz 40 – 55% Lithics 10-25% Mica < 6% Garnet up to 5% HM% = 5-17% Glaucony <5% (mixed glaucony type mainly)	SiO_2 70-80% SiO_2/Al_2O_3 5-7 Fe_2O_3 5-7% Al_2O_3 10-13% P_2O_3 <0.2% Y/Ni >1.0	Foraminifera <1% in HCH c. 15% in CCH tributary canyon

[a]Textural names based on Folk (1968)
[b]Mineralogy based on point counting of sand fraction only
[c]HM=Heavy mineral % determined from the very fine to fine sand fraction via liquid separation method
[d]Geochemistry determined from bulk samples via XRF method
[e]The dominant skeletal components identified from the sand fraction only via binocular inspection

The inner shelf of the SWCM is the most active sediment transport zone, particularly when southwesterly storm swells, wind drift currents, and the Westland Current combine to transport vast quantities of inner shelf sediments northwards. Near Westport, the littoral zone (< 30 m depth) transports ~ 3.8 x 10^6 m^3 of sediment annually (Probert & Swanson 1985), but further south in the SWCM this supply is larger due to more numerous high sediment yield rivers (Hicks & Shankar 2003). In addition, contributions from coastal cliff erosion to the littoral zone would be higher south of the Waitaha River, where coarse coastal moraines and fluvio-glacial deposits are more common. The narrower widths of the Haast and South shelves may explain the coarser, well sorted Facies 1a textures. Incoming swells will shoal less before reaching the inner shelf on narrower shelves, resulting in greater sorting and winnowing of fine sediments.

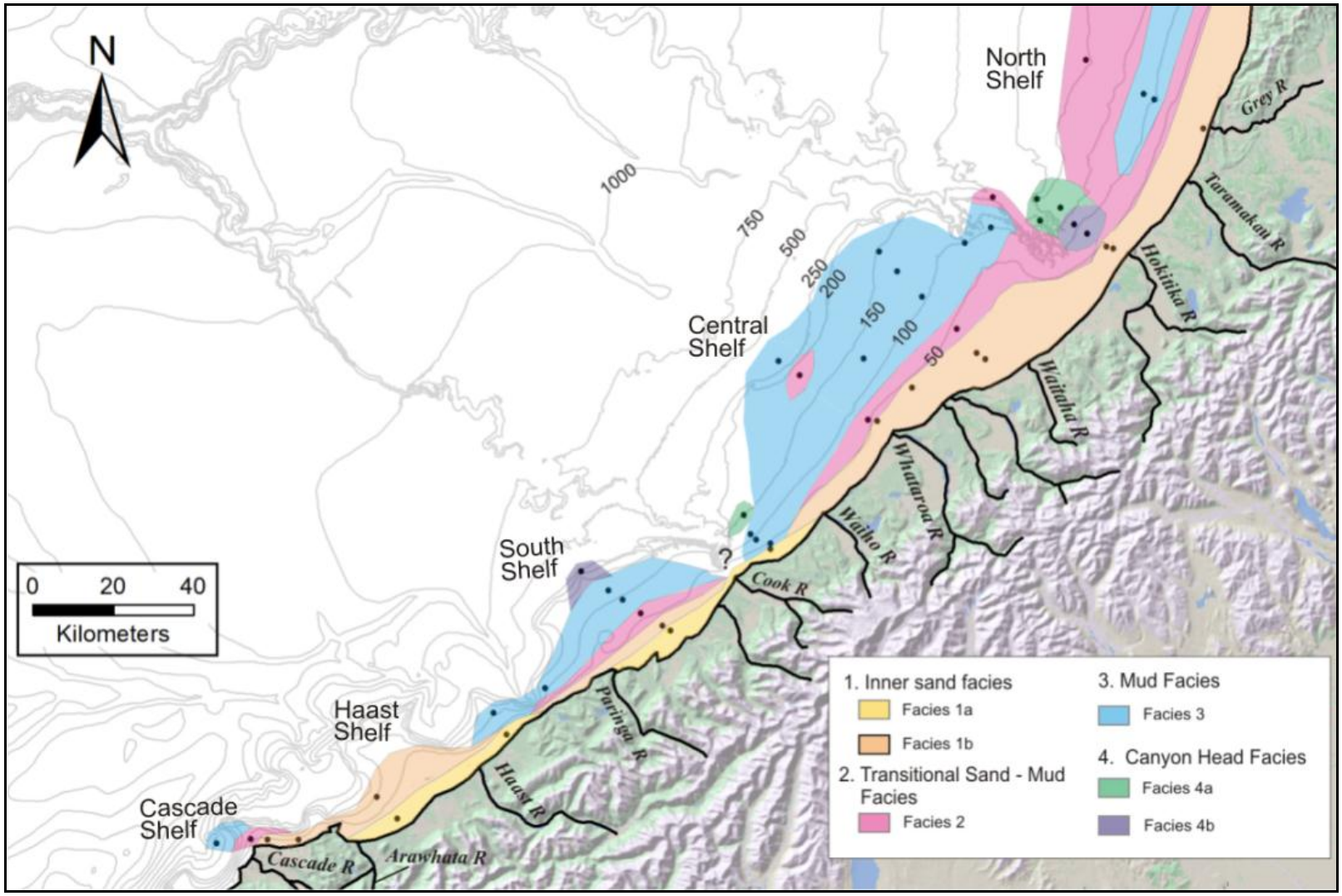

Figure 7-1 Distribution of modern facies on the SWCM. Based on properties in Table 7-1.

7.1.2 Transitional Sand-Mud Facies (Facies 2)

Description

Facies 2 mainly forms a transitional facies between the high energy sand dominated Facies 1a and 1b, and the lower energy mud dominated Facies 3 (Figure 7-1). Between 40 – 50 m depth, a gradational transition from the inner shelf sands into Facies 2 occurs. Facies 2 is poorly sorted, sandy mud to muddy sand, with 30 – 70 % sand, and up to 5 % clay. Micas become more common in Facies 2, and SiO_2 and Al_2O_3 decrease and increase respectively. Skeletal components, while rare (<1% of the sand fraction), are dominated by benthic Foraminifera and less common bivalves and gastropods. Facies 2 lies mainly between 40 – 70 m depth, but other locations include the Hokitika Canyon Head (HCH) canyon floor at the foot of the south rim, and the outer shelf of the North Shelf (Figure 7-1).

Interpretation

Facies 2 primarily represents a decrease in the frequency and magnitude of wave orbital remobilisation of shelf sediments. Increasing clay, silt, mica, and Al_2O_3 content, and lower SiO_2/Al_2O_3 ratios reflect this, with conditions more favorable for mud deposition. Less frequent remobilization of Facies 2 sediment will reduce the rate of sediment transport compared to Facies 1a and 1b. Storm waves (mainly from the southwest) are very capable of stirring sediments at these depths (40 - 70m), and Carter (1980) has shown that wind drift currents at 75 m depth on the Westland Shelf can have velocities of up to 15 cm/s. During these events northward transport of Facies 2 sediment would be significant.

The occurrence of Facies 2 textures on the outer North Shelf suggests significant coarsening here, contrary to a typical ‘graded shelf’ trend. It should be noted that only one sample in transect A occurs on the outer North Shelf. Previous work by Carter (1980) and Probert & Swanson (1985) have shown that this outer shelf coarsening extends northwards from the HCH for the entire western South Island shelf. Increasing shelf width, falling fluvial supplies, and upwelling have been suggested as factors for this coarsening.

7.1.3 Mud Facies (Facies 3)

Description

At middle shelf depths (50 -150m), poorly sorted, mud dominated (80-90%), and clay rich (7-9%) sediments comprise Facies 3. Within the sand fraction, quartz content is low, while mica content is the highest of all the SWCM Facies. The Central and South shelves have the most extensive coverage of Facies 3 sediments, often extending to the shelf break (Figure 7-1). The south rim of the HCH (and probably the Cook Canyon Head (CCH)) is covered mainly in Facies 3.

Interpretation

The muds of Facies 3 are terrigenous muds that bypass the energetic inner shelves of the SWCM. Active margin middle shelf muds are commonly interpreted as depocenters where maximum rates of

sediment accumulation exist (Alexander et al. 2010; Carter et al. 2010; Rose & Kuehl 2010). In addition, clay rich sediments strongly correlate with zones of maximum sediment accumulation (Puig et al. 2003). The low levels of skeletal grains (1-4 % Foraminifera in the sand fraction) also reflect a high sediment accumulation rate. Facies 3 lies well beneath fair weather wave base (~48m), with wave orbital resuspension less frequent. This favors mud deposition and intensive bioturbation (Rose & Kuehl 2010). Hemipelagic sedimentation from nepheloid layers and bioturbation will be major processes in facies 3.

Episodic transport during large storms is probable at Facies 3 water depths, with shelf muds resuspended by storm wave orbitals and transported approximately northwards. The blanketing of the Central and South shelves with Facies 3 muds to the shelf break is a testament to the very high fluvial supply to these shelves (Table 1-1 & Figure 7-1). Facies 3 muds are found less than a kilometre from the active gully networks along the south and east rims of the HCH and CCH. These sediments will almost certainly be involved with these gullies that actively feed into the canyon heads.

7.1.4 Canyon Head Facies (Facies 4a &4b)

Description

Facies 4a and 4b possess textures and compositions that contrast with the other SWCM facies and are only found to the north HCH and CCH central axes. Facies 4a is characterised by mature glaucony grains (20-60% of the sand fraction), poor to very poorly sorted sands, rare relict siliciclastic pebbles, and 15 – 35 % mud. Mica and heavy mineral content is low, and skeletal grains are typically foraminifera and rare bored shell fragments. Unique to Facies 4a is very high levels of Fe_2O_3 and P_2O_3 compared to the other SWCM facies. Facies 4a occurs across a narrow depth range of 180 – 200 m.

Facies 4b is a poor to very poorly sorted mixed facies of relict and modern siliciclastic sediments. It is found at shallower depths on the HCH north rim (90 – 125 m), and at 250 m depth at the head of a tributary canyon to the CCH (Figure 7-1). Rounded quartz and metamorphic lithic pebbles (up to 10%), coarse to fine sands, and 30 – 50% mud is typical of Facies 4b. Glaucony content is very low and dominantly of the mixed siliciclastic-glaucony variety. Mica content is low, while quartz and heavy minerals are common (5 -15% of fine to very fine sand fraction). Geochemically, Facies 4b has high SiO_2 contents and SiO_2/Al_2O_3 ratios, and a higher Y/Ni ratio than Facies 4a.

Interpretation

Facies 4a: This facies represents a mixture of glaucony, relict siliciclastics and modern fine terrigenous sediment. It denotes a zone of low to very low sediment deposition found only on the north HCH and CCH rims (and several kilometres to the north of this) (Figure 7-1). The abundance of glaucony and lack of micas and muds suggest there is little influx of modern fine terrigenous sediments. The abundance of mature, often limonitised glaucony grains suggest extended periods of low sedimentation on the deeper north canyon rims areas. The glaucony grains exert a strong control on the bulk geochemistry compared to other SWCM facies, elevating Fe_2O_3 and P_2O_3 in particular

(Chapter 5). Relict siliciclastic components are commonly very coarse to fine quartz sands and metamorphic lithics. Rare, rounded pebbles are usually from the Alpine Schist. These coarser siliciclastic components are out of equilibrium with the modern hydraulic regime. Facies 4a is spatially associated with relict topography (i.e. terraces and channels in Chapter 3), providing further evidence for a relict origin.

Facies 4b: This facies is dominated by a mixture of relict and modern siliciclastic sediments with a higher mud content (30-50%) suggesting a greater influx of modern fine sediments than at Facies 4a. Sedimentation rates are still low compared to the modern SWCM facies, allowing coarse sediments to remain exposed at depths normally blanketed by Facies 2 and 3. Relict sediments are a major component, dominantly as pebble to fine sand, sub-rounded to rounded quartz and metamorphic lithics. The relatively high Zr content, high heavy mineral percentages (especially garnet), and high SiO_2/Al_2O_3 and Y/Ni ratios all indicate the presence of siliciclastics associated with a near shore to beach environment. During the Last Glacial Cold Period (LGCP) lowstand and the early stages of the post-LGCP transgression, the Facies 4b area was a beach or littoral zone environment which could impart these relict characteristics. On the upper slope at the head of a tributary canyon to the CCH, Facies 4b sediments may be exposed due to internal waves and tides which are often accentuated at the shelf edge (Puig et al. 2003).

7.2 SWCM SEDIMENTATION MODEL

7.2.1 SWCM Shelf Sedimentation

Shelf sedimentation on the SWCM shelves is probably a dynamic balance between hemipelagic and active sediment gravity flows such as hyperpycnal plumes and fluid mud flows, particularly beyond the inner shelf. Hemipelagic sedimentation would typically prevail during calm periods beyond the mean H_{sig} wave base, contributing to Facies 3. Suspended sediments would be transported as terrigenous, low density intermediate and bottom nepheloid layers generated by river discharge, wave resuspension, or internal waves (Sommerfield et al. 2007; Walsh & Nittrouer 2009).

Sediment gravity flows will be a major shelf transport mechanism on the SWCM. Where shelf slopes on the SWCM are > 0.7˚, autosuspension of silts and clays may generate sediment gravity flows (Walsh & Nittrouer 2009). Southern portions of the Central and South shelves could produce autosuspending flows due to widespread Facies 3 silts and clays and slope angles commonly between 0.5-1.0˚ (Figure 2-3 B & Figure 7-2). However, slope angles on the majority of the SWCM shelves are < 0.5˚, requiring wave orbitals and/or currents to create conditions for sediment gravity flows (i.e. fluid mud flows).

The frequency and magnitude of storm events, particularly ‘wet’ storms, will be a major influence on SWCM sedimentation. Wet storms occur when large ocean waves coincide with peak river flow and sediment discharge (Sommerfield et al. 2007), resulting in extensive dispersal of fine shelf sediments via fluid mud flows. Conditions for fluid mud flows require near bed suspended sediment

concentrations of >10 g/l (Puig et al. 2003). In addition, numerous small to medium sized mountainous SWCM rivers with high sediment yields could generate hyperpycnal conditions on the inner shelf (Figure 7-2). These in turn can produce fluid mud flows which transfer fluvial sediment from the near shore to middle shelf depths (Traykovski et al. 2000; Addington et al. 2007).

Given the extensive coverage of silts and clays on the SWCM, the energetic wave climate, and numerous high yield mountainous rivers, fluid mud flow conditions would be common on the shelves south of the HCH during wet storms. The ability of wet storms to generate sediment gravity flows will be more profound on the SWCM than other regions such as the South Islands east coast. This is because short, steep rivers with few coastal embayments on the SWCM are able to rapidly transfer high flows and sediment loads to the coast to coincide with peak storm waves during a wet storm event.

Net transport of SWCM shelf sediments will be to the north as previous workers have demonstrated (Carter 1980; Probert & Swanson 1985; Carter & Heath 1975). Particularly during storm events, sediment gravity flows will create significant offshore transport controlled by the SWCM shelf gradient. Large volumes of bedload and suspended sediments are frequently transferred to the north in the littoral zone beneath fairweather wave base (e.g. Facies 1a and 1b). Northward directed transport of the deeper Facies 2 and 3 sediments will be less frequent, with maximum transport of these finer sediments occurring when south-westerly storms coincide with peak tidal flows aligned with the Westland Current (Carter & Heath 1975).

The narrower shelf widths in the north of the SWCM were alluded to by Probert & Swanson (1985) as a contributing factor causing finer sediments to blanket the northern Central Shelf. This trend clearly continues further south, with the Central and South shelves draped in Facies 3 clays and silts to the shelf break as shelf width narrows and fluvial sediment supply increases (Figure 7-2). Offshelf export of terrigenous sediments would increase to the south of the HCH as a result, becoming a major phenomenon on the narrow Haast and Cascade shelves. North of the HCH the shelf is more storm dominated, since shelf width increases as fluvial supply falls, modern silts and clays cannot blanket the outer shelf under the prevailing hydraulic regime (Probert & Swanson 1985). On the Central and South shelves, narrower, higher fluvial supplies result in more fluvial dominated shelves (Figure 7-2). A similar trend was observed on the Monterey continental shelf in California. Here, a northern storm dominated shelf with coarse relict sands on the outer shelf prevails due to widening shelf width and lower fluvial input. Further south, the shelf is fluvial dominated as the shelf narrows and fluvial input increases (Edwards 2002).

7.2.2 SWCM Canyon Head Sedimentation:

The interaction of the Hokitika and Cook Canyon Heads with SWCM sedimentation has major implications for sediment textures and compositions (Figure 7-2). The high volumes of modern fine grained shelf sediments transported and deposited on the SWCM (e.g. Facies 3) are key factors maintaining the active Hokitika and Cook Canyon Heads. Transport of these fines via nepheloid layers

and sediment gravity flows result in across shelf and northwards directed transport towards the SWCM canyon heads. This causes the buildup and storage of unconsolidated fine sediments at the canyon rims. South rim samples from the HCH show this, with Facies 3 muds draping the slopes leading towards the south rim (Figure 7-2). The storage zones on the south and east rims of the HCH and CCH will be favorable environments for the generation of sediment gravity flows feeding into the canyon systems (Figure 7-2). Erosive, active gully networks in these areas provide strong evidence for this (Chapter 3). Stored unconsolidated shelf sediments are common on other active margin canyon rims where high sedimentation rates and energetic wave climates persist (e.g. Eel canyon, Puig et al. (2004) or Monterey canyon, Kunze et al. (2002)).

The generation of canyon rim submarine gravity flows could be due to autosuspending gravity flows, wave orbital affects, seismic activity, or a combination of these. Considerable areas of the shelves leading towards the HCH and CCH south and east rims have slope angles between 0.5 -2.0˚ which could generate fluid mud flows via autosuspension (e.g. > 0.7˚) (Figure 2-3 B). Fluid mud flows generated by wave orbitals are the most probable driver of HCH and CCH sediment transport. Resuspension during storm events on canyon rims and the surrounding shelves would produce high near bed suspended sediment concentrations. The wave base for maximum H_{sig} incident on the SWCM (Chapter 3) suggests storm wave orbitals can episodically stir most south and east rim canyon sediments. The shallower CCH rims may experience more intensive resuspension of during storms. The active margin setting of the SWCM probably generates episodic, earthquake induced mass failures on the south and east rims of the CCH and HHC. These would be less frequent than sediment gravity flows produced by wave orbitals (i.e. decades to centuries between events).

Shelf sediment interception

Canyon head interception of modern shelf transport paths on the SWCM is evident in the sediment texture, composition, and geomorphology of areas adjacent to the HCH and CCH. This interception creates a sediment deficit to the north of the canyon heads, leeward of the net shelf transport direction on the SWCM (Figure 7-2). Exposed relict siliciclastics and abundant glaucony strongly indicate little to no deposition of modern fine sediments leeward of the canyon heads (i.e. Facies 4a & 4b). In the CCH, abundant glaucony but no coarse siliciclastics are exposed in the leeward zone, which may be due to the higher sediment supply here compared to the location of the HCH leeward zone (Figure 7-2). Canyon morphology may be contributing to the lack of fine sediment deposition on the north rims, which can direct or accentuate internal waves and tides that flush the leeward zones. (Sommerfield et al. 2007).

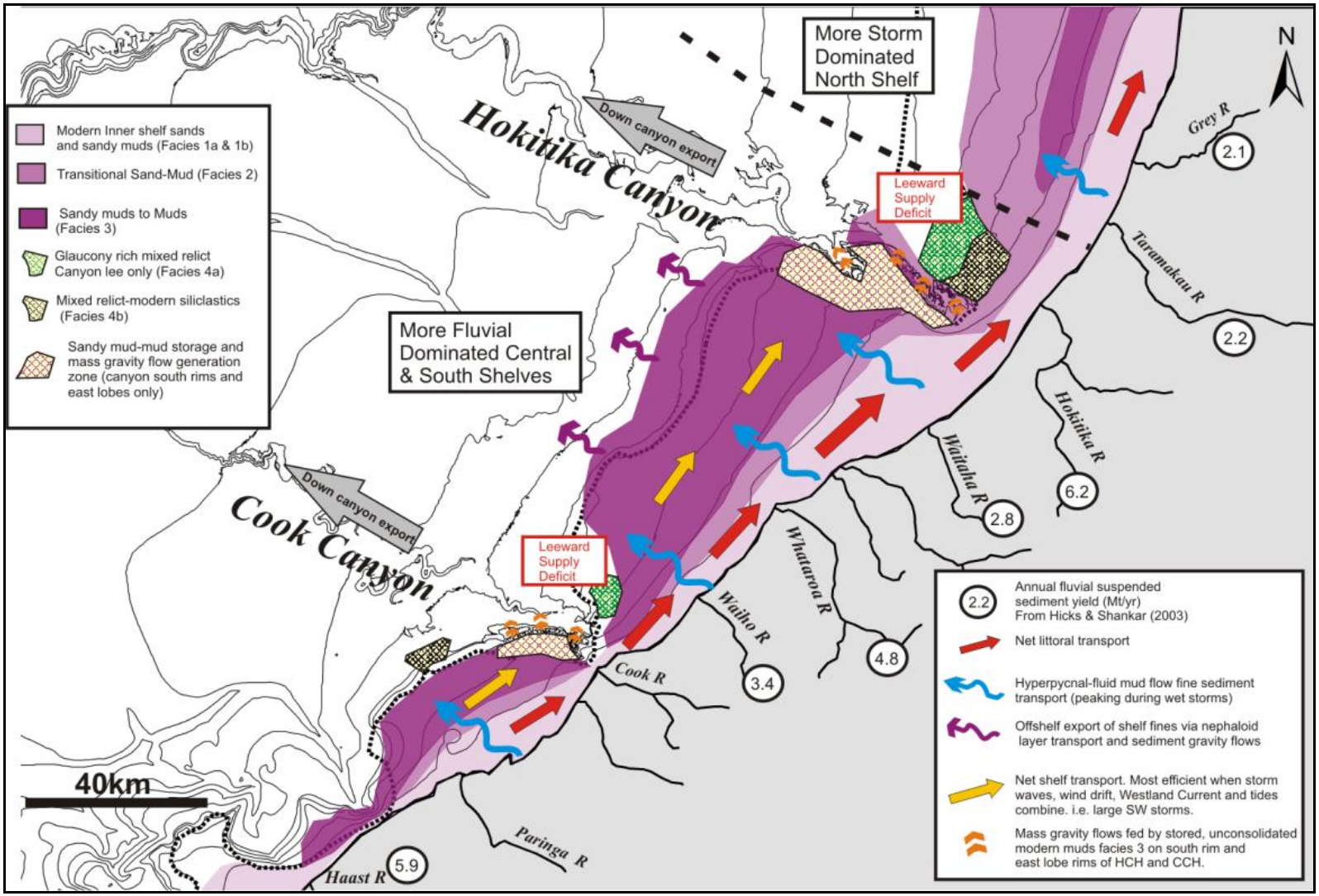

Figure 7-2 Schematic model of shelf and canyon head sedimentation on the modern SWCM.

The Hokitika Canyon is bypassed by the littoral zone but would still export significant amounts of the SWCM sediment budget (Figure 7-2). For example, up to ~1/3 of the Ganges-Brahmaputra fluvial supply is exported into a canyon system not directly connected to rivers or the littoral zone (Walsh & Nittrouer 2009). The deeply incised, more shoreward location of the CCH (Figure 2-3 & Figure 7-2) may result in greater export of shelf sediments than the HCH, including sediments from the seaward limit of the littoral zone.

Canyon incision and leeward outer shelf coarsening

Beyond the leeward supply deficit zone (e.g. Facies 4a and 4b) the interception of shelf sediments may be exerting a far reaching influence on Westland shelf textures. In addition to outer shelf coarsening on the North Shelf caused by increasing shelf width and falling fluvial supply (Probert & Swanson 1985), the export of modern fines from the Central Shelf into the HCH is probably a significant contributing factor for this coarsening. This reduction in outer shelf fines due to canyon export will contribute to the more storm dominated North Shelf, where coarse relict sands are more exposed to the hydraulic regime (Figure 7-2). The export of large volumes of shelf sediment into the CCH does not produce outer shelf coarsening on the Central Shelf to the north, probably due to the high fluvial supply from the Central Shelf catchments (Cook to Waitaha Rivers).

7.3 DISPERSAL AND PROVENANCE

Regional trends in the geology of the SWCM catchments have produced broad differences in shelf composition. The influence of ultramafic outcrops in the Cascade – Arawhata catchments (Dun Mountain Ultramafics) and the Hokitika – Waitaha catchments (Pounamu Ultramafics) were identified in river, beach, and shelf sediments through Cr enriched spinels and Cr enriched bulk geochemistry. In particular, Cr/V and Y/Ni ratios were reliable indicators of these ultramafic source rocks since they are less affected by the effects of dilution by the Alpine Schists. These ultramafic signals were strongest on the Cascade and North shelves (Dun Mountain and Pounamu Ultramafics respectively). The net northward transport direction on the SWCM was reinforced by the Cr/V ratio, with shelf sediments to the south of the Hokitika - Waitaha catchments depleted in this ratio, indicating no southward transport of the Cr ‘enriched’ river sediments.

The Alpine Schists overwhelm the SWCM shelves, diluting and restricting the influence of the ultramafic components from dispersing great distances (i.e. > 50km). On the shelves between the Haast and Mikonui Rivers, depleted Cr/V ratios and no Cr enriched spinels demonstrate the lack of ultramafic outcrops in these catchments. The influence of catchment lithologies other than the Ultramafics were not significant (i.e. the Greenland Group, Cretaceous – Pliocene sediments, or Granitoids). This is probably due to the small outcrop area of these units and their similarity in composition to the Alpine Schist compared to the

ultramafics. Hydrodynamic sorting of modern SWCM sediments produces major variations in mineralogy and geochemistry, providing a basis to define modern facies on the SWCM (Table 7-1).

7.4 GLACIAL-INTERGLACIAL SCENARIOS

The effects of lowstand sea levels on SWCM shelf and canyon sedimentation is displayed in (Figure 7-3). This interpretation is based on work from Chapter 7 on paleoshorelines, and textural and compositional results in Chapters 3-6. Assuming a similar continental margin morphology, lowstand sea levels (-120 m below present) had dramatic effects on the level of canyon interception of shelf sediments, and the connectivity between rivers and submarine canyon heads on the SWCM. The shelves were clearly compartmentalised during lowstands, divided by the HCH and CCH which intercepted a variety of shelf material, from littoral bed load gravels and sands to dilute suspended sediments such as bottom nepheloid layers on the shelf.

During lowstands, local fluvial systems are more directly connected to the HCH and CCH. Both canyon heads probably received the majority of the sediment load from more than one river (e.g. Hokitika and Waitaha Rivers into the HCH, and the Cook, Karangarua, and possibly the Paringa rivers into the CCH). The net result during lowstands is major increases in the volume and grain size of terrigenous sediment intercepted and exported offshore. Evidence for this textural 'spike' was identified in the Hokitika Canyon core samples from the LGCP (Chapter 7). Tributary canyons which are inactive today were probably active during the LGCP (Figure 7-3).

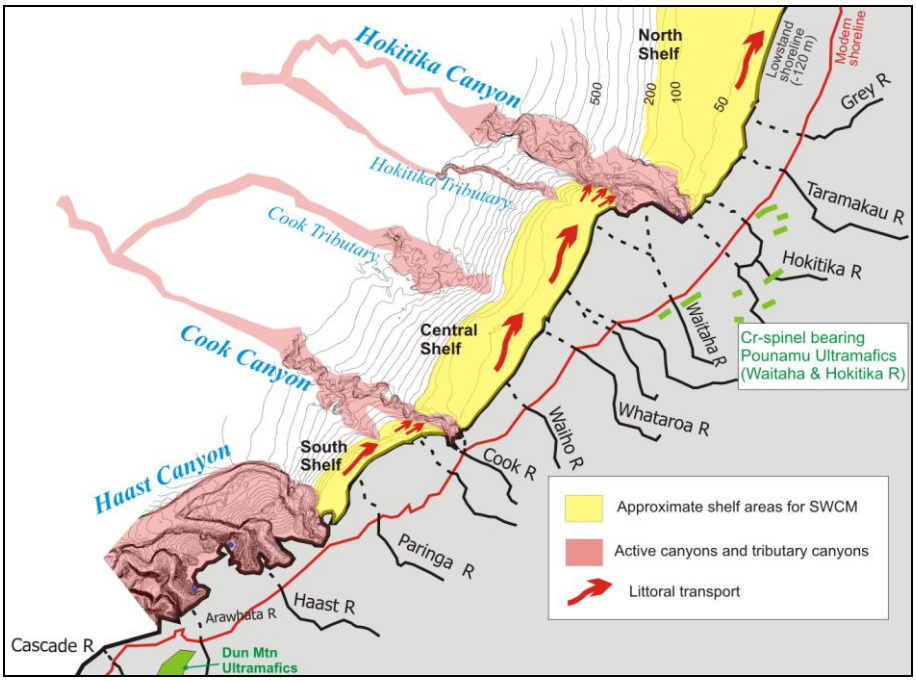

Figure 7-3 Schematic interpretation of the SWCM during a glacial lowstand. Note the compartmentalisation of the shelves and direct connection of several fluvial systems to the HCH and CCH. Lowstand shoreline is projected as – 120 m below the present sea level and bathymetry is based on the modern bathymetry of the SWCM. Yellow shaded area is a projection of the shelf ~200m below the LGCP shoreline.

Coarse relict sediments exposed today at the head of a CCH tributary canyon on the South Shelf (Facies 4a) were probably associated with littoral sediments during the LGCP. Deposition of Facies 4a and 4b on the HCH north rim were probably associated with the Waitaha – Hokitika outwash systems, where Cr-spinels from Pounamu Ultramafics were delivered to the LGCP beaches and littoral zones (Figure 7-3). The increased connectivity of the Waitaha – Hokitika fluvial system to the HCH was observed in LGCP trace element ratios in core samples. Slight enrichments in ferromagnesian and Cr bearing minerals suggest a greater influx of terrigenous material from the Pounamu Ultramafic bearing catchments. These changes in the composition of canyon sediments between lowstands and highstands demonstrate that trace element ratios can be a useful proxy of glacial-interglacial sea level change.

7.5 COMPARISONS TO OTHER SHELVES

7.5.1 Comparisons to other New Zealand Shelves

Continental shelves around New Zealand have a variety of similarities and differences in surface sediment textures with the SWCM shelves. Sediment supply and shelf width are major factors controlling shelf textures between these regions. Other factors include the nature of the hydraulic regime, and structural or geomorphic controls on sediment distribution.

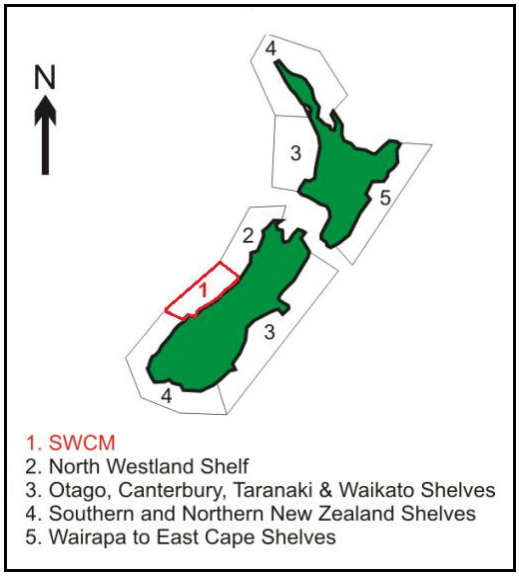

Figure 7-4 Shelf regions of New Zealand

The North Westland Shelf (2)

North of the SWCM between the Grey River and Farewell Spit (Figure 7-4), shelf sediments become progressively coarser and richer in biogenic material (Carter 1975,1980; Probert and Swanson 1985). Despite a comparable hydraulic regime to the SWCM, decreased sediment supply and broader shelf widths produce these notable textural differences. The supply of suspended sediment reaching the North Westland shelf is almost an order of magnitude less than the SWCM (Table 1-1). This reduction in fluvial

supply combined with increasing shelf width (typically 60 – 80 km wide), results in less sediment available to blanket the shelf with modern terrigenous sediments. Consequently, coarser muddy sands prevail from middle to outer shelf depths. With less modern fine material reaching the shelf edge, relict or palimpsest sands and skeletal grains become common beyond the middle shelf (Probert and Swanson 1985), reflecting less dilution with terrigenous sediments on the North Westland outer shelf. In contrast, the ability of the hydraulic regime on the SWCM to disperse fine sediments is over whelmed by the higher sediment supply and progressively narrower shelf widths.

The Otago, Canterbury, Taranaki, and Waikato Shelves (3)

Textures are notably different on the Otago, Canterbury, Taranaki, and Waikato shelves to the SWCM (Figure 7-4). Shelf sediment supply is low compared to the SWCM due to a lack of major rivers (Waikato and Taranaki) or a relatively low sediment yield in rivers discharging to the coast (Canterbury and Otago) (Carter 1975). The net result is an irregular textural distribution consisting of a near shore modern sand prism up to several kilometres wide (Lewis & Barnes 1999) that grades into middle and outer shelf relict and biogenic sediments (Carter 1986). Similar sand rich prisms occur on the SWCM shelves, but these grade into modern muds and muddy sands. Without high suspended sediment input, waves and currents inhibit any significant fine sediment deposition beyond the inner shelf in the Otago, Canterbury, Taranaki, and Waikato regions.

Southern and Northern NZ shelves (4)

The northern and southern New Zealand shelves differ the most from the SWCM (Figure 7-4). In Fiordland, coastal embayments (in this case fiords) dramatically reduce sediment supply, resulting in mainly relict and biogenic sediments out to the shelf edge. In Southland, wide shelves and low sediment supplies also result in relict and biogenic shelf covers (Carter 1975). Despite a similar shelf width and hydraulic regime as the SWCM, Payne et al. (2010) found on the western Northland shelf an overall coarser (fine sand- very fine sand) shelf lacking muds. Here, carbonate content beyond the inner shelf is over 5 %, with middle to outer shelf sediments dominantly relict and palimpsest due to much lower sediment supplies (Payne et al. 2010). The more distal location of the western Northland shelf to the New Zealand active margin would result in low river sediment yields and increased trapping of sediments in coastal embayments. High uplift rates in SWCM catchments results in a lack of coastal embayments, allowing for more direct input of fluvial sediments and consequently a finer, modern sediment cover towards the SWCM shelf edge.

Wairarapa to East Cape Shelves (5)

Sediment supply is high to the Eastern North Island shelves given the active margin setting and lack of coastal embayments to trap sediments (Figure 7-4). Lithology is also a key factor here, with soft, erodible, fine grained Cretaceous to Paleocene sediments elevating sediments loads via frequent landslides and

gully erosion (Hicks et al. 1996; Rose & Kuehl 2010). Shelf widths are narrow, allowing modern fine sediments to frequently reach the outer shelf. The Waipaoa and Waiapu sedimentary systems have received significant research attention as part of an international collaboration (US-NZ Source-to-Sink program) investigating sediment transfer at several temporal scales (Alexander et al. 2010; Carter et al. 2010; Rose & Kuehl 2010). This research provides a useful reference for interpreting sedimentary textures and processes on the SWCM shelves.

Inner shelf sands prevail at depths shallower than 50 m and grade into a trasitional sand-mud facies termed the 'Mixed Layers and Mottles Facies'on the Poverty Bay shelf by Rose & Kuehl (2010). This then grades into modern muds and muddy sands at middle shelf depths which extend towards the outer shelf (Alexander et al. 2010; Rose & Kuehl 2010). Middle shelf mud depocenters with maximum rates of sediment accumulation are widely recognized on the Poverty Bay – East Cape shelves (Alexander et al. 2010; Carter et al. 2010; Rose & Kuehl 2010). Sediment gravity flows are cited as major transport mechanism on the Poverty Bay shelf (Addington et al. 2007). Structural controls on shelf sediment accumulation are important on the Eastern North Island shelves. For example, synclinal basins provide accommodation space for depocenters on the Poverty Bay shelf (Rose & Kuehl 2010). In addition, anticlinal structures may attenuated or pruturb southern swells and currents (Rose & Kuehl 2010). Relict sediments are rarely documented on the Poverty Bay to East Cape shelves due to an inundation with fine modern sediments. An exception is relict gravels and sands observed near anticlinal ridges on the Poverty Bay shelf (Foster & Carter 1997).

The Wairarapa to East Cape shelves are most similar to the SWCM shelves than other New Zealand regions. Both are active margins with narrow shelf widths, high sediment supplies, and a lack of coastal embayments, resulting in volumionous fine terrigenous sediment deposition on the shelf. Across shelf textural patterns on the SWCM are similar to the Poverty Bay and Waiapu shelves with inner shelf sands indicative of the high bed shear stresses from waves and currents that prevent silts and clays from settling and limit benthic organism activity. Facies 2 on the SWCM (Table 7-1) is analogous to the transitional sand – mud 'Mixed Layers and Mottles' facies on the Poverty Bay shelf (Rose & Kuehl 2010). The Central and South shelves of the SWCM are both blanketed in muds to the shelf edge like the Eastern North island shelves. Storm wave resuspension is likely to occur at greater depths on the SWCM shelves due to exposure to more frequent, larger period swells from the W to SW quadrants. Deeper stirring depths on the SWCM will likely push the boundaries between each facies to greater depths than seen in the Poverty Bay shelf. For example, the Poverty Bay shelf transisional sand-mud facies lies between 30 – 60 m water depth, shallower than Facies 2 on the SWCM which is between 40 - 70 m depth.

A significant difference between the SWCM and the Poverty Bay shelves is the contrast in physiohydrographic sheltering or buffering of swells and currents by coastline morphology and structural features. The SWCM coastline is straighter with fewer large bays and headlands to attenuate swell energy.

The smooth SWCM shelf also lacks any notable anticlinal sturctures which could influence swells. Unlike the Poverty Bay shelves, there is little evidence for localised structural control of depocenters on the SWCM except for regional subsidence on the downthrown sides of the South Westland and Cape Fowlwind fault zones. On the SWCM, the smooth shelf morphology suggests relict sediments exposed by structural features like anticlines on the Poverty Bay shelf are unlikely.

Comparisons to the Kaikoura Canyon

The Kaikoura Canyon is major active conduit on the South Islands east coast which incises the 18 m depth contour to within 1 km of the coastline (Lewis & Barnes 1999). The close proximity of the Kaikoura Canyon to an active margin results in a large supply of terrigenous gravels and sands to beaches and the near shore surrounding the canyon head. The canyon intercepts northward migrating pebble gravels to fine sands within the littoral zone, acting as a major sink for shelf sediments (Lewis & Barnes 1999). Partly due to the interception of the mobile inner shelf sediments, gravels on the middle to outer shelf remain exposed on the north rim and several kilometres to the north as a consequence (Figure 7-5 B) (Lewis & Barnes 1999).

A similar south versus north textural pattern exists in the Hokitika Canyon Head due to the interception and offshore export of northwards transported modern sands and muds (Figure 7-5 A). Facies 4a and 4b on the HCH are analogous to the gravels exposed on the Kaikoura Canyon north rim. Glaucony in the Kaikoura Canyon north rim gravels is not reported by Lewis & Barnes (1999) and is likely due to the shallower depths of these gravel compared to the HCH north rim. While the Hokitika and Cook Canyon Heads are seperated from the coast by up to 10 km of shelf, the modern Kaikoura Canyon provides a useful analogue of how sediment textures and processes may have operated on the SWCM during the LGCP lowstand. Similar coarse terrigenous materials fed by glaciers and outwash plains would have surrounded and fed the HCH and CCH during the LGCP, which are partially exposed as Facies 4a and 4b on the HCH north rim.

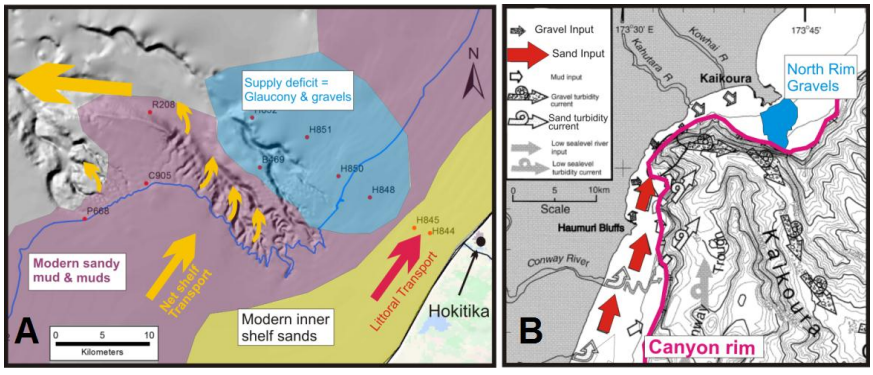

Figure 7-5 Schematic figures comparing modern canyon head interception. A) The Hokitika Canyon Head and the SWCM shelf. B) The Kaikoura Canyon and the North Canterbury shelf. Blue areas are interpreted as areas with supply deficits due the canyon heads intercepting mobile shelf transport paths. Kaikoura figure is modified from Lewis & Barnes (1999).

7.5.2 Comparison to the Eel Margin, Northern California

The Eel shelf and canyon in Northern California and is a region charcterised by high rainfall, steep catchments, a high fluvial supply and an energetic wave climate (mean wave height ~ 3m) (Walsh & Nittrouer 2009; Puig et al. 2004; Sommerfield et al. 2007). Shelf widths are typically 20 km narrowing to ~ 10 km by the Eel canyon head. The entire margin is blanketed in modern sediments consisting of inner shelf sands that grade into muds near the 50 to 60 m isobaths (Puig et al. 2003). A clay rich middle shelf mud belt strongly correlates with maximum accumulation rates measured using radioisotopes (Puig et al. 2003).

Nepheloid bottom boundary layer transport and sediment gravity flows are the main transport mechanisms on the Eel shelf and canyon (Walsh & Nittrouer 2009; Puig et al. 2003). During wet storm events, fluid mud flows transfer sediment concentrated in the near shore from hyperpycnal plumes, across the shelf to middle shelf depths and beyond (Traykovski et al. 2000). Observations from the Eel canyon head using tripods to measure opacity found high suspended sediment concentrations coincident with large wave orbitals and high fluvial input during wet storms. These measurments are interpreted as consistent with bottom boundary layer sediment transport and fluid mud flows at the Eel canyon head (Ogston & Sternberg 1999; Puig et al. 2003).

Decadal core records of clay-rich flood layers sourced from the Eel River represent evidence for the rapid emplacement and storage of flood deposits on the Eel canyon rims (Sommerfield et al. 2007; Puig et al. 2004). These deposits in turn provide a ready supply of fines where Puig et al. (2004) have observed fluid mud flow transport during both wet and dry storms. In addition to the generation of sediment gravity flows from wave-current resuspenion, oscillations in sediment pore pressure from wave orbitals can produce liquefaction induced sediment gravity flows. In the Eel canyon, sediment gravity flows from wave orbital liquefaction are considered more significant than resuspension (Puig et al. 2004).

The wave climate and high sediment supply make the Eel continental margin a useful analogue to the SWCM. The transition depth between inner shelf sands and muds is similar on both the Eel and SWCM shelves, reflecting very energetic wave climates operating in both regions. High clay contents on the SWCM middle shelf, particularly the central and south shelves, are consistent with accumulation maximums as observed on the Eel shelf. Given the similar shelf textures (modern inner shelf sands and muds towards the shelf egde), wave climates, shelf dimensions, and high fluvial sediment supply, nepheloid bottom boundary layer transport and sediment gravity flows will also be key transport mechanisms on the SWCM. Fluid mud flow transfer of fine sediments across the SWCM shelves during wet storms is highly likely on the SWCM. The less seasonal climate of the SWCM would result in a more consistent, year round occurrences of wet storms compared to California's Eel margin. Storage zones of modern fines on the south and east rims of the HCH and CCH are comparable to the fine flood event

layers in recent Eel canyon head cores. This supports the notion that, south and east rims of the HCH and CCH will be favorable environments for the generation of sediment gravity flows that feed into the canyon systems (Figure 7-2). Erosive, active gully networks on the SWCM canyon rims described in Chapter 3 provide strong evidence for this. The unconsolidated nature of HCH and CCH south and east rim sediments could also generate fluid mud flow conditions through wave orbital induced liquefaction.

7.6 CONCLUSIONS

The SWCM has an energetic south-westerly dominated wave climate and numerous high yield mountainous rivers. Consequently the shelf has an extensive coverage of silts and clays, with sediment transport most likely dominated by nepheloid layers and fluid mud flows during wet storms. North of the Hokitika Canyon, shelf width increases as fluvial supply falls, resulting in a more storm dominated shelf as the prevailing hydraulic conditions prevent modern silts and clays from blanketing the outer shelf. Narrower shelf widths and higher fluvial supply between the Hokitika Canyon and the Haast region results in more fluvial dominated shelves.

Four main surficial facies are defined from textural and compositional results, primarily reflecting the supply and storm dominated nature of the SWCM. Mineralogy, geochemistry and skeletal content of these facies is primarily controlled by hydrodynamics. Facies 1 is comprised of inner shelf very fine to medium sand sized quartz, metamorphic lithics, and feldspar. This facies occurs above the mean H_{sig} wave base (48 m) where silts, clays, and sand sized micas are bypassed further offshore. Facies 2 is a transitional sand to mud facies between 40 -70 m depth where increasing clay, silt, and mica reflect a decrease in the frequency and magnitude of wave orbital remobilisation. Facies 3 is a mud dominated (80-90%), clay rich (7-9%) facies with the highest mica and Al_2O_3 content of all the SWCM facies. The shelves south of the Hokitika Canyon are blanketed beyond the inner shelf in facies 3 towards the shelf break. Facies 4 is restricted to the canyon head north rims and is characterised by mixed relict and modern terrigenous sediments and glaucony. Net transport on the SWCM shelf is to the north, particularly during south-westerly storms where wind drift and storm swells may stir and transport the deeper Facies 2 and 3 sediments.

The mineralogy and geochemistry of SWCM sediments is controlled mainly by the hydrodynamic sorting of the Alpine Schist, which comprises most of the SWCM catchments. Broad regional trends in geology are identified in shelf sediments, particularly on the Cascade and North shelves where ultramafic lithologies are found in catchments. Ultramafic signals (i.e. enriched trace element patterns and Cr/V and Ni/Y ratios) suggest enrichments in Cr bearing and ferromagnesian minerals from the Pounamu Ultramafics and Dun Mountain Ultramafics on the North and Cascade shelves respectively. Chromim-rich spinels and magnetites are present in the modern shelf sediments of the Cascade and North shelves but have limited dispersal. Dispersal of shelf sediments beyond the shelves adjacent to catchments associated

with ultramafics is masked by dilution with Alpine Schist sediments. Compositional and textural variations, particularly perpendicular to shore, reflect strong hydrodynamic sorting which help to delineate modern facies on the SWCM.

The Hokitika and Cook Canyon Heads exert a significant influence on SWCM textures during the present day sea level highstand. Net northward transported shelf sediments are intercepted, creating a leeward supply deficit. This deficit is apparent on the north rims and several kilometres to the north where coarser, often glaucony rich, mixed relict-modern siliciclastics remain exposed. Glaucony grains in both canyon lees are probably parautochthonous, representing mature glaucony that as experienced limited transport and indicates a long period of little to no modern sediment deposition on the north canyon rims.

In contrast, the south and east canyon rims represent areas of buildup and storage of modern terrigenous sandy muds and muds where sediment gravity flows are generated. These flows maintain the open nature of the canyon heads and are primarily caused by storm wave orbitals and less frequent autosuspending flows or seismic events. The active nature of the canyons is manifest as submarine gully networks along the south and east rims.

Glacial sea level lowstands represented periods of compartmentalisation of the SWCM shelves and increased connectivity of fluvial systems to the HCH and CCH. Consequently increased volumes of coarse terrigenous sediments were intercepted by the canyon heads and exported down the canyon systems. The unusually coarse, beach to nearshore composition of the relict fraction in the lee of the HCH suggests they were lowstand beach or littoral zones (facies 4b). The occurrence of Cr-spinels in the coarse relict fraction of facies 4a is indicative of the stronger connection of the Hokitika River with the HCH.

The Hokitika Canyon core stratigraphy documents coarsening textures and increases in siliciclastics during the Last Glacial Cold Period due to the lowstand configuration of the SWCM. The export of most of the Waitaha – Hokitika River sediment loads into the HCH during lowstands is supported by enrichments in Cr bearing and ferromagnesian minerals in the terrigenous fraction of LGCP sediments. The Cr/V ratio in particular demonstrates its effectiveness as a proxy for interglacial – glacial sea level change in submarine canyon stratigraphy.

Interglacial periods represent periods of decreased export to SWCM submarine canyons, where littoral transport paths bypass the canyon heads and fluvial systems are more disconnected from the canyon heads. Interglacial highstand signals in the Hokitika cores show up as finer textures with increased carbonate content, and decreased Cr and ferromagnesian enrichments as much of the Hokitika - Waitaha sediment load bypasses the HCH in the northward propagating littoral zone. The more severely incised Cook Canyon would have exported large volumes of shelf sediment and maintained a more direct connection to fluvial systems longer than the HCH as sea levels transgressed after ca. 18ka.

REFERENCES

Addington, L. D., Kuehl, S. A., & McNinch, J. E. (2007). Contrasting modes of shelf sediment dispersal off a high-yield river: Waiapu River, New Zealand. *Marine Geology*, *243*(1-4), 18-30.

Alexander, CR, Walsh, JP & Orpin, AR 2010, 'Modern sediment dispersal and accumulation on the outer Poverty continental margin', *Marine Geology*, vol. 270, no. 1-4, pp. 213-26.

Alloway, B. V., Lowe, D. J., Barrell, D. J. A., Newnham, R. M., Almond, P. C., Augustinus, P. C., Bertler, N. A. N., et al. (2007). Towards a climate event stratigraphy for New Zealand over the past 30 000 years (NZ-INTIMATE project). *Journal of Quaternary Science*, *22*(1), 9–35. Wiley Online Library. doi:10.1002/jqs

Amorosi, A. (1995). Glaucony and sequence stratigraphy; a conceptual framework of distribution in siliciclastic sequences. *Journal of Sedimentary Research*, *65*(4b), 419.

Amorosi, Alessandro. (1997). Detecting compositional , spatial , and temporal attributes of glaucony : a tool for provenance research. *Sedimentary Geology*, *109*, 135-153.

Baker, ET & Hickey, BM 1986, 'Contemporary sedimentation processes in and around an active west coast submarine canyon', *Marine Geology*, vol. 71, no. 1-2, pp. 15-34.

Basu, A., Young, S., & Lee, A. (1975). Re-evaluation of the Use of Undulatory Extinction and Polycrystallinity in Detrital Quartz for Provenance Interpretation. *Journal of sedimentary research*, *45*(4), 873.

Bhuiyan, M. A. H., Rahman, M. J. J., Dampare, S. B., & Suzuki, S. (2011). Provenance, tectonics and source weathering of modern fluvial sediments of the Brahmaputra–Jamuna River, Bangladesh: Inference from geochemistry. *Journal of Geochemical Exploration*. Elsevier B.V. doi:10.1016/j.gexplo.2011.06.008

Blott, S. J., & Pye, K. (2001). GRADISTAT: a grain size distribution and statistics package for the analysis of unconsolidated sediments. *Earth Surface Processes and Landforms*, *26*(11), 1237-1248.

Boggs, S. (2001). *Principles of sedimentology and stratigraphy* (3rd ed., p. xviii, 726). Upper Saddle River, N.J.: Prentice Hall.

Boggs, S. (2009). *Petrology of sedimentary Rocks* (2nd ed., p. 600). Cambridge: Cambridge University Press.

Bradford, J. (1983). Physical and chemical oceanographic observations off Westland, New Zealand, June 1979. *New Zealand journal of marine and freshwater research*, *17*(1), 71–81. Taylor & Francis.

Bradley, J. P. (1977). A study of the detrital heavy minerals of Westland. Christchurch: University of Canterbury, University of Canterbury, 1977.

Bradley, J. P., Chew, P. M., & Wilkins, C. J. (2002). Transport and distribution of magnetite and ilmenite on Westland beaches of New Zealand. *Journal of the Royal Society of New Zealand*, *32*(1), 169–181. Taylor & Francis. doi:10.1080/03014223.2002.9517689

Bradshaw, J. D. (1989). Cretaceous geotectonic patterns in the New Zealand region. *Tectonics*, *8*(4), 803–820. American Geophysical Union.

Campos, R. H. S., & Dominguez, J. M. L. (2010). Mobility of sediments due to wave action on the continental shelf of the Northern coast of the state of Bahia. *Brazilian Journal of Oceanography*, *58*(SPE2), 57–63. SciELO Brasil.

Carpenter, R, Peterson, ML & Bennett, JT 1982, '210Pb-derived sediment accumulation and mixing rates for the Washington continental slope', *Marine Geology*, vol. 48, no. 1-2, pp. 135-64.

Carter, L. (1975). Sedimentation on the continental terrace around New Zealand: a review. *Marine geology*, *19*(4), 209–237. Elsevier.

Carter, L, Manighetti, B., Elliot, M., Trustrum, N., & Gomez, B. (2002). Source, sea level and circulation effects on the sediment flux to the deep ocean over the past 15 ka off eastern New Zealand. *Global and PLanetary Change*, *33*, 339-355.

Carter, L, Orpin, A. R., & Kuehl, S. A. (2010). From mountain source to ocean sink - the passage of sediment across an active margin, Waipaoa Sedimentary System, New Zealand. *Marine Geology*, *270*(1-4), 1-10.

Carter, L. (1980). Ironsand in continental shelf sediments off Western new zealand. *New Zealand journal of geology and geophysics*, *23*(4), 455–468.

Carter, L., & Heath, R. (1975). Role of mean circulation, tides, and waves in the transport of bottom sediment on the New Zealand continental shelf. *New Zealand journal of marine and freshwater research*, *9*(4), 423–448. Taylor & Francis.

Carter, L., & Herzer, R. (1979). The hydraulic regime and its potential to transport sediment on the Canterbury continental shelf. *New Zealand Oceanographic Institute Memoires*, (83), 33 pp.

Carter, R M, Carter, L., & Johnson, D. P. (1986). Submergent shorelines in the SW Pacific: evidence for an episodic post-glacial transgression. *Sedimentology*, *33*(5), 629–649. Wiley Online Library.

Carter, R.M., Carter, L., Williams, J., & Landis, C. (1985). Modern and relict sedimentation on the South Otago continental shelf, New Zealand. *New Zealand Oceanographic Institute Memoir*, (93). New Zealand Dept. of Scientific and Industrial Research.

Chew, P. M. (1981). *MAGNETITE AND ILMENITE OF WESTLAND BEACHES: ANALYTICAL STUDIES BEARING ON THEIR SOURCES AND ACCUMULATION PATTERNS (Unpublished Masters thesis)*. *Unpublished MSc*. University of Canterbury, 1981.

Clifton, H. E., & Dingler, J. R. (1984). Wave-formed structures and paleoenvironmental reconstruction. *Marine Geology*, *60*(1-4), 165–198. Elsevier.

Coombs, D., Landis, C., Norris, R., Sinton, J., Borns, D., & Craw, D. (1976). The Dun Mountain Ophiolite Belt, New Zealand, its tectonic setting, constitution, and origin, with special reference to the southern portion. *American journal of science*, *276*(5), 561.

Cooper, A. F., & Lovering, J. F. (1970). Greenschist amphiboles from Haast river, New Zealand. *Contributions to Mineralogy and Petrology*, *27*(1), 11-24.

Cox, S., & Barrell, D. J. A. (2007). *Geology of the Aoraki Area: 1:250 000 geological map 15*. (p. 71). Lower Hutt, New Zealand: Institute of Geological & Nuclear Sciences Limited.

Deer, W. A., Howie, R. A., & Zussman, J. (1992). *An introduction to the rock-forming minerals* (2nd ed., p. 696). Pennsylvania State University: Longman Scientific & Technical.

Dickonson, W. (1982). Provenance of Franciscan graywackes in coastal California. *Geological Society of America bulletin*, *93*(2), 95-.

Dunbar, G. B., & Barrett, P. J. (2005). Estimating palaeobathymetry of wave-graded continental shelves from sediment texture. *Sedimentology*, *52*(2), 253-269. doi:10.1111/j.1365-3091.2004.00695.x

Edwards, B. D. (2002). Variations in sediment texture on the northern Monterey Bay National Marine Sanctuary continental shelf. *Marine Geology*, *181*(1-3), 83-100.

Evans, B., & Frost, B. (1975). Chrome-spinel in progressive metamorphism—a preliminary analysis. *Geochimica et Cosmochimica Acta*, *39*(6-7), 959-972. doi:10.1016/0016-7037(75)90041-1

Fischer, H. (1990). Glauconite formation: discussion of the terms authigenic, perigenic, allogenic, and meta-allogenic. *Eclogae geologicae Helvetiae*, *83*(1), 1.

Folk, R. L. (1968). *Petrology of sedimentary rocks* (Vol. 169). USA: Hemphill Publishing, USA.

Foster, G & Carter, L 1997, 'Mud sedimentation on the continental shelf at an accretionary margin—Poverty Bay, New Zealand', *New Zealand journal of geology and geophysics*, vol. 40, no. 2, pp. 157-73.

Gorman, R. M., Bryan, K. R., & Laing, A. K. (2003). Wave hindcast for the New Zealand region: Nearshore validation and coastal wave climate. *New Zealand Journal of Marine and Freshwater Research*, *37*(3), 567-588. doi:10.1080/00288330.2003.9517190

Gorman, R., Bryan, K. R., & Laing, A. K. (2003). Wave hindcast for the New Zealand region: deep-water wave climate. *New Zealand Journal of Marine and Freshwater Research*, *37*(3), 567–588. EUROSPAN LTD. doi:10.1080/00288330.2003.9517190

Grapes, R. H. (1995). Uplift and exhumation of Alpine schist, Southern Alps, New Zealand: thermobarometric constraints. *New Zealand journal of geology and geophysics*, *38*(September), 525–534.

Grapes, R., Watanabe, J., & Palmer, K. (1982). *XRF analyses of quartzo-feldspathic schists and metacherts, Franz Josef—Fox Glacier area, Southern Alps of New Zealand : Victoria University of Wellington Geology Department Publication 25. 11 p*. *Victoria University of Wellington Geology Department Publication* (p. 11 p.). Wellington.

Griffin, J. D., Hemer, M. A., & Jones, B. G. (2008). Mobility of sediment grain size distributions on a wave dominated continental shelf, southeastern Australia. *Marine Geology*, *252*(1-2), 13-23.

Griffin, Windom, & Goldberg. (1968). The distribution of clay minerals in the World Ocean. *Deep Sea Research*, *15*, 433 - 459.

Griffiths, G., & Glasby, G. (1985). Input of river-derived sediment to the New Zealand continental shelf: I. Mass. *Estuarine, coastal and shelf science*, *21*(6), 773–787. Elsevier.

Grigsby, J. D. (1990). Detrital magnetite as a provenance indicator. *Journal of Sedimentary Research*, *60*(6), 940-951.

Hayward, B., Grenfell, H. ., Reid, C. ., & Hayward, K. . (1999). *Recent New Zealand shallow-water benthic foraminifera : taxonomy, ecologic distribution, biogeography, and use in paleoenvironmental assessment* (21st ed., p. 264 p.). Lower Hutt, New Zealand: Institute of Geological & Nuclear Sciences monograph ; 21.

Heath, R. A. (1985). A review of the physical oceanography of the seas around New Zealand—1982. *New Zealand journal of marine and freshwater research*, *19*(1), 79-124.

Heath, RA. (1982). What drives the mean circulation on the New Zealand west coast continental shelf? *New Zealand journal of marine and freshwater research*, *16*(2), 215–226. Taylor & Francis.

Hedges, J. I., & Keil, R. G. (1995). Sedimentary organic matter preservation: an assessment and speculative synthesis. *Marine Chemistry*, *49*(2-3), 81-115.

Henderson, R., & Thompson, S. M. (1999). Extreme rainfalls in the Southern Alps of New Zealand. *Journal of Hydrology (NZ)*, *38*(2), 309 -330.

Herron, M. (1988). Geochemical Classification of Terrigenous Sands and Shales from Core or Log Data. *Journal of Sedimentary Research*, *58*(5), 820.

Hessell, J. W. D. (1982). *The climate and weather of Westland* (NZ Met. S., p. 44). Wellington: Ministry of Transport New Zealand Meteorological Service.

Hicks, DM, Hill, J & Shankar, U 1996, 'Variation of suspended sediment yields around New Zealand: the relative importance of rainfall and geology', *Exeter Symposium - Erosion and Sediment Yield: Global and Regional Perspectives*, IAHS pp. 149-56.

Hicks, & Shankar. (2003). Sediments from New Zealand Rivers - NIWA Chart. Wellington, N.Z.: NIWA.

Hicks, M., Shankar, U., & McKerchar, A. (2003). Sediment yield estimates: a GIS tool. *Water and Atmosphere (NIWA)*, *11*(4), 26–27.

Hoogakker, B. a. a., Rothwell, R. G., Rohling, E. J., Paterne, M., Stow, D. a. V., Herrle, J. O., & Clayton, T. (2004). Variations in terrigenous dilution in western Mediterranean Sea pelagic sediments in response to climate change during the last glacial cycle. *Marine Geology*, *211*(1-2), 21-43. doi:10.1016/j.margeo.2004.07.005

Jones, G. A., & Kaiteris, P. (1983). A vacuum-gasometric technique for rapid and precise analysis of calcium carbonate in sediments and soils. *Journal of Sedimentary Research*, *53*(3467), 1-6.

Kautz, C., & Martin, C. (2007). Chemical and physical weathering in New Zealand's Southern Alps monitored by bedload sediment major element composition. *Applied Geochemistry*, *22*(8), 1715–1735.

Komar, P. D. (2007). The entrainment, transport and sorting of heavy minerals by waves and currents. *Developments in Sedimentology*, *58*, 3-48.

Korup, O., Schmidt, J., & Mcsaveney, M. (2005). Regional relief characteristics and denudation pattern of the western Southern Alps, New Zealand. *Geomorphology*, *71*(3-4), 402-423. doi:10.1016/j.geomorph.2005.04.013

Kunze, E., Rosenfeld, L. K., Carter, G. S., & Gregg, M. C. (2002). Internal waves in Monterey submarine canyon. *Journal of physical Oceanography*, 1890-1913.

Laird, M. G. (1972). Sedimentology of the Greenland Group in the Paparoa Range, west coast, south island. *New Zealand journal of geology and geophysics*, *15*(3), 372-393.

Le Roux, J. P. (2010). Sediment entrainment under fully developed waves as a function of water depth, boundary layer thickness, bottom slope and roughness. *Sedimentary Geology*, *223*(1-2), 143-149. Elsevier B.V. doi:10.1016/j.sedgeo.2009.11.006

Lewis, D. W., & McConchie, D. (1994). *Analytical sedimentology* (2nd ed., p. 197 p). New York: Chapman & Hall.

Lewis, K. B., & Barnes, P. M. (1999). Kaikoura Canyon, New Zealand: active conduit from near-shore sediment zones to trench-axis channel. *Marine Geology*, *162*(1), 39–69. Elsevier.

McLennan, SM, Hemming, S., McDaniel, D., & Hanson, G. (1993). Geochemical approaches to sedimentation, provenance, and tectonics. *SPECIAL PAPERS-GEOLOGICAL SOCIETY OF AMERICA*, 21–21. GEOLOGICAL SOCIETY OF AMERICA, INC.

Moore, M. I., & Murdoch, R. C. (1993). Physical and biological observations of coastal squirts under nonupwelling conditions. *Journal of geophysical research*, *98*(C11), 20043–20. American Geophysical Union.

Mortimer, N. (2000). Metamorphic discontinuities in orogenic belts: example of the garnet-biotite-albite zone in the Otago Schist, New Zealand. *International Journal of Earth Sciences*, *89*(2), 295-306. doi:10.1007/s005310000086

Mortimer, N. (2004). New Zealand's geological foundations. *Gondwana Research*, *7*(1), 261–272. Elsevier.

Morton, A. C., & Hallsworth, C. R. (1999). Processes controlling the composition of heavy mineral assemblages in sandstones. *Sedimentary Geology*, *124*(1-4), 3-29.

Morton, A. C., & Smale, D. (1990). The effects of transport and weathering on heavy minerals from the Cascade River, New Zealand. *Sedimentary Geology*, *68*(1-2), 117-123.

Mount, J. F. (1984). Mixing of siliciclastic and carbonate sediments in shallow shelf environments. *Geology*, *12*(7), 432.

Mountjoy, J. J. (2009). The Hikurangi Subduction Margin. PhD thesis, University of Canterbury.

NIWA Voyage Report. (2005). *NIWA Voyage Report - West Coast Canyons - TAN0513*. Wellington, N.Z.

Nathan, Anderson, Cook, Herzer, R., Raine, & Smale, D. (1986). *Cretaceous and Cenozoic sedimentary basins of the West Coast region, South Island, New Zealand* (p. 90). Wellington, N.Z.: Dept. of Scientific and Industrial Research.

Nathan, S., Rattenbury, M. S., & Suggate, R. P. (2002). *Geology of the Greymouth Area: 1:250 000 geological map 14.* (p. 58). Lower Hutt, New Zealand: Institute of Geological & Nuclear Sciences Limited.

Neil, H. L., Carter, L., & Morris, M. Y. (2004). Thermal isolation of Campbell Plateau, New Zealand, by the Antarctic Circumpolar Current over the past 130 kyr. *Paleoceanography*, *19*(4).

Nittrouer, C. A. A., & Wright, L. D. D. (1994). Transport of particles across continental shelves. *Reviews of Geophysics*, *32*(1), 85–113. American Geophysical Union.

Norris, R. M. (1978). Late Cenozoic geology of the West Coast Shelf between Karamea and teh Waiho River, South Island, New Zealand. *New Zealand Oceanographic Institute Memoir*, (81). Dept. of Scientific and Industrial Research.

Odin, G. S., & Fullagar, P. D. (1988). Geological Significance of the Glaucony Facies. In G. S. Odin (Ed.), *Developments in Sedimentology - Green Marine Clays* (pp. 295–332). Amsterdam: Elsevier.

Ogston, A & Sternberg, R 1999, 'Sediment-transport events on the northern California continental shelf', *Marine Geology*, vol. 154, no. 1-4, pp. 69-82.

Ooi, K. H. (1982). *Electron-microprobe analysis on magnetite sand from Westland - MSc thesis*. University of Canterbury.

Palanques, A, Guillén, J, Puig, P & Durrieu de Madron, X 2008, 'Storm-driven shelf-to-canyon suspended sediment transport at the southwestern Gulf of Lions', *Continental Shelf Research,* vol. 28, no. 15, pp. 1947-56.

Payne, D. S. (2008). *Shelf-to-slope sedimentation on the north Kaipara continental margin, northwestern North Island, New Zealand - Masters Thesis. North*. The University of Waikato.

Phillips, W. R., & Griffen, D. T. (1981). *Optical mineralogy : the nonopaque minerals* (p. 677). San Francisco: Freeman.

Porter-smith, R., Harris, & Anderson. (2004). Classification of the Australian continental shelf based on predicted sediment threshold exceedance from tidal currents and swell waves. *Marine Geology*, *211*, 1 - 20. doi:10.1016/j.margeo.2004.05.031

Portersmith, R. (2004). Classification of the Australian continental shelf based on predicted sediment threshold exceedance from tidal currents and swell waves. *Marine Geology*, *211*, 1 - 20. doi:10.1016/j.margeo.2004.05.031

Price, G. D. (1983). *Final report on West Coast offshore project - Central exploration licences, New Zealand, including Harvester Prospect. (Mineral report series MR1381)*.

Probert, P. K., & Swanson, K. M. (1985). Sediment texture of the continental shelf and upper slope off the west coast of South Island, New Zealand. *New Zealand journal of marine and freshwater research*, *19*(4), 563-573.

Puig, Ogston, Mullenbach, Nittrouer, & Parsons. (2004). Storm-induced sediment gravity flows at the head of the Eel submarine canyon, northern California margin. *Journal of Geophysical Research*, *109*(C3), 1-10. doi:10.1029/2003JC001918

Puig, P., Ogston, A. S., Mullenbach, B. L., Nittrouer, C. A., & Sternberg, R. W. (2003). Shelf-to-canyon sediment-transport processes on the Eel continental margin (northern California). *Marine Geology*, *193*(1-2), 129–149. Elsevier.

Rattenbury, M. S., Jongens, R., & Cox, S. (2010). *Geology of the Haast Area: 1:250 000 geological map 14*. (p. 58). Lower Hutt, New Zealand: GNS Science.

Rollinston, H. (1993). *Using geochemical data : evaluation, presentation, interpretation* (1st ed., p. 352 p). London: Longman Scientific & Technical.

Rose, L. E., & Kuehl, S. A. (2010). Recent sedimentation patterns and facies distribution on the Poverty Shelf, New Zealand. *Marine Geology*, *270*(1-4), 160-174.

Roser, B P, & Korsch, R. (1986). Determination of Tectonic Setting of Sandstone-Mudstone Suites Using Content and Ratio. *The Journal of Geology*, *94*(5), 635–650. JSTOR.

Roser, B P, & Korsch, R. J. (1988). Provenance signatures of sandstone-mudstone suites determined using discriminant function analysis of major-element data. *Chemical geology*, *67*(1-2), 119-139.

Roser, BP P, & Nathan, S. (1997). An evaluation of elemental mobility during metamorphism of a turbidite sequence (Greenland Group, New Zealand). *Geological Magazine*, *134*(2), 219–234. Cambridge Univ Press.

Ryan, M. (2010). *A palynological record of the vegetation and climate of Westland since 210 ka : a thesis submitted to the Victoria University of Wellington in partial fulfilment of the requirements for the degree of Master of Science in Geology*. Victoria University, Wellington.

Schattner, U., Lazar, M., Tibor, G., Ben-Avraham, Z., & Makovsky, Y. (2010). Filling up the shelf - A sedimentary response to the last post-glacial sea rise. *Marine Geology*, *278*(1-4), 165-176.

Sinton, J. M. (1975). *Structure, petrology and metamorphism of the Red mountain ophiolite complex, New Zealand - PhD thesis*. University of Otago.

Smale, D. (1991). Provenance changes and movement on the Alpine Fault indicated by heavy minerals from Cretaceous-Cenozoic sediments in south Westland. *Journal of the Royal Society of New Zealand*.

Sommerfield, Ogston, Mullenbach, Drake, Alexander, Nittrouer, Borgeld, et al. (2007). Oceanic Dispersal and Accumulation of River Sediment. *Continental Margin Sedimentation: From Sediment Transport to Sequence Stratigraphy* (p. 531). Oxford, UK: Blackwell Scientific Publications.

Stanton, B. (1976). Circulation and hydrology off the west coast of the South Island, New Zealand. *New Zealand journal of marine and freshwater research*, *10*(3), 445–467. Taylor & Francis.

Stanton, B. R. (1971). Hydrology of Karamea Bight, New Zealand. *New Zealand journal of marine and freshwater research*, *5*(1), 37-41.

Stanton, B. R. (1998). Ocean surface winds off the west coast of New Zealand: a comparison of ocean buoy, ECMWF model, and land-based data. *Journal of Atmospheric and Oceanic Technology*, *15*(5), 1164-1170.

Stoffers, P., Pluger, W., & Walter, P. (1984). Geochemistry and mineralogy of continental margin sediments from Westland, New Zealand. *New Zealand Journal of Geology & Geophysics*, *27*(3), 351-365.

Stoffers, P., Plüger, W., Walter, P., & Pluger, W. (1984). Geochemistry and mineralogy of continental margin sediments from Westland, New Zealand. *New Zealand journal of geology and geophysics*, *27*(3), 351–365. Department of Scientific and Industrial Research.

Suggate, R. P. (1990). Late pliocene and quaternary glaciations of New Zealand. *Quaternary Science Reviews*, *9*(2-3), 175-197.

Suter, J. R. (2006). Facies models revisited: clastic shelves. *SPECIAL PUBLICATION-SEPM*, *84*, 339.

Swift, DJP, Stanley, DJ & Curray, JR 1971, 'Relict sediments on continental shelves: a reconsideration', *The Journal of Geology*, vol. 79, no. 3, pp. 322-46.

Taylor, S., & McLennan, S. (1985). *The continental crust: Its composition and evolution* (p. 312 p.). Oxford: Blackwells.

Traykovski, P., Geyer, W. R., Irish, J. D., & Lynch, J. F. (2000). The role of wave-induced density-driven fluid mud flows for cross-shelf transport on the Eel River continental shelf. *Continental Shelf Research*, *20*(16), 2113-2140.

Uysal, I., Tarkian, M., Sadiklar, M. B., & \cSen, C. (2007). Platinum-group-element geochemistry and mineralogy of ophiolitic chromitites from the Kop Mountains, northeastern Turkey. *The Canadian Mineralogist*, *45*(2), 355–377. Mineralogical Association of Canada. doi:10.2113/gscanmin.45.2.355

Vry, J., Powell, R., & Williams, J. (2008). Establishing the P–T path for Alpine Schist, Southern Alps near Hokitika, New Zealand. *Journal of Metamorphic Geology*, *26*(1), 81–97. Wiley Online Library. doi:10.1111/j.1525-1314.2007.00746.x

Walling, D. E., & Fang, D. (2003). Recent trends in the suspended sediment loads of the world's rivers. *Global and Planetary Change*, *39*(1-2), 111-126. doi:10.1016/S0921-8181(03)00020-1

Walsh, J. P., & Nittrouer, C. A. (2003). Contrasting styles of off-shelf sediment accumulation in New Guinea. *Marine Geology*, *196*(3-4), 105-125.

Walsh, J. P., & Nittrouer, C. A. (2009). Understanding fine-grained river-sediment dispersal on continental margins. *Marine Geology*, *263*(1-4), 34-45.

Winter, J. D. (2001). *An Introduction to Igneous and Metamorphic petrology*. New Jersey: Prentice Hall.

Youngson, J. (2006). *Placer Gold Deposits on the Westland Continental Shelf: An introdution to Onshore, Geology, Mineralisation and previous offshore investigations. - Unpublished Mineral Report MR4329. Offshore (Conroe, TX).*

APPENDIX

APPENDIX A: SAMPLE INFORMATION AND LOCATIONS

A1: SWCM Locality maps

A2: Shelf and canyon surface locality infromation

A3: Beach and river sample locality infromation

A4: Canyon core information

A5: Sample treatments

Appendix A1: Detailed locality maps of river and beaches discussed in this thesis.

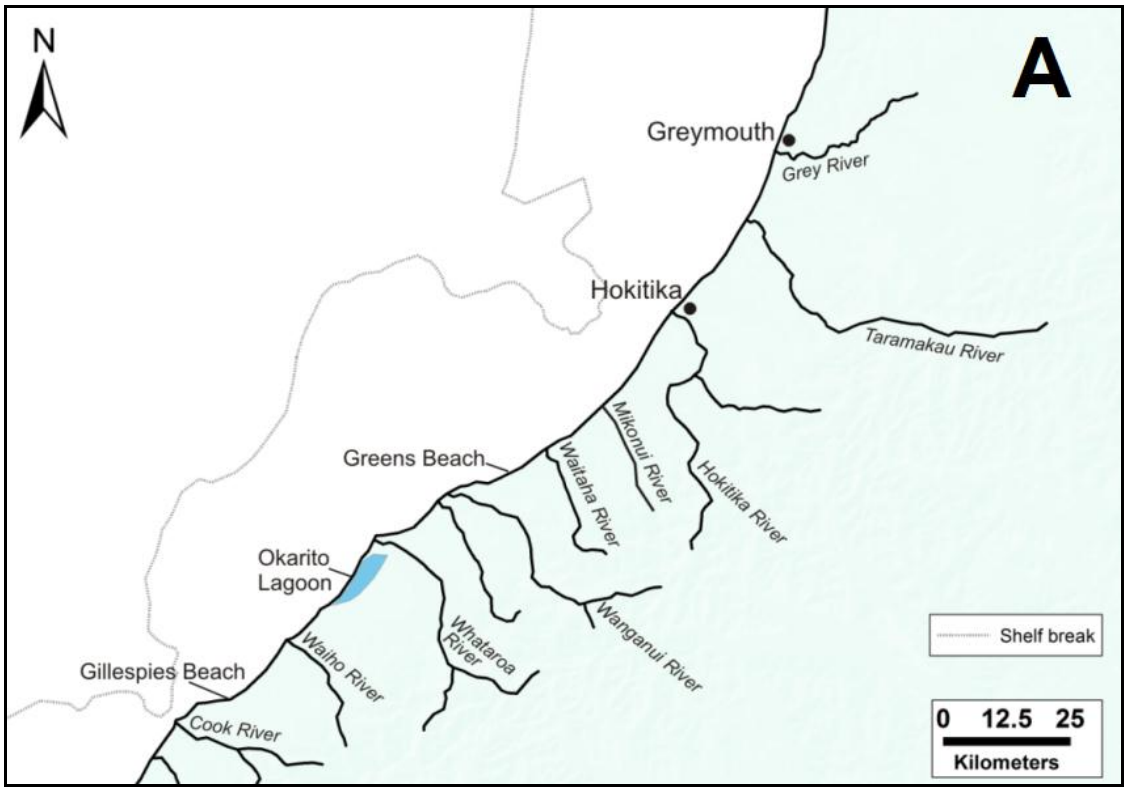

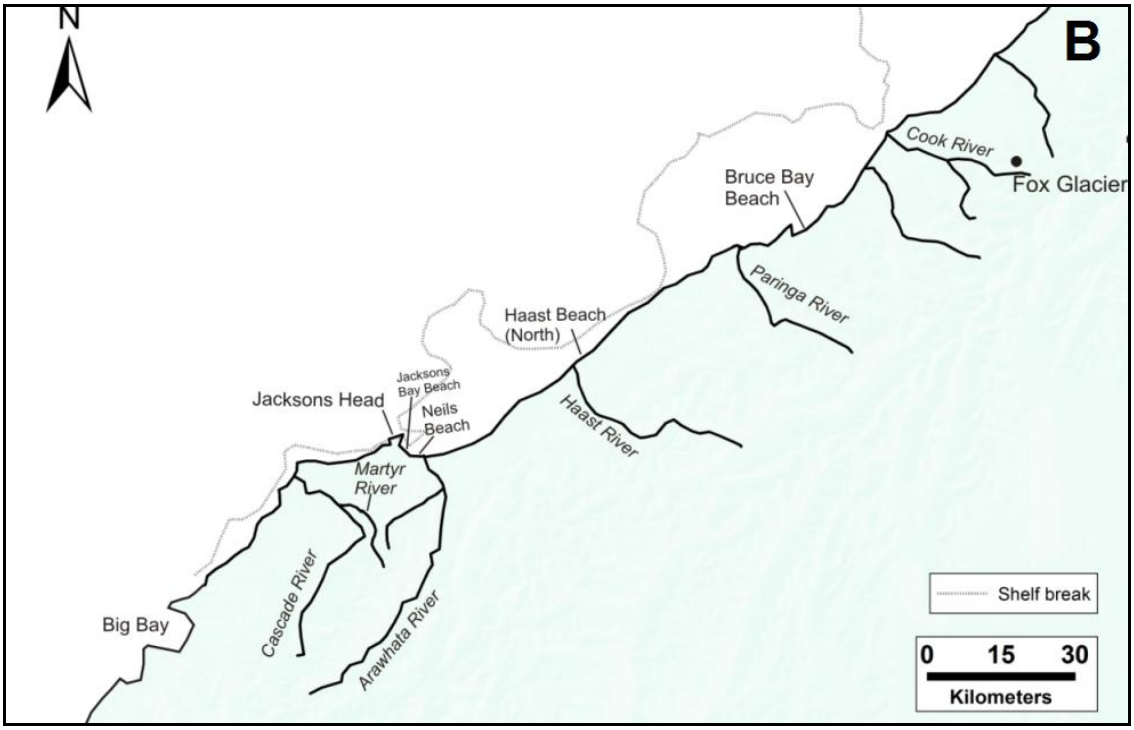

Appendix A2: Location, depth and environment of shelf and canyon surface sediment samples. HCH = Hokitika Canyon Head, CCH= Cook Canyon Head.

Station No.	Lat	Long	Depth	Transect	Environment
H843	-42.448	171.175	15	A	Inner shelf
H838	-42.383	171.032	99	A	Middle shelf
H837	-42.372	171.000	119	A	Middle shelf
H833	-42.297	170.828	207	A	Outer shelf
H845	-42.707	170.890	44	B	Inner shelf
H844	-42.712	170.910	30	B	Inner shelf
H848	-42.678	170.833	94	B	HCH- North rim
H850	-42.658	170.793	126	B	HCH- North rim
H851	-42.622	170.753	182	B	HCH- North rim
H852	-42.603	170.683	198	B	HCH- North rim
B469	-42.65	170.6933	188	B	HCH- North rim
R208	-42.598	170.553	450	B	HCH- South rim
P668	-42.6983	170.47	105	-	HCH- South rim
C905	-42.665	170.5483	241	-	HCH- South rim
H854	-42.953	170.532	17	C	Inner shelf
H855	-42.940	170.505	21	C	Inner shelf
H858	-42.887	170.447	45	C	Inner shelf
H862	-42.817	170.343	107	C	Middle shelf
H864	-42.762	170.270	137	C	Middle shelf
H865	-42.718	170.218	153	C	Outer shelf
S368	-42.9517	170.1717	133	C - D	Middle shelf
P663	-43.015	170.315	49	C - D	Inner shelf
H874	-43.088	170.212	29	D	Inner shelf
H873	-43.085	170.185	45	D	Inner shelf
H867	-42.988	169.983	173	D	Outer shelf
H866	-42.957	169.920	312	D	Upper slope
H876	-43.365	169.897	21	E	Inner shelf
H877	-43.353	169.897	60	E	Middle shelf
H878	-43.345	169.853	86	E	Middle shelf
H879	-43.333	169.838	116	E	Middle shelf
H882	-43.292	169.817	186	E	CCH
H884	-43.542	169.600	20	F	Inner shelf
H885	-43.532	169.577	29	F	Inner shelf
H888	-43.505	169.513	62	F	Middle shelf
H890	-43.475	169.460	98	F	Middle shelf
H891	-43.455	169.417	118	F	Middle shelf
H893	-43.413	169.337	256	F	CCH
H894	-43.9467	168.7933	14	Haast - Cascade shelves	Inner shelf
H898	-43.9	168.7317	41	Haast - Cascade shelves	Inner shelf
H900	-43.7667	169.1167	28	Haast - Cascade shelves	Inner shelf
H902	-43.72	169.0767	280	Haast - Cascade shelves	Upper slope
C901	-43.6667	169.23	99	Haast - Cascade shelves	Middle shelf
B474	-43.9917	168.5	28	Haast - Cascade shelves	Inner shelf
B622	-43.9917	168.4083	68	Haast - Cascade shelves	Middle shelf
C898	-43.99	168.36	95	Haast - Cascade shelves	Middle shelf
E786	-44	168.2583	454	Haast - Cascade shelves	Upper slope

Appendix A3: Location of SWCM river and beach sediment samples.

Station No.	Location	Lat	Long	Comments
AA2	Hokitika Beach	-42.7184	170.9573	200-300 m Nth of Hokitika river mouth
AB2	Hokitika River	-42.7258	170.9722	North bank
AF3	Mokonui Beach	-42.9165	170.74	
AG2	Waitaha Beach	-42.9548	170.6651	500 m Nth of river mouth
AH3	Waitaha River	-42.9775	170.6832	
AK2	Whataroa River	-43.2036	170.4037	
AN1	Gillespies Beach	-43.4075	169.8275	
AO2	Cook River	-43.4621	169.9089	
AQ2	Bruce Bay Beach	-43.5948	169.6036	
AR2	Paringa River	-43.7127	169.4947	
AT1	Haast River	-43.8543	169.0544	
AU3	Haast Beach	-43.8221	169.062	~ 2km Nth of river mouth
01a	Hannahs Clearing beach	-43.923	168.873	
02b	Martyr River	-44.104	168.532	
03a	Arawhata River	-44.032	168.712	
04b	Neils Beach	-43.995	168.666	200-300 Sth of Arawhata river mouth
05a	Jacksons Bay Beach	-43.976	168.616	

Appendix A4: South Westland canyon core information. Cores collected on NIWA's research vessel Tangaroa during the Westcoast Canyons voyage TAN0513. Details of core collection and locations form NIWZ voyage report TAN0513 – 2005.

Station ID	Latitude	Longitude	Depth	Core Method	Date collected	Location	Core Length Recovered	General Description	Sample Depth intervals
TAN0513-15	-42.30	169.88	956	Kasten	13/10/2005	Hokitika Canyon North Levee	2.91 m	Hemipelagic (mica/foram) mud	5-6cm, 30-35cm, 55-60cm, 85-90cm, 250-255cm
TAN0513-19	-42.11	168.87	1253	Kasten	15/10/2005	Hokitika Canyon North Levee	2.83 m	Gray sandy silty muds and sandy foraminiferal muds	5-6cm, 30-35cm, 70-75cm, 85-90cm, 250-255cm
TAN0513-21	-42.35	167.93	1806	Kasten	17/10/2005	10km west of Hoki-Cook Canyon Junction	2.1 m	Gray to olive gray sandy muds and silts	4-5cm, 24-25cm, 45-50cm, 60-65cm, 190-195cm
TAN0513-29	-42.48	167.05	2923	Kasten	20/10/2005	Hokitika Canyon North Levee	3.06 m	Light gray to gray sandy silts	20-21cm, 140-145cm
TAN0513-37	-42.62	168.42	1505	Kasten	23/10/2005	Cook canyon North levee	3.62 m	Light gray to gray sandy silts	20-21cm, 95-100cm
TAN0712-17	-43.58	168.22	1375	Kasten	24/10/2005	Haast Canyon	?	Light gray to gray sandy silts	40-45cm, 120-125 cm

Appendix A5 SAMPLE TREATMENTS

Station No.	Transect - Environment	Depth	Grain size analysis	> 63µm Binocular inspection	Thin Section Description - Bulk sample	Point Count (>63 µm)	Carbonate analysis	XRF	XRD	Heavy Mineral Seperation	Microprobe (Detrital magnetites)
H843	A	15	1	1	1	1	1	1	1	1	1
H837	A	119	1	1			1	1			
H833	A	99	1	1	1		1	1	1	1	
H838	A	207	1	1	Too fine	1	1	1		1	
H844	B	30	1	1	1	1	1	1	1	1	1
H845	B	40	1	1			1	1			
H848	HCH	94	1	1		1	1	1	1	1	
H850	HCH	126	1	1		1	1	1	1	1	1
H851	HCH	182	1	1	1	1	1	1		1	
B469	HCH	188	1	1	1	1	1	1		1	1
H852	HCH	198	1	1	1	1	1	1	1	1	1
R208	HCH	450	1	1	Too fine	1	1	1	1	1	
P668	HCH	105	1	1	Too fine		1	1	1	1	
C905	HCH	241	1	1	Too fine	1	1	1	1	1	1
H854	C	17	1	1			1	1	1		
H855	C	21	1	1	1	1	1	1		1	
H858	C	45	1	1			1	1		1	
H862	C	107	1	1	1 (sand fraction only)	1	1	1	1	1	
H864	C	137	1	1			1	1			
H865	C	153	1	1	1 (sand fraction only)		1	1	1	1	1
P663	C_D	49	1	1	1	1	1	1		1	
S368	C_D	133	1	1			1	1		1	
H874	D	29	1	1			1	1	1	1	1
H873	D	45	1	1	1	1	1	1		insufficient sample	
H867	D	173	1	1	Too fine	1	1	1		1	
H866	D	312	1	1	Too fine		1	1	1	1	
H876	E	21	1	1	1	1	1	1	1	1	1
H877	E	60	1	1	Too fine		1	1			
H878	E	86	1	1	Too fine		1	1		insufficient sample	
H879	E	116	1	1	Too fine	1	1	1	1	1	1

Station No.	Transect - Environment	Depth	Grain size analysis	> 63µm Binocular inspection	Thin Section Description - Bulk sample	Point Count (>63 µm)	Carbonate analysis	XRF	XRD	Heavy Mineral Seperation	Microprobe (Detrital magnetites)
H882	CCH	186	1	1	1	1	1	1	1	1	1
H884	F	20	1	1	1	1	1	1	1	1	1
H885	F	29	1	1			1	1	1	insufficient sample	
H888	F	62	1	1	1	1	1	1		1	1
H890	F	98	1	1	Too fine		1	1	1	insufficient sample	
H891	F	118	1	1			1	1		1	
H893	CCH	256	1	1	1	1	1	1	1	1	1
H894	Haast Shelf	14	1	1			1	1	1	1	1
H898	Haast Shelf	41	1	1			1	1		1	1
H900	Haast Shelf	28	1	1			1	1		1	1
H902	Haast Shelf	280	1	1			1	1	1		
C901	Haast Shelf	99	1	1			1	1	1	1	1
B474	Cascade Shelf	28	1	1			1	1	1	1	1
B622	Cascade Shelf	68	1	1			1	1		1	
C898	Cascade Shelf	95	1	1			1	1	1	1	1
E786	Cascade Shelf	454	1	1			1	1	1		
KASTEN CORES											
TAN0513-15 a	Hokitika Canyon		1				1	insufficient	1		
TAN0513-15 b	Hokitika Canyon		1				error	1	1		
TAN0513-15 c	Hokitika Canyon		1				1	1	1		
TAN0513-15 d	Hokitika Canyon		1				1	1	1		
TAN0513-15 e	Hokitika Canyon		1				1	1	1		
TAN0513-19a	Hokitika Canyon		1				1	insufficient			
TAN0513-19b	Hokitika Canyon		1				1	1	1		
TAN0513-19c	Hokitika Canyon		1				error	1	1		
TAN0513-19d	Hokitika Canyon		1				1	1	1		
TAN0513-19e	Hokitika Canyon		1				1	1	1		
TAN0513-21a	Hokitika Canyon		1				1		1		
TAN0513-21b	Hokitika Canyon		1				1		1		
TAN0513-21c	Hokitika Canyon		1				1	1	1		
TAN0513-21d	Hokitika Canyon		1				1	1	1		
TAN0513-21e	Hokitika Canyon		1				1	1	1		

Station No.	Transect - Environment	Depth	Grain size analysis	> 63µm Binocular inspection	Thin Section Description - Bulk sample	Point Count (>63 µm)	Carbonate analysis	XRF	XRD	Heavy Mineral Seperation	Microprobe (Detrital magnetites)
TAN0712-17a	Haast Canyon						1	1	1		
TAN0712-17b	Haast Canyon						1	1	1		
BEACH/RIVER SAMPLES											
AA 2	Hokitika Beach				1 - (2-4 phi only)	1 - (2-4 phi only)		1	1	1	1
AB 2	Hokitika River				1 - (2-4 phi only)	1 - (2-4 phi only)		1	1	1	1
AF 3	Mokonui Beach							1			
AG 2	Waitaha Beach (Nth)							1		1	
AH 3	Waitaha River							1	1	1	1
AK 2	Whataroa River				1 - (2-4 phi only)	1 - (2-4 phi only)		1	1	1	
AN 1	Gillespies Beach				1 - (1.5 - 4 phi only)	1 - (1.5 - 4 phi only)		1	1	1	1
AO 2	Cook River							1			
AQ 2	Bruce Bay Beach				1 - (1.5 - 4 phi only)	1 - (1.5 - 4 phi only)		1	1	1	
AR 2	Paringa River							1			
AT 1	Haast River				1 - (2-4 phi only)	1 - (2-4 phi only)		1	1	1	1
AU 3	Haast Beach (Nth)							1	1	1	1
01a	Hannahs Clearing (beach)							1			
02b	Martyr River				1 - (1.5 - 4 phi only)	1 - (1.5 - 4 phi only)		1	1	1	1
03a	Arawhata River				1 - (2-4 phi only)	1 - (2-4 phi only)		1	1	1	1
04b	Neils Beach (Sth beach)				1 - (2-4 phi only)	1 - (2-4 phi only)		1	1	1	1
05a	Jacksons Bay Beach				1 - (2-4 phi only)	1 - (2-4 phi only)		1	1		

APPENDIX B: GRAIN SIZE ANALYSIS

B1: Laser sizing results for SWCM marine surface sediments

B2: Laser sizing results for Hokitika Canyon core sediments

B3: Coarse fraction sieving analysis (>1600μm)

Appendix B1 – Laser sizing results for SWCM surface sediments. Textural group is after Folk (1968). * Gravel, sand and mud percentages have been normalized to include gravel content determined from sieving.

Sample ID	Transect	Textural Group	Mean Grain size (μm)	Mean Grain Size	Sorting (μm)	Sorting Term	Skew (μm)	Gravel* %	Sand* %	Mud* %	Very Coarse Sand %	Coarse Sand %	Medium Sand %	Fine Sand %	Very Fine Sand %	Silt %	Clay % (<4μm)
H843	A	Muddy Sand	120.5	Very Fine Sand	1.8	Moderately Sorted	-0.3	0.0	84.9	15.1	0.0	0.0	3.5	51.8	29.6	14.5	0.6
H838	A	Sandy Mud	23.6	Coarse Silt	3.6	Poorly Sorted	0.0	0.0	25.7	74.3	0.0	0.0	0.0	8.5	17.2	65.1	9.2
H837	A	Sandy Mud	22.8	Coarse Silt	3.6	Poorly Sorted	0.1	0.0	26.3	73.7	0.0	0.0	0.0	7.9	18.4	64.6	9.2
H833	A	Sandy Mud	42.9	Very Coarse Silt	3.1	Poorly Sorted	-0.5	0.0	49.1	50.9	0.0	0.0	0.0	12.8	36.3	45.8	5.1
H844	B	Muddy Sand	103.1	Very Fine Sand	1.8	Moderately Sorted	-0.3	0.0	81.9	18.1	0.0	0.0	0.2	40.3	41.4	17.2	0.8
H845	B	Muddy Sand	71.7	Very Fine Sand	2.5	Poorly Sorted	-0.5	0.0	65.6	34.4	0.0	0.0	0.3	30.3	35.0	32.4	2.0
H848	B/HCH	Gravelly Mud	48.2	Very Coarse Silt	4.9	Very Poorly Sorted	0.0	9.9	43.1	47.0	2.6	5.1	3.0	20.8	11.7	42.0	4.9
H850	B/HCH	Muddy Sand	74.2	Very Fine Sand	3.2	Poorly Sorted	-0.6	0.0	69.3	30.7	0.0	0.0	3.1	45.6	20.6	27.3	3.5
H851	B/HCH	Slightly gravelly Muddy Sand	67.6	Very Fine Sand	4.2	Very Poorly Sorted	-0.6	0.2	65.4	34.4	0.0	2.2	8.9	41.7	12.6	28.5	5.8
B469	B/HCH	Muddy Sand	109.3	Very Fine Sand	2.5	Poorly Sorted	-0.6	0.0	79.8	20.2	0.0	0.0	6.7	53.7	19.5	17.8	2.4
H852	B/HCH	Slightly gravelly Muddy Sand	169.6	Fine Sand	2.7	Poorly Sorted	-0.5	2.8	82.7	14.4	0.4	2.6	32.0	34.9	12.8	12.1	2.3
R208	HCH	Muddy Sand	47.7	Very Coarse Silt	3.1	Poorly Sorted	-0.4	0.0	50.4	49.6	0.0	0.0	0.1	18.2	32.1	45.0	4.7
P668	HCH	Sandy Mud	24.7	Coarse Silt	2.4	Poorly Sorted	-0.2	0.0	12.8	87.2	0.0	0.0	0.0	1.1	11.7	82.7	4.6
C905	HCH	Sandy Mud	20.7	Coarse Silt	2.8	Poorly Sorted	-0.1	0.0	13.1	86.9	0.0	0.0	0.0	2.6	10.5	79.7	7.3

Sample ID	Transect	Textural Group	Mean Grain size (μm)	Mean Grain Size	Sorting (μm)	Sorting Term	Skew (μm)	Gravel* %	Sand* %	Mud* %	Very Coarse Sand %	Coarse Sand %	Medium Sand %	Fine Sand %	Very Fine Sand %	Silt %	Clay % (<4μm)
H854	C	Muddy Sand	104.6	Very Fine Sand	1.6	Moderately Well Sorted	-0.2	0.0	86.5	13.5	0.0	0.0	0.0	36.3	50.2	12.8	0.7
H855	C	Muddy Sand	95.2	Very Fine Sand	1.6	Moderately Sorted	-0.3	0.0	82.1	17.9	0.0	0.0	0.0	28.4	53.7	17.1	0.8
H858	C	Muddy Sand	59.2	Very Coarse Silt	2.7	Poorly Sorted	-0.6	0.0	62.2	37.8	0.0	0.0	0.0	19.9	42.3	34.9	2.9
H862	C	Sandy Mud	22.3	Coarse Silt	2.8	Poorly Sorted	-0.1	0.0	15.4	84.6	0.0	0.0	0.0	2.5	12.9	77.7	6.9
H864	C	Slightly gravelly Sandy Mud	24.0	Coarse Silt	2.6	Poorly Sorted	-0.1	3.1	14.6	82.3	0.0	0.0	0.0	1.9	12.7	76.8	5.5
H865	C	Sandy Mud	24.8	Coarse Silt	2.7	Poorly Sorted	-0.2	0.0	16.8	83.2	0.0	0.0	0.0	2.7	14.2	77.0	6.2
P663	C_D	Muddy Sand	62.5	Very Coarse Silt	2.8	Poorly Sorted	-0.6	0.0	60.4	39.6	0.0	0.0	0.0	29.6	30.8	36.6	3.0
S368	C_D	Sandy Mud	21.0	Coarse Silt	3.1	Poorly Sorted	0.0	0.0	17.9	82.1	0.0	0.0	0.0	4.5	13.5	73.6	8.5
H874	D	Muddy Sand	91.1	Very Fine Sand	2.0	Moderately Sorted	-0.4	0.0	73.5	26.5	0.0	0.0	0.0	37.9	35.6	25.4	1.1
H873	D	Slightly gravelly Muddy Sand	66.9	Very Fine Sand	2.8	Poorly Sorted	-0.6	0.5	63.5	36.0	0.0	0.0	0.0	34.2	29.5	33.4	2.8
H867	D	Sandy Mud	34.4	Very Coarse Silt	3.3	Poorly Sorted	-0.2	0.0	36.6	63.4	0.0	0.0	0.0	12.5	24.1	57.6	5.7
H866	D	Sandy Mud	27.1	Coarse Silt	2.6	Poorly Sorted	-0.2	0.0	17.2	82.8	0.0	0.0	0.0	2.4	14.8	77.8	5.0
H876	E	Sand	127.1	Fine Sand	1.4	Well Sorted	-0.1	0.0	96.0	4.0	0.0	0.0	0.0	54.3	41.6	3.7	0.3
H877	E	Sandy Mud	19.1	Coarse Silt	3.0	Poorly Sorted	0.0	0.0	14.1	85.9	0.0	0.0	0.0	5.1	9.1	77.1	8.8
H878	E	Mud	16.0	Coarse Silt	2.7	Poorly Sorted	-0.1	0.0	7.0	93.0	0.0	0.0	0.0	0.5	6.5	83.1	9.9
H879	E	Sandy Mud	20.3	Coarse Silt	3.2	Poorly Sorted	0.0	0.0	17.0	83.0	0.0	0.0	0.0	5.6	11.5	73.9	9.1

Sample ID	Transect	Textural Group	Mean Grain size (μm)	Mean Grain Size	Sorting (μm)	Sorting Term	Skew (μm)	Gravel* %	Sand* %	Mud* %	Very Coarse Sand %	Coarse Sand %	Medium Sand %	Fine Sand %	Very Fine Sand %	Silt %	Clay % (<4μm)
H882	CCH	Slightly gravelly Muddy Sand	100.5	Very Fine Sand	4.1	Very Poorly Sorted	-0.4	2.4	72.7	24.9	0.0	6.6	17.2	34.8	14.1	21.6	3.3
H884	F	Sand	129.8	Fine Sand	1.4	Well Sorted	-0.2	0.0	95.2	4.8	0.0	0.0	0.0	57.9	37.3	4.3	0.5
H885	F	Muddy Sand	106.5	Very Fine Sand	1.6	Moderately Well Sorted	-0.3	0.0	86.1	13.9	0.0	0.0	0.0	40.1	46.0	13.2	0.7
H888	F	Sandy Mud	41.7	Very Coarse Silt	2.7	Poorly Sorted	-0.3	0.0	41.1	58.9	0.0	0.0	0.0	8.6	32.5	54.9	4.0
H890	F	Sandy Mud	21.9	Coarse Silt	2.7	Poorly Sorted	-0.2	0.0	12.8	87.2	0.0	0.0	0.0	1.2	11.7	79.6	7.5
H891	F	Sandy Mud	21.8	Coarse Silt	2.6	Poorly Sorted	-0.2	0.0	11.6	88.4	0.0	0.0	0.0	0.7	10.9	81.7	6.7
H893	CCH	Muddy Sand	91.2	Very Fine Sand	6.3	Very Poorly Sorted	-0.1	0.0	56.9	43.1	6.0	16.0	6.4	14.9	13.5	38.7	4.4
H894	Haast	Sand	136.4	Fine Sand	1.4	Moderately Well Sorted	-0.3	0.0	94.1	5.9	0.0	0.0	0.4	64.1	29.6	5.6	0.4
H900	Haast	Sand	148.4	Fine Sand	1.4	Well Sorted	-0.2	0.0	96.0	4.0	0.0	0.0	0.6	73.3	22.0	3.6	0.4
H898	Haast	Slightly gravelly Sand	120.9	Very Fine Sand	1.5	Moderately Well Sorted	-0.3	2.2	89.7	8.2	0.0	0.0	0.0	50.4	41.3	7.6	0.8
C901	Haast	Sandy Mud	20.6	Coarse Silt	2.9	Poorly Sorted	-0.2	0.0	14.7	85.3	0.0	0.0	0.0	1.1	13.6	76.3	9.0
H902	Haast _Jackson	Sandy Mud	18.8	Coarse Silt	2.7	Poorly Sorted	-0.1	0.0	10.4	89.6	0.0	0.0	0.0	2.0	8.4	81.6	8.0
B474	Cascade	Muddy Sand	93.3	Very Fine Sand	1.7	Moderately Sorted	-0.2	0.0	77.8	22.2	0.0	0.0	0.0	30.2	47.6	21.6	0.7
C898	Cascade	Slightly gravelly Muddy Sand	46.4	Very Coarse Silt	2.5	Poorly Sorted	-0.3	3.0	40.7	56.3	0.0	0.0	0.0	8.1	32.7	53.5	2.7
B622	Cascade	Slightly gravelly Muddy Sand	62.9	Very Fine Sand	2.2	Poorly Sorted	-0.4	0.4	59.3	40.3	0.0	0.0	0.0	12.6	46.7	38.2	2.1
E786	Cascade	Sandy Mud	23.8	Coarse Silt	2.7	Poorly Sorted	-0.2	0.0	15.8	84.2	0.0	0.0	0.0	1.0	14.8	78.3	5.9

Appendix B2: Laser sizing results for Hokitika Canyon core sediments. Textural name is after Folk (1968).

Core ID	Core sample depth (cm)	Textural name	MEAN (µm)	SORTING (µm)	SKEWNESS (µm)	SORTING TERM	% GRAVEL:	% SAND:	% MUD:	% Silt	% Clays
TAN0513 - 15 a	5.5	Sandy Mud	14.68	3.492	0.029	Poorly Sorted	0.00	13.02	86.98	70.48	16.50
TAN0513 - 15 b	32.5	Sandy Mud	10.68	3.634	0.125	Poorly Sorted	0.00	10.62	89.38	65.78	23.60
TAN0513 - 15 c	57.5	Sandy Mud	10.69	4.023	0.148	Very Poorly Sorted	0.00	12.47	87.53	61.73	25.80
TAN0513 - 15 d	87.5	Mud	9.053	3.272	0.055	Poorly Sorted	0.00	5.80	94.20	67.90	26.30
TAN0513 - 15 e	252.5	Mud	8.052	2.848	-0.006	Poorly Sorted	0.00	2.33	97.67	71.17	26.50
TAN0513 - 19 a	5.5	Sandy Mud	11.77	4.583	0.335	Very Poorly Sorted	0.00	17.27	82.73	56.26	26.47
TAN0513 - 19 b	32.5	Sandy Mud	13.87	5.597	0.324	Very Poorly Sorted	0.00	22.69	77.31	50.41	26.90
TAN0513 - 19 c	72.5	Sandy Mud	14.68	4.854	0.236	Very Poorly Sorted	0.00	21.25	78.75	56.85	21.90
TAN0513 - 19 d	87.5	Sandy Mud	11.91	4.635	0.228	Very Poorly Sorted	0.00	17.41	82.59	56.01	26.58
TAN0513 - 19 e	252.5	Sandy Mud	8.928	4.685	0.310	Very Poorly Sorted	0.00	14.51	85.49	49.29	36.20
TAN0513 - 21 a	4.5	Sandy Mud	10.10	3.718	0.218	Poorly Sorted	0.00	10.53	89.47	62.34	27.13
TAN0513 - 21 b	24.5	Sandy Mud	12.26	4.374	0.213	Very Poorly Sorted	0.00	17.54	82.46	56.96	25.50
TAN0513 - 21 c	47.5	Sandy Mud	13.19	4.161	0.140	Very Poorly Sorted	0.00	16.78	83.22	61.25	21.97
TAN0513 - 21 d	62.5	Sandy Mud	11.29	4.212	0.148	Very Poorly Sorted	0.00	14.75	85.25	58.70	26.55
TAN0513 - 21 e	192.5	Sandy Mud	17.81	6.013	0.184	Very Poorly Sorted	0.00	28.75	71.25	48.48	22.77

Appendix B3: Weight percent of grains > 1600 µm and > 2000 µm in SWCM marine surface samples. Determined by wet sieving. 'Trace' = < 0.2 % wt.

Sample	*Location*	*1.6 - 2mm (% wt.)*	*>2mm (% wt.)*	*Dominant clast type*
H882	*CCH (Transect E)*	*-*	*2.44*	*Terrigenous or authigenic?*
H864	*Central (Transect C)*	*-*	*3.22*	*Bioclast*
H873	*Central (Transect D)*	*Trace*	*0.50*	*Bioclast*
H898	*Haast - Jackson B*	*Trace*	*2.20*	*Bioclast*
B474	*Haast - Jackson B*	*-*	*Trace*	*Bioclast*
B622	*Haast - Jackson B*	*Trace*	*0.40*	*Bioclast*
C898	*Haast - Jackson B*	*Trace*	*3.10*	*Bioclast*
H851	*HCH (Transect B)*	*Trace*	*0.25*	*Terrigenous*
H852	*HCH (Transect B)*	*0.60*	*2.88*	*Terrigenous (bored shells too!!)*
B469	*HCH (Transect B)*	*Trace*	*-*	*Terrigenous*
H848	*HCH (Transect B)*	*1.80*	*10.90*	*Terrigenous*
H893	*South (Transect F)*	*Trace*	*-*	*Bioclast*

APPENDIX C: MINERALOGY AND SKELETAL COMPOSITION

C1: Thin section preparation

C2: Abbreviations used in petrographic descriptions

C3: Petrographic descriptions of bulk sediment thin sections

C4: Point count data from the sand fraction

C5: Foraminifera in SWCM shelf and canyon head sand fractions

C6: Skeletal grains and glaucony in SWCM shelf and Canyon head sediments

C7: X-ray Diffraction (XRD) method

C8: Bulk XRD results for SWCM shelf, canyon head, and terrestrial samples

C9: Bulk XRD resultsHokitika Canyon kasten core samples

C10: Heavy mineral separation method

C11: Heavy mineral and magnetic fraction seperation results

Appendix C1: Thin section preparation:

Thin section preparation

Shelf and canyon sediments for bulk thin sections were split from the main sample, ~5 -10g of this split was placed into 25mm diametre plastic moulds. These moulds were lined with Vaseline® to allow easier removal of the epoxy resin once set. Epoxy resin was added to the moulds and allowed to set for 24 hrs. The epoxy blocks were then glued to thin section slides and then cut to the required thickness.

Shelf and canyon sediments for point counting were sieved with a 63 µm mesh sieve. The beach and river samples were sieved with 63 µm and 2000 µm mesh sieves to isolate the coarse to very fine sand fraction to allow comparisons with the shelf and canyon sand fraction. Thin sections were made following the same technique as above for the bulk thin sections. Point counting was conducted on a Prior James Swift point counter, with 300 grains per slide counted. Thin sections for point counting were stained for plagioclase and alkali feldspar before cover slips were glued onto the thin section.

Staining methods:

Thin sections to be point counted were stained for plagioclase and alkali feldspars with Rhodizonic acid and sodium cobalt nitrite respectively following the methods from Lewis & McConchie, (1994). The dyes bond to calcium and potassium respectively, staining alkali feldspar yellow and plagioclase red. Only half the thin section was stained by wrapping masking tape across one half of the section. This was most useful for distinguishing untwinned plagioclase and quartz.

Appendix C2: Abbreviations used in petrographic descriptions

Sorting = S	**Rounding = R**
1 - Very poorly sorted	1 – Angular
2 – Poorly sorted	2- Sub angular
3 – Moderately sorted	3- Sub rounded
4 - Well sorted	4- Rounded
5 – Very well sorted	5- Well rounded

Mode = modal grain size (µm) (measured on long axis)
Max = maximum grain size (µm)

Plag = feldspars dominantly plagioclase
Poly = Polysynthetic twinning
Poik = Poikilitic texture
Part alt = Partially altered
Alt = Altered
V. alt = Very altered
Seric = sericitised
Fe = Fe stained
Lim = Limonite
Frac = fractured
Q.Und= undulose extinction most common
Q.PolyCr=polycrystalline most common
Q.Str =Straight extinction most common

Lmet = Metamorphic lithics
Lplut= Plutonic lithics
Lsed= Sedimentary lithics
Fol = Foliated

Bio undiff = undifferentiated bioclasts
Foraminifera P = Foraminifera dominantly planktic
Foraminifera B = Foraminifera dominantly benthic
Ech = Echinoids
Moll = Molluscs

G.mat = Mature/evolved glaucony pellets (well-rounded and >90% glaucanitised)
G. mix = Mixed pellets of glaucony and remnant mica and quartz
G. nac = Nacent glaconite (early stage gloauconite, irregular boundaries)
G. mld = glaucony mould (replaced Foraminifera etc…)

Appendix C3: Petrographic descriptions of bulk sediment thin sections for SWCM shelf and canyon samples.

Sample ID	Transect	Depth (m)	Textural Name (after Folk 1968)	Quartz	Feldspar	Lithics	Muscovite	Biotite	Amphibole + Pyroxene	Garnet	Fines + epoxy	Glaucony grains	Skeletal Grains	Others	Comments
H843	A	15	Muddy Sand	20%, R=2-3, S=3 Mode 250 µm,	<5%, poly, Alt,	10%, Lmet, R=3-4,	3%	4%, R= 1-2, S=2, Alt,	<1%	-	35%	-	-	Chlorite 2%, Epidote <1%	
H833	A	207	Sandy Mud	20%, R=3, S=2, Mode 150µm,	5 %, poly, Plag	rare	R= 1, S=2, Mode 400µm, 5%	R= 1, S=2, Mode 400µm, 7%	-	-	40%	-	Foraminifera P, 1-2%	Opaques <1%, Chlorite 2%,	Higher mica than inner shelf, mica v. elongate
H844	B	30	Muddy Sand	30%, R=2, S=2, Mode 100µm, 30%	10 %, poly, Plag	6%, fol, Lmet,	2%	3%	<1%	-	35%	-	<1%	Chlorite 1%, Opaques 1% , Zircon <1% , Epidote 1%	Felds alt to clay+calcite+chlorite
H851	B - HCH	182	Slightly gravelly Muddy Sand	25%, R=2-3, S=2, Mode 250µm,	5-10%, R=2, poly, Plag,	5%, Lmet, R=3, Mode 500µm,	2%	1-2%	1%,	<1%, R=4, max 700µm, poik,	40-45%	15%, Grn/brwn, R= 5, S=3, Max 500µm, Lim, G.mat, G.mix, G.mld,	Foraminifera P, 1-2%	Chlorite <1%, Epidote <1%, Olivine Max 100µm <1%, Zircon v. rare.	Glauc rims common on siliclasctic grains
B469	B - HCH	188	Muddy Sand	Mode 250µm, R=4, S=2, Und, 25%	R= 1-2, S=2, Mode 200µm, Plag, alt, rare microcline, 10-15%	R=3-4, Mode 300µm, Lmet, 5%	S=1, 3%	2%	alt to chorite, <1%	<1%	45%	7-10%, R=3-4, S=3, Gmat, Gmix, Lim/frac, Mode 150µm, Max 500µm,	Bio undiff, 1%	Epidote <1%, Opaques <1% Hematite <1%	Glauc rims on siliclasctic grains. Epoxy bubbles problematic
H852	B - HCH	198	Slightly gravelly Muddy Sand	20%, R=2, S=2, Mode 125µm, und,	5-10%, Mode 100µm, Plag,	5% , R=3, Fol, Lmet, Qtz/feld dom.	1%	1%	-	<1%, R=4-5, max 400µm,	35%	30%, R=4, S=3, Gmat, Gmix, Gmld, Lim/frac, Mode 300µm, Max 500µm,	Foraminifera P, Ech, 5%	Epidote <1%, Zircon v. rare, Limonite <1%, opaques <1%	Glauc more deeply Alt/frac than H851
H855	C	21	Muddy Sand	40% max 400µm	5-10% , Part. Alt to sericite/clay	10% , Lmet, rare Lsed	4% , Part. alt to clays	3% , Part. alt to clays	<1%		up to 40%	-	<1%, bio undiff	Epidote 1-2% , Opaques <1% Chlorite 1%,	
P663	C_D	49	Muddy Sand	30%,	5%, poly, plag	5%, dom Lmet	2%, Part. alt	4%, Part. Alt	-	-	up to 50%	-	-	-	Fine grain size = diificult ID's
H873	D	45	Slightly gravelly Muddy Sand	25%	<5%	5-10%	4%	2%	<1%, Part. Alt to clays	-	up to 50%	-	<1%, bio undiff	Epidote <1%	Fine grain size = diificult ID's
H876	E	21	Sand	25%	3%, poly, plag	5%,m Lmet	2%	2%	<1%	<1%	30-40%	-	<1%, bio undiff	Epidote 2-3% , Opaques 10-15%	**Heavy mineral rich,** esp opaques
H882	E	186	Slightly gravelly Muddy Sand	25-30% , mode 150µm, max 300µm, S=2-3, R=2-3,	2-3%, plag, poly	<5% , Lmet, max 600µm	1-2%	1%	<1%		40%	10-15%. Mode 300-400µm, max 700µm, S=3, R=4-5, pale green, Lim fractures common	<1% , bio undiff, max=700µm	Epidote <1% , Opaques 1%	G.mat common, Lim rims, G.mix w Qtz/feld/mica core, less common, G.mld rare.
H884	F	20	Sand	30-35%	2-3%, poly, plag	5%	1%	1%	1-2%	<1%	40%	-	-	Epidote <1% , Opaques 1-2%, unknowns 1%	heavy minerals relatively common
H888	F	62	Sandy Mud	25%	<5%, poly	<5%, very fine grained	8%, max 500µm, S=2 , R=1-2, highly tabular	5%, S=2 , R=1-2, highly tabular	<1%	-	45-50%	-	-	Opaques <1%,	Grains very fine = difficult ID's, Mica rich, mica more tablar than inner shelf mica.
H893	F	256	Muddy Sand	20% Q.und, rare Q.poly, mode = 200-300 µm, up to 600 µm	<5% , poly	15-20%, S=2-3, R=4 , max 2.5mm, Lmet, rare Lsed, very rare serpentenised lithic seen	3%	2% , max 700µm	<1%	-	35-40%	-	10%, Foraminifera (5%), planktic>>benthic, Ech (1%), Ech spines, rare worm, Moll, Lim common		Lmet rich, schist to phyllite common. serpentenised lithic

Appendix C3: Petrographic descriptions the sand fraction of river and beach samples from the South Westland region. Abbreviations detailed in Appendix C2.

Location	Quartz	Feldspar	Lithics	Muscovite	Biotite	Amphibole + Pyroxene	Garnet	Fines + epoxy	Others	Comments
Hokitika Beach (north)	10-15 %, Qund, Qpoly, S=3, R=2/3	<1%, poly	40-45%, S=3, R=3/4, Lmet dominant, rare Lplut.	1%	1-2%, Part alt to chlorite	<1%	2% , poik,	45-50%	Chlorite <<1%	Lmet mainly quartzofeldspathic phyllite & slates
Hokitika River	20-25%, S=2, R=2/3	<5%, plag, poly	30%	2-3%	3-4%	<1%	<1%		Chlorite <<1% , Opaques <1%, Epidote <1%	rare serpentinised Lmet up to 0.4mm
Whataroa River	25%, R=2/3,	5%	20%, mainly quartzofelds schists to slates	2%, R=1	1-2%, R=1/2	<1%	-	40%	Epidote <1%, Opaques <1%,	Poor thin section quality
Gillespies Beach	30%, dominantly Qund	<5%	20%, S=3, R=4, quartzofelds	<1%	<%	<1%, Amphibole	5-10%, poik, colourless, R=3/4,	45%	Epidote <1%, Opaques 2-3%, Hematite <1%	
Bruce Bay Beach	25%, R=3, Qpoly + Qund>Qstr	<5%, poly, R=2 , Part alt to sericite	25%, dominatly quartzofelds schist/phyllite	3%	1%	<1%, R=3	1-2%, poik, R=3-4	45%	Hematite <1%	rare serpentinised Lmet , much less garnet than Gillespies beach (AN1)
Haast River	15%	1%, Qstr very rare	35%, R=2/3, quartzofelds Lmet dominant	1%, R=1	<1%	-	-	40%	Chlorite <1% , Opaques <1%, Epidote <1%	
Martyr River	10-15%	<3%, poly	35%, Lmet dominantly quartzofelds serpentinised Lmet com	1%	<1%	1%, Pyrox>Amph	-	40%	Chlorite <% , Opaques <1%, Epidote <1%, Olivine <1%,	rare Limestone Lsed, Olivine commonly alt to Fe oxide
Arawhata River	25-30%, Qpoly common	<5%	10-15%, Lmet dominant, Schist>phyllite	5%,	3%, Part alt to chlorite	-	-	45%	Chlorite <% , Opaques <1%, Epidote 1%, Olivine <<1%	Rare serpentinised Lmet. Lmet with occasional sericite alt.
Neils Beach (Sth beach)	25-30%, R=2-3,	5-10%, R=2, poly, poik	20%, Lmet dominant, rare Lsed (Greenland Gp?)	1%	1%, part alt to chlorite	1%, Pyroxene dominant	<1% , prob uvarovite (Green ppl)	40-45%	Chlorite <1% , Opaques 1%, Epidote 1%, Olivine <<1%	Rare serpentinised Lmet , Msed with calcite veinlets prob Greenland Gp?
Jacksons Bay Beach	15%	1%	30%, R=3/4, Lmet dominantly quartzofelds schist, rare Lsed	<1%	<1%	-	-	45-50%	Chlorite <1% , Opaques 1%,	

Appendix C4 : Point count data of the sand fraction in SWCM sediments

Sample ID	H843	H838	H844	H848	H850	H851
Environment	Inner shelf	Middle shelf	Inner shelf	HCH	HCH	HCH
Mean Grain size (µm)	120.5	23.6	103.1	48.2	74.2	67.6
Qtz (undulose)	76	65	47	54	93	58
Qtz (Polycrystalline)	15	24	17	18	20	17
Qtz (Straight)	27	34	33	44	49	37
Plagioclase	11	11	15	9	15	9
K-Feldspar	1	0	*	3	*	3
Undiff Feldspar	12	15	9	5	9	7
Schist Lithic	40	7	19	32	11	20
Phyllite Lithic	7	13	33	25	24	14
Slate Lithic	0	10	17	10	4	7
Sedimentary Lithic	3	2	2	3	0	5
Plutonic Lithic	0	0	0	1	0	0
Muscovite	20	19	15	1	9	3
Biotite	21	13	19	2	9	7
Fines/clays	14	39	18	21	23	11
Opaques	2	3	2	11	6	6
Epidote	2	4	8	5	2	1
Amphibole/Pyroxene	10	5	2	2	3	*
Chlorite	2	8	3	1	3	2
Garnet	*	*	*	17	2	5
Limonite	4	3	0	0	0	13
Sericite	0	4	4	0	0	1
Olivine	0	0	0	0	0	0
Zircon	1	1	*	0	0	0
Unknown grains	6	14	12	4	2	1
Highly altered grains	22	2	24	9	5	4
Planktic Foraminifera	0	0	0	1	1	1
Benthic Foraminifera	0	0	0	1	0	0
Mollusc	0	0	0	0	0	0
Undiff Bioclast	4	4	2	4	6	9
G.mat	0	0	0	1	*	41
G. mld	0	0	0	0	0	7
G. mix	0	0	0	5	10	11
G. nac	0	0	0	0	0	0
TOTAL	300	300	301	289	306	300

* = Observed, not counted:

G.mat = Mature/evolved glaucony pellets (well rounded and >90% glaucanitised)

G. mix = Mixed pellets of glaucony and remnant mica and quartz

G. nac = Nacent glaucony (early stage gloauconite, irregular boundaries)

G. mld = Mature glaucony as moulds (replaced Foraminifera etc…)

HCH = Hokitika Canyon Head

CHC = Cook Canyon Head

Appendix C4 : Point count data of the sand fraction in SWCM sediments (continued)

Sample ID	B469	H852	R208	C905	H855	H862
Environment	HCH	HCH	HCH	Middle shelf	Inner shelf	Middle shelf
Mean Grain size (µm)	109.3	169.6	47.7	20.7	95.2	22.3
Qtz (undulose)	59	22	44	40	47	61
Qtz (Polycrystalline)	12	4	9	6	21	8
Qtz (Straight)	43	32	44	36	79	56
Plagioclase	13	5	18	4	10	3
K-Feldspar	0	1	1	0	1	0
Undiff Feldspar	11	1	8	6	6	1
Schist Lithic	17	8	0	0	3	3
Phyllite Lithic	27	7	12	13	16	16
Slate Lithic	3	1	16	11	7	1
Sedimentary Lithic	6	2	1	1	0	0
Plutonic Lithic	0	1	0	0	0	0
Muscovite	6	2	23	30	16	22
Biotite	6	2	26	50	10	39
Fines/clays	8	5	48	56	28	57
Opaques	2	*	*	3	9	1
Epidote	1	1	6	2	11	1
Amphibole/Pyroxene	2	1	3	1	3	0
Chlorite	6	1	2	6	3	1
Garnet	2	0	2	0	0	0
Limonite	5	2	0	0	1	1
Sericite	1	0	1	2	2	1
Olivine	0	0	0	0	0	0
Zircon	0	0	0	0	0	*
Unknown grains	2	0	12	11	8	6
Highly altered grains	6	1	10	11	14	11
Planktic Foraminifera	1	6	4	1	0	1
Benthic Foraminifera	0	2	0	0	0	*
Mollusc	0	0	0	0	0	*
Undiff Bioclast	1	10	6	10	5	10
G.mat	27	160	2	0	0	*
G. mld	6	6	0	0	0	0
G. mix	25	15	0	0	0	0
G. nac	2	2	0	0	0	0
TOTAL	300	300	298	300	300	300

* = Observed, not counted:

G.mat = Mature/evolved glaucony pellets (well rounded and >90% glaucanitised)

G. mix = Mixed pellets of glaucony and remnant mica and quartz

G. nac = Nacent glaucony (early stage gloauconite, irregular boundaries)

G. mld = Mature glaucony as moulds (replaced Foraminifera etc…)

HCH = Hokitika Canyon Head

CHC = Cook Canyon Head

Appendix C4 : Point count data of the sand fraction in SWCM sediments (continued)

Sample ID	P663	H873	H867	H876	H879	H882
Environment	Inner shelf	Inner shelf	Outer shelf	Inner shelf	Middle shelf	CCH
Mean Grain size (µm)	62.5	66.9	34.4	127.1	20.3	100.5
Qtz (undulose)	55	48	54	41	50	46
Qtz (Polycrystalline)	13	19	21	15	17	21
Qtz (Straight)	78	69	64	57	70	58
Plagioclase	10	5	3	4	3	3
K-Feldspar	1	0	0	0	1	1
Undiff Feldspar	3	9	3	1	4	10
Schist Lithic	15	11	4	8	4	4
Phyllite Lithic	27	23	26	20	19	14
Slate Lithic	6	13	15	3	0	1
Sedimentary Lithic	3	2	1	0	0	1
Plutonic Lithic	0	0	0	0	0	0
Muscovite	12	14	12	5	24	6
Biotite	10	10	20	5	22	10
Fines/clays	27	23	26	17	39	3
Opaques	1	5	4	26	5	8
Epidote	7	6	3	27	2	6
Amphibole/Pyroxene	2	2	1	7	2	4
Chlorite	4	3	9	*	*	*
Garnet	0	0	0	7	0	1
Limonite	0	2	1	3	3	9
Sericite	2	1	0	2	1	7
Olivine	0	0	0	0	0	0
Zircon	0	0	0	0	0	0
Unknown grains	6	9	7	14	1	5
Highly altered grains	16	17	14	31	25	18
Planktic Foraminifera	0	0	4	0	2	0
Benthic Foraminifera	0	0	0	0	2	0
Mollusc	0	0	0	0	0	0
Undiff Bioclast	2	9	9	7	4	4
G.mat	0	0	0	0	0	45
G. mld	0	0	0	0	0	0
G. mix	0	0	*	0	*	13
G. nac	0	0	0	0	0	2
TOTAL	300	300	301	300	300	300

* = Observed, not counted:

G.mat = Mature/evolved glaucony pellets (well rounded and >90% glaucanitised)

G. mix = Mixed pellets of glaucony and remnant mica and quartz

G. nac = Nacent glaucony (early stage gloauconite, irregular boundaries)

G. mld = Mature glaucony as moulds (replaced Foraminifera etc…)

HCH = Hokitika Canyon Head

CHC = Cook Canyon Head

Appendix C4 : Point count data of the sand fraction in SWCM sediments (continued)

Sample ID	H884	H888	H893
Environment	Inner shelf	Middle shelf	Upper slope
Mean Grain size (µm)	129.8	41.7	91.2
Qtz (undulose)	57	67	42
Qtz (Polycrystalline)	19	18	29
Qtz (Straight)	103	61	46
Plagioclase	13	9	8
K-Feldspar	1	0	0
Undiff Feldspar	4	5	2
Schist Lithic	8	1	20
Phyllite Lithic	17	6	12
Slate Lithic	3	1	0
Sedimentary Lithic	0	0	4
Plutonic Lithic	0	0	3
Muscovite	11	26	8
Biotite	8	36	10
Fines/clays	20	29	14
Opaques	5	*	*
Epidote	5	1	1
Amphibole/Pyroxene	10	2	3
Chlorite	1	1	*
Garnet	*	0	2
Limonite	1	1	5
Sericite	1	1	0
Olivine	0	0	0
Zircon	0	0	0
Unknown grains	4	13	5
Highly altered grains	8	20	1
Planktic Foraminifera	0	0	20
Benthic Foraminifera	0	0	2
Mollusc	0	0	0
Undiff Bioclast	0	2	63
G.mat	0	0	0
G. mld	0	0	0
G. mix	1	0	0
G. nac	0	0	0
TOTAL	300	300	300

* = Observed, not counted:

G.mat = Mature/evolved glaucony pellets (well rounded and >90% glaucanitised)

G. mix = Mixed pellets of glaucony and remnant mica and quartz

G. nac = Nacent glaucony (early stage gloauconite, irregular boundaries)

G. mld = Mature glaucony as moulds (replaced Foraminifera etc…)

HCH = Hokitika Canyon Head

CHC = Cook Canyon Head

Appendix C4 : Point count data of the sand fraction in SWCM sediments (continued)

Sample ID	AA2	AB2	AK2	AN1	AQ2
Environment	Hokitika Beach	Hokitika River	Whataroa River	Gillespies Beach	Bruce Bay Beach
Mean Grain size (µm)					
Qtz (undulose)	18	48	33	23	42
Qtz (Polycrystalline)	35	29	45	26	57
Qtz (Straight)	16	43	41	23	32
Plagioclase	2	8	*	1	*
K-Feldspar	0	0	0	0	0
Undiff Feldspar	0	4	2	1	1
Schist Lithic	106	42	58	94	80
Phyllite Lithic	37	19	41	31	23
Slate Lithic	39	20	3	36	15
Sedimentary Lithic	7	4	2	2	3
Plutonic Lithic	2	0	0	2	0
Muscovite	0	15	17	2	9
Biotite	2	25	10	1	2
Fines/clays	1	6	3	1	2
Opaques	8	2	4	9	1
Epidote	1	*	2	2	2
Amphibole/Pyroxene	1	1	0	*	4
Chlorite	1	2	3	1	0
Garnet	19	2	0	39	12
Limonite	0	0	0	0	0
Sericite	0	0	7	0	2
Olivine	0	0	0	0	0
Zircon	0	0	0	0	0
Unknown grains	0	6	14	0	2
Highly altered grains	5	23	14	4	13
Planktic Foraminifera	0	0	0	0	0
Benthic Foraminifera	0	0	0	0	0
Mollusc	0	0	0	0	0
Undiff Bioclast	0	1	1	2	0
G.mat	0	0	0	0	0
G. mld	0	0	0	0	0
G. mix	0	0	0	0	0
G. nac	0	0	0	0	0
TOTAL	300	300	300	300	302

* = Observed, not counted:

G.mat = Mature/evolved glaucony pellets (well rounded and >90% glaucanitised)

G. mix = Mixed pellets of glaucony and remnant mica and quartz

G. nac = Nacent glaucony (early stage gloauconite, irregular boundaries)

G. mld = Mature glaucony as moulds (replaced Foraminifera etc…)

HCH = Hokitika Canyon Head

CHC = Cook Canyon Head

Appendix C4 : Point count data of the sand fraction in SWCM sediments (continued)

Sample ID	AT1	2b	3a	4b	5a
Environment	Haast River	Martyr River	Arawhata River	Neils Beach (Sth)	Jacksons Beach
Mean Grain size (µm)					
Qtz (undulose)	39	10	69	64	32
Qtz (Polycrystalline)	81	15	43	76	20
Qtz (Straight)	9	0	50	32	20
Plagioclase	1	*	3	17	0
K-Feldspar	0	1	0	0	0
Undiff Feldspar	3	3	13	11	2
Schist Lithic	77	126	22	44	212
Phyllite Lithic	53	57	8	10	1
Slate Lithic	16	19	1	0	1
Sedimentary Lithic	1	2	0	7	8
Plutonic Lithic	1	0	0	0	0
Muscovite	1	1	27	8	0
Biotite	0	1	6	1	1
Fines/clays	6	0	27	3	0
Opaques	1	1	1	2	*
Epidote	*	2	9	7	0
Amphibole/Pyroxene	*	11	1	1	*
Chlorite	*	*	2	4	*
Garnet	0	0	0	*	1
Limonite	0	*	0	*	*
Sericite	3	0	6	4	0
Olivine	0	4	0	0	0
Zircon	0	0	0	0	0
Unknown grains	0	0	5	5	0
Highly altered grains	7	47	7	4	2
Planktic Foraminifera	0	0	0	0	0
Benthic Foraminifera	0	0	0	0	0
Mollusc	0	0	0	0	0
Undiff Bioclast	1	0	0	0	0
G.mat	0	0	0	0	0
G. mld	0	0	0	0	0
G. mix	0	0	0	0	0
G. nac	0	0	0	0	0
TOTAL	300	300	300	300	300

* = Observed, not counted:

G.mat = Mature/evolved glaucony pellets (well rounded and >90% glaucanitised)

G. mix = Mixed pellets of glaucony and remnant mica and quartz

G. nac = Nacent glaucony (early stage gloauconite, irregular boundaries)

G. mld = Mature glaucony as moulds (replaced Foraminifera etc…)

HCH = Hokitika Canyon Head

CHC = Cook Canyon Head

Appendix C5 :Foraminifera in SWCM shelf and canyon head sand fraction, including identified species and an estimate of relative dominance of Benthic vs. Planktic tests. Observed under binocular microscope.

Sample ID	Transect	Depth	Benthic species	Planktics	Dominant Foraminifera
H838	A	99	various	Y	B
H837	A	119	various	-	-
H833	A	207	*Bulimina* spiral benthics?	Y	B
H848	HCH	94	*Elphidium* uniserial benthics?	Y	-
H850	HCH	126	various	Y	-
H851	HCH	182	various	Y	B
H852	HCH	198	various	Y	P
B469	HCH	188	very rare	-	-
R208	HCH	450	various	Y	P
P668	HCH	105	various	Y	-
C905	HCH	241	various	Y	-
H858	C	45	spiral benthics?	Y	B
H862	C	107	various	Y	P
H864	C	137	various	Y	P
H865	C	153	various	Y	P
S368	C - D	133	various	Y	P
P663	C - D	49	Rare spiral benthics?	-	-
H867	D	173	various	Y	P
H866	D	312	various	Y	P
H877	E	60	Rare, various.	-	-
H878	E	86	various	Y	B
H879	E	116	*Elphidium* *Bolivina* *Saidovina*	Y	B
H882	CCH	186	Rare, various.	Y	-
H885	F	29	very rare	-	-
H888	F	62	*Saidovina?* + various	Y	-
H890	F	98	*Saidovina?* + various	Y	B
H891	F	118	various	Y	-
H893	CCH	256	*Elphidium* *Bolivina* *Cibicides* *Uvigerina*	Y	P

Appendix C6: Skeletal grains and glaucony in Westland shelf and Canyoin head sediments. Based on binocular examination of > 63µm sediments. F= Foraminifera, B=bivalves, E= echinoids.

Sample ID	Transect	Depth	Textural name	Total Biogenics > 63 µm (%)	Dominant Bioclast	Foraminifera	Bivalves	Gastropods	Others	Glaucony Grains	Comments
H843	A	15	Muddy Sand	-	-	-	-	-	-		-
H838	A	99	Sandy Mud	<<1	F	Benthic > Planktic	-	-	-		-
H837	A	119	Sandy Mud	3	F	various	-	-	-		-
H833	A	207	Sandy Mud	~ 1	F	Possibly Benthic > Planktic	-	-	-		-
H845	B	44	Muddy Sand	-	-	-	-	-	-	Rare Dk grey/green pellet w Fe fractures	-
H844	B	30	Muddy Sand	-	-	-	-	-	-		-
H848	HCH	94	Gravelly Mud	<1	F	Biserail + spirals	-	-	-		-
H850	HCH	126	Muddy Sand	<1	F	poss Benthic > Planktic	-	-	-	<1 % Rare Dk grey/green pellet w Fe fractures	-
H851	HCH	182	Muddy Sand	2	F	biserial most dom	fragmented bivalves	-	rare ech spines	15% . R=4-5, S=2/1. Dk grn/gry pellets, Often Frac. Fe-stained. Internal foram moulds but less common. All pellets 0.1 - 1 mm.	-
H852	HCH	198	Slightly gravelly Muddy Sand	2 to 3	F	poss planktic > bethic	rare bivalve fragments max 5mm	-	silciceous spines com, Fe - stained & bored shell frags (up to 5mm)	30%. 0.2 - 1mm Diverse types, dk green to black, light brown.	-
B469	HCH	188	Muddy Sand	<<1	-	rare	-	-	-	10%. some internal moulds. Full glauc replacement common	rare biogenics
R208	HCH	450	Muddy Sand	1	F	planktics > Benth	-	-	-	<1 % Dk green pellets	-
P668	HCH	105	Sandy Mud	<1	F	?	-	-	-		-
C905	HCH	241	Sandy Mud	<1	F	both observed	-	-	rare ech spines		-

Sample ID	Transect	Depth	Textural name	Total Biogenics > 63 µm (%)	Dominant Bioclast	Foraminifera	Bivalves	Gastropods	Others	Glaucony Grains	Comments
H854	C	17	Muddy Sand	-	-	-	-	-	-		-
H855	C	21	Muddy Sand	-	-	-	-	-	-		-
H858	C	45	Muddy Sand	<1	F	spiral Foraminifera dom	Bivalve frags	-	ech spines		-
H862	C	107	Sandy Mud	1	F	Biserial, spiral + planktic bulbus	-	-	ech spines		-
H864	C	137	Sandy Mud	2	F	planktics > Benth	-	-	rare undiff shell frags up to 5mm		-
H865	C	153	Sandy Mud	3	F	planktics > Benth	-	-	-	< 1% vry dk red - blck.	-
S368	C - D	133	Sandy Mud	1	F	planktics > Benth	-	-	-		-
P663	C - D	49	Muddy Sand	<<1	-	rare spiral Foraminifera	-	-	-		-
H874	D	29	Muddy Sand	-	-	-	-	-	-		-
H873	D	45	Slightly gravelly Muddy Sand	<1	B	-	Bivalve frags up to 5mm. Whole up to 10mm (*Scalpomactra scalpellum*)	-	sponge fragments common		-
H867	D	173	Sandy Mud	<1	F	planktics > Benth	-	-	-		-
H866	D	312	Sandy Mud	4	F	planktics > Benth. Frag Foraminifera com	-	-	-		-
H876	E	21	Sand	-	-	-	-	-	-		-
H877	E	60	Sandy Mud	<1	F	rare Foraminifera	-	-	-		-
H878	E	86	Mud	1	F	Benthic > Planktic	-	-	ech spines		-
H879	E	116	Sandy Mud	1	F	Saidovina karreriana most com, followed by planktics	-	-	-		increase in planktic Foraminifera from H878
H882	CCH	186	Muddy Sand	<1	-	rare spiral & biserial	rare bivelve frags max 2mm	-	-	15%. R = 4-5. range from dk green to orange/red Fe - stained. Frac and un-Frac both common.	-

Sample ID	Transect	Depth	Textural name	Total Biogenics > 63 µm (%)	Dominant Bioclast	Foraminifera	Bivalves	Gastropods	Others	Glaucony Grains	Comments
H884	F	20	Sand	-	-	-	-	-	-	very rare Dk grey/green pellets ,Fe stained	-
H885	F	29	Muddy Sand	<<1	-	very rare benthics	-	-	-		-
H888	F	62	Sandy Mud	<1	F	Saidovina karreriana & frag Foraminifera com.	-	-	-		-
H890	F	98	Sandy Mud	1 to 2	F	whole & frag Foraminifera , spiral most com. S karreriana seen					
H891	F	118	Sandy Mud	1	F	Diverse range	-	-	-		-
H893	CCH	256	Muddy Sand	15	F	Planktics>>benthic	-	-	ech spines very com.	4%. Forams moulds common	
H894	Haast - Cascade	14	Sand	-	-	-	-	-	-		-
H898	Haast - Cascade	41	Slightly gravelly Sand	1 to 2	B	-	Whole and frag up to 15mm. mainly S. *scalpellum*	yes, less com than bivalve, up to 3mm	-		-
H900	Haast - Cascade	28	Sand	<1	B	-	rare bivalves up to 8mm, mainly S. *scalpellum*	-	-		-
H902	Haast - Cascade	280	Sandy Mud	<<1	-	-	-	-	undiff fragments		-
C901	Haast - Cascade	99	Sandy Mud	<1	F	rare undiff Foraminifera	-	-	-		-
B474	Haast - Cascade	28	Muddy Sand	1	B	-	up to 3mm	-	ech spines, sponge, undiff frags com.		-
B622	Haast - Cascade	68	Muddy Sand	1	G	rare. poss Benthic > Planktic	rare frags	2 species present, up to 2-3mm	Single 20mm worm tube		-
C898	Haast - Cascade	95	Slightly gravelly Muddy Sand	1 to 2	B/G	rare	Whole and frag up to 4m	frags up to15mm	-		-
E786	Haast - Cascade	454	Sandy Mud	1	F	planktics > Benth	-	-	-		-

Appendix C7: X-ray Diffraction method (XRD)

A selection of shelf, kasten core and terrestrial samples were analyzed to characterize the bulk mineralogy. This was particularly useful for samples where the mean grain size was too fine for petrographic analysis (i.e. kasten cores) or where modal composition in thin section became difficult to estimate due to alteration or confusion between fine grained quartz and feldspars. were analyzed from A 2-3 g split from the bulk sample was crushed in a mortar and pestle and ran at the Canterbury University using a Philips PW1820/1710 X-ray Diffractometre with a Copper tube (Cu Ka = 1.54178Å). Each powdered bulk sample was pipetted onto glass slides (oriented mounts) and operated at 50Kv/40mA in steps of 0.02° 2θ with a step speed of 0.02° 2θ per second. The slides were air dried and scanned at 3-70° 2θ. Where clay minerals were anticipated (i.e. marine shelf and core samples), further analysis by treatment with ethylene glycol for 12 hours at 60°C followed by heating each sample to 550°C helped to distinguish clay mineral species (Hardy and Tucker 1988 pg. 213) .

A quantitative estimate of the percentage composition of crystalline material present in the air dried samples was determined using peak area. This technique is only an approximation of the percentage composition (Hardy and Tucker 1988 pg. 213) and consequently an error of ± 5% is acknowledged for all samples. Minerals with less than a 5% composition of the bulk sample are reported as trace.

Appendix C8: Bulk XRD results for SWCM shelf, canyon, beach, and river samples. 'tr.' = < 5 % of the bulk composition.

Sample ID	Transect	Depth	Qtz	Albite	Kaolinite	Muscovite	Calcite
H843	A	15	90	10	tr.	tr.	
H837	A	119					
H833	A	99	90	10	tr.	tr.	
H838	A	207					
H844	B	30	90	10	tr.	tr.	
H845	B	40					
H848	HCH	94	80	20	tr.	tr.	
H850	HCH	126	85	15	tr.	tr.	
H851	HCH	182					
B469	HCH	188					
H852	HCH	198	90	10	tr.	tr.	
R208	HCH	450	80	20	tr.	tr.	
P668	HCH	105	60	30	10	tr.	
C905	HCH	241	65	25	10	tr.	
H854	C	17	90	10	tr.	tr.	
H855	C	21					
H858	C	45					
H862	C	107	70	30	tr.	tr.	
H864	C	137					
H865	C	153	60	30	5	5	
P663	C_D	49					
S368	C_D	133					
H874	D	29	80	20	tr.	tr.	
H873	D	45					
H867	D	173					
H866	D	312	60	25	10	5	
H876	E	21	85	15	tr.	tr.	
H877	E	60					
H878	E	86					
H879	E	116	65	30	5	tr.	
H882	E	186	70	30	tr.	tr.	
H884	F	20	75	25	tr.	tr.	
H885	F	29					
H888	F	62					
H890	F	98	70	30	tr.	tr.	
H891	F	118					
H893	F	256	80	10	tr.	10	10
H894	Haast - Cascade		70	30	tr.	tr.	
H898	Haast - Cascade		70	30	tr.	tr.	
H900	Haast - Cascade						
H902	Haast - Cascade		60	25	10	5	
C901	Haast - Cascade		65	20	10	5	
B474	Haast - Cascade		65	35	tr.	tr.	
B622	Haast - Cascade						
C898	Haast - Cascade						
E786	Haast - Cascade		65	15	15	5	

Sample ID	Transect	Depth	Qtz	Albite	Kaolinite	Muscovite	Calcite
AA2	Hokitika Beach		90	10	tr.	tr.	
AB2	Hokitika River		90	10	tr.	tr.	
AF3	Mokonui Beach						
AG2	Waitaha Beach (Nth)						
AH3	Waitaha River		85	15	tr.	tr.	
AK2	Whataroa River		90	10	tr.	tr.	tr.
AN1	Gillespies Beach		90	10	tr.		
AO2	Cook River		85	15	tr.	tr.	
AQ2	Bruce Bay Beach						
AR2	Paringa River						
AT1	Haast River		90	10	tr.		
AU3	Haast Beach (Nth)		85	15	tr.		
1a	Hannahs Clearing (beach)						
2b	Martyr River		65	20	15	tr.	
3a	Arawhata River		80	20	tr.		
4b	Neils Beach (Sth beach)		90	10	tr.		
5a	Jacksons Bay Beach		90	10	tr.	tr.	

Appendix C9: Bulk XRD results (in %) for South Westland canyon kasten core samples. 'tr.' = < 5 % of the bulk composition.

Sample_ID	Core sample depth (cm)	Quartz	Albite	Kaolinite	Muscovite	Calcite
TAN0513 - 15 A	5.5	60	15	tr.	tr.	25
TAN0513 - 15 B	32.5	25	10	5	tr.	60
TAN0513 - 15 C	57.5	35	25	tr.	tr.	40
TAN0513 - 15 D	87.5	50	10	5	tr.	35
TAN0513 - 15 E	252.5	40	15	10	tr.	35
TAN0513 - 19 B	32.5	10	10	tr.		80
TAN0513 - 19 C	72.5	10	5	tr.	tr.	85
TAN0513 - 19 D	87.5	10	tr.			90
TAN0513 - 19 E	252.5	10	tr.			90
TAN0513 - 21 A	4.5	10	tr.	tr.		90
TAN0513 - 21 B	24.5	5	tr.			95
TAN0513 - 21 C	47.5	5	tr.	tr.		95
TAN0513 - 21 D	62.5	10	tr.			90
TAN0513 - 21 E	192.5	5				95
TAN0712 - 17 A	42.5	55	20	10	tr.	15
TAN0712 - 17 B	122.5	45	20	5	tr.	30

Appendix C10: Heavy mineral separation method and separation of the magnetic fraction

Heavy mineral separation (LST liquid):

Splits from the bulk samples were taken and sieved to retain the fine to very fine sand fraction (63 – 250 μm). This size fraction was used to be comparable to other heavy mineral studies in the area (i.e. Bradley et al. 2002). In most shelf samples, wet sieving was required to remove the silt and clay fraction. This was then dried at 50 degrees C for at least 12 hrs. In several shelf samples there was insufficient material in the sand fraction to perform the analysis on; these are noted in the sample treatments table in Appendix A4.

Heavy minerals were separated using LST heavy liquids (lithium heteropolytungstate) with a specific gravity of 2.85. The specific gravity of the liquid was checked between each run and adjusted by heating or adding distilled water to increase or decrease the specific gravity respectively. After recording the sample weight, up to 10 g of sample was floated using an apparatus setup similar to that outlined in Lewis and McConchie (1994, pg. 138) and Figure C1. Once the sample was added, the liquid was stirred vertically and left for approximately 2 hours with 2-3 stirs in between. Prior to each stirring, the separated heavy minerals accumulated at the funnel base were siphoned off onto filter paper within the lower funnel. The separated heavy and light mineral fractions were then rinsed into a small beakers using distilled water and dried at 60˚C for at least 12 hours. These were then weighed and recorded, allowing the heavy mineral percentage to be calculated (Appendix C9).

Figure C1: Apparatus used for heavy liquid separation of SWCM sediments.

Magnetic fraction separation:

The magnetic fraction was separated from the heavy mineral fraction using a strong hand magnet and non-stick lab paper. The magnetic fraction removed was then subjected to further passes with the hand magnet to improve the purity of magnetite grains recovered. This repeated passing of the magnet removed many composite grains containing small amounts of magnetite. The final magnetic fraction was checked for purity under the binocular microscope; most samples contained ≥ 90% magnetite grains (Figure C2). Heavy mineral separates containing coarser composite grains were difficult to isolate from the final magnetic fraction in some cases (i.e. Martyr River). Each magnetite fraction was weighed to give a percentage weight of the heavy mineral separate (Appendix C9).

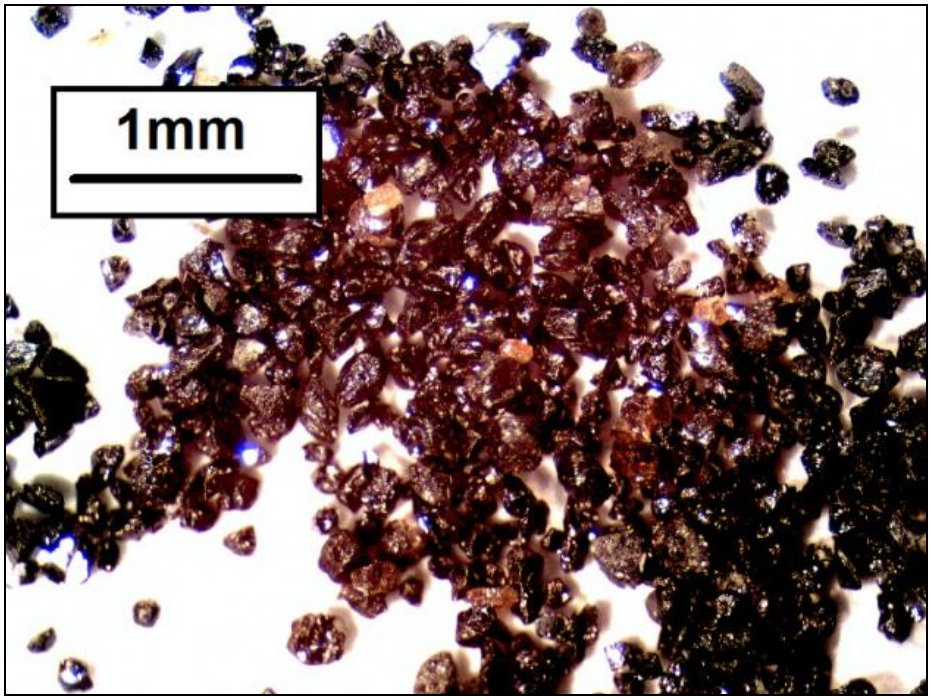

Figure C2: Photo of the magnetic fraction removed from the heavy mineral fraction. Sample is from H876 and is clearly dominated by magnetite grains.

Appendix C11: Heavy mineral and magnetic fraction seperation results. All weights are in grams. Note that heavy mineral separations were conducted on the very fine to fine sand fractions only. HM = heavy mineral

Sample ID	Total wt.	Wt. HM	Wt. Lights	% HM	% Lights	Wt. HM	Magnetic Fraction Wt.	Magnetic % of HM
H843	14.21	0.82	13.56	5.67	94.33	0.80	0.0020	0.25
H838	6.90	0.45	6.82	6.18	93.82	0.36	0.0000	0.00
H833	7.13	0.23	7.05	3.20	96.80	0.19	0.0003	0.16
H844	9.18	0.90	8.30	9.77	90.23	0.87	0.0010	0.11
H848	8.90	1.48	7.36	16.77	83.23	1.45	0.0110	0.76
H850	11.30	0.62	10.45	5.58	94.42	0.60	0.0049	0.82
H851	10.34	0.51	9.60	5.03	94.97	0.49	0.0009	0.18
H852	11.80	0.42	11.18	3.59	96.41	0.39	0.0014	0.36
B469	12.60	0.51	12.04	4.09	95.91	0.50	0.0020	0.40
R208	4.33	0.17	4.15	3.98	96.02	0.15	0.0000	0.00
P668	1.72	0.05	1.45	3.34	96.66	0.01	0.0000	0.00
C905	9.64	0.46	9.00	4.85	95.15	0.41	0.0005	0.12
H855	11.81	0.99	10.79	8.43	91.57	0.95	0.0002	0.02
H858	11.32	0.91	10.29	8.08	91.92	0.87	0.0000	0.00
H862	1.92	0.21	1.50	12.15	87.85	0.17	0.0000	0.00
H865	4.37	0.25	3.74	6.31	93.69	0.25	0.0008	0.32
P663	8.22	0.63	7.55	7.68	92.32	0.61	0.0004	0.07
S368	4.02	0.07	3.77	1.82	98.18	0.06	0.0000	0.00
H874	13.33	1.38	11.99	10.35	89.65	1.37	0.0028	0.20
H867	8.03	0.24	8.16	2.89	97.11	0.24	0.0000	0.00
H866	0.83	0.03	0.73	3.94	96.06	0.22	0.0000	0.00
H876	4.48	6.24	8.03	43.73	56.27	6.23	0.0960	1.54
H879	14.33	0.36	2.97	10.81	89.19	0.35	0.0009	0.25
H882	7.45	0.97	6.36	13.23	86.77	0.97	0.0030	0.31
H884	11.00	1.91	8.99	17.49	82.51	1.88	0.0040	0.21
H888	7.57	0.61	7.05	7.96	92.04	0.60	0.0000	0.00
H891	0.72	0.02	0.35	4.11	95.89	0.01	0.0000	0.00
H893	11.53	1.02	10.11	9.16	90.84	1.01	0.0060	0.60
C901	6.19	0.55	5.25	9.48	90.52	0.54	0.0006	0.11
H900	12.60	1.80	7.86	10.99	89.01	1.36	0.0071	0.52
H894	9.56	3.23	9.57	18.61	81.39	1.79	0.0040	0.22
H898	12.60	3.06	10.55	25.21	74.79	2.98	0.0045	0.15
B474	13.71	0.69	6.49	22.48	77.52	3.03	0.0353	1.16
B622	7.44	0.31	5.08	9.62	90.38	0.68	0.0035	0.52
C898	5.48	1.41	11.40	5.70	94.30	0.29	0.0033	1.13
Hokitika Beach	12.64	9.48	3.86	71.08	28.92	9.38	0.2715	2.89
Hokitika River	8.26	0.75	7.54	9.00	91.00	0.74	0.0040	0.54
Waitaha Beach	6.11	1.41	4.79	22.67	77.33	1.40	0.0050	0.36
Waitaha River	10.50	2.22	8.28	21.15	78.85	2.17	0.0151	0.70
Whataroa River	10.14	0.96	9.37	9.32	90.68	0.95	0.0001	0.01
Gillespies Beach	10.60	8.48	2.16	79.70	20.30	8.43	0.3620	4.30
Bruce Bay Beach	9.62	7.22	2.40	75.08	24.92	7.13	0.0590	0.83
Haast River	11.85	1.32	10.54	11.14	88.86	1.29	0.0330	2.56
Haast Beach	11.39	0.80	10.58	6.99	93.01	0.78	0.0120	1.54
Arawhata River	5.98	0.64	5.96	9.65	90.35	0.59	0.0120	2.04
Neils Beach	6.45	0.80	5.62	12.49	87.51	0.78	0.0300	3.84
Martyr River	6.07	1.41	4.68	23.15	76.85	1.40	0.2210	15.83

APPENDIX D: CARBONATE ANALYSIS

Appendix D1: Gasometric quantitative analysis after acidification method for determining carbonate content of SWCM surface and core sediments.

Bulk samples were split, crushed using a hand mortar, and dried at 110°C for approximately 2 hours before weighing out ~ 0.333g. For every 10 samples, one standard sample of pure calcium carbonate powder was included to monitor the accuracy of each run. Following measurements of atmospheric pressure, temperature and pressure within each reaction bomb, samples were reacted with 5 ml of 70% orthophosphoric acid and the reaction bomb pressure was recorded once again to determine the percentage carbonate within each sample. Samples with greater than 2 % difference to replicate samples were either rejected or rerun. Further details of this technique can be found in Jones & Kaiteris (1983).

Appendix D2: Carbonate results for the three Hokitika Canyon core. Gray shaded values had an error > 2%.

HOLE ID	Sample	Depth (cm)	Carbonate %
TAN 0513-15	**T15a**	5.5	28.05
	T15b	32.5	53.6
	T15c	57.5	-
	T15d	87.5	30.15
	T15e	252.5	34.2
TAN 0513-19	**T19a**	5.5	72.6
	T19b	32.5	62.5
	T19c	72.5	63.1
	T19d	87.5	58.05
	T19e	252.5	67.7
TAN 0513- 21	**T21a**	4.5	71.55
	T21b	24.5	71.1
	T21c	47.5	67.7
	T21d	62.5	68.4
	T21e	192.5	71.4

Appendix D3: Table of carbonate results for SWCM surface sediments determined by Gasometric quantitative analysis after acidification.

Sample_ID	Transect	Depth	Carbonate %
H843	A	15	0.0
H838	A	99	0.0
H837	A	119	0.3
H833	A	207	1.4
H844	B	30	0.0
H845	B	44	0.0
H851	HCH	182	0.1
H850	HCH	126	0.0
H852	HCH	198	6.0
B469	HCH	188	0.0
H848	HCH	94	0.0
R208	HCH	450	0.2
C905	HCH	241	0.0
P668	HCH	105	0.0
H854	C	17	1.0
H864	C	137	0.5
H865	C	153	1.0
H862	C	107	0.4
H858	C	45	0.0
P663	C_D	49	0.0
S368	C _D	133	0.0
H873	D	45	0.0
H874	D	29	0.0
H876	E	21	0.0
H882	CCH	186	0.0
H879	E	116	0.0
H878	E	86	0.0
H884	F	20	0.0
H885	F	29	0.9
H891	F	118	1.0
H893	CCH	256	9.2
H888	F	62	0.0
H890	F	98	0.1
C901	Haast - Cascade	99	0.0
H900	Haast - Cascade	28	0.1
H902	Haast - Cascade	280	0.9
H898	Haast - Cascade	41	0.5
B474	Haast - Cascade	28	0.5
B622	Haast - Cascade	68	0.2
C898	Haast - Cascade	95	0.0
E786	Haast - Cascade	454	0.0

APPENDIX E: GEOCHEMICAL ANALYSES

E1: X-ray Fluorescence (XRF) method

E2: Raw XRF major element results for all shelf, canyon head, and terrestrial samples

E3: Raw XRF trace element results for all shelf, canyon head, and terrestrial samples

E4: Mean and standard deviation for all marine surface sediments by region

E5: Mean and standard deviations for all marine surface sediments by depositional environment

E6: Raw XRF major and trace element results for canyon kasten core samples

E7: Pearson correlation analysis

E8: Bulk major and trace element ratios used in this study of SWCM sediments

Appendix E1: X-ray Fluorescence (XRF)

The bulk geochemistry of SWCM sediments was analysed using X-ray Fluorescence (XRF). Samples included: shelf and canyon head surface samples, kasten core, river, and beach sediments. Sample preparation involved removing a 10-12 g split from the bulk samples and washing with distilled water to remove any marine salts. Samples were then oven dried at 60°C for at least 12 hours and crushed to a fine powder using a tungsten-carbide *Rocklabs* Standard Ring Mill for 45 seconds per sample.

Samples were analysed at the University of Canterbury on a Philips PW2400 Sequential Wavelength Dispersive X-ray Fluorescence Spectrometre with a Rhodium target tube. Fusion beads were made from the powdered samples for major elements using Fusilux furnace, and pressed powder pellets were made for trace element analysis. Major elements were analyzed at 50 KV and 55MA, while trace elements were ran at 60KV and 46 MA. For each sample, the weight percentage of 10 major oxides and 16 trace elements in parts per million (ppm) were determined (Appendix E2 & E3). Major elements for the shelf, canyon heads, and terrestrial samples have been normalized to 100% to account for Loss On Ignition (LOI).

Appendix E2: Raw XRF major element results for all shelf, canyon head, river an beach samples. HCH=Hokitika Canyon Head, CHC= Cook Canyon Head. All values in weight percent.

Sample ID	Environment	SiO2	TiO2	Al2O3	Fe2O3T	MnO	MgO	CaO	Na2O	K2O	P2O5	LOI	Total
H833	North Shelf	69.63	0.56	13.10	4.04	0.05	1.69	2.38	2.97	2.23	0.14	3.13	99.94
H837	North Shelf	66.56	0.69	14.57	4.57	0.07	1.84	2.18	3.20	2.61	0.16	3.01	99.46
H838	North Shelf	65.56	0.67	15.21	4.81	0.07	1.96	2.14	3.11	2.74	0.17	3.34	99.77
H843	North Shelf	73.45	0.69	12.07	3.91	0.06	1.50	1.56	2.50	2.14	0.13	1.94	99.93
H844	North Shelf	73.85	0.96	11.54	4.02	0.10	1.39	1.97	2.56	1.75	0.16	1.65	99.93
H845	North Shelf	72.42	0.71	12.29	4.02	0.07	1.53	1.96	2.71	1.95	0.15	2.07	99.88
H848	HCH north rim	67.67	1.66	12.73	6.47	0.24	1.59	2.40	2.61	2.08	0.15	2.13	99.72
H850	HCH north rim	73.81	0.91	10.50	4.62	0.10	1.37	2.02	2.45	1.88	0.13	2.10	99.88
H851	HCH north rim	65.84	0.75	9.82	11.49	0.08	1.66	1.96	1.93	2.65	0.37	3.27	99.82
H852	HCH north rim	58.06	0.47	8.53	15.99	0.06	2.15	3.12	1.53	3.99	0.47	5.08	99.45
C905	HCH south rim	62.20	0.62	16.94	5.10	0.07	2.09	2.29	3.90	2.94	0.19	3.28	99.62
P668	HCH south rim	60.70	0.60	18.00	5.45	0.07	2.22	2.00	4.00	3.12	0.18	3.57	99.92
R208	HCH south rim/floor	69.85	0.61	12.70	3.80	0.06	1.46	2.62	3.70	1.93	0.18	2.83	99.74
B469	HCH north rim	69.71	0.74	10.47	7.75	0.08	1.54	1.94	2.21	2.42	0.25	2.83	99.95
H854	Central Shelf	75.12	0.87	11.07	3.49	0.07	1.15	2.25	2.66	1.53	0.18	1.55	99.94
H855	Central Shelf	76.26	0.78	10.66	3.10	0.06	1.01	2.27	2.80	1.33	0.20	1.50	99.97
H858	Central Shelf	70.69	0.64	12.58	3.93	0.06	1.48	2.14	3.29	1.99	0.17	2.90	99.87
H862	Central Shelf	63.03	0.62	16.59	4.87	0.06	1.96	2.43	3.98	2.77	0.20	3.33	99.85
H864	Central Shelf	62.92	0.60	16.96	4.89	0.06	1.98	2.48	3.86	2.80	0.20	3.21	99.95
H865	Central Shelf	64.93	0.62	15.85	4.53	0.06	1.73	2.74	3.91	2.38	0.21	2.99	99.96
P663	Central Shelf	71.20	0.67	12.83	3.91	0.06	1.45	2.12	3.11	2.01	0.16	2.45	99.96
S368	Central Shelf	62.80	0.63	16.59	5.29	0.07	2.09	2.51	3.47	2.99	0.18	3.36	99.97
H866	Central Shelf	65.10	0.60	15.94	4.30	0.06	1.71	2.75	3.91	2.40	0.21	2.96	99.94
H867	Central Shelf	68.61	0.61	14.23	4.16	0.06	1.60	2.38	3.36	2.22	0.17	2.55	99.96
H873	Central Shelf	73.40	0.88	11.72	3.67	0.07	1.20	2.47	2.77	1.62	0.18	1.97	99.95
H874	Central Shelf	73.53	1.04	11.63	3.73	0.08	1.13	2.63	2.87	1.50	0.21	1.64	99.97
H876	Central Shelf	58.23	6.46	11.48	11.01	0.38	1.26	5.44	1.88	1.16	0.49	1.37	99.15
H877	Central Shelf	63.12	0.70	16.86	5.23	0.08	2.05	2.15	3.54	2.96	0.19	3.08	99.97
H878	Central Shelf	59.81	0.63	17.42	5.36	0.08	2.17	2.45	4.55	3.11	0.20	3.68	99.45
H879	Central Shelf	61.89	0.68	17.03	5.30	0.07	2.11	2.34	3.94	3.06	0.19	3.18	99.79
H882	CHC	60.16	1.01	10.27	14.23	0.10	1.83	2.59	2.19	2.84	0.73	3.58	99.52
H884	South Shelf	73.21	1.55	11.39	4.16	0.13	1.04	2.74	3.51	0.92	0.29	0.97	99.89
H885	South Shelf	73.80	1.23	11.53	3.69	0.10	1.03	2.54	3.57	1.02	0.26	1.05	99.82

Sample ID	Environment	SiO2	TiO2	Al2O3	Fe2O3T	MnO	MgO	CaO	Na2O	K2O	P2O5	LOI	Total
H888	South Shelf	67.76	0.65	14.92	4.07	0.06	1.52	2.32	4.23	2.03	0.21	2.19	99.95
H890	South Shelf	62.62	0.67	17.00	5.06	0.07	1.97	2.43	4.05	2.81	0.20	2.98	99.85
H891	South Shelf	63.56	0.65	16.84	4.90	0.06	1.92	2.29	3.95	2.70	0.20	2.89	99.97
H893	CHC	67.05	0.47	10.11	4.76	0.06	1.35	6.16	2.49	1.55	0.19	5.67	99.85
E786	Haast - Cascade Shelf	58.96	0.84	17.28	6.33	0.09	2.80	2.40	3.31	3.33	0.20	4.17	99.70
B474	Haast - Cascade Shelf	68.61	0.84	12.62	4.20	0.07	2.72	3.29	3.56	1.48	0.27	2.26	99.92
B622	Haast - Cascade Shelf	67.63	0.74	14.28	4.33	0.07	1.81	2.78	4.03	1.73	0.24	2.19	99.83
C898	Haast - Cascade Shelf	63.70	0.82	15.21	5.04	0.07	2.28	3.11	3.78	2.31	0.22	3.22	99.77
C901	Haast - Cascade Shelf	62.56	0.68	16.89	5.04	0.07	1.95	2.11	3.94	2.85	0.20	3.64	99.92
H894	Haast - Cascade Shelf	72.76	0.63	12.94	3.50	0.06	1.19	1.67	4.40	1.20	0.15	1.45	99.94
H898	Haast - Cascade Shelf	73.35	0.67	12.26	3.18	0.05	1.03	2.17	4.12	1.20	0.19	1.74	99.97
H900	Haast - Cascade Shelf	74.84	0.73	11.61	3.14	0.05	1.04	1.87	3.54	1.28	0.16	1.64	99.91
H902	Haast - Cascade Shelf	61.40	0.70	17.79	5.50	0.07	2.19	2.05	3.50	3.27	0.19	3.24	99.89
AA2	Hokitika Beach	66.99	2.27	12.57	8.16	0.60	1.59	2.62	1.86	1.94	0.15	1.23	99.97
AB2	Hokitika River	73.72	0.66	11.60	4.35	0.07	1.73	1.46	2.33	1.95	0.12	1.94	99.93
AF3	Mokonui Beach	79.39	0.41	9.69	2.65	0.06	0.98	1.47	2.34	1.52	0.11	1.30	99.92
AG2	Waitaha Beach (Nth)	73.67	0.73	12.12	3.99	0.12	1.40	1.94	2.39	2.09	0.15	1.36	99.97
AH3	Waitaha River	71.16	1.13	13.03	4.76	0.16	1.41	1.75	2.89	2.10	0.14	1.41	99.93
AK2	Whataroa River	70.92	0.82	13.04	4.33	0.08	1.57	1.97	2.56	2.28	0.16	2.17	99.89
AN1	Gillespies Beach	65.01	3.06	12.22	10.52	0.67	1.14	2.87	2.14	1.34	0.14	0.76	99.87
AO2	Cook River	68.13	0.92	13.75	5.30	0.13	1.48	2.78	3.13	1.95	0.15	2.19	99.91
AQ2	Bruce Bay Beach	74.83	1.30	10.57	5.59	0.34	0.98	1.63	2.06	1.55	0.10	0.96	99.91
AR2	Paringa River	71.05	0.64	13.73	4.03	0.06	1.37	1.68	4.00	1.58	0.14	1.65	99.93
AT1	Haast River	82.93	0.34	8.12	2.29	0.04	0.72	0.83	2.39	1.04	0.08	1.15	99.94
AU3	Haast Beach	83.47	0.37	7.72	2.19	0.04	0.71	0.88	2.29	1.00	0.07	1.20	99.94
1a	Hannahs Clearing Beach	88.84	0.17	5.42	1.09	0.02	0.43	0.60	2.46	0.27	0.05	0.59	99.95
2b	Martyr River	58.30	0.50	10.02	6.69	0.09	13.73	2.14	1.96	1.56	0.11	4.87	99.96
3a	Arawhata River	84.15	0.18	7.58	1.94	0.05	0.73	0.65	3.16	0.47	0.08	0.86	99.86
4b	Neils Beach	81.36	0.28	8.05	2.26	0.04	0.80	1.76	2.79	0.75	0.09	1.74	99.93
5a	Jacksons Bay Beach	76.60	0.48	10.29	3.93	0.04	1.90	0.66	1.13	2.33	0.12	2.42	99.89

Appendix E3: Raw XRF trace element results for all shelf, canyon head, river an beach samples. HCH=Hokitika Canyon Head, CHC= Cook Canyon Head. All values are in parts per million (ppm).

Sample ID	V	Cr	Ni	Zn	Zr	Nb	Ba	La	Ce	Nd	Ga	Pb	Rb	Sr	Th	Y
H833	86.04	54.22	24.27	69.62	172.42	9.82	513.79	20.18	43.19	47.48	16.61	17.61	110.20	318.25	11.47	22.09
H837	94.80	59.05	22.91	75.16	227.49	11.48	560.33	21.83	45.84	45.43	18.01	18.97	121.92	320.89	11.09	25.23
H838	108.02	71.11	27.32	88.64	213.94	11.83	624.09	23.07	52.58	37.20	19.34	19.66	128.29	325.88	13.92	25.33
H843	81.84	50.35	19.41	62.09	211.42	11.48	463.61	20.36	52.79	45.05	15.55	14.26	103.89	294.33	13.90	24.90
H844	87.83	47.76	17.64	56.42	278.77	13.86	417.44	22.30	55.86	39.59	14.83	12.97	84.82	327.76	11.12	30.17
H845	88.64	52.70	18.85	65.86	228.87	10.84	450.20	20.66	40.82	37.71	15.62	16.70	93.69	313.05	10.65	25.37
H848	93.77	58.15	22.04	85.50	412.72	20.31	464.41	27.16	72.09	28.37	15.18	24.59	97.39	287.99	15.40	39.07
H850	69.35	45.46	19.77	81.06	323.89	13.26	381.62	19.81	55.51	27.83	13.05	20.07	88.60	255.58	10.82	22.96
H851	135.54	119.53	22.02	81.17	157.99	12.73	305.27	8.23	38.00	27.57	12.56	67.47	98.11	233.13	6.60	20.79
H852	129.65	104.99	23.28	103.29	111.23	8.28	242.90	2.65	37.06	28.49	12.89	59.74	116.55	246.04	3.46	19.90
C905	119.69	67.75	27.58	89.02	186.40	11.05	684.94	24.43	48.96	38.62	22.07	21.53	132.10	351.77	15.96	25.89
P668	125.98	68.54	26.55	95.96	167.07	10.49	750.14	18.75	52.80	36.06	23.60	19.01	140.28	354.69	12.04	24.48
R208	61.10	34.37	15.43	55.01	223.81	10.24	340.12	26.86	58.32	14.04	12.82	14.38	88.44	330.18	9.73	24.40
B469	95.22	80.55	20.15	72.40	173.34	10.82	360.80	12.95	36.17	32.38	13.17	35.91	97.42	245.70	10.38	21.32
H854	76.85	33.76	13.27	49.22	290.16	13.04	367.12	27.57	51.78	40.71	14.03	11.34	72.78	371.97	11.70	29.35
H855	69.65	29.07	11.18	43.19	308.62	11.61	325.11	20.03	50.54	39.17	13.00	8.18	63.05	366.14	13.33	28.14
H858	85.43	41.11	16.78	62.42	227.27	11.09	457.66	27.52	59.57	38.89	15.10	14.95	90.65	338.14	9.42	24.88
H862	110.34	59.26	23.75	84.93	199.63	11.04	655.42	25.44	61.06	40.62	20.13	17.16	125.21	372.87	9.15	26.45
H864	115.35	58.93	21.31	82.48	191.29	10.76	664.31	22.38	58.59	31.27	21.37	14.12	126.29	372.00	11.84	25.68
H865	100.91	53.30	19.81	77.23	223.87	10.37	553.60	23.80	50.25	36.61	19.18	12.72	107.14	376.16	10.45	26.88
P663	93.93	44.77	16.63	65.52	208.54	11.06	492.37	19.93	51.46	34.17	15.24	17.37	91.36	355.48	15.71	24.11
S368	118.19	65.57	23.91	91.93	176.32	11.19	723.95	26.51	41.19	36.69	21.46	21.69	137.88	355.61	13.27	24.19
H866	99.91	54.76	21.21	77.71	215.47	10.23	563.02	24.47	51.15	46.47	19.48	15.30	108.07	380.80	11.69	27.40
H867	92.69	48.29	17.97	70.48	197.55	10.27	506.58	26.84	51.32	46.93	17.61	14.04	102.36	354.32	12.72	25.32
H873	79.44	36.25	14.34	64.35	264.78	13.24	385.93	26.30	57.81	49.10	15.26	16.23	74.47	402.44	13.25	29.47
H874	77.37	35.64	14.53	51.42	309.61	15.11	334.37	28.04	71.50	45.59	14.69	15.02	69.37	438.94	15.85	32.74
H876	163.60	47.13	21.06	67.29	1441.23	64.90	312.75	56.88	144.82	73.64	20.53	15.75	50.25	642.72	39.83	87.82
H877	116.72	59.89	23.99	91.70	201.79	11.57	707.03	27.17	50.95	34.60	21.92	23.84	132.96	364.81	12.52	25.84
H878	62.21	34.11	17.23	68.98	174.16	10.10	381.03	17.54	39.72	29.86	16.45	21.89	124.84	351.30	8.19	24.25
H879	101.98	53.25	22.73	88.65	185.22	11.50	631.25	30.02	53.63	33.51	19.59	20.04	132.54	355.97	9.17	25.78
H882	145.31	71.27	27.64	85.63	233.19	15.04	338.08	17.37	44.91	32.63	14.89	89.42	98.97	300.99	10.48	25.52
H884	77.77	34.79	12.31	41.45	401.02	18.17	213.34	27.20	62.81	38.03	12.47	11.98	43.61	304.33	16.07	33.94
H885	76.44	34.13	13.64	40.14	304.40	15.53	243.68	22.11	48.57	46.67	12.47	14.14	48.07	305.22	17.10	31.26
H888	90.32	43.11	17.64	67.62	234.37	11.18	475.43	22.06	73.05	23.15	15.71	17.26	90.83	346.94	10.82	26.57
H890	109.63	54.75	22.48	86.78	203.30	10.96	651.08	28.33	77.97	29.28	19.86	16.30	123.47	363.93	12.82	27.66

Sample ID	V	Cr	Ni	Zn	Zr	Nb	Ba	La	Ce	Nd	Ga	Pb	Rb	Sr	Th	Y
H891	110.29	57.86	21.45	81.67	194.22	11.22	637.01	27.32	49.29	27.06	21.17	14.82	120.46	357.06	11.28	25.95
H893	81.97	48.56	19.19	62.38	137.97	8.70	339.04	17.37	28.17	15.87	12.61	26.74	74.60	354.65	8.04	15.98
E786	126.49	88.88	43.49	96.07	190.19	13.27	667.01	20.74	43.29	30.23	22.50	18.41	150.28	310.75	16.98	25.92
B474	95.70	274.75	70.78	51.76	340.76	12.78	313.09	27.43	45.92	47.94	14.58	15.56	70.70	362.10	12.81	33.35
B622	98.99	82.59	28.68	60.33	224.09	11.22	404.20	25.52	47.14	42.37	15.91	14.42	78.70	338.75	12.66	29.47
C898	109.71	88.64	35.74	72.84	233.08	13.06	493.39	24.51	46.84	37.82	18.95	14.03	103.92	355.66	15.46	29.09
C901	118.03	58.33	20.73	84.73	198.84	11.34	685.40	25.39	49.10	32.42	20.92	23.18	126.46	346.20	13.75	26.10
H894	73.46	35.71	14.06	47.55	135.35	9.44	284.22	18.63	23.16	22.73	13.04	9.56	57.33	226.59	7.48	20.39
H898	73.78	32.29	10.46	44.74	201.57	10.07	278.36	21.17	33.10	19.72	12.56	11.85	56.67	264.12	9.12	22.01
H900	69.89	30.54	10.19	44.06	182.65	11.67	296.80	22.97	38.36	33.23	12.68	10.76	61.26	268.73	10.75	24.54
H902	129.13	65.65	23.36	94.79	184.72	11.78	761.37	26.92	42.66	26.08	23.76	20.37	145.50	331.80	14.27	25.66
Hokitika Beach	104.95	133.38	25.17	61.44	195.58	26.80	501.70	31.39	76.84	38.36	15.24	11.60	89.04	292.92	16.18	61.34
Hokitika River	83.38	67.08	28.61	74.55	187.86	11.03	477.02	25.31	54.58	17.76	14.36	15.49	96.19	260.17	9.56	22.41
Mokonui Beach	54.27	29.71	11.49	35.60	116.13	7.29	354.91	19.19	36.56	16.70	10.94	11.47	67.08	238.10	6.46	16.10
Waitaha Beach (Nth)	87.82	46.45	15.49	52.79	163.69	11.86	520.83	20.51	53.07	33.57	14.90	12.08	92.17	297.07	10.50	25.92
Waitaha River	89.39	45.01	14.56	63.27	180.20	15.19	546.74	24.48	59.44	30.18	15.15	15.02	92.10	279.11	9.30	26.69
Whataroa River	90.13	49.39	18.86	69.77	228.91	13.62	586.20	29.68	64.85	31.28	16.71	16.17	103.40	346.29	12.70	29.12
Gillespies Beach	104.79	38.14	12.12	53.68	188.98	26.78	353.75	20.58	56.68	35.66	12.73	7.42	56.66	308.77	13.68	89.38
Cook River	94.50	45.68	17.80	63.06	178.36	11.59	521.80	21.62	57.72	29.69	16.49	18.76	82.45	362.23	11.09	28.34
Bruce Bay Beach	75.06	34.53	10.71	45.94	174.10	14.28	443.02	20.83	48.68	33.07	12.29	12.86	64.79	189.17	12.34	47.48
Paringa River	81.64	36.39	16.43	63.14	183.02	10.00	423.02	21.73	39.89	25.19	15.09	14.63	71.14	264.07	9.91	21.57
Haast River	45.06	18.28	8.39	33.75	100.60	6.38	255.99	10.60	32.38	18.36	8.85	9.81	47.03	149.01	6.11	12.92
Haast Beach	43.78	22.26	8.32	32.18	88.29	6.72	255.09	18.79	41.94	26.56	8.42	9.46	46.18	146.43	4.73	12.54
Hannahs Clearing Beach	21.94	16.11	10.61	52.00	43.77	3.11	84.56	9.63	15.08	11.68	4.07	7.99	15.62	74.93	1.58	6.21
Martyr River	99.88	1175.49	634.00	66.86	106.20	7.42	297.02	12.35	33.90	18.72	12.86	12.73	75.08	148.46	5.81	18.54
Arawhata River	30.05	26.11	15.83	29.23	51.50	3.71	150.72	7.64	21.72	5.05	6.12	30.47	22.42	98.87	2.38	7.03
Neils Beach	39.70	47.26	13.14	30.90	72.80	5.15	173.21	9.57	29.54	16.28	8.26	10.50	39.71	141.93	3.33	12.42
Jacksons Bay Beach	70.40	70.07	26.34	55.34	163.76	9.94	369.07	30.38	64.54	22.66	13.16	15.93	119.32	61.96	10.96	24.46

Appendix E4: Mean and standard deviations for all marine surface sediments by region. $\bar{x}$=sample mean, s = standard deviation.

	North Shelf (n=6)		Canyon heads (n=10)		Central Shelf (n=16)		South Shelf (n=5)		Haast – Cascade (n=9)	
	$\bar{x}$	s	$\bar{x}$	s	$\bar{x}$	s	$\bar{x}$	s	$\bar{x}$	s
SiO2	72.2	3.1	68.0	4.8	68.8	5.5	69.6	4.7	68.9	5.2
TiO2	0.7	0.1	0.8	0.4	1.1	1.5	1.0	0.4	0.8	0.1
Al2O3	13.5	1.6	12.5	3.2	14.8	2.7	14.7	2.9	15.0	2.6
Fe2O3T	4.3	0.4	8.3	4.6	4.9	1.9	4.5	0.6	4.6	1.2
MnO	0.1	0.0	0.1	0.1	0.1	0.1	0.1	0.0	0.1	0.0
MgO	1.7	0.2	1.8	0.3	1.7	0.4	1.5	0.5	1.9	0.7
CaO	2.1	0.3	2.8	1.4	2.7	0.8	2.5	0.2	2.5	0.6
Na2O	2.9	0.3	2.8	0.9	3.5	0.7	3.9	0.3	3.9	0.3
K2O	2.3	0.4	2.6	0.8	2.3	0.7	1.9	0.9	2.1	0.9
P2O5	0.2	0.0	0.3	0.2	0.2	0.1	0.2	0.0	0.2	0.0
SiO2/Al2O3	5.4	0.8	5.8	1.3	4.9	1.3	5.0	1.4	4.8	1.1
Na2O/K2O	1.3	0.1	1.1	0.5	1.6	0.2	2.5	1.1	2.2	1.0
V	91.2	9.3	105.8	29.4	97.8	24.6	92.9	16.5	99.5	23.1
Cr	55.9	8.4	69.9	26.4	47.2	11.2	44.9	11.0	84.2	75.2
Ni	21.7	3.7	22.4	4.0	18.7	4.1	17.5	4.5	28.6	19.4
Zn	69.6	11.3	81.1	14.6	71.1	15.0	63.5	21.9	66.3	21.3
Zr	222.2	34.5	212.8	92.0	301.0	307.3	267.5	86.3	210.1	56.3
Nb	11.6	1.3	12.1	3.5	14.8	13.4	13.4	3.3	11.6	1.3
Ba	504.9	77.1	420.7	166.8	503.8	143.2	444.1	208.8	464.9	193.8
La	21.4	1.2	17.6	7.9	26.9	8.7	25.4	3.1	23.7	3.0
Ce	48.5	6.1	47.2	13.0	59.1	24.1	62.3	13.4	41.1	8.3
Nd	42.1	4.4	28.2	7.9	41.1	10.4	32.8	9.5	32.5	9.1
Ga	16.7	1.7	15.3	4.1	17.8	3.0	16.3	4.1	17.2	4.4
Pb	16.7	2.6	37.9	25.4	16.2	4.1	14.9	2.0	15.3	4.5
Rb	107.1	16.5	103.2	20.4	100.6	28.3	85.3	38.2	94.5	38.0
Sr	316.7	12.2	296.1	49.3	387.5	72.0	335.5	28.7	311.6	47.6
Th	12.0	1.5	10.3	3.8	13.6	7.3	13.6	2.8	12.6	3.0
Y	25.5	2.6	24.0	6.1	30.5	15.5	29.1	3.4	26.3	3.9

Appendix E5: Mean and standard deviations for all marine surface sediments by depositional environment.

	Inner Shelf (n=16)		Middle Shelf (n=14)		Outer shelf - upper slope (n=6)		Canyons (n=10)		Rivers (n=8)		Beaches (n=9)	
	$\bar{x}$	s	$\bar{x}$	s	$\bar{x}$	s	$\bar{x}$	s	$\bar{x}$	s	$\bar{x}$	s
SiO2	73.5	4.1	66.0	2.1	66.9	3.9	68.0	4.8	74.0	7.6	77.7	7.7
TiO2	1.2	1.5	0.7	0.1	0.7	0.1	0.8	0.4	0.7	0.3	1.0	1.0
Al2O3	12.1	0.7	16.7	1.2	16.2	1.9	12.5	3.2	11.6	2.6	10.0	2.4
Fe2O3T	4.2	1.9	5.1	0.4	5.0	1.0	8.3	4.6	4.3	1.6	4.5	3.1
MnO	0.1	0.1	0.1	0.0	0.1	0.0	0.1	0.1	0.1	0.0	0.2	0.3
MgO	1.3	0.4	2.0	0.2	2.0	0.5	1.8	0.3	3.0	4.7	1.1	0.5
CaO	2.5	0.9	2.5	0.3	2.5	0.3	2.8	1.4	1.7	0.7	1.6	0.8
Na2O	3.2	0.7	4.0	0.4	3.6	0.4	2.8	0.9	2.9	0.6	2.2	0.5
K2O	1.5	0.4	2.8	0.4	2.7	0.6	2.6	0.8	1.7	0.6	1.4	0.7
P2O5	0.2	0.1	0.2	0.0	0.2	0.0	0.3	0.2	0.1	0.0	0.1	0.0
SiO2/Al2O3	6.1	0.5	4.0	0.4	4.2	0.8	5.8	1.3	6.8	2.4	8.5	3.5
Na2O/K2O	2.2	0.9	1.5	0.3	1.4	0.3	1.1	0.5	2.3	1.9	2.4	2.6
V	85.7	22.2	104.6	14.9	105.9	17.9	105.8	29.4	76.8	25.2	67.0	29.3
Cr	53.8	59.4	60.5	13.9	60.9	14.9	69.9	26.4	182.9	401.3	48.7	35.5
Ni	18.4	14.3	23.6	4.7	25.0	9.3	22.4	4.0	94.3	218.1	14.8	6.5
Zn	53.6	9.7	80.5	9.9	81.0	11.7	81.1	14.6	58.0	16.8	46.7	11.1
Zr	333.4	302.8	204.1	19.9	197.4	19.3	212.8	92.0	152.1	59.2	134.1	55.3
Nb	15.9	13.3	11.3	0.7	11.0	1.3	12.1	3.5	9.9	3.8	12.4	8.8
Ba	352.3	84.4	592.4	111.2	594.2	100.0	420.7	166.8	407.3	156.1	339.6	146.2
La	25.6	9.0	24.8	3.2	23.8	2.9	17.6	7.9	19.2	7.9	20.1	7.6
Ce	55.6	26.5	53.4	11.1	47.0	4.3	47.2	13.0	45.6	15.6	47.0	18.7
Nd	40.7	12.0	34.4	6.1	39.0	9.4	28.2	7.9	22.0	8.9	26.1	9.7
Ga	14.5	2.0	19.3	2.1	19.9	2.8	15.3	4.1	13.2	3.8	11.1	3.6
Pb	13.5	2.7	18.4	3.4	16.4	2.9	37.9	25.4	16.6	6.2	11.0	2.6
Rb	70.7	18.0	119.6	16.8	120.6	21.4	103.2	20.4	73.7	27.1	65.6	31.2
Sr	348.9	95.1	352.0	15.4	345.3	29.7	296.1	49.3	238.5	96.6	194.6	95.0
Th	14.3	7.4	11.9	2.1	12.9	2.4	10.3	3.8	8.4	3.3	8.9	5.0
Y	31.4	15.6	26.3	1.6	25.5	1.9	24.0	6.1	20.8	7.8	32.9	27.7

Appendix E6: Raw XRF major and trace element results for South Westland canyon core samples. Major elements are in wt % and trace element values are in parts per million (ppm)

	TAN0513 - 15				TAN0513 - 19				TAN0513 - 21			TAN0712 - 17	
Sample_ID	T15B	T15C	T15D	T15E	T19B	T19C	T19D	T19E	T21C	T21D	T21E	T17A	T17B
Core sample depth (cm)	32.5	57.5	87.5	252.5	32.5	72.5	87.5	252.5	47.5	62.5	192.5	42.5	122.5
SiO2	33.43	39.03	41.98	39.29	19.43	23.18	22.42	16.39	17.50	16.83	12.95	51.25	49.04
TiO2	0.39	0.48	0.51	0.50	0.28	0.34	0.32	0.24	0.28	0.27	0.21	0.71	0.74
Al2O3	10.05	11.64	12.54	12.76	6.41	7.77	7.59	5.69	5.93	5.59	4.30	17.38	15.45
Fe2O3T	3.11	3.87	4.15	4.17	2.53	2.93	2.87	2.22	2.51	2.28	1.77	6.07	5.91
MnO	0.04	0.05	0.05	0.05	0.03	0.04	0.03	0.03	0.03	0.03	0.02	0.07	0.07
MgO	1.43	1.76	1.88	1.85	1.23	1.47	1.45	1.13	1.32	1.21	0.96	2.67	2.91
CaO	25.60	20.50	17.90	19.26	36.67	32.70	33.14	39.02	37.79	38.73	42.45	7.39	10.27
Na2O	1.92	2.04	2.18	2.19	1.01	1.41	1.41	0.91	0.97	0.95	0.73	2.60	2.50
K2O	1.94	2.31	2.51	2.64	1.37	1.66	1.62	1.23	1.27	1.18	0.90	3.72	3.10
P2O5	0.13	0.13	0.13	0.14	0.08	0.09	0.09	0.09	0.08	0.07	0.07	0.16	0.17
LOI	21.84	17.87	15.83	16.82	30.52	27.82	28.32	32.58	32.01	32.17	34.49	7.69	9.61
Total	99.88	99.67	99.66	99.66	99.55	99.40	99.26	99.53	99.68	99.30	98.83	99.71	99.75
V	78	87	91	98	66	69	69	58	64	59	48	137	126
Cr	47	59	61	58	40	46	44	38	45	42	34	82	101
Ni	19	24	24	23	19	21	21	18	21	19	18	34	42
Zn	66	78	82	82	58	66	63	56	61	55	49	108	101
Zr	104	116	126	116	64	74	73	55	62	61	51	149	153
Nb	8	9	9	9	6	7	6	6	6	6	5	12	12
Ba	550	598	597	691	608	581	617	513	692	658	708	965	732
La	14	15	20	20	13	11	11	8	5	7	<5	19	21
Ce	26	36	46	38	10	21	16	6	14	19	15	40	39
Nd	38	42	37	37	49	35	41	45	40	44	48	31	35
Ga	14	16	17	18	10	12	11	9	9	9	6	24	21
Pb	5	10	12	11	5	9	8	5	2	<1	1	16	16
Rb	91	111	118	122	63	80	78	55	57	53	40	166	142
Sr	929	779	699	785	1163	993	1042	1263	1075	1120	1239	462	488
Th	9	11	11	13	7	8	7	4	6	5	5	14	14
Y	16	20	20	20	16	15	14	15	16	16	14	22	23
Y/Al	3.09	3.17	3.05	2.98	4.66	3.72	3.42	4.90	5.09	5.29	6.09	2.39	2.83
SiO2/Al2O3	3.33	3.35	3.35	3.08	3.03	2.98	2.95	2.88	2.95	3.01	3.01	2.95	3.17
Cr/V	0.60	0.68	0.67	0.59	0.61	0.67	0.65	0.65	0.70	0.71	0.70	0.60	0.80
Y/Ni	0.87	0.83	0.86	0.87	0.82	0.73	0.67	0.82	0.77	0.84	0.78	0.65	0.55

Appendix E7: Pearson correlation analysis (r) for all shelf and canyon surface sediments, water depth, and mean grain size. Significant correlation at the 0.01 level with correlation coefficients > 0.6 are highlighted in bold. (n=46).

	SiO_2	TiO_2	Al_2O_3	Fe_2O_3T	MnO	MgO	CaO	Na_2O	K_2O	P_2O_5	V	Cr	Ni	Zn
SiO_2	1.00													
TiO_2	-0.22	1.00												
Al_2O_3	**-0.61**	-0.21	1.00											
Fe_2O_3T	-0.57	0.30	-0.25	1.00										
MnO	-0.25	**0.93**	-0.19	0.35	1.00									
MgO	**-0.76**	-0.21	**0.65**	0.29	-0.14	1.00								
CaO	-0.27	0.50	-0.18	0.27	0.43	0.01	1.00							
Na_2O	-0.19	-0.34	**0.75**	-0.55	-0.39	0.27	-0.23	1.00						
K_2O	**-0.77**	-0.32	0.58	0.48	-0.22	**0.80**	-0.16	0.09	1.00					
P_2O_5	-0.43	0.39	-0.33	**0.85**	0.36	0.11	0.35	-0.42	0.16	1.00				
V	**-0.81**	0.38	0.30	**0.69**	0.37	0.56	0.23	-0.19	0.57	0.58	1.00			
Cr	-0.27	-0.06	0.01	0.29	-0.03	0.62	0.13	-0.09	0.21	0.26	0.35	1.00		
Ni	-0.42	-0.02	0.26	0.18	0.02	**0.78**	0.17	0.06	0.30	0.17	0.40	**0.90**	1.00	
Zn	**-0.79**	-0.10	0.55	0.50	0.02	**0.74**	-0.04	-0.01	**0.91**	0.17	**0.71**	0.20	0.33	1.00
Zr	-0.13	**0.98**	-0.22	0.20	**0.90**	-0.25	0.49	-0.33	-0.39	0.33	0.29	-0.04	0.00	-0.17
Nb	-0.23	1.00	-0.19	0.30	**0.93**	-0.19	0.48	-0.35	-0.30	0.39	0.40	-0.05	0.00	-0.08
Ba	-0.55	-0.23	**0.87**	-0.15	-0.19	**0.62**	-0.22	0.43	0.67	-0.33	0.44	0.01	0.24	**0.72**
La	-0.14	**0.71**	0.23	-0.24	0.62	-0.11	0.32	0.15	-0.32	-0.04	0.17	-0.13	0.04	-0.13
Ce	-0.22	**0.82**	0.01	0.11	**0.77**	-0.16	0.33	-0.17	-0.20	0.20	0.31	-0.14	-0.05	0.01
Nd	-0.01	0.57	-0.08	-0.01	0.45	-0.08	0.16	-0.24	-0.24	0.14	0.21	0.11	0.16	-0.15
Ga	**-0.73**	0.07	**0.88**	0.00	0.06	**0.66**	-0.03	0.41	0.63	-0.11	**0.62**	0.07	0.32	**0.70**
Pb	-0.37	-0.04	-0.30	**0.87**	0.05	0.22	0.07	-0.50	0.44	**0.78**	0.51	0.27	0.14	0.43
Rb	**-0.69**	-0.35	**0.76**	0.18	-0.26	**0.80**	-0.24	0.25	**0.93**	-0.12	0.49	0.14	0.32	**0.88**
Sr	-0.31	0.67	0.22	-0.05	0.51	0.01	0.53	0.03	-0.12	0.12	0.31	-0.08	0.07	0.00
Th	-0.19	**0.87**	0.04	0.03	**0.78**	-0.10	0.37	-0.16	-0.29	0.17	0.36	-0.06	0.09	-0.08
Y	-0.22	**0.96**	-0.10	0.18	**0.90**	-0.15	0.44	-0.23	-0.32	0.32	0.35	0.00	0.06	-0.12
Depth	-0.40	-0.21	0.25	0.25	-0.15	0.44	0.16	0.01	0.50	0.09	0.24	0.10	0.22	0.47
M.G.S.	0.48	0.28	**-0.85**	0.23	0.20	-0.58	0.16	-0.53	-0.57	0.35	-0.23	-0.01	-0.23	-0.59

Appendix E7: Pearson correlation analysis continued.

Zr	Nb	Ba	La	Ce	Nd	Ga	Pb	Rb	Sr	Th	Y	Depth	M.G.S.
1.00													
0.98	1.00												
-0.25	-0.20	1.00											
0.76	**0.72**	0.16	1.00										
0.85	**0.83**	0.02	**0.78**	1.00									
0.61	0.58	-0.04	0.54	0.54	1.00								
0.05	0.10	**0.91**	0.37	0.23	0.18	1.00							
-0.13	-0.03	-0.16	-0.48	-0.19	-0.20	-0.15	1.00						
-0.40	-0.33	**0.87**	-0.17	-0.17	-0.19	**0.78**	0.18	1.00					
0.71	**0.68**	0.19	**0.81**	**0.77**	**0.62**	0.43	-0.30	-0.05	1.00				
0.87	**0.88**	0.03	**0.79**	**0.79**	**0.65**	0.30	-0.26	-0.21	**0.74**	1.00			
0.98	**0.97**	-0.15	**0.81**	**0.88**	**0.66**	0.16	-0.16	-0.32	**0.76**	**0.90**	1.00		
-0.25	-0.20	0.29	-0.21	-0.21	-0.36	0.26	0.26	0.48	-0.14	-0.16	-0.26	1.00	
0.26	0.25	**-0.84**	-0.15	-0.02	0.09	**-0.74**	0.15	**-0.76**	-0.20	0.05	0.18	-0.37	1

Appendix E8: Bulk sediment major and trace element ratios used in this study of SWCM sediments.

SAMPLE	TRANSECT	SiO_2/Al_2O_3	Na_2O/K_2O	$Log(SiO_2/Al_2O_3)$	$Log(Na_2O/K_2O)$	Cr/V	Y/Ni
H843	A	6.09	1.16	0.78	0.07	0.62	1.28
H838	A	4.31	1.13	0.63	0.05	0.66	0.93
H837	A	4.57	1.23	0.66	0.09	0.62	1.10
H833	A	5.32	1.33	0.73	0.12	0.63	0.91
H844	B	6.40	1.46	0.81	0.17	0.54	1.71
H845	B	5.90	1.39	0.77	0.14	0.59	1.35
H848	B	5.31	1.26	0.73	0.10	0.62	1.77
H850	B	7.03	1.31	0.85	0.12	0.66	1.16
H851	B	6.71	0.73	0.83	-0.14	0.88	0.94
B469	B	6.66	0.91	0.82	-0.04	0.85	1.06
H852	B	6.81	0.38	0.83	-0.42	0.81	0.85
R208	B	5.50	1.92	0.74	0.28	0.56	1.58
P668	B_sth	3.37	1.28	0.53	0.11	0.54	0.92
C905	B_sth	3.67	1.33	0.56	0.12	0.57	0.94
H882	E	5.86	0.77	0.77	-0.11	0.49	0.92
H893	F	6.63	1.60	0.82	0.20	0.59	0.83
H854	C	6.79	1.74	0.83	0.24	0.44	2.21
H855	C	7.15	2.11	0.85	0.32	0.42	2.52
H858	C	5.62	1.65	0.75	0.22	0.48	1.48
H862	C	3.80	1.44	0.58	0.16	0.54	1.11
H864	C	3.71	1.38	0.57	0.14	0.51	1.20
H865	C	4.10	1.64	0.61	0.22	0.53	1.36
P663	C_D	5.55	1.55	0.74	0.19	0.48	1.45
S368	C_D	3.78	1.16	0.58	0.06	0.55	1.01
H874	D	6.32	1.92	0.80	0.28	0.46	2.25
H873	D	6.26	1.72	0.80	0.23	0.46	2.06
H867	D	4.82	1.51	0.68	0.18	0.52	1.41
H866	D	4.08	1.63	0.61	0.21	0.55	1.29
H876	E	5.07	1.61	0.71	0.21	0.29	4.17
H877	E	3.74	1.20	0.57	0.08	0.51	1.08
H878	E	3.43	1.46	0.54	0.16	0.55	1.41
H879	E	3.63	1.29	0.56	0.11	0.52	1.13
H884	F	6.43	3.83	0.81	0.58	0.45	2.76
H885	F	6.40	3.50	0.81	0.54	0.45	2.29
H888	F	4.54	2.08	0.66	0.32	0.48	1.51
H890	F	3.68	1.44	0.57	0.16	0.50	1.23
H891	F	3.77	1.46	0.58	0.17	0.52	1.21
H894	Haast _Cascade	5.62	3.66	0.75	0.56	0.49	1.45
H900	Haast _Cascade	6.45	2.76	0.81	0.44	0.44	2.41
B474	Haast _Cascade	5.44	2.40	0.74	0.38	2.87	0.47
H898	Haast _Cascade	5.98	3.44	0.78	0.54	0.44	2.10
B622	Haast _Cascade	4.74	2.33	0.68	0.37	0.83	1.03
C898	Haast _Cascade	4.19	1.64	0.62	0.22	0.81	0.81

SAMPLE	TRANSECT	SiO_2/Al_2O_3	Na_2O/K_2O	$Log(SiO_2/Al_2O_3)$	$Log(Na_2O/K_2O)$	Cr/V	Y/Ni
C901	Haast _Cascade	3.70	1.38	0.57	0.14	0.49	1.26
H902	Haast _Cascade	3.45	1.07	0.54	0.03	0.51	1.10
E786	Haast _Cascade	3.41	0.99	0.53	0.00	0.70	0.60
AA2	Hokitika Beach	5.33	0.96	0.73	-0.02	1.27	2.44
AB2	Hokitika River	6.35	1.19	0.80	0.08	0.80	0.78
AF3	Mokonui Beach	8.19	1.54	0.91	0.19	0.55	1.40
AG2	Waitaha Beach (Nth)	6.08	1.14	0.78	0.06	0.53	1.67
AH3	Waitaha River	5.46	1.37	0.74	0.14	0.50	1.83
AK2	Whataroa River	5.44	1.12	0.74	0.05	0.55	1.54
AN1	Gillespies Beach	5.32	1.59	0.73	0.20	0.36	7.38
AO2	Cook River	4.96	1.60	0.70	0.21	0.48	1.59
AQ2	Bruce Bay Beach	7.08	1.33	0.85	0.12	0.46	4.43
AR2	Paringa River	5.18	2.53	0.71	0.40	0.45	1.31
AT1	Haast River	10.21	2.30	1.01	0.36	0.41	1.54
AU3	Haast Beach (Nth)	10.81	2.29	1.03	0.36	0.51	1.51
1a	Hannahs Clearing (beach)	16.40	8.99	1.21	0.95	0.73	0.59
2b	Martyr River	5.82	1.26	0.76	0.10	11.77	0.03
3a	Arawhata River	11.10	6.67	1.05	0.82	0.87	0.44
4b	Neils Beach (Sth beach)	10.11	3.70	1.00	0.57	1.19	0.95
5a	Jacksons Bay Beach	7.45	0.49	0.87	-0.31	1.00	0.93

APPENDIX F: DETRITAL MAGNETITES

F1: Sample preparation and microprobe use

F2: Microporbe results

F3: SWCM detrital magnetite descriptive statistics by region

F4: Descriptive statistics by spinel grain type

Appendix F1: <u>Stub preparation (University of Canterbury)</u>

A total of 254 magnetite grains were analysed from 20 shelf and 9 Beach/River samples. The magnetic fraction was first removed from the heavy mineral separate using the procedures outlined in Appendix C8. Up to 15 magnetite grains per sample were then hand picked at random from the magnetic fraction under a binocular microscope using a needle. The magnetite grains were then placed onto double sided tape and affixed to the bottom of 1-inch plastic moulds with the grains facing up. Grains from each sample were arranged in rows and a sketch map was made to keep track these rows (Figure F1, B). An epoxy resin (Epotek 301) was then added using an eye dropper and the moulds were left to set for at least 24 hours. Five stubs in total contained the 254 grains. Once set, the epoxy moulds were ground until the core of the grains were exposed and then sanded with 1200, followed by 2000 grit sand paper. Polishing then commenced with 3 µm followed by 1 µm diamond paste.

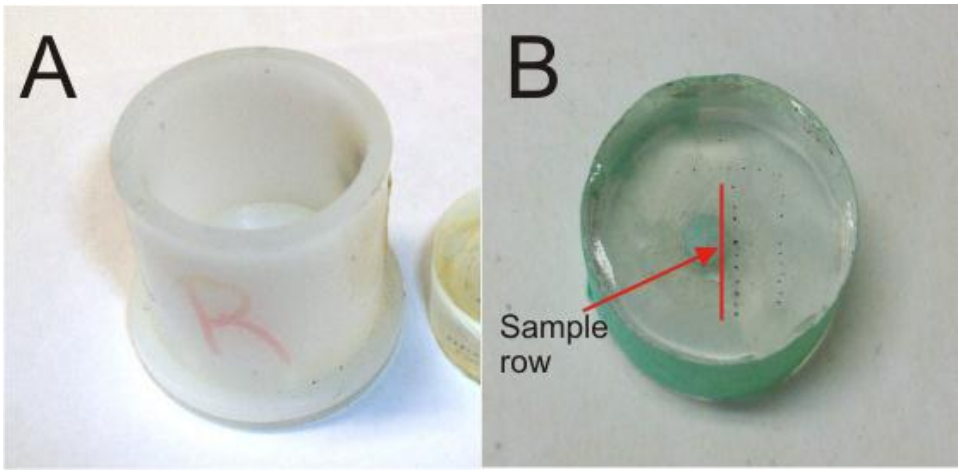

Figure F1: A) Plactic 1 inch mould used for making epoxy stubs. B) Finished epoxy stub with with polished magnetite grains aligned by sediment sample.

<u>Microprobe (Victoria University)</u>

Detrital magnetites from the SWCM were analysed at Victoria University, Wellington on the JEOL JXA-8230 SuperProbe Electron Probe Microanalyser (Figure F2). A combination of 5 wavelength dispersive X-ray spectrometres (WDS) were used to analyse the weight percent of Al_2O_3, MgO, TiO_2, V_2O_3, FeO, Cr_2O_3, Fe_2O_3, MnO in individual grains. A 5 µm beam diametre was typically used but this was reduced to 2 µm when only small areas of polished grain were exposed. Three points per grain were analysed and then averaged to reduce the effects of internal variation in composition. Standards used are outlined below in Table F1.Back scatter images were taken for selected grains, particularly those with anomalous values of Cr. FeO has been recalculated to give FeO and Fe2O3 based on the 32 oxygen method. Weight % oxides, elemental concentration of Cr, and parts per million Cr are provided in Appendix F2. Cr proved the most useful proxy for provenance/dispersal in this study.

Table F1: Standards used to calibrate oxides measured in the microprobe analysis of SWCM detrital magnetites.

Oxide	Standard
TiO2	Ilmenite 96189
MgO	Cr-Augite
FeO	Magnetite Minas Gerais, Brazil
MnO	Ilmenite 96189
Cr2O3	Cr-Augite
Al2O3	Cr-Augite
V2O3	Vanadinite

Figure F2: The JEOL JXA-8230 SuperProbe at Victoria University, Wellington.

Appendix F2 : Microporbe results for oxides in individual detrital magnetite grains (wt. %), elemental Cr by wt, and Cr in parts per million (ppm). FeO and Fe2O3 have been recalculated based on 32 oxygens.

Transect	Sample-grain	MgO	Al_2O_3	TiO_2	V_2O_3	Cr_2O_3	MnO	FeO	Fe_2O_3	Total	Cr	Cr ppm
A	H843-3	0.01	0.07	0.00	0.19	0.21	0.08	46.06	51.29	97.91	0.14	1426
A	H843-4	0.01	0.04	0.05	0.04	0.01	0.31	45.91	51.34	97.72	0.01	100
A	H843-5	0.01	0.20	0.14	0.12	0.00	0.06	46.08	51.16	97.78	0.00	33
A	H843-6	0.01	0.03	0.01	0.15	0.20	0.08	46.07	51.29	97.83	0.14	1362
A	H843-7	0.36	0.10	0.01	0.03	10.52	0.45	36.67	40.97	89.10	7.20	71952
A	H843-9	0.04	0.08	0.09	0.08	0.29	0.08	45.65	50.82	97.14	0.20	1991
A	H843-10	0.01	0.05	0.03	0.07	1.09	0.04	45.87	51.00	98.15	0.74	7436
A	H843-11	0.02	0.51	0.08	0.10	0.04	2.23	41.61	48.69	93.28	0.03	287
A	H843-13	0.02	0.07	0.07	0.07	0.00	0.09	45.87	51.04	97.21	0.00	10
A	H843-14	0.00	0.04	0.03	0.07	0.04	0.09	45.97	51.17	97.41	0.03	274
A	H843-15	0.00	0.01	0.01	0.05	0.12	0.06	45.96	51.15	97.37	0.08	843
A	H844-1	0.01	0.09	0.08	0.11	0.05	0.01	46.17	51.25	97.77	0.03	333
A	H844-2	0.01	0.03	0.00	0.03	0.03	0.13	46.00	51.27	97.51	0.02	233
A	H844-3	0.03	0.17	0.08	0.06	0.05	0.01	45.79	50.88	97.09	0.03	327
A	H844-4	0.01	0.01	0.00	0.07	0.09	0.04	45.98	51.17	97.38	0.06	610
A	H844-5	0.02	0.06	0.05	0.07	0.02	0.35	45.52	50.97	97.06	0.01	140
A	H844-6	0.00	0.01	0.00	0.07	0.02	0.06	45.58	50.72	96.46	0.01	147
A	H844-7	0.00	0.01	0.00	0.06	0.05	0.08	46.20	51.42	97.82	0.03	349
A	H844-10	0.01	0.19	0.04	0.08	0.01	0.01	46.20	51.34	97.88	0.01	51
A	H844-11	0.02	0.13	0.07	0.11	0.01	0.01	46.25	51.37	97.97	0.00	37
A	H844-12	0.02	0.16	0.18	0.10	0.01	0.06	46.03	51.08	97.65	0.00	40
A	H844-13	0.00	0.02	0.00	0.00	0.07	0.37	45.45	50.93	96.83	0.05	480
A	H844-14	0.00	0.04	0.05	0.05	0.00	0.06	46.52	51.72	98.43	0.00	0
B	H850-2	0.01	0.09	0.07	0.10	0.13	0.03	46.13	51.25	97.81	0.09	911
B	H850-3	0.01	0.07	0.03	0.09	0.10	0.03	46.30	51.48	98.11	0.07	676
B	H850-5	0.04	0.41	0.89	0.22	0.03	0.84	45.20	50.31	97.94	0.02	230
B	H850-6	0.01	0.13	0.02	0.18	0.03	0.03	46.24	51.42	98.05	0.02	217
B	H850-7	0.01	0.02	0.01	0.10	0.04	0.13	45.83	51.08	97.22	0.03	306
B	H850-8	0.01	0.25	0.19	0.11	0.25	0.04	46.02	51.01	97.88	0.17	1683
B	H850-10	0.01	0.05	0.02	0.07	0.10	0.09	45.35	50.51	96.22	0.07	705
B	B469-1	0.00	0.05	0.01	0.10	0.03	0.03	46.21	51.39	97.81	0.02	176
B	B469-2	0.01	0.11	0.07	0.10	0.08	0.05	45.90	51.02	97.34	0.05	525
B	B469-3	0.00	0.13	0.06	0.34	0.64	0.02	45.87	50.93	97.98	0.44	4357
B	H852-1	0.00	0.04	0.02	0.18	0.13	0.09	45.71	50.88	97.07	0.09	922
B	H852-3	0.01	0.02	0.07	0.15	0.15	0.03	44.31	49.23	93.98	0.11	1051
B	H852-4	0.42	1.51	6.27	0.30	0.02	0.39	45.29	43.67	97.87	0.01	121
B	H852-5	0.01	0.04	0.03	0.08	0.06	0.04	46.22	51.40	97.89	0.04	443
B	H852-6	0.00	0.00	0.00	0.11	0.14	0.04	46.12	51.29	97.71	0.09	936
B	H852-7	0.01	0.26	0.21	0.36	2.17	0.06	45.16	49.98	98.21	1.48	14843
B	H852-9	0.00	0.03	0.01	0.03	0.03	0.04	45.25	50.32	95.70	0.02	193
B_sth	C905	0.00	0.02	0.01	0.04	0.01	0.01	45.22	50.26	95.58	0.01	81
C	H865-3	0.00	0.02	0.01	0.08	0.02	0.03	46.11	51.27	97.54	0.01	137
C	H865-4	0.00	0.04	0.06	0.05	0.01	0.33	46.05	51.49	98.03	0.00	40
D	H874-1	0.01	0.04	0.03	0.10	0.52	0.04	45.80	50.93	97.55	0.36	3553
D	H874-2	0.03	0.23	0.04	0.09	0.04	0.08	45.83	51.04	97.45	0.03	298
D	H874-6	0.01	0.11	0.06	0.12	0.07	0.03	45.71	50.78	96.98	0.05	489
D	H874-7	0.03	0.04	0.05	0.16	0.01	0.01	45.58	50.68	96.67	0.01	96
D	H874-9	0.03	0.16	0.12	0.18	0.01	0.05	45.96	51.06	97.71	0.00	40
D	H874-11	0.02	0.08	0.05	0.09	0.06	0.05	45.65	50.79	96.85	0.04	431
D	H874-12	0.01	0.07	0.05	0.11	0.24	0.03	45.67	50.76	97.01	0.16	1639
D	H874-13	0.03	0.21	0.09	0.18	0.00	0.04	45.89	51.01	97.57	0.00	32
D	H874-14	0.03	0.19	0.07	0.11	0.27	0.04	45.70	50.81	97.28	0.18	1822

D	H874-15	0.01	0.04	0.01	0.05	0.24	0.07	46.05	51.25	97.77	0.17	1673
Transect	**Sample-grain**	**MgO**	**Al_2O_3**	**TiO_2**	**V_2O_3**	**Cr_2O_3**	**MnO**	**FeO**	**Fe_2O_3**	**Total**	**Cr**	**Cr ppm**
E	H876-1	0.02	0.12	0.05	0.09	0.01	0.04	45.83	50.98	97.22	0.01	59
E	H876-2	0.01	0.08	0.03	0.10	0.17	0.05	45.67	50.80	96.98	0.12	1172
E	H876-3	0.00	0.02	0.00	0.01	0.02	0.05	16.13	17.98	34.24	0.02	169
E	H876-5	0.01	0.09	0.04	0.05	0.50	0.03	44.19	49.13	94.07	0.34	3417
E	H876-8	0.02	0.08	0.06	0.14	0.01	0.04	42.65	47.42	90.51	0.00	34
E	H876-7	1.09	1.09	0.12	0.09	0.07	0.01	38.16	44.42	85.12	0.05	452
E	H879-1	0.02	0.51	0.69	0.20	0.02	0.09	45.74	50.25	97.50	0.01	110
E	H879-2	0.00	0.19	0.24	0.05	0.01	0.02	45.69	50.55	96.75	0.00	44
E	H879-3	0.05	0.15	0.10	0.05	0.27	0.02	45.73	50.84	97.22	0.19	1881
E	H879-4	0.00	0.04	0.05	0.08	0.00	0.03	45.67	50.74	96.61	0.00	0
E	H879-5	0.00	0.03	0.01	0.04	0.00	0.08	45.98	51.18	97.33	0.00	10
E	H879-6	0.05	0.10	0.09	0.12	0.02	0.03	45.69	50.82	96.91	0.01	113
E	H879-7	0.01	0.02	0.00	0.03	0.05	0.08	45.80	51.00	97.00	0.04	375
E	H879-8	0.01	0.03	0.00	0.06	0.02	0.06	46.11	51.33	97.63	0.01	103
E	H879-9	0.02	0.32	0.26	0.15	0.01	0.03	45.83	50.74	97.36	0.01	59
E	H879-10	0.00	0.01	0.01	0.06	0.00	0.04	46.07	51.24	97.43	0.00	18
E	H879-11	0.01	0.01	0.01	0.05	0.06	0.04	45.73	50.87	96.77	0.04	378
E	H879-12	0.03	0.10	0.02	0.11	0.01	0.02	45.57	50.71	96.57	0.01	71
E	H882-1	0.01	0.11	0.07	0.45	0.03	0.02	46.20	51.30	98.19	0.02	196
E	H882-2	0.03	0.02	0.01	0.04	0.10	0.06	45.75	50.95	96.96	0.07	669
E	H882-3	0.01	0.03	0.01	0.04	0.01	0.05	45.99	51.17	97.31	0.01	54
E	H882-4	0.05	0.21	0.08	0.09	0.01	0.06	45.77	50.95	97.21	0.01	66
E	H882-6	0.00	0.07	0.24	0.20	0.01	0.03	46.35	51.30	98.20	0.01	100
E	H882-7	0.00	0.11	0.05	0.07	0.02	0.04	45.71	50.79	96.79	0.01	110
E	H882-8	0.01	0.02	0.00	0.04	0.00	0.07	45.89	51.09	97.12	0.00	0
E	H882-9	0.01	0.22	0.16	0.07	0.01	0.04	45.91	50.92	97.35	0.01	62
E	H882-10	0.02	0.18	0.09	0.11	0.02	0.10	46.03	51.21	97.76	0.01	108
E	H882-11	0.01	0.04	0.01	0.05	0.03	0.06	45.98	51.17	97.36	0.02	231
E	H882-12	0.00	0.02	0.01	0.04	0.06	0.11	45.96	51.20	97.40	0.04	419
F	H888-5	0.01	0.00	0.00	0.06	0.13	0.13	46.16	51.46	97.96	0.09	887
F	H888-6	0.01	0.09	0.06	0.02	0.00	0.04	46.28	51.44	97.95	0.00	0
F	H888-7	0.00	0.11	0.11	0.14	0.00	0.02	46.33	51.40	98.11	0.00	29
F	H884-1	0.00	0.04	0.01	0.14	0.02	0.05	45.73	50.87	96.87	0.02	162
F	H884-2	0.01	0.05	0.05	0.14	0.00	0.04	46.10	51.24	97.63	0.00	10
F	H884-4	0.01	0.00	0.00	0.07	0.34	0.01	45.99	51.12	97.53	0.23	2307
F	H884-5	0.02	0.03	0.04	0.08	0.00	0.03	46.22	51.42	97.84	0.00	0
F	H884-6	0.01	0.03	0.03	0.19	0.09	0.02	46.12	51.27	97.76	0.06	598
F	H884-7	0.01	0.07	0.04	0.08	0.04	0.07	46.04	51.23	97.57	0.02	240
F	H884-8	0.01	0.02	0.01	0.16	0.01	0.02	46.37	51.55	98.16	0.01	96
F	H884-9	0.00	0.03	0.03	0.05	0.00	0.00	45.74	50.81	96.66	0.00	0
F	H884-11	0.00	0.06	0.11	0.02	0.00	0.12	45.79	50.92	97.02	0.00	17
F	H884-13	0.00	0.14	0.05	0.09	0.05	0.00	45.83	50.88	97.04	0.04	360
F	H884-14	0.01	0.03	0.00	0.15	0.07	0.05	45.96	51.15	97.41	0.05	458
F	H884-15	0.01	0.02	0.00	0.15	0.02	0.03	45.91	51.06	97.19	0.02	158
F	H893-1	0.02	0.08	0.11	0.04	0.03	0.06	46.01	51.14	97.49	0.02	220
F	H893-2	0.01	0.03	0.01	0.05	0.03	0.12	45.74	50.96	96.95	0.02	239
F	H893-3	0.01	0.08	0.04	0.13	0.00	0.07	45.89	51.06	97.30	0.00	29
F	H893-4	0.01	0.03	0.01	0.11	0.00	0.02	46.03	51.18	97.39	0.00	12
F	H893-5	0.02	0.09	0.07	0.11	2.16	0.03	45.23	50.22	97.94	1.47	14747
F	H893-6	0.01	0.07	0.03	0.03	0.00	0.05	45.81	50.96	96.96	0.00	11
F	H893-7	0.02	0.01	0.00	0.03	0.01	0.44	45.21	50.77	96.50	0.01	59
F	H893-8	0.01	0.04	0.05	0.11	0.01	0.14	45.89	51.11	97.35	0.01	76
F	H893-9	0.01	0.07	0.04	0.04	0.03	0.09	46.11	51.32	97.70	0.02	223
F	H893-10	0.03	0.06	0.03	0.15	0.03	0.01	45.45	50.55	96.31	0.02	171
F	H893-11	0.01	0.05	0.02	0.09	0.01	0.07	45.91	51.11	97.28	0.01	73

F	H893-13	0.01	0.02	0.03	0.13	0.12	0.05	46.15	51.32	97.84	0.09	852
Transect	**Sample-grain**	**MgO**	**Al_2O_3**	**TiO_2**	**V_2O_3**	**Cr_2O_3**	**MnO**	**FeO**	**Fe_2O_3**	**Total**	**Cr**	**Cr ppm**
F	H893-14	0.00	0.02	0.00	0.16	0.01	0.06	45.90	51.09	97.26	0.01	91
F	H893-15	0.01	0.03	0.00	0.03	0.00	0.03	45.98	51.15	97.23	0.00	22
F	H893-16	0.01	0.06	0.03	0.09	0.15	0.02	45.49	50.57	96.43	0.10	1024
South Shelf	C901-1	0.00	0.03	0.02	0.06	0.00	0.02	45.66	50.75	96.54	0.00	15
South Shelf	C901-2	0.00	0.02	0.02	0.08	0.14	0.01	45.79	50.88	96.95	0.10	988
South Shelf	C901-3	0.03	0.14	0.10	0.11	0.01	0.04	45.56	50.64	96.63	0.00	34
South Shelf	C901-4	0.04	0.15	0.07	0.09	0.22	0.11	45.48	50.68	96.83	0.15	1477
South Shelf	C901-5	0.00	0.03	0.01	0.09	0.01	0.15	45.97	51.25	97.52	0.01	91
South Shelf	C901-6	0.01	0.25	0.15	0.03	0.00	0.01	45.79	50.77	97.01	0.00	22
South Shelf	C901-7	0.03	0.13	0.04	0.15	0.05	0.00	46.06	51.20	97.66	0.03	342
Haast Shelf	H900-1	0.02	0.01	0.00	0.08	0.09	0.05	45.45	50.59	96.28	0.06	588
Haast Shelf	H900-2	0.00	0.02	0.00	0.04	0.01	0.08	46.10	51.32	97.57	0.01	55
Haast Shelf	H900-3	0.00	0.02	0.02	0.08	0.04	0.03	45.93	51.06	97.18	0.03	283
Haast Shelf	H900-7	0.02	0.01	0.00	0.06	0.00	0.02	46.04	51.21	97.37	0.00	22
Haast Shelf	H900-9	0.01	0.03	0.01	0.06	0.01	0.00	46.02	51.15	97.29	0.01	51
Haast Shelf	H894-1	0.01	0.05	0.07	0.01	0.00	0.08	45.87	51.02	97.10	0.00	15
Haast Shelf	H894-2	0.00	0.04	0.01	0.07	0.03	0.07	46.13	51.34	97.70	0.02	209
Haast Shelf	H894-3	0.03	0.03	0.05	0.16	0.01	0.05	45.94	51.12	97.38	0.01	91
Haast Shelf	H894-4	0.00	0.03	0.01	0.07	0.00	0.07	45.73	50.90	96.83	0.00	32
Haast Shelf	H894-5	0.00	0.01	0.00	0.02	0.00	0.08	45.97	51.18	97.25	0.00	0
Haast Shelf	H894-6	0.00	0.04	0.02	0.08	0.01	0.08	46.21	51.42	97.87	0.01	88
Haast Shelf	H894-7	0.00	0.01	0.01	0.11	0.02	0.03	46.16	51.32	97.67	0.01	132
Haast Shelf	H894-9	0.01	0.01	0.01	0.09	0.01	0.03	45.84	50.99	97.00	0.01	66
Haast Shelf	H894-10	0.01	0.03	0.00	0.11	0.00	0.05	46.01	51.20	97.42	0.00	0
Haast Shelf	H894-11	0.02	0.01	0.00	0.06	0.02	0.07	46.12	51.37	97.66	0.01	125
Haast Shelf	H894-12	0.00	0.03	0.02	0.11	0.04	0.06	46.20	51.40	97.85	0.03	252
Haast Shelf	H894-13	0.00	0.00	0.00	0.04	0.19	0.05	46.09	51.28	97.65	0.13	1293
Haast Shelf	H894-15	0.00	0.02	0.00	0.03	0.03	0.05	46.18	51.38	97.71	0.02	206
Haast Shelf	H898-1	0.00	0.01	0.00	0.07	0.02	0.06	45.85	51.02	97.04	0.01	125
Haast Shelf	H898-3	0.01	0.02	0.00	0.09	0.07	0.05	46.06	51.26	97.57	0.05	478
Haast Shelf	H898-4	0.03	0.02	0.00	0.09	0.04	0.03	46.04	51.25	97.50	0.03	287
Haast Shelf	H898-6	0.03	0.03	0.04	0.17	0.02	0.05	45.86	51.03	97.23	0.01	140
Haast Shelf	H898-7	0.00	0.01	0.00	0.12	0.02	0.04	45.85	51.01	97.07	0.01	132
Haast Shelf	H898-9	0.00	0.00	0.00	0.09	0.04	0.05	45.92	51.08	97.19	0.03	304
Haast Shelf	H898-10	0.01	0.01	0.00	0.04	0.01	0.06	46.08	51.29	97.50	0.01	77
Haast Shelf	H898-13	0.01	0.02	0.00	0.12	0.03	0.02	45.58	50.69	96.48	0.02	209
Cascade Shelf	B474-2	13.45	21.53	0.09	0.09	39.26	0.26	13.93	8.69	97.31	26.86	268621
Cascade Shelf	B474-3	11.97	18.47	0.05	0.12	46.85	0.33	16.32	5.64	99.74	32.05	320520
Cascade Shelf	B474-4	8.20	10.89	0.05	0.10	54.56	0.42	21.50	6.19	101.92	37.33	373301
Cascade Shelf	B474-5	10.05	7.65	0.15	0.05	59.88	0.37	18.77	6.40	103.33	40.97	409692
Cascade Shelf	B474-6	0.00	0.01	0.00	0.05	0.02	0.01	46.24	51.39	97.71	0.02	157
Cascade Shelf	B474-8	0.23	0.00	0.03	0.02	1.40	0.08	44.57	50.02	96.35	0.96	9611
Cascade Shelf	B474-9	9.76	7.42	0.14	0.07	59.39	0.38	18.91	6.48	102.55	40.63	406341
Cascade Shelf	B474-10	0.24	0.00	0.01	0.01	2.79	0.17	44.72	50.29	98.24	1.91	19068
Cascade Shelf	B474-11	11.56	16.78	0.06	0.18	47.31	0.31	16.77	6.91	99.89	32.37	323713
Cascade Shelf	B474-12	0.31	0.01	0.08	0.02	0.16	0.06	45.63	51.32	97.59	0.11	1124
Cascade Shelf	B474-13	1.63	0.53	0.46	0.08	45.79	1.33	30.40	20.87	101.09	31.33	313290
Cascade Shelf	B474-14	9.42	11.29	0.59	0.11	51.27	0.37	20.10	8.15	101.31	35.08	350790
Cascade Shelf	B474-15	0.01	0.09	0.21	0.35	0.24	0.01	46.07	51.01	97.99	0.16	1628
Cascade Shelf	C898	0.14	0.24	0.34	0.56	0.59	0.01	45.77	50.76	98.41	0.40	4012
Cascade Shelf	C898	0.88	0.00	0.01	0.02	1.96	0.06	43.76	50.39	97.08	1.34	13437
Cascade Shelf	C898	0.03	0.40	0.05	0.52	0.13	0.02	46.22	51.37	98.73	0.09	896
Cascade Shelf	C898	0.01	0.05	0.02	0.07	0.01	0.00	46.05	51.17	97.37	0.00	47
Cascade Shelf	C898	0.02	0.07	0.01	0.33	0.17	0.00	46.00	51.14	97.73	0.12	1161
Cascade Shelf	C898	0.02	0.07	0.01	0.02	0.00	0.07	46.06	51.29	97.54	0.00	22

Cascade Shelf	C898	0.12	0.00	0.05	0.01	0.90	0.07	45.38	50.68	97.20	0.62	6153
Transect	**Sample-grain**	**MgO**	**Al_2O_3**	**TiO_2**	**V_2O_3**	**Cr_2O_3**	**MnO**	**FeO**	**Fe_2O_3**	**Total**	**Cr**	**Cr ppm**
Cascade Shelf	C898	0.00	0.08	0.10	0.28	0.02	0.05	46.26	51.35	98.14	0.02	152
Cascade Shelf	C898	0.45	0.01	0.06	0.02	5.24	0.17	43.24	48.84	98.03	3.58	35849
Cascade Shelf	C898	0.01	0.31	0.05	0.44	0.18	0.01	46.47	51.61	99.08	0.13	1252
Cascade Shelf	C898	0.01	0.04	0.02	0.21	0.05	0.06	46.31	51.52	98.22	0.03	340
Cascade Shelf	C898	0.01	0.07	0.02	0.34	0.10	0.02	46.16	51.32	98.03	0.07	681
Cascade Shelf	C898	0.01	0.06	5.64	0.31	0.03	0.20	46.60	45.39	98.25	0.02	239
Cascade Shelf	C898	1.76	0.73	0.23	0.14	27.20	0.46	34.34	35.54	100.40	18.61	186110
Hokitika Beach	AA2-1	0.02	0.05	0.00	0.09	1.26	0.05	45.68	50.84	97.97	0.86	8595
Hokitika Beach	AA2-2	0.01	0.10	0.16	0.10	0.01	0.07	44.30	49.17	93.90	0.00	40
Hokitika Beach	AA2-3	0.01	0.07	0.04	0.08	0.02	0.12	46.05	51.30	97.68	0.01	125
Hokitika Beach	AA2-4	0.09	0.04	0.07	0.13	0.41	0.11	45.94	51.28	98.06	0.28	2792
Hokitika Beach	AA2-5	0.03	0.14	0.09	0.04	0.00	0.13	45.96	51.18	97.56	0.00	22
Hokitika Beach	AA2-6	0.02	0.11	0.03	0.04	0.01	0.28	46.06	51.49	98.04	0.01	54
Hokitika Beach	AA2-7	0.02	0.09	0.05	0.04	0.01	0.30	45.78	51.21	97.51	0.01	78
Hokitika Beach	AA2-8	0.10	0.01	0.03	0.06	5.82	0.29	43.72	48.82	98.86	3.98	39787
Hokitika Beach	AA2-9	0.03	0.05	0.01	0.05	0.14	0.10	46.24	51.54	98.15	0.10	955
Hokitika Beach	AA2-10	0.08	0.02	0.02	0.08	7.08	0.11	43.13	47.79	98.31	4.84	48409
Hokitika Beach	AA2-12	0.06	0.09	0.02	0.08	0.03	0.26	45.90	51.39	97.82	0.02	208
Hokitika Beach	AA2-13	0.30	0.24	0.15	0.12	18.90	1.09	38.42	41.38	100.61	12.93	129310
Hokitika River	AB2-1	0.01	0.04	0.00	0.04	1.03	0.14	45.41	50.63	97.29	0.70	7028
Hokitika River	AB2-2	3.02	8.32	0.01	0.03	51.87	1.33	28.06	8.89	101.53	35.49	354855
Hokitika River	AB2-3	0.04	0.05	0.00	0.05	0.20	0.10	45.56	50.83	96.83	0.14	1389
Hokitika River	AB2-4	0.31	0.00	0.00	0.02	2.69	0.06	44.25	49.79	97.12	1.84	18407
Hokitika River	AB2-5	0.16	0.00	0.01	0.05	4.27	0.22	43.83	49.11	97.67	2.92	29245
Hokitika River	AB2-6	0.01	0.04	0.00	0.08	1.81	0.09	45.57	50.74	98.35	1.24	12389
Waitaha River	AH3-1	0.07	0.10	0.00	0.04	0.26	0.10	45.55	50.86	96.96	0.18	1766
Waitaha River	AH3-2	0.19	0.04	0.35	0.16	1.13	0.12	45.30	50.47	97.76	0.78	7757
Waitaha River	AH3-3	0.01	0.09	0.11	0.13	0.04	0.02	46.12	51.19	97.71	0.03	279
Waitaha River	AH3-4	0.02	0.08	0.11	0.10	0.04	0.15	45.95	51.16	97.62	0.03	296
Waitaha River	AH3-5	0.00	0.06	0.12	0.08	0.04	0.15	46.01	51.17	97.63	0.03	296
Waitaha River	AH3-6	0.02	0.09	0.19	0.05	0.01	0.24	45.87	51.09	97.56	0.00	44
Waitaha River	AH3-7	0.01	0.08	0.07	0.06	0.02	0.19	45.94	51.22	97.58	0.01	145
Waitaha River	AH3-8	0.02	0.22	0.00	0.03	0.01	0.05	46.26	51.50	98.09	0.01	61
Waitaha River	AH3-9	0.02	0.09	0.09	0.09	0.06	0.09	45.95	51.11	97.50	0.04	386
Waitaha River	AH3-10	0.02	0.17	0.39	0.11	1.65	0.15	45.48	50.28	98.24	1.13	11313
Waitaha River	AH3-11	0.00	0.16	0.17	0.10	0.03	0.02	46.29	51.29	98.05	0.02	186
Waitaha River	AH3-12	0.02	0.12	0.09	0.01	0.00	1.31	44.78	51.19	97.53	0.00	12
Gillespies Beach	AN1-1	0.02	0.15	0.08	0.06	0.05	0.02	46.10	51.21	97.70	0.04	367
Gillespies Beach	AN1-2	0.02	0.29	0.34	0.07	0.00	0.35	45.82	51.01	97.90	0.00	29
Gillespies Beach	AN1-3	0.02	0.22	0.12	0.08	0.02	0.06	46.01	51.10	97.62	0.01	135
Gillespies Beach	AN1-4	0.01	0.12	0.09	0.08	0.12	0.01	46.17	51.24	97.83	0.08	818
Gillespies Beach	AN1-5	0.02	0.13	0.07	0.13	0.01	0.00	46.17	51.29	97.83	0.01	86
Gillespies Beach	AN1-6	0.03	0.09	0.06	0.09	0.05	0.08	46.09	51.31	97.80	0.03	331
Gillespies Beach	AN1-7	0.03	0.03	0.04	0.05	0.04	0.03	45.89	51.05	97.17	0.03	301
Gillespies Beach	AN1-11	0.01	0.08	0.07	0.08	0.12	0.09	46.09	51.26	97.80	0.09	855
Gillespies Beach	AN1-12	0.03	0.12	0.10	0.11	0.03	0.03	46.31	51.46	98.20	0.02	198
Gillespies Beach	AN1-13	0.03	0.23	0.34	0.11	0.01	0.11	45.90	50.84	97.57	0.01	91
Gillespies Beach	AN1-14	0.02	0.20	0.15	0.07	0.00	0.03	45.90	50.93	97.30	0.00	20
Haast River	AT1-1	0.01	0.03	0.05	0.16	0.02	0.03	46.48	51.65	98.43	0.01	110
Haast River	AT1-2	0.02	0.14	0.12	0.05	0.00	0.09	46.15	51.29	97.86	0.00	11
Haast River	AT1-3	0.00	0.00	0.01	0.05	0.02	0.01	45.82	50.93	96.84	0.01	121
Haast River	AT1-4	0.01	0.01	0.00	0.07	0.08	0.03	46.49	51.72	98.41	0.06	551
Haast River	AT1-5	0.01	0.09	0.10	0.11	0.03	0.03	46.20	51.30	97.87	0.02	186
Haast River	AT1-6	0.01	0.01	0.00	0.07	0.82	0.03	45.93	51.09	97.95	0.56	5611
Haast River	AT1-7	0.02	0.04	0.01	0.08	0.04	0.06	45.66	50.83	96.75	0.03	282

Haast Beach	AU3-1	0.00	0.01	0.00	0.07	0.01	0.04	46.25	51.45	97.83	0.00	39
Transect	**Sample-grain**	**MgO**	**Al_2O_3**	**TiO_2**	**V_2O_3**	**Cr_2O_3**	**MnO**	**FeO**	**Fe_2O_3**	**Total**	**Cr**	**Cr ppm**
Haast Beach	AU3-2	0.00	0.03	0.01	0.18	0.10	0.04	46.13	51.30	97.78	0.07	656
Haast Beach	AU3-3	0.00	0.02	0.00	0.08	0.04	0.03	46.18	51.35	97.69	0.03	277
Haast Beach	AU3-4	0.00	0.02	0.00	0.14	0.10	0.03	46.15	51.32	97.75	0.07	652
Haast Beach	AU3-5	0.00	0.03	0.01	0.08	0.00	0.09	46.55	51.83	98.59	0.00	29
Haast Beach	AU3-6	0.00	0.00	0.00	0.06	0.10	0.02	45.97	51.11	97.27	0.07	698
Haast Beach	AU3-7	0.01	0.02	0.03	0.01	0.00	0.08	46.36	51.60	98.11	0.00	22
Haast Beach	AU3-8	0.01	0.02	0.01	0.10	0.01	0.01	45.85	50.97	96.97	0.01	71
Haast Beach	AU3-9	0.01	0.11	0.08	0.09	0.00	0.03	45.98	51.07	97.37	0.00	32
Haast Beach	AU3-10	0.01	0.08	0.02	0.05	0.15	0.06	46.30	51.52	98.19	0.11	1058
Haast Beach	AU3-11	0.00	0.04	0.03	0.02	0.02	0.03	46.18	51.32	97.64	0.01	115
Martyr River	2b-1	7.96	9.96	0.23	0.09	49.03	0.43	22.03	11.88	101.61	33.55	335481
Martyr River	2b-2	0.36	0.00	0.18	0.03	0.13	0.07	45.47	51.14	97.37	0.09	914
Martyr River	2b-3	0.02	0.03	0.02	0.11	0.02	0.07	46.13	51.37	97.76	0.01	105
Martyr River	2b-4	0.01	0.02	0.00	0.06	0.00	0.04	46.31	51.53	97.97	0.00	15
Martyr River	2b-5	0.07	0.06	0.02	0.09	0.02	0.08	45.77	51.08	97.18	0.01	103
Martyr River	2b-8	0.00	0.02	0.00	0.07	0.11	0.05	46.24	51.45	97.96	0.07	725
Martyr River	2b-9	0.01	0.04	0.02	0.14	0.04	0.05	46.16	51.35	97.80	0.03	287
Martyr River	2b-10	0.00	0.02	0.00	0.03	0.11	0.08	46.10	51.32	97.68	0.08	759
Arawhata River	3a-1	0.02	0.02	0.34	0.04	0.00	0.08	46.11	51.03	97.63	0.00	15
Arawhata River	3a-2	0.01	0.05	0.03	0.04	0.01	0.07	46.18	51.37	97.75	0.01	51
Arawhata River	3a-3	0.00	0.02	0.00	0.00	0.00	0.05	46.27	51.47	97.82	0.00	26
Arawhata River	3a-4	0.00	0.02	0.00	0.02	0.00	0.21	45.88	51.23	97.36	0.00	18
Arawhata River	3a-5	0.00	0.02	0.00	0.12	0.01	0.04	46.34	51.54	98.06	0.01	66
Arawhata River	3a-6	0.00	0.03	0.01	0.07	0.01	0.04	45.90	51.05	97.10	0.01	66
Arawhata River	3a-7	0.00	0.02	0.01	0.11	0.01	0.05	46.33	51.54	98.07	0.01	73
Arawhata River	3a-9	0.01	0.01	0.00	0.05	0.02	0.08	46.44	51.71	98.34	0.02	157
Arawhata River	3a-10	0.01	0.01	0.00	0.01	0.00	0.02	46.15	51.33	97.53	0.00	2
Arawhata River	3a-11	0.00	0.02	0.01	0.04	0.11	0.04	46.14	51.32	97.68	0.08	764
Neils Beach	4b-1	0.01	0.04	0.01	0.05	0.02	0.05	45.22	50.32	95.72	0.01	137
Neils Beach	4b-2	0.00	0.01	0.00	0.06	0.06	0.04	46.04	51.21	97.43	0.04	424
Neils Beach	4b-3	0.00	0.03	0.01	0.12	0.05	0.04	46.20	51.37	97.81	0.03	309
Neils Beach	4b-4	1.60	0.29	0.14	0.03	23.10	1.92	33.46	37.90	98.45	15.81	158078
Neils Beach	4b-5	0.02	0.03	0.01	0.15	0.09	0.03	45.77	50.92	97.01	0.06	590

Appendix F3: SWCM Detrital magnetite descriptive statistics by region

North Shelf +HCH

	MgO	Al2O3	TiO2	V2O3	FeO	Cr2O3	Fe2O3	MnO
Mean	0.03	0.13	0.22	0.11	45.51	0.42	50.52	0.16
Standard Deviation	0.08	0.24	0.98	0.08	1.62	1.66	1.99	0.37
Minimum	0.00	0.00	0.00	0.00	36.67	0.00	40.97	0.01
Maximum	0.42	1.51	6.27	0.36	46.52	10.52	51.72	2.23
Count	41.00	41.00	41.00	41.00	41.00	41.00	41.00	41.00

Hokitika Beach- AA2

	MgO	Al2O3	TiO2	V2O3	FeO	Cr2O3	Fe2O3	MnO
Mean	0.06	0.08	0.06	0.08	44.77	2.81	49.78	0.24
Standard Deviation	0.08	0.06	0.05	0.03	2.25	5.63	2.93	0.28
Minimum	0.01	0.01	0.00	0.04	38.42	0.00	41.38	0.05
Maximum	0.30	0.24	0.16	0.13	46.24	18.90	51.54	1.09
Count	12.00	12.00	12.00	12.00	12.00	12.00	12.00	12.00

Hokitika River - AB2

	MgO	Al2O3	TiO2	V2O3	FeO	Cr2O3	Fe2O3	MnO
Mean	0.59	1.41	0.00	0.04	42.11	10.31	43.33	0.32
Standard Deviation	1.20	3.39	0.01	0.02	6.93	20.41	16.89	0.49
Minimum	0.01	0.00	0.00	0.02	28.06	0.20	8.89	0.06
Maximum	3.02	8.32	0.01	0.08	45.57	51.87	50.83	1.33
Count	6.00	6.00	6.00	6.00	6.00	6.00	6.00	6.00

Central Shelf

	MgO	Al2O3	TiO2	V2O3	FeO	Cr2O3	Fe2O3	MnO
Mean	0.04	0.13	0.08	0.10	45.54	0.08	50.67	0.05
Standard Deviation	0.17	0.18	0.12	0.07	1.34	0.13	1.22	0.05
Minimum	0.00	0.01	0.00	0.03	38.16	0.00	44.42	0.01
Maximum	1.09	1.09	0.69	0.45	46.35	0.52	51.49	0.33
Count	40.00	40.00	40.00	40.00	40.00	40.00	40.00	40.00

Gillespies Beach

	MgO	Al2O3	TiO2	V2O3	FeO	Cr2O3	Fe2O3	MnO
Mean	0.02	0.15	0.13	0.08	46.04	0.04	51.16	0.08
Standard Deviation	0.01	0.07	0.11	0.02	0.15	0.04	0.19	0.10
Minimum	0.01	0.03	0.04	0.05	45.82	0.00	50.84	0.00
Maximum	0.03	0.29	0.34	0.13	46.31	0.12	51.46	0.35
Count	11.00	11.00	11.00	11.00	11.00	11.00	11.00	11.00

Waitaha River

	MgO	Al2O3	TiO2	V2O3	FeO	Cr2O3	Fe2O3	MnO
Mean	0.03	0.11	0.14	0.08	45.79	0.27	51.04	0.21
Standard Deviation	0.05	0.05	0.12	0.04	0.44	0.54	0.35	0.35
Minimum	0.00	0.04	0.00	0.01	44.78	0.00	50.28	0.02
Maximum	0.19	0.22	0.39	0.16	46.29	1.65	51.50	1.31
Count	12.00	12.00	12.00	12.00	12.00	12.00	12.00	12.00

South Shelf

	MgO	Al2O3	TiO2	V2O3	FeO	Cr2O3	Fe2O3	MnO
Mean	0.01	0.06	0.04	0.09	45.88	0.10	51.04	0.06
Standard Deviation	0.01	0.05	0.04	0.05	0.28	0.35	0.29	0.08
Minimum	0.00	0.00	0.00	0.02	45.21	0.00	50.22	0.00
Maximum	0.04	0.25	0.15	0.19	46.37	2.16	51.55	0.44
Count	37	37	37	37	37	37	37	37

Haast Shelf

	MgO	Al2O3	TiO2	V2O3	FeO	Cr2O3	Fe2O3	MnO
Mean	0.0082	0.0199 6	0.0116 05	0.0799 83	45.972 11	0.0295 69	51.149 72	0.0501 23
Standard Deviation	0.0090	0.0119 54	0.0174 03	0.0392 24	0.1846 11	0.0386 65	0.2089 59	0.0214 56
Minimum	0	0	0	0.0101 1	45.454 79	0	50.591 7	0.0019 69
Maximum	0.0297	0.0452 17	0.0715 62	0.1704 42	46.211 53	0.1890 21	51.423 3	0.0823 53
Count	26	26	26	26	26	26	26	26

Haast river

	MgO	Al2O3	TiO2	V2O3	FeO	Cr2O3	Fe2O3	MnO
Mean	0.0094 72	0.0448 48	0.0420 58	0.0840 75	46.105 58	0.1435 05	51.257 84	0.0405 44
Standard Deviation	0.0052 37	0.0507 01	0.0499 06	0.0404 54	0.3190 49	0.2994 49	0.3403 47	0.0258 92
Minimum	0	0	0	0.0493 47	45.663 02	0.0016 11	50.831 38	0.0137 8
Maximum	0.0158 18	0.1356 51	0.1243 18	0.1610 42	46.493 86	0.8201 67	51.720 4	0.0895 71
Count	7	7	7	7	7	7	7	7

Haast Beach Nth

	MgO	Al2O3	TiO2	V2O3	FeO	Cr2O3	Fe2O3	MnO
Mean	0.00	0.03	0.02	0.08	46.17	0.05	51.35	0.04
Standard Deviation	0.00	0.03	0.02	0.05	0.20	0.05	0.25	0.02

Minimum	0.00	0.00	0.00	0.01	45.85	0.00	50.97	0.01
Maximum	0.01	0.11	0.08	0.18	46.55	0.15	51.83	0.09
Count	11.00	11.00	11.00	11.00	11.00	11.00	11.00	11.00

Arawhata river

	MgO	Al2O3	TiO2	V2O3	FeO	Cr2O3	Fe2O3	MnO
Mean	0.01	0.03	0.03	0.07	46.13	0.11	51.29	0.04
Standard Deviation	0.01	0.04	0.04	0.04	0.26	0.25	0.28	0.02
Minimum	0.00	0.00	0.00	0.01	45.66	0.00	50.83	0.01
Maximum	0.02	0.14	0.12	0.16	46.49	0.82	51.72	0.09
Count	10.00	10.00	10.00	10.00	10.00	10.00	10.00	10.00

Cascade Shelf

	MgO	Al2O3	TiO2	V2O3	FeO	Cr2O3	Fe2O3	MnO
Mean	2.97	3.59	0.32	0.17	37.50	16.50	37.62	0.20
Standard Deviation	4.72	6.51	1.07	0.16	12.34	23.39	19.57	0.27
Minimum	0.00	0.00	0.00	0.01	13.93	0.00	5.64	0.00
Maximum	13.45	21.53	5.64	0.56	46.60	59.88	51.61	1.33
Count	27.00	27.00	27.00	27.00	27.00	27.00	27.00	27.00

Neils Beach

	MgO	Al2O3	TiO2	V2O3	FeO	Cr2O3	Fe2O3	MnO
Mean	0.33	0.08	0.03	0.08	43.34	4.66	48.35	0.42
Standard Deviation	0.71	0.12	0.06	0.05	5.53	10.31	5.85	0.84
Minimum	0.00	0.01	0.00	0.03	33.46	0.02	37.90	0.03
Maximum	1.60	0.29	0.14	0.15	46.20	23.10	51.37	1.92
Count	5.00	5.00	5.00	5.00	5.00	5.00	5.00	5.00

Martyr River

	MgO	Al2O3	TiO2	V2O3	FeO	Cr2O3	Fe2O3	MnO
Mean	1.06	1.27	0.06	0.08	43.03	6.18	46.39	0.11
Standard Deviation	2.79	3.51	0.09	0.04	8.49	17.31	13.94	0.13
Minimum	0.00	0.00	0.00	0.03	22.03	0.00	11.88	0.04
Maximum	7.96	9.96	0.23	0.14	46.31	49.03	51.53	0.43
Count	8.00	8.00	8.00	8.00	8.00	8.00	8.00	8.00

Appendix F4: Descriptive statistics by spinel grain type

	Wt %	Mean	Min	Max	Median	Std. error	Variance	Stand. dev
Chromites	**MgO**	9.49	3.02	13.45	9.76	1.00	9.03	3.01
n=9	**Al_2O_3**	12.48	7.42	21.53	10.89	1.72	26.61	5.16
	TiO_2	0.15	0.01	0.59	0.09	0.06	0.03	0.18
	V_2O_3	0.09	0.04	0.18	0.09	0.01	0.00	0.04
	FeO	19.60	13.93	28.06	18.91	1.36	16.67	4.08
	Cr_2O_3	51.05	39.26	59.88	51.27	2.16	41.91	6.47
	Fe_2O_3	7.69	5.64	11.88	6.91	0.65	3.80	1.95
	MnO	0.47	0.27	1.33	0.37	0.11	0.11	0.33
Ferrian Chromites	**MgO**	1.13	0.30	1.76	1.60	0.33	0.54	0.73
n=5	**Al_2O_3**	0.38	0.10	0.73	0.29	0.11	0.06	0.25
	TiO_2	0.20	0.01	0.46	0.15	0.07	0.03	0.17
	V_2O_3	0.08	0.03	0.14	0.08	0.02	0.00	0.05
	FeO	34.66	30.40	38.43	34.34	1.38	9.49	3.08
	Cr_2O_3	25.10	10.52	45.79	23.11	5.86	171.90	13.11
	Fe_2O_3	35.33	20.87	41.38	37.90	3.77	71.01	8.43
	MnO	1.05	0.45	1.92	1.09	0.28	0.39	0.62
Cr- Magnetites	**MgO**	0.14	0.00	0.88	0.08	0.05	0.04	0.21
n=21	**Al_2O_3**	0.06	0.00	0.27	0.04	0.02	0.01	0.08
	TiO_2	0.08	0.00	0.40	0.03	0.03	0.02	0.13
	V_2O_3	0.11	0.01	0.56	0.07	0.03	0.02	0.14
	FeO	44.94	43.13	45.93	45.30	0.20	0.85	0.92
	Cr_2O_3	2.24	0.52	7.08	1.65	0.40	3.41	1.85
	Fe_2O_3	50.17	47.79	51.09	50.39	0.19	0.75	0.87
	MnO	0.10	0.01	0.30	0.07	0.02	0.01	0.07
Low Cr -Magnetites (I)	**MgO**	0.03	0.00	0.36		0.01	0.01	0.07
n= 40	**Al_2O_3**	0.07	0.00	0.40		0.01	0.01	0.09
	TiO_2	0.04	0.00	0.21		0.01	0.00	0.05
	V_2O_3	0.12	0.02	0.52		0.02	0.01	0.11
	FeO	45.84	44.19	46.47		0.07	0.21	0.46
	Cr_2O_3	0.19	0.10	0.50		0.01	0.01	0.09
	Fe_2O_3	51.02	49.13	51.61		0.08	0.26	0.51
	MnO	0.05	0.00	0.13		0.01	0.00	0.03
Low Cr -Magnetites (II)	**MgO**	0.02	0.00	1.09		0.01	0.01	0.09
n = 178	**Al_2O_3**	0.09	0.00	1.51		0.01	0.02	0.15
	TiO_2	0.12	0.00	6.27		0.05	0.40	0.63
	V_2O_3	0.09	0.00	0.45		0.00	0.00	0.06
	FeO	45.87	38.16	46.60		0.06	0.60	0.77
	Cr_2O_3	0.03	0.00	0.10		0.00	0.00	0.02
	Fe_2O_3	50.98	43.68	51.83		0.07	0.94	0.97
	MnO	0.09	0.00	2.23		0.02	0.04	0.21

APPENDIX G: WAVE HIND CASTING METHODS AND DATA

Appendix G1: WAM (WAve Model)

The WAve generation Model (WAM) enables the creation of a hindcast for the generation and propagation of deep-water waves incident on the New Zealand coastline (Gorman et al. 2003). This hindcast is based on wind data from the European Centre for Meduim-Range Weather Forecasts (EMCMWF).Validation of WAM wave spectra with measured wave statistics have shown that for coastlines exposed to deep-water waves the modeled wave spectra are comparable (Gorman et al. 2003).

Wave data from a selection of West Coast sites between Greymouth and the Wanganui River (Appendix A1) for the period 1979 – 1998 were made available from NIWA. The wave spectra have been interpolated from model output spectra and filtered to correct for limited fetch to the coast, and undergone 'parallel-contour' refraction calculations. One of the main assumptions of the WAM model is that contours are approximately parallel. This becomes a disadvantage where bathymetry is complex (i.e. Canyon heads), and requires higher resolution near shore modeling called SWAN (Simulating WAves Nearshore) to account for this. Given the scope and time frame required for this study, only WAM wave statistics are used providing an approximation of the general wave climate of the region.

Comparisons between the West Coast WAM sites available showed only small variations in wave direction, significant wave height, and significant wave period. Consequently, a single WAM hindcast site was chosen for analysis and subsequent results are applied to the rest of the study region between Greymouth and Haast. This is site '011- Greens Beach' offshore form the Wanganui River. The hind cast period is between 01/01/79 and 31/12/98, with predictions of significant wave height (H_{sig}), period (T_{sig}), and mean wave direction every 3 hours. For the 20-year hindcast period a total of 58,440 recordings of wave statistics were made.

Appendix G2: Wave orbitals and sediment entrainment background, equations and assumptions.

Near bed wave orbital velocity calculations

Water particles in waves move in circular paths (orbitals) in the direction of wave travel. The diametre of the orbitals decreases with depth until there is no motion. This typically occurs at a depth equivalent to half the wavelength. When waves move into shallow water (i.e. $h < 0.5L$), the orbitals become more elliptical, resulting in an increase in wave height and decrease in wave length (shoaling) (Porter-smith et al. 2004). The maximum orbital velocity, U_{max}, for a given water depth, *h*, may be calculated using Airy's wave theory provided the wave height, H, and wave period, T, are known (Portersmith et al 2004). The orbital velocity for as given wave height, period, and fixed point on the shelf bed will vary from zero to U_{max} according to the relationship:

$$\mathbf{U_{max} = \pi H/(T\sinh(2\pi h/L))} \quad \text{(Eq 1)}$$

The wave length (L) in used in Eq (1) was calculated according to the equations:

$$L_o = gT^2/2\pi \quad \text{(Eq 2a)}$$

$$L_i = L_o(T\tanh(2\pi h/L_o))^{1/2} \quad \text{(Eq 2b)}$$

Where L_o, is the deep water wave length, when $h>L_o/2$, and L_i is the expression for intermediate wave length when $1/2 > L_o > 1/20$.

U_{max} was calculated for 25, 50, and 100 m depth for each wave statistic recording in the 20 year hindcast (n=58440).

Estimation of sediment entrainment thresholds

The sediment entrainment threshold is based on flat-bed, spherical, unconsolidated, quartz silt and sand (Porter-Smith et al. 2004), therefore providing an approximation of the mobility of more heterogeneous shelf sediments. Simplified empirical threshold equations have been published by Clifton and Dingler (1984), for flat-bed, spherical, cohesionless, quartz silt and fine sand.

For silt and fine sand and grain size D< 0.05 cm in diametre the threshold speed is given by:

$$\mathbf{U_{cr} = 33.3(TD)^{0.33}} \quad \text{(Eq 3)}$$

Units for U_{cr} are in cm/s.

Potential for sediment entrainment

Where the maximum wave orbital velocity (U_{max}) is greater than the U_{cr} for a given grain size and water depth, the grains may become suspended. With this knowledge, the percentage of time that U_{max} exceeds U_{cr} for 125μm sediments (fine sand) at 25, 50, and 100 m water depth could be calculated from the 20 year

hind cast data. Since U_{cr} varies with T_{sig}, the mean T_{sig} for the entire hind cast was used to calculate the most *common* U_{cr} for 125µm sediment.

Table G1: Summary wave statistics for 20 year hind cast for Greens Beach-Wanganui River, South Westland. (n=58440)

	Hsig (m)	Tsig (sec)	Mean direction (from)
Mean	2.07	7.86	263.3
Min	0.44	4.31	227.8
Max	8.39	13.43	377.2
Standard Deviation	0.91	1.18	-

Table G2: Summary statistics for maximum wave orbital velocities at 25, 50 and 100 m water depth from the Wanganui river 20 year hindcast. [a]each recording represents a 3 hourly set of wave statistics out of 58440 recordings.

Umax (cm/s)	Number of recordings at 25m[a]	% @ 25m	Number of recordings at 50m[a]	% @ 50m	Number of recordings at 100m[a]	% @ 100m
< 10	5006	8.57	42082	72.01	58305	99.77
10 to 30	27205	46.55	14582	24.95	135	0.23
30 - 50	16399	28.06	1581	2.71	0	0.00
50 - 100	9034	15.46	195	0.33	0	0.00
> 100	796	1.36	0	0.00	0	0.00